Role of GABA-dependent hippocampal network oscillations in anxiety and learned fear

Thesis

for the degree of

doctor rerum naturalium (Dr. rer. nat.)

approved by the Faculty of Natural Sciences of Otto von Guericke University Magdeburg

by

Evangelia Pollali, MD, M.Sc.

born on 11 July 1986 in Corinth

Examiners: Prof. Dr. Oliver Stork

Prof. Dr. Costas Papatheodoropoulos

submitted on: 25 April 2022

defended on: 15 December 2022

Τὰ πάντα ῥεῖ, Ηράκλειτος, ~ 500 πΧ

panta rhei: everything flows, accredited to Heracleitus, approx. 500 BC [from Buzsáki, 2006]

Summary

Role of GABA-dependent hippocampal network oscillations in anxiety and learned fear

Evangelia Pollali, MD, M.Sc.

Sharp wave-ripples (SW-R) and gamma oscillations are network activity patterns linked to cognition and memory processes. The ventral hippocampus (vHP) is a structure particularly involved in emotional memories and anxiety and displays robust network oscillatory activity, which critically depends on the interplay between GABAergic inhibition and excitation. Dysregulation of the GABAergic system has been connected with anxiety and post-traumatic stress disorder (PTSD). To further understand how hippocampal network oscillations and excitation/inhibition balance are implicated in learned fear and anxiety, I used slice electrophysiology and fear memory tasks in different animal models.

Firstly, I observed enhanced ripples and pharmacologically-induced gamma oscillations in the vHP of GAD65 KO mice, an animal model of GABA deficiency that exhibits emotional processing deficits. In addition, SW components were enhanced in the CA3 region but diminished in CA1, a dissociation more prominent after a contextual fear conditioning paradigm. Along with a decreased SW incidence in the CA1 region, CA1 pyramidal neurons exhibited hyperpolarized membrane potential and a trend for faster inhibitory current kinetics. Interestingly, the network oscillatory alterations observed in GAD65 KO mice were not present upon local GAD65 reduction in the ventral HP.

Next, I observed enhanced SW-R of the vHP in wild-type mice specifically after adverse training that normalized after fear memory extinction, indicating a potential role of SW-R in the recall of adverse recent memories. Interestingly, reduced CA1 SW incidence was associated with extinction deficits and in combination with similar electrophysiological findings in GAD65 KO mice I would postulate that reduced SW incidence could be a correlate of a predisposition for PTSD-like traits.

Last, by pharmacological excitation of different signaling pathways, I could directly connect the reported molecular alterations of cholinergic and glutamatergic systems with the gamma oscillopathy of Fmr1 KO mice, an animal model of Fragile X syndrome that exhibits cognitive impairments and excitation/inhibition imbalance.

In conclusion, this study could show alterations in the ventral hippocampal network oscillations in animal models of imbalanced excitation/inhibition and phenotypes of increased anxiety and stress susceptibility and would suggest a potential representation of the environmental adversity in SW-R properties.

Zusammenfassung

Die Rolle GABA-abhängiger Netzwerk-Oszillationen des Hippocampus bei Angst und erlernter Furcht

Evangelia Pollali, MD, M.Sc.

Sharp wave-Ripples (SW-R) und Gamma-Oszillationen sind Netzwerkaktivitätsmuster, die mit Kognitions- und Gedächtnisprozessen verbunden sind. Der ventrale Hippocampus (vHP) ist eine Struktur, die besonders an emotionalen Erinnerungen und Angst beteiligt ist und eine robuste oszillatorische Netzwerkaktivität aufweist, die entscheidend vom Zusammenspiel zwischen GABA-ergischer Hemmung und Erregung abhängt. Eine Dysregulation des GABA-ergen Systems wurde mit Angst und posttraumatischen Belastungsstörungen (PTBS) in Verbindung gebracht. Um besser zu verstehen, wie die Oszillationen des Hippocampus-Netzwerks und das Gleichgewicht zwischen Erregung und Hemmung mit erlernter Angst und Furcht zusammenhängen, habe ich elektrophysiologische Methoden und Furchtgedächtnisaufgaben in verschiedenen Tiermodellen verwendet.

Erstens beobachtete ich verstärkte Ripples und pharmakologisch induzierte Gamma-Oszillationen im vHP von GAD65-KO-Mäusen, einem Tiermodell für GABA-Mangel, das Defizite bei der emotionalen Verarbeitung aufweist. Außerdem waren die SW-Komponenten in der CA3-Region verstärkt, in der CA1-Region jedoch vermindert, eine Dissoziation, die nach einem Paradigma der kontextuellen Angstkonditionierung noch deutlicher hervortrat. Zusammen mit einer verringerten SW-Inzidenz in der CA1-Region, zeigten CA1-Pyramidenneuronen ein hyperpolarisiertes Membranpotenzial und einen Trend zu einer schnelleren hemmenden Stromkinetik. Interessanterweise waren die oszillatorischen Veränderungen des Netzwerks, die bei GAD65-KO-Mäusen beobachtet wurden, bei einer lokalen GAD65-Reduktion in der ventralen HP nicht vorhanden.

Als Nächstes beobachtete ich bei Wildtyp-Mäusen erhöhte SW-R im vHP, speziell nach einem negativen Training, die sich nach der Löschung des Furchtgedächtnisses normalisierte, was auf eine mögliche Rolle der SW-R beim Abruf negativer Erinnerungen hinweist. Interessanterweise war eine verringerte SW-Inzidenz in CA1 mit Extinktionsdefiziten verbunden, und in Kombination

mit ähnlichen elektrophysiologischen Befunden bei GAD65 KO-Mäusen würde ich postulieren, dass eine verringerte SW-Inzidenz ein Korrelat für eine Prädisposition für PTBS-ähnliche Merkmale sein könnte.

Schließlich konnte ich durch pharmakologische Anregung verschiedener Signalwege die berichteten molekularen Veränderungen der cholinergen und glutamatergen Systeme direkt mit der Gamma-Oszillopathie von Fmr1-KO-Mäusen, einem Tiermodell des Fragilen-X-Syndroms, das kognitive Beeinträchtigungen und ein Ungleichgewicht von Erregung und Hemmung aufweist, in Verbindung bringen.

Zusammenfassend lässt sich sagen, dass diese Studie Veränderungen in den Oszillationen des ventralen Hippocampus-Netzwerks in Tiermodellen mit unausgeglichener Erregung/Hemmung und Phänotypen erhöhter Angst und Stressanfälligkeit aufzeigen konnte und auf eine potenzielle Darstellung von Umweltbelastungen in den SW-R-Eigenschaften hindeutet.

Table of contents

2 METHODS

List of figures

List of tables

List of abbreviations

°C	degrees Celcius
µM	micromolar
µV	microvolt
ACC	anterior cingulate cortex
ACh	acetylcholine
aCSF	artificial cerebrospinal fluid
ANOVA	analysis of variance
AP	action potential
AP5	d,l-2-Amino-5-phosphonopentanoic acid
AUC	area under the curve
BA	basal amygdala
BC	basket cell
BLA	basolateral amygdala
CA	cornu amonis
$CaCl_2$,	calcium cloride
CCh	carbachol
CEA	central amygdala
CGG	cytosine-guanine-guanine triplet
CO2	carbon dioxide
CORT	corticosterone
CRF	corticotropin-releasing factor
CS	conditioned stimulus
CsOH	cesium hydroxide
ctr	control
DG	dentate gyrus
dHP	dorsal hippocampus
DHPG	(RS)-3,5-dihydroxyphenylglycine
DMSO	dimethylsulfoxid
DNQX	6-cyano-7-nitroquinoxoxaline-2,3-dione
E1-E5	extinction session 1-5
EC	entorhinal cortex
EDTA	Ethylenediaminetetraacetic acid
EEG	electroencephalogram
EPM	elevated plus maze
EPSC	excitatory postsynaptic current
FC	fear conditioning
fEPSP	field excitatory postsynaptic potential
FFT	fast Fourier transformaiton
Fmr1	Fragile X mental retardation gene
FMRP	Fragile X mental retardation protein
fv	fiber volley

FXS	Fragile X syndrome
GABA	gamma-amino-butyric acid
GAD	glutamic acid decarboxylase
GFP	green fluorescent protein
h	hour
HCl	hydrocloride
HCO_3^-	Bicarbonate ion
HEPES	4-(2-hydroxyethyl)-1-piperazineethanesulfonic acid
HFS	high frequency stimulation
HP	hippocampus
Hz	hertz
iHP	intermediate hippocampus
IL	infralimbic cortex
IN	interneuron
ING	interneuron network gamma model
I-O	input- output
IPSC	inhibitory postsynaptic current
ISI	interstimulus interval
KA	kainic acid or kainate
KCl	potassium chloride
KD	knock-down
K-gluconate	potassium-gluconate
KO	knock-out
KOH	potassium hydroxide
LA	lateral amygdala
lEC	lateral entorhinal cortex
LFP	local field potential
LIA	large amplitude irregular activity
LTD	long-term depression
LTP	long-term potentiation
M1-M4	muscarinic receptor type 1 and type 4
mA	milliamper
mAChR	muscarinic cholinergic receptor
mEC	medial entorhinal cortex
MEG	magnetic electrogram
Mg	magnesium
mg	milligram
MgATP	adenosine triphosphate magnesium
$MgCl_2$	magnesium cloride
mGluR	metabotropic glutamate receptor
ml	milliliter
mm	millimeter
mM	millimolar
mOsm	milliosmol
mPFC	medial prefrontal cortex

ms	millisecond
mV	millivolt
MΩ	megaohm
Na	sodium
NaCl	sodium cloride
NaGTP	guanosine -triphosphate sodium
NaH_2PO_4	sodium diphosphate
$NaHCO_3$	sodium bicarbonate
NPY	neuropeptide Y
O2	oxygen
O-LM	oriens- lacunosum moleculare
pA	picoamper
PBS	phosphate buffer saline
PC	pyramidal cells
PCR	polymerase chain reaction
PFA	paraformaldehyde
PFC	prefrontal cortex
PING	pyramidal-interneuron gamma model
PL	prelimbic cortex
PP	paired-pulse
PTSD	post-traumatic stress disorder
PV	parvalbumin
REM	rapid eye movement sleep
s.l-m.	stratum lacunosum-moleculare
s.o.	stratum oriens
s.p.	stratum pyramidale
s.r.	startum radiatum
SC	Schaffer collateral
sec	second
SEM	standard error of the mean
SOM	somatostatin
SR	spontaneous recovery
STP	short-term plasticity
SW	sharp wave
SW-R	sharp wave-ripples
UC	unconditioned stimulus
vHP	ventral hippocampus
WT	wild type

CHAPTER 1. INTRODUCTION

1.1 Hippocampus and Memory

1.1.1 Memory processes

Studies from human brain lesions have demonstrated cognitive deficits characterized by the location of the lesion. The famous case of Henry Molaison (H.M.), a patient who suffered from severe epileptic seizures, shed light on the critical role of the hippocampus in memory. H.M. underwent a brain operation and had his medial temporal lobes surgically removed, including the anterior two-thirds of both hippocampi. The epileptic episodes substantially decreased, but consequently, anterograde and retrograde amnesia were developed, an inability to form new or recall relatively recent episodic memories. Episodic memories, a subgroup of declarative memories, contain information about events we have experienced regarding time, place and context. Interestingly, other non-episodic memory types, such as working memory or procedural memory, which includes motor learning, were left intact in the case of H.M. (Scoville & Milner, 1957). Therefore, from this and other later studies, it was shown that the hippocampus is critical for the three stages of episodic memory: encoding, consolidation, and retrieval (Burgess et al., 2002; Eichenbaum et al., 1992; Hirsh, 1974; Nadel & Moscovitch, 1997; Squire & Zola-Morgan, 1991). During encoding, the first exposure to an event takes place and relational information is initially processed in the hippocampus. Deficits in encoding, such as lesions in the hippocampus, can explain the anterograde amnesia. Then, to sustain the acquired information, the following step of consolidation is needed. According to the two-stage model of memory consolidation (Buzsáki, 1989; Marr, 1971), the fresh, new memories, transiently stored in the hippocampus, are transferred to the neocortex and become more stable for long-term storage. Consolidation happens during sleep or quiet immobility when a planned action has ended. In contrast, encoding happens during motivational or preparatory activity, such as exploration. During retrieval, the consolidated information from a past event is reactivated in the hippocampus to facilitate decisions based on experience. Inhibiting the retrieval results in retrograde amnesia (Joo & Frank, 2018).

1.1.2 Emotional memories, adaptive & maladaptive responses

1.1.2.1 Defense mechanisms: anxiety and fear

Episodic memories become stronger when paired with emotions (Cahill & McGaugh, 1998). Negative emotions, such as fear, which is elicited in the presence of real danger, can attach importance to an initially indifferent environment (Davis, 1997; Fanselow, 1986). Emotional memories prepare a person for a possible negative outcome based on a negative experience and send a warning as a reminder. Therefore, they are protective, contributing to safe decisions and avoiding harmful situations in the future. Additionally, traits, such as anxiety, which is an innate state of alertness and anticipation of vague, distal threats, can support this safety mechanism (Davis et al., 2010; Gray & McNaughton, 1982). Therefore, both, fearful memories and anxiety are considered defensive behaviors and contribute to survival. Defensive responses include risk assessment when a threat is relatively distant or fight and flight response when the danger is imminent (Blanchard et al., 2011; Davis, 1997). However, this adaptive mechanism might be dysregulated, become uncontrollable and lead to inappropriate outcomes, rendering the system maladaptive. Such conditions include psychiatric disorders, such as anxiety disorders and post-traumatic stress disorder (PTSD) (McEwen, 2004).

1.1.2.2 Anxiety disorders and PTSD

Heightened anxiety is described by overestimation of threat and highly avoidant behavior. This exaggeration can cause psychiatric conditions, such as panic disorder and phobias. Highly anxious individuals are nervous, restless, and hypersensitive to sensory stimuli. Symptomatology includes worrying and a sense of body rigidity, along with physiological alterations, such as increased blood pressure, heart rate, and sweating (Calhoon & Tye, 2015). Anxiety disorders appear with a 20% twelve-month prevalence and 33% lifetime prevalence (Bandelow & Michaelis, 2015). They cause mild to serious distress, deteriorating productivity and the quality of life (Bereza et al., 2009).

Post-traumatic stress disorder (PTSD) is a psychiatric condition categorized in the disorders associated with stress, according to the International Classification of Diseases (ICD-11). It has an incidence of 5-10% in the general population, which is higher in women (Kessler et al., 2005) and military populations after a war (Richardson et al., 2011). PTSD often co-occurs with anxiety and affective disorders and it was considered an anxiety disorder by older classification (Siegmund &

Wotjak, 2006). It might occur as a result of a single or repetitive highly frightening or harmful episodes, such as war, accident, or violence. The symptomatology lasts for weeks and interferes with the normal functional life of the person, causing severe distress in personal, interpersonal and professional aspects of life. Three major conditions describe PTSD. First, re-experiencing the traumatic episodes in sleep or awake with the same emotional and physiological responses, as when it actually happened. Second, avoidance of situations that might remind the traumatic episode and third, hyperarousal and increased perceptions of immediate threats that might be exaggerated with stimuli, such as sudden noises (World Health Organization, ICD-11, 2018; Barbano et al., 2019).

1.1.2.3 Fear Conditioning, a tool to study emotional memories

Fear conditioning (FC) is established as a tool to investigate emotional memories and maladaptive responses, such as fear memory over-generalization or extinction deficits. It is based on the classical conditioning, discovered by Pavlov (Pavlov, 1927), according to which neutral stimuli (conditioned stimulus: CS) are paired with appetitive (or aversive) stimuli (unconditioned stimulus: US) and provoke the physiological responses that the US alone would cause. The form of (pure) contextual FC describes the association of an initially neutral context with an unconditioned fearful stimulus, such as an electrical shock. Thus, the context, characterized by polymodal sensory elements, such as odors, texture, and light intensity, becomes the conditioned stimulus (CS) (Neves et al., 2008). On the other hand, during the cued FC, the animal associates the fearful stimuli (shock) with a static, originally neutral cue, such as a tone (CS) that precedes the shock. In this case, the context is only a background characteristic and contributes to a much lesser extent to the fear association. However, when the cue does not precede the shock and thus is not predictive of it, the context is in the foreground and contributes more to the fear memory association. Pure, foreground, and background context are represented in different neural circuits (Calandreau et al., 2010; Phillips & LeDoux, 1994; Raza et al., 2017; Zelikowsky et al., 2014). In all FC paradigms, associative learning is assessed based on defensive responses towards fear. One robust fear indicator is the freezing behavior, characterized by immobility and tensed posture (Davis, 1992). When the animal is repeatedly exposed to the CS but not to the US, the freezing response decreases, and fear extinction develops. It has been shown that fear extinction is a non-permanent state since the CS can elicit fear responses even after extinction

training, spontaneously, or after re-exposure to the US. Thus, it is supported that fear extinction does not delete the fear memories that are formed, but rather facilitates additional learning that inhibits the conditioned fear (Bouton et al., 2006; Quirk et al., 2006). During FC, different systems interact; the amygdalar circuits encode valence, while the hippocampal complex is involved in the contextual information and memory formation (Janak & Tye, 2015; Phelps, 2004; Richardson et al., 2004). Additional circuits involving the prefrontal cortex (PFC) are activated during fear extinction to suppress the fear responses (Myers & Davis, 2007; Quirk et al., 2006).

1.2 Main structures and connections involved in emotional memories

1.2.1 The hippocampus and main anatomical connections

Studying hippocampal anatomy and connectivity provides substantial knowledge in understanding the neural substrates and the physiological mechanisms underlying memory. The hippocampus is a structure in the medial temporal lobe that belongs to the limbic system (Fig. 1.1). It consists of three main Cornu Amonis subregions; CA3, CA2, and CA1, the dentate gyrus (DG), and the subiculum. The Cornu Amonis areas are characterized by a laminar organization with four main regions. From deep to superficial, it consists of five layers or strata: the alveus, the stratum (str.) oriens (s.o.), where the basal dendrites of pyramidal cells (PC) reside, and the str. pyramidale (s.p.), where the somata of the PC are located. The proximal and distal dendrites of pyramidal cells are found in str. radiatum (s.r.) and str. lacunosum-moleculare (s.l-m.), respectively. In the CA3 exists one additional stratum, the str. lucidum. The DG consists of four layers; the polymorphic, the most superficial layer, where interneurons reside; the str. granulosum, which contains the granule cell somata; the str. moleculare, which includes the fibers and synapses and the hilus, which contains the mossy cells.

The hippocampus communicates with its adjacent structures, such as entorhinal and perirhinal cortices, from where it receives its main input and projects its main output. Medial and lateral entorhinal cortices (mEC and lEC) send excitatory input to the hippocampus that contains polymodal sensory information about space. Specifically, fibers starting from EC layer II project

via the perforant path to DG. DG projects to CA3 via the mossy fibers and subsequently sends fibers to CA1 via the Schaffer collateral (SC) path. After information processing within the trisynaptic pathway (EC-DG-CA3-CA1), CA1 projects mainly back to EC, directly or indirectly through subiculum. Additionally, CA3 and CA1 regions receive direct excitatory input from EC that targets principally the s.l-m. Except for the above main pathways, the CA3 region projects through commissural connections to contralateral CA3 and CA1 pyramidal neurons (Neves et al., 2008; O'Keefe & Nadel, 1978).

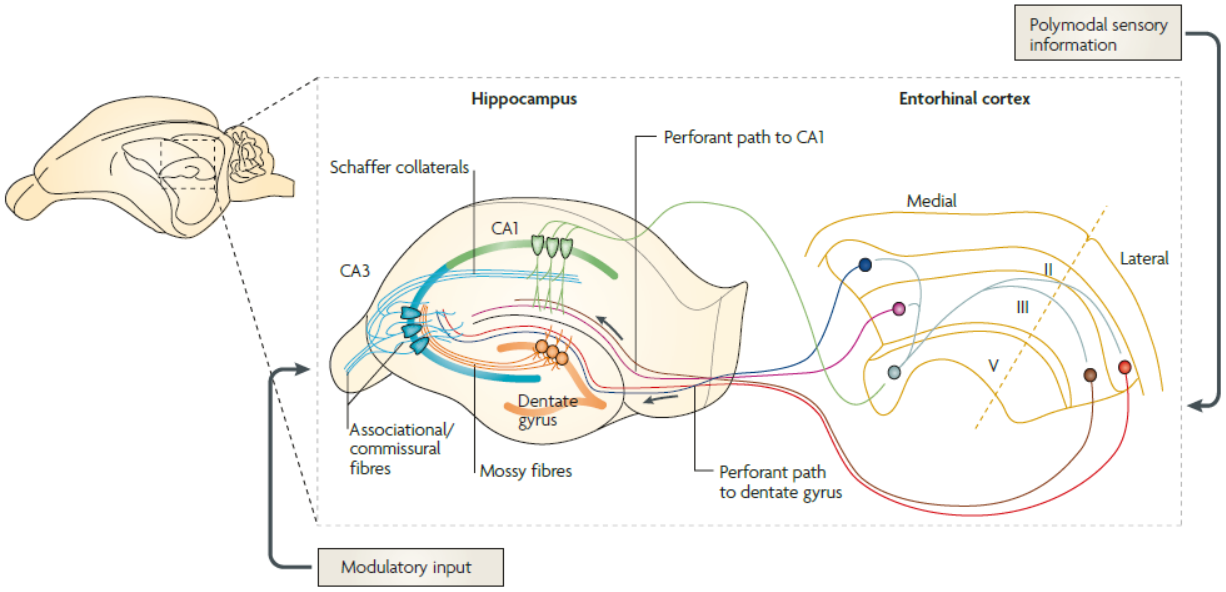

Fig. 1.1: Hippocampus: basic anatomy and connections. *The hippocampus is a structure in the temporal lobe. It receives polymodal sensory information from the medial and lateral entorhinal cortices, which is further processed within the trisynaptic hippocampal network. Initially, DG receives input from EC via the perforant path, which is further transferred via the mossy fibers to the CA3 region. Subsequently, CA3 pyramidal cells project to the CA1 region via the Schaffer collaterals and finally, CA1 pyramidal neurons send the main hippocampal output back to EC and other cortical regions. Additionally, the CA1 subregion receives direct input from mEC through the perforant path to the CA1 or temporoammonic path. DG: Dentate gyrus; CA1-CA3: Cornu Ammonis 1-3 (Reproduced from Neves et al., [2008] with permission from Springer Nature).*

1.2.2 Other important structures in emotional processing

Even though the hippocampus is a crucial region involved in emotional memories, it does not act alone. Other limbic regions, such as the amygdala and prefrontal cortex contribute substantially to emotional processing (Fig. 1.2). The amygdala is a critical structure involved in defense mechanisms and fear conditioning. It gives either positive or negative valence to events. It consists of the lateral (LA), basolateral (BLA), basal (BA), central (CEA) and medial nuclei. The LA

is the main nucleus to receive the sensory input from the thalamus and cortex which is further processed towards the other nuclei that later project to other areas and mediate physiological responses, such as endocrine or autonomic. The BLA shares direct and reciprocal connections with the hippocampus, which mediates the contextual FC (Adolphs, 2013; Janak & Tye, 2015). The medial prefrontal cortex (mPFC) participates in the extinction of conditioned fear and the maintenance of the extinction (Milad & Quirk, 2002; Morgan et al., 1993; Quirk et al., 2000). It consists of the anterior cingulate cortex (ACC), the prelimbic (PL), infralimbic (IL) cortices (Anastasiades & Carter, 2021).

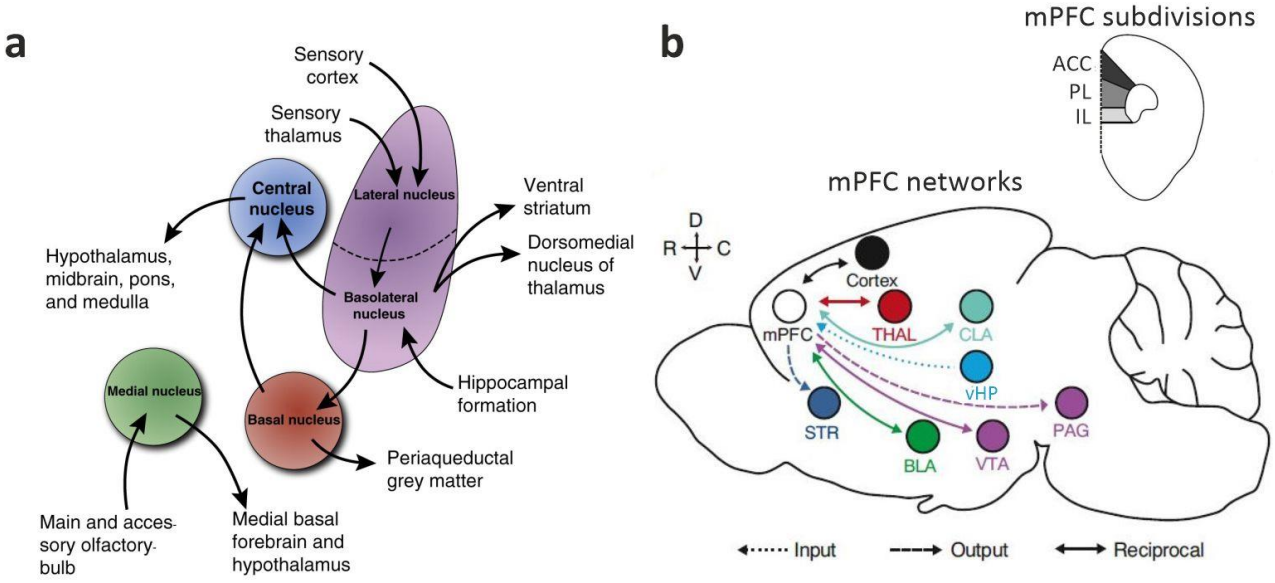

Fig. 1.2: Anatomy of the amygdala, the mPFC, and their networks. (a) *Amygdala consists of an accumulation of nuclei that interact with each other and process the incoming information. The sensory input from the cortex and thalamus enters the lateral nucleus of the amygdala that further projects to the basolateral nucleus (BLA). BLA also receives input from the hippocampus and projects to other nuclei and external areas.* ***(b)*** *The medial prefrontal cortex (mPFC) consists of the anterior cingulate cortex (ACC), the prelimbic (PL), and the infralimbic (IL) cortices. It is connected with other limbic areas, including the ventral hippocampus and the amygdala, with one-directional or reciprocal connections. THAL: thalamus; CLA: claustrum; vHP: ventral hippocampus; PAG: periaqueductal gray; VTA: ventral tegmental area; STR: striatum. (****(a)*** *Reproduced from Adolphs, [2013] and* ***(b)*** *from Anastasiades & Carter [2021], with permissions from Elsevier).*

1.2.3 Hippocampal functional segregation along the septo-temporal axis

The role of the hippocampus in episodic, spatial, and fear memory is widely accepted. Studies using animal experimentation in tasks, such as spatial navigation and FC, assessed episodic-like memories and investigated how the subparts of the hippocampus contribute to each of these

behaviors. Hippocampal lesions in rats showed that the dorsal pole (dHP) but not the ventral (vHP) is required for spatial learning in the water-maze task (Bannerman et al., 2003; Kjelstrup et al., 2002; Moser et al., 1995). Place cell receptive fields are smaller and thus more sensitive in the dHP than in the vHP. Therefore, internal cognitive space maps are mediated more precisely by dHP (Kjelstrup et al., 2008).

However, both dHP and vHP are involved in contextual fear FC but not cued FC. Specifically, dHP or vHP are sufficient to mediate pure (Kjelstrup et al., 2002) or foreground contextual FC, and only lesions to both of them disrupt the contextual FC (Zhang et al., 2014). Additionally, dHP or vHP lesions disrupted the acquisition of background contextual FC (Phillips & LeDoux, 1994; Zhang et al., 2014). Therefore, it is supported that contextual FC requires both dHP and vHP with the view that dHP contributes to the spatial representations, and the vHP mediates the association of these representations with the fear through its close connections with the amygdala and other subcortical regions (Zhang et al., 2014).

Nonetheless, studies have shown the selective role of vHP as part of the defense mechanism, demonstrated by animal behavioral tests that assess anxiety. For example, distinct lesions in vHP but not dHP had an anxiolytic effect by increasing open arm exploration on the elevated plus-maze (Bannerman et al., 2004; Kjelstrup et al., 2002). Selective lesions of vHP decreased the stress responses (defecation, corticosterone blood levels) during the stay in a bright lit chamber and confinement test (Kjelstrup et al., 2002). In line, lesions of vHP but not dHP increased social interaction and reduced hyponeophagia, a test during which animals placed in a novel, potentially anxiogenic environment show increased latency to eat (Bannerman et al., 2004).

Thus, the hippocampus is not a functional entity but rather divided into two main functional zones along the septotemporal (or longitudinal) axis: the dorsal and the ventral poles, with an intermediate zone (iHP) (Bannerman et al., 2014; Fanselow & Dong, 2010; Strange et al., 2014). According to this, the dHP is mainly important for cognitive functions and declarative memories, such as spatial memory and locomotion. The vHP mainly mediates emotions, unconditioned fear, motivations and stress responses (Strange et al., 2014). Last, the iHP is a mixture of both functions and its role might be a combination and translation of both kinds of information to critical actions for survival (Bast et al., 2009; Ciocchi et al., 2015; Fanselow & Dong, 2010). However, all functional

regions maintain the same trisynaptic circuit with fibers passing from DG to CA3 and then to CA1, which implies a common algorithm in computations for all functions (Bannerman et al., 2014).

1.2.4 Synaptic plasticity along the septo-temporal axis of the hippocampus

Synaptic plasticity entails activity-dependent changes that increase or decrease the synaptic weights between neurons and can have a short- or long-term duration (Zucker & Regehr, 2002). This process is considered a mechanism that mediates learning and memory (Hebb, 1949). According to Hebbian theory, when a neuron is activated persistently after the firing of another synaptically connected neuron, then metabolic changes will occur that increase the efficacy of the synaptic transmission. Additionally, such cells while connected into cells assemblies will be characterized by sequential activity. Therefore, activation of only a part of the assembly can activate the whole assembly and resemble the activity that was originally evoked during the first experience of the event (Hebb, 1949; Langille & Brown, 2018).

Experimentally, long-term synaptic plasticity is achieved by high-frequency repetitive electrical stimulation on the presynaptic fibers that modifies the responses of the postsynaptic neurons. Long-term potentiation (LTP) occurs when the responses are enhanced whereas long-term depression LTD occurs with reduced responses (Bliss & Lomo, 1973; Neves et al., 2008). Similarly, induction of short-term plasticity (STP) occurs with methods, such as paired-pulse facilitation and depression, by which two stimuli are applied with a small delay (5-200 Hz). Within a short interval (<20 ms) depression is achieved, whereas with longer intervals (20-500 ms) augmentation is observed. The determining factors of whether the postsynaptic responses would be facilitated or depressed involve presynaptic and postsynaptic mechanisms. Such factors include accumulation of calcium in the presynapse, neurotransmitter probability release and depletion of neurotransmitter vesicles, inactivation of voltage-dependent channels, activity state of protein kinases and activation states of neurotransmitter receptors (Citri & Malenka, 2008).

Synaptic plasticity can reach lengthy durations in the hippocampus, but it exhibits differences along its septo-temporal axis. Previous studies have shown that high frequency stimulation (HFS) exhibits inefficiency to induce LTP in the SC-CA1 synapse of rat ventral hippocampal slices compared to dorsal (Papatheodoropoulos & Kostopoulos, 2000a), which is also observed *in vivo* (Maruki et al., 2001). Furthermore, LTP magnitude is smaller and not persistent in slices of vHP compared to dHP (Maggio & Segal, 2007b). Similarly, induction of STP in the CA1 subregion of rat

hippocampal slices, assessed by a paired-pulse paradigm, is less robust in vHP compared to dHP (Papatheodoropoulos & Kostopoulos, 2000b).

Moreover, stress differentially modifies LTP induction in the hippocampus. Previous studies (Diamond et al., 1990; Shors et al., 1989) have shown that behavioral stress suppresses LTP in dorsal CA1 and DG and administration of the stress hormone corticosterone (CORT) (Joëls, 2006) has similar results, tested both *in vivo* and *in vitro* (Pavlides et al., 1993, 1996). However, behavioral stress reverses the deficits of the vHP to exhibit LTP (Maggio & Segal, 2007a) and furthermore rats exposed to stress both in juvenile age and adulthood show enhanced and long-lasting LTP in CA1 of ventral but not dorsal HP (Maggio & Segal, 2011).

1.2.5 Functional and anatomical connectivity of the ventral hippocampus

The hippocampus demonstrates distinct connectivity with cortical and subcortical brain regions along its septo-temporal axis. The ventral HP shows solid connections with limbic structures implicated in emotional processing (Fanselow & Dong, 2010). For example, the ventral CA1 region projects to the olfactory bulb and olfactory cortices (Cenquizca & Swanson, 2007). Interestingly, studies have shown that depression symptomatology occurs after olfactory bulbectomy which is not explained by the loss of olfaction (Song & Leonard, 2005; Dayong Wang et al., 2007).

Additionally, ventral but not dorsal HP communicates directly with the BLA (Maren & Fanselow, 1995; Pitkänen et al., 2000). Inputs from the vHP to the BA are critical for the contextual fear memory retrieval and activation of these projections impairs fear extinction (Xu et al., 2016). Direct projections from the vHP to the CEA (Cenquizca & Swanson, 2007; Kishi et al., 2000) are required for cued memory retrieval (Xu et al., 2016). Furthermore, activated projections from the BLA to the vHP enhance the consolidation of fear memory after FC (Huff et al., 2016) and heighten anxiety-like behaviors, whereas their optogenetic inhibition has the opposite effect (Felix-Ortiz et al., 2013). Similarly, connections between the vHP to mPFC but not dHP are direct (Hoover & Vertes, 2007). Optogenetically inhibiting the vHP-mPFC pathway results in an anxiolytic effect (Padilla-Coreano et al., 2016).

The vHP shows oscillatory synchronization with the amygdala and the mPFC. In particular, theta power and synchrony between the mPFC and the vHP but not the dHP are increased in anxiogenic environments tested in the open field and elevated plus maze (EPM) (Adhikari et al., 2010). mPFC

neurons, active in the anxiogenic regions of the EPM, are correlated with the vHP inputs (Adhikari et al., 2011). On the other hand, strong gamma synchrony with directionality from mPFC to BLA and to vHP indicates safety in anxiogenic environments (Adhikari et al., 2010; Likhtik et al., 2014; Stujenske et al., 2014).

Among other limbic structures differentially connected with the vHP is the hypothalamus, a structure with a central role in the neuroendocrine, the autonomic nervous system and in the control of motivational and reward-related behaviors (Fanselow & Dong, 2010).

1.3 Network Oscillations

Neural networks show electrical oscillatory activity that spans in frequencies from 0.05 Hz to 500 Hz. This activity can be further categorized into bands with each mean band-value being at a constant distance from the next value, namely at a distance of one natural logarithm (Penttonen & Buzsáki, 2003). Thus, the representation of the frequency bands in the natural logarithmic scale is linear, as shown in Figure 1.3 (Buzsáki & Draguhn, 2004). These frequency bands are preserved across species and they have been connected with cognition and behaviors, such as immobility or spatial navigation (Buzsáki, 2005; Gray et al., 1989; Kahana et al., 2001; Laurent, 2002; Llinas & Ribary, 1993). Therefore, accumulating evidence supports that the network oscillations hold a functional role rather than just being an epiphenomenon or a by-product of brain activity (Buzsáki, 2015).

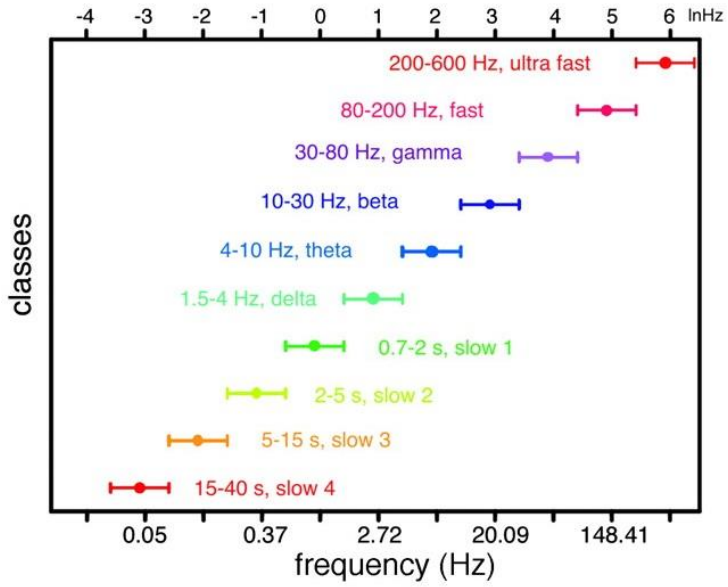

Fig. 1.3: Oscillation classes. *Oscillations are classified according to their frequency, from slow to ultrafast. Note the step from one frequency range to the next that equals the natural logarithm (Reproduced from Buzsáki & Draguhn, [2004] with permission from AAAS and Elsevier).*

The term local field potential (LFP) describes the electrical activity of a brain region recorded by locally inserted electrodes. It represents the extracellular collective voltage deflections that arise from the communication among neurons, mainly from slow synaptic currents but also fast action potentials. However, other sources of electrical activity, such as intrinsic membrane currents or neuronal-glial interactions, might also contribute to the LFP, but to a lesser extent (Buzsáki et al., 2012).

1.3.1. Sharp wave-ripples

1.3.1.1 Basic features of SW-R

One type of electrical activity recorded in the LFP is the sharp wave-ripple events (SW-R). They were described by Buzsaki et al., 1983, even though previous observations reported similar activity, such as "EEG spikes" by Jouvet et al., 1959, "large amplitude irregular activity" (LIA) by (Vanderwolf, 1969), or ripples by (O'Keefe, 1976; O'Keefe & Nadel, 1978). SW-R is a complex event with two elements, the sharp wave, and the ripple. The sharp wave (SW) is a slow, irregular and high magnitude deflection of negative polarity when recorded in s.r. SW events *in vivo* have an incidence of 0.5-1 per sec and 40-100 ms duration. On the other hand, the ripple component, superimposed on the SW, is a regular, smaller amplitude fast oscillation (~110-200 Hz). The ripple frequency varies, depending on whether it is recorded during sleep (140 Hz), wake immobility (160 Hz), or *in vitro* (>180 Hz) (Buzsáki, 2015; Maier et al., 2003; Oliva et al., 2016).

The SW-R were described in the hippocampus of behaving rats during immobility (Buzsáki et al., 1983). Apart from rodents, similar activity has been previously observed in other species, such as humans, primates, and cats (Freemon et al., 1969; Freemon & Walter, 1970; Hartse et al., 1979). SW-R appear during quiet wakefulness and consummatory behaviors, such as drinking and eating, but also during slow-wave sleep (Bragin et al., 1999; Buzsáki et al., 1983). Additionally, they occur spontaneously *in vitro*, such as in ventral to intermediate slices of rodent hippocampus (Maier et al., 2003; Papatheodoropoulos & Kostopoulos, 2002a; Wu et al., 2002) or more rarely in dorsal

hippocampal slices (Kouvaros & Papatheodoropoulos, 2017). In the rat hippocampus, they have also been reported after high-frequency stimulation in the dorsal and ventral-mid parts (Behrens et al., 2005).

The SW-R complex is also observed in the olfactory bulb, olfactory cortex, and para-hippocampal areas, such as the entorhinal cortex and parasubiculum, basolateral amygdala & piriform cortex (Manabe et al., 2011; Narikiyo et al., 2014; Perumal et al., 2021; Ponomarenko et al., 2003). The ripple component is described in associative cortices, including ACC, retrosplenial cortex, medial prefrontal cortex, posterior parietal cortex, and occurs in synchrony with the hippocampal ripples (Khodagholy et al., 2017).

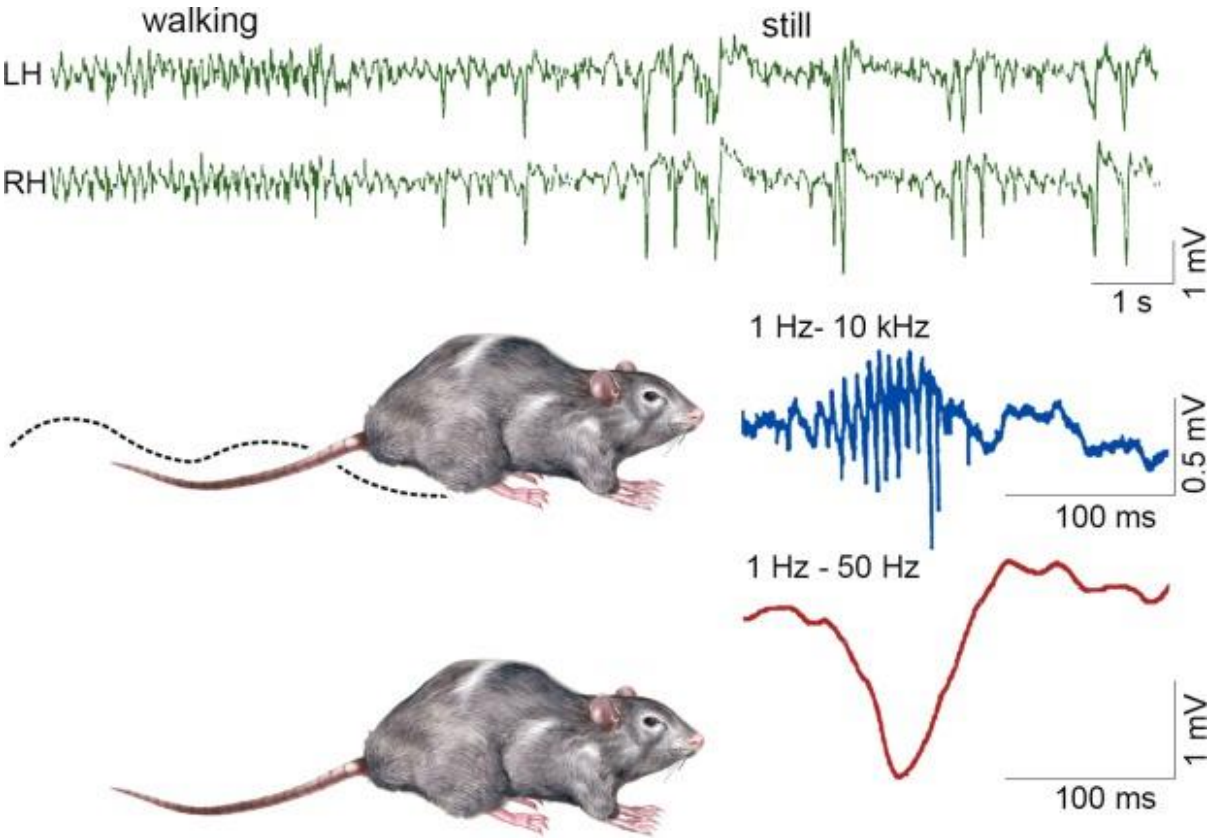

Fig. 1.4: Basic features of sharp wave-ripples (SW-R). *LFP activity recorded from the CA1 subregion of the dorsal hippocampus of a rat while moving and after the transition to stillness. Regular activity in theta range is recorded while walking, whereas in immobility irregular activity, the SW-R complex is observed. In higher magnification the filtered ripple component (in blue) and the sharp wave component in red (Reproduced from Buzsaki, [2015], with permission from John Wiley & Sons).*

1.3.1.2 SW-R generation mechanisms

CA3 region, due to its recurrent collateral excitatory profile, is suggested to be the initiator of SW bursts (Amaral & Witter, 1989; Buzsáki, 2015; Traub & Wong, 1982; Wittner et al., 2007). One recently identified CA3 pyramidal cell type that exhibits bursting firing, absence of dendritic thorns and receives no mossy-fiber activation has been proposed to initiate the sharp waves (Hunt et al., 2018). Alternatively, the CA2 region could be the initiator of SW-R because the firing rate of CA2 pyramidal neurons increases before the initiation of ripples and decreases when firing of CA1 and CA3 is increased (Oliva et al., 2016), or a combined activity of CA2 - CA3 synchronous activity would be possible (Buzsáki, 2015; Csicsvari et al., 2000). Some studies have shown that CA1 ripples occur even with blocking CA3 input (Maier et al., 2003; Nakashiba et al., 2009), possibly due to sufficient excitatory drive from the entorhinal cortex (Buzsáki, 2015). Additionally, a recent study shows the emergence of a proportion of atypical SW-R that originate from the subiculum (Imbrosci et al., 2021).

To explain the SW-R generation, previous studies have suggested an important role of gap junctions (Draguhn et al., 1998), reciprocal interneuronal inhibition (Maier et al., 2003) and of feedback inhibition with interactions between pyramidal neurons and interneurons (Ramirez-Villegas et al., 2018). However, a very prominent model suggests a combinatory mechanism with pyramidal cell and interneuron interactions that also involves a refractory and a spontaneous component (Schlingloff et al., 2014). According to the model, initially, through a stochastic mechanism, a number of CA3 pyramidal neurons start to fire, and this excitation is further transferred to a bigger population of CA3 neurons due to their recurrent collateral connections. Then, this high excitatory drive is conveyed via the SC to the CA1 apical dendrites and causes a negative LFP deflection at the s.r. The excitatory potential from the dendrites travels to the soma of the CA1 pyramidal cells, which elicit action potentials. At the same time, the local CA1 perisomatic interneurons, through reciprocal and feedback inhibition, set the rhythm for the CA1 neuronal firing and thus the rhythm for a ripple activity. Therefore, the SW component recorded in the apical dendrites of CA1 pyramidal neurons (CA1 s.r.) reflects the excitatory afferents from the CA3 region.

The ripple component, recorded where the pyramidal cell body is located, arises at the str. pyramidale from a local mechanism of pyramidal neuron - interneuron interaction in a reciprocal

and feedback manner. The troughs of ripple oscillation represent the synchronous firing of a population of CA1 neurons, whereas the positive peaks represent the perisomatic inhibition. Thus the magnitude of the ripples represents the population of active CA1 pyramidal cells (Buzsáki et al., 1983, 1992; Csicsvari et al., 1999; English et al., 2014; Schomburg et al., 2012; Stark et al., 2014).

It has been shown that inhibiting either the glutamatergic or the GABAergic transmission impedes the SW-R generation (Behrens et al., 2005; Ellender et al., 2010; Hofer et al., 2015; Maier et al., 2003; Papatheodoropoulos & Kostopoulos, 2002; Wu et al., 2002). In particular, perisomatic fast-spiking parvalbumin-positive (PV^+) basket cells, are critical for ripple generation, but also sufficient to initiate ripples. This counter-intuitive finding that PV^+ cells promote and do not inhibit PC might be explained by a disinhibition mechanism. According to this process, PV^+ cells inhibit dendritic targeting interneurons, which results in a net excitatory effect on the PC (Butler & Paulsen, 2015; Buzsáki, 2015; Schlingloff et al., 2014). Except for the PV^+ basket cells, other types of interneurons are linked to SW-R, such as the oriens-lacunosum-moleculare (O-LM) cells, which show coherent synaptic excitation coupled to LFP ripples (Pangalos et al., 2013). The O-LM cells have a particular location of their anatomical components; their somata are located in the s.o., while their axons reach the s.l-m., where they provide with inhibition the apical dendrites of CA1 pyramidal cells. Interestingly, s.l-m. is the same compartment where the input from the EC and thalamus arrives at the CA1 region (Colbert & Levy, 1992; Empson & Heinemann, 1995). Therefore, it is suggested that activation of O-LM interneurons modulates the competition between the cortical afferents against the CA3 input (Pangalos et al., 2013). Supporting mechanisms involve the augmentation of the entorhinal input by a disinhibition approach, such as reducing the feedforward inhibition from the EC (Elfant et al., 2008; Empson & Heinemann, 1995). On the other hand, attenuation of the entorhinal input is also proposed by the direct hyperpolarizing action of the O-LM to the CA1 pyramidal dendrites (Maccaferri et al., 2000).

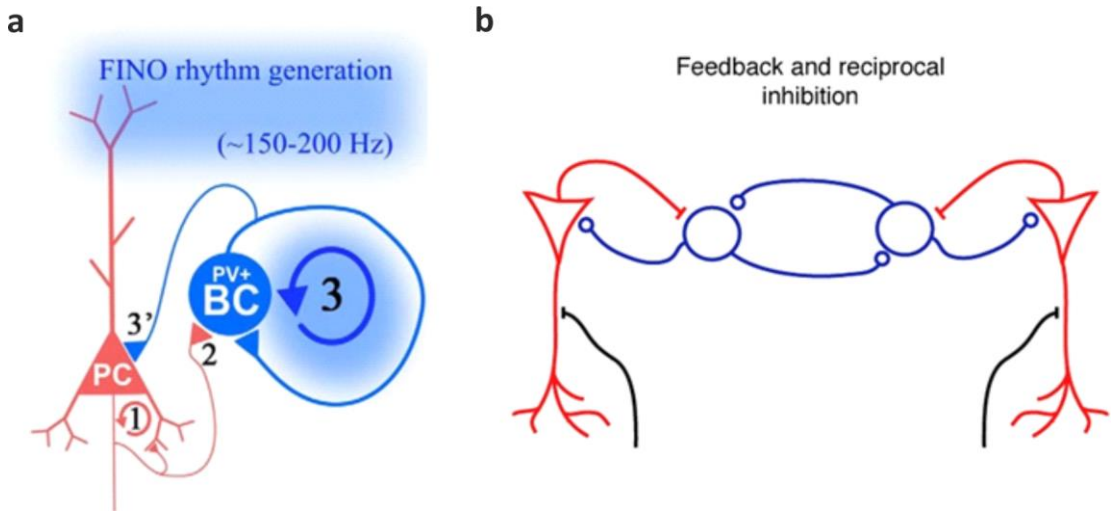

Fig. 1.5: FINO and P-IN-IN models of ripple generation in the CA3 and CA1 subregions of the hippocampus*. Feedback inhibition onto the pyramidal neurons and reciprocal inhibition between the interneurons pace the firing rate of pyramidal cells and set the rhythm of ripples. Of note, the PC-IN interaction is not cycle-by-cycle but is mediated by the reciprocal inhibition of IN. It is suggested that PV+ BC is a crucial IN type for the ripple rhythm. PV+ BC: parvalbumin-positive basket cell, PC: pyramidal cell (**(a)** Reproduced from Schlingloff et al., [2014] with permission from the Society for Neuroscience; **(b)** Reproduced from Stark et al., [2014] with permission from Elsevier).*

Studying the SW-R in vitro

Previous studies, such as (Colgin et al., 2004; Kubota et al., 2003; Maier et al., 2003; Papatheodoropoulos & Kostopoulos, 2002a; Wu et al., 2002), have shown that SW-R occur in the isolated hippocampus (e.g., slice preparations), when the connecting fibers from subcortical or cortical regions have been sectioned. This suggests that SW-R could be an intra-hippocampal phenomenon, probably when the cholinergic drive, which gives rise to gamma/theta oscillations in the same structure, is suppressed (Buzsáki, 2015). The SW-R observed *in vitro* share similar properties with those *in vivo*, even though differences in the artificial cerebrospinal fluid (aCSF), the slice preparation and the incubation protocols might slightly change the exact characteristics of the *in vitro* SW-R (Hájos & Mody, 2009; Maier et al., 2012; Papatheodoropoulos, 2007; Wu et al., 2005). Additionally, ex vivo SW-R carry information relevant to previous experience (Mizunuma et al., 2014). This study shows that the CA1 pyramidal cells, active during novel spatial exploration, participate in the SW-R in slice preparations. On the other hand, SW-R properties show slight differences, such as in the frequency when recorded *in vivo* (140-160 Hz) (Ponomarenko et al., 2008; Sullivan et al., 2011) and *in vitro* (>180 Hz) (Maier et al., 2011). Furthermore, the ripples recorded in the CA1 region *in vitro* are coherent with the CA3 ripples, which is not observed in the *in vivo* recordings (Behrens et al., 2005, 2007; Both et al., 2008). In

total, despite minor differences to *in vivo* SW-R, slice preparations have been consistently used as a model to study the network and cellular correlates of SW-R.

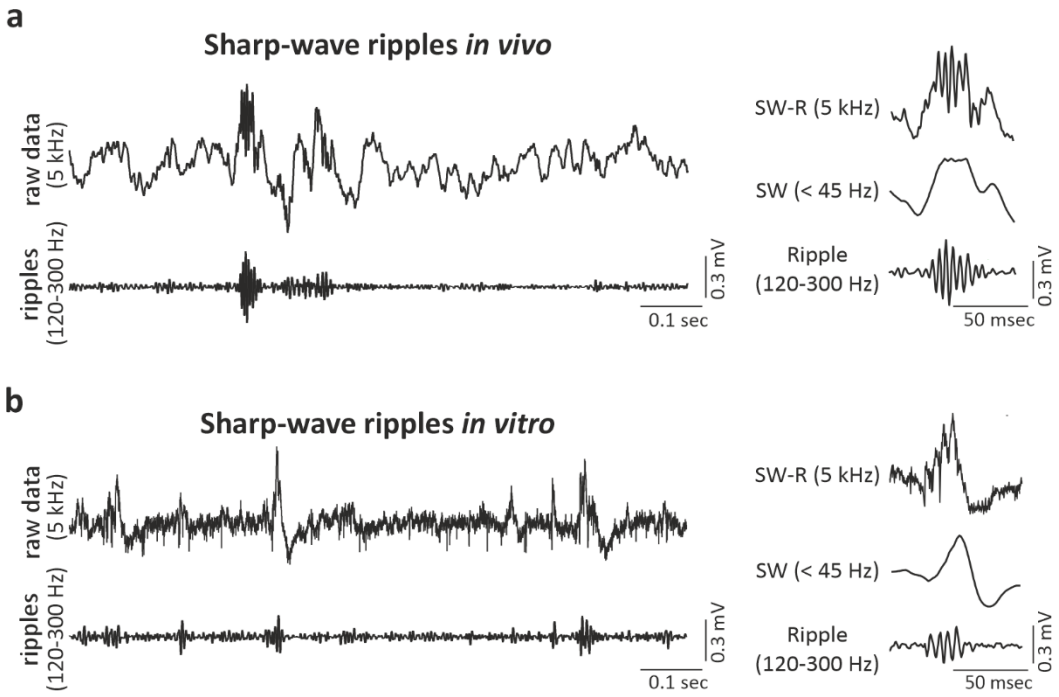

Fig. 1.6: Similarities between in vivo and in vitro sharp wave-ripples. (a) *SW-R recorded from str. pyramidale of the CA1 subregion of rodent hippocampus during slow-wave sleep with the raw trace and the ban-pass filtered (120-300 Hz) ripple. On the right, single traces of sampling rate 5 kHz are low-pass filtered (<45 Hz), illustrating the sharp wave component, and band-pass filtered (120-300 Hz), illustrating the ripple component.* ***(b)*** *SW-R from slices containing the vHP with the raw trace and the filtered ripple (band-pass 120-300 Hz) recording. Note the higher LIA in vivo as well as the striking similarity of the single traces. (****(a)*** *Unpublished data from Dr. Caliskan, Otto-von-Guericke-Universität, Magdeburg).*

1.3.1.3 Memory processes related to SW-R

Previous studies have demonstrated the role of SW-R in cognition, such as spatial navigation, and have suggested their involvement in the planning of future actions, imagination, and memory processes, in particular consolidation and retrieval (Buzsáki, 2015; Jai & Frank, 2015; Joo & Frank, 2018; O'Neill et al., 2006; Pfeiffer & Foster, 2013). According to the two-stage model of memory consolidation (Buzsáki, 1989; Marr, 1971), the transfer of liable memories from the hippocampus to the neocortex for long-term storage happens during SW-R. This is supported by the replay phenomenon, when previous experience is re-activated in a time-compressed manner during SW-R (Carr et al., 2011; Foster, 2017; O'Neill et al., 2010). During the replay, place cells are re-activated in the same or reverse order, but shortened during SW-R before or after an animal

crosses an environment. Preplay is also observed during SW-R when place cells fire even before an animal transverses a novel environment and is connected with a role of SW-R in planning (Diba & Buzsáki, 2007; Dragoi & Tonegawa, 2011).

Additional evidence of SW-R being involved in learning is that their incidence increases in novel environments, after learning, and after reward (Girardeau et al., 2014; Joo & Frank, 2018). Studies that interfere with SW-R and reduce or increase their incidence substantially affect memory consolidation. For example, disrupting the SW-R development with electrical manipulation in the hippocampus during rest (sleep or awake), after a spatial memory task, results in learning deficits (Ego-Stengel & Wilson, 2010; Girardeau et al., 2009; Jadhav et al., 2012). Additionally, transgenic mice with decreased CA3 activity (and thus CA1 SW-R impairments) after FC show contextual fear memory consolidation deficits (Nakashiba et al., 2009). On the other hand, facilitating the coupling of hippocampal SW-R and cortical oscillatory activity enhances spatial memory consolidation (Maingret et al., 2016).

1.3.2. Gamma rhythm

1.3.2.1 Basic features of gamma rhythm and generation mechanisms

Gamma rhythm represents a fast oscillatory activity in the range of 30-140 Hz, which can be further divided into slow (30-50 Hz), mid (50-90 Hz), and fast (90-140 Hz) gamma (Buzsáki & Wang, 2012). Gamma oscillations are superimposed on the slower theta oscillation (4-12 Hz) and are modulated in power and frequency (Bragin et al., 1995). They appear during exploration, navigation, or other motivation-related movements and are critical for encoding sensory information (Gray, 1994; Singer, 1993) and maintaining working memory (Fell et al., 2001) and attention (Fries et al., 2001). Additionally, they occur during REM sleep, when information storage and recall are thought to occur (Bartos et al., 2007). Gamma rhythm is generated in brain areas with recurrent excitatory collateral activity, such as the hippocampus, the neocortex, and the amygdala (Bragin et al., 1995; Collins et al., 2001; Hájos & Paulsen, 2009a; König et al., 1995), the striatum, the olfactory bulb and the thalamus (Adrian, 1942; Berke et al., 2004; Buzsáki & Wang, 2012; Pinault & Deschenes, 1992).

In the hippocampus, CA3 and CA1 regions show synchronicity in the slower gamma range (30-80 Hz), whereas the CA1 region and mEC synchronize in the faster gamma range (60-120 Hz) (Colgin et al., 2009). Therefore, it is suggested that a slower gamma rhythm originates from the CA3 region, which reaches the CA1 area through the SC. Furthermore, the faster gamma rhythm is supported to arise in the mEC and through the direct perforant path reaches the s.l-m. of the CA1 region (Colgin et al., 2009). However, it has been shown that local CA1 faster gamma (100 Hz) can be generated in CA1 s.p. independently of the mEC input (Schomburg et al., 2014).

In vitro, gamma rhythm can be induced by several methods, such as increasing the tonic excitation, the cholinergic tonus, or the glutamatergic tonus. Such examples include the application of the muscarinic cholinergic receptor (M) agonist carbachol (CCh) (Fisahn et al., 1998), the ionotropic glutamatergic receptor agonist kainate (KA) (Traub et al., 2003), and the group I metabotropic glutamate receptor (mGluR) agonist (RS)-3,5-dihydroxyphenylglycine (DHPG) (Pálhalmi et al., 2004). Except for the pharmacological methods, electrical (Whittington et al., 1995; Wójtowicz et al., 2009) or optogenetic stimulation can also induce gamma *in vitro* (Butler et al., 2016). In hippocampal slices, subiculum, CA1, CA3 and mEC are proposed to be gamma generators (Butler & Paulsen, 2015; Jackson et al., 2011; Pietersen et al., 2014).

To explain the generation of gamma rhythm, mechanisms of interactions among interneurons, or among interneurons and pyramidal cells, or sparse and persistent gamma have been suggested (ter Wal & Tiesinga, 2013). According to the Interneuron Network Gamma model (IN-G) (Wang & Buzsáki, 1996; Whittington et al., 1995, 2000), interneurons are initially activated by an excitatory afferent. Then, due to their mutual connections, they tune each other's firing and inhibit the pyramidal cells they are connected to, enabling one gamma cycle, which repeats the same way. Notably, the pyramidal cells' firing is not involved in a feedback loop with the interneurons, but they excite other pyramidal cells that boost the magnitude of the oscillation. Therefore, interneurons pace the gamma cycle, characterized by their fast kinetics resulting in a fast oscillation (Buzsáki & Wang, 2012).

On the other hand, the Pyramidal-Interneuron Network Gamma (P-IN-G) model (Traub et al., 1999; Whittington et al., 2000) suggests that initially, pyramidal cells receive sufficient excitatory input that leads to firing. Then, interneurons, which receive heavily convergent pyramidal cell input (Whittington et al., 2011), will be depolarized and subsequently inhibit the firing of the

connected pyramidal cells. Thus, only when the inhibition has ceased are the pyramidal cells able to initiate another cycle. Therefore, in the P-IN-G model, the firing of pyramidal cells is tuned by feedback inhibition, while pyramidal cells and interneurons interact in each cycle reciprocally. Of note, in this model, pyramidal cells have a high likelihood to fire (ter Wal & Tiesinga, 2013).

Interneuron-types suggested to mediate the gamma rhythm generation are perisomatic-innervating fast-spiking interneurons, such as the PV^+ BC. PV^+ BC fire in synchrony with the LFP gamma rhythm, and their synaptic inputs on the connected pyramidal cells are phase-locked in gamma. The contribution of other interneuron classes is also studied, such as O-LM and bistratified IN (Tukker et al., 2007). Nevertheless, a critical role is less clearly supported (Buzsáki & Wang, 2012).

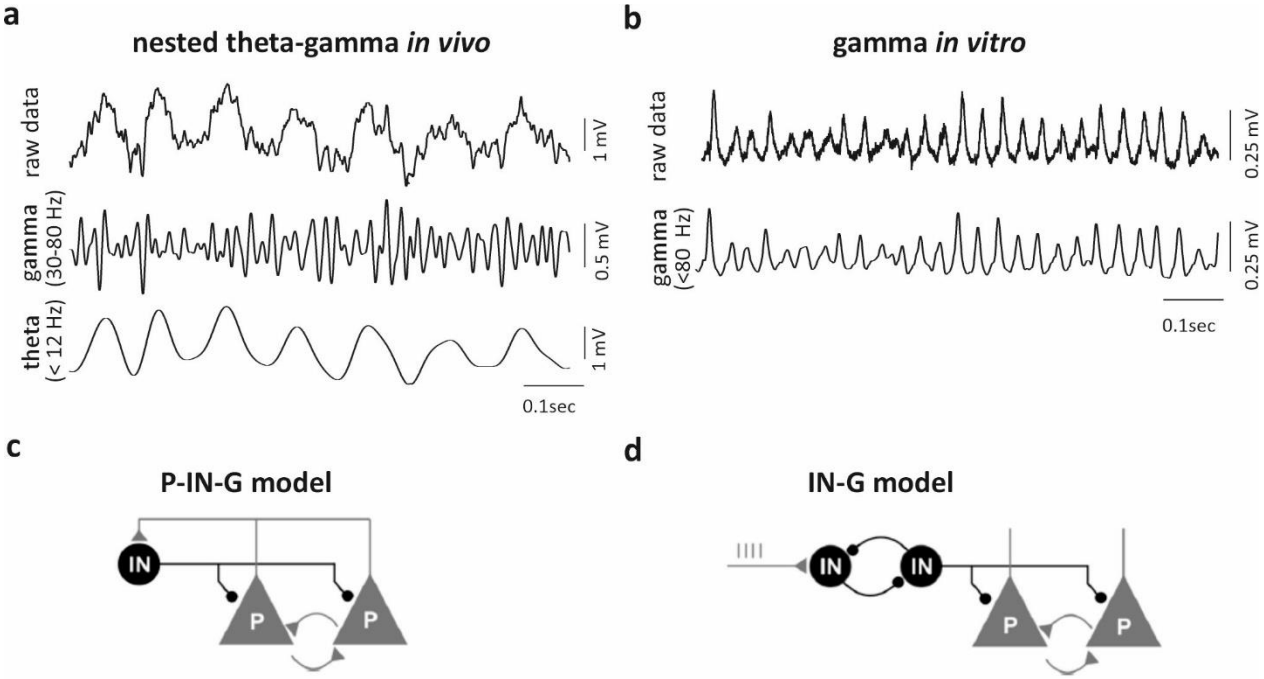

Fig. 1.7: Similarities of in vivo and in vitro gamma oscillations and models of rhythm generation. ***(a)*** *In vivo traces that show on top unfiltered data then band-pass filtered (30-100 Hz) gamma rhythm and low pass filtered (12 Hz). Note the gamma oscillations on top of the theta rhythm in the unfiltered trace.* ***(b)*** *Pharmacologically-induced gamma rhythm recorded from the vHP in vitro occurs independently of the theta. Note the striking similarity of the band-pass filtered gamma between the in vivo and in vitro recordings.* ***(c)*** *According to the P-IN-G model for gamma rhythm generation, pyramidal cells (P) and local perisomatic interneurons (IN) interact cycle-by-cycle with feedback inhibition. On the other side,* ***(d)*** *based on the interneuron network gamma (IN-G) generation model, reciprocal inhibition of local IN sets the firing of P after their activation by excitatory afferents (****(a)*** *unpublished data from Dr. Çalışkan, Otto-von-Guericke-Universität, Magdeburg* ***(c*** *&* ***d)*** *modified from Çalışkan & Stork, [2018] with permission from Springer Nature)*

1.3.2.2 Memory and emotional processing connected with gamma rhythm

Previous studies have indicated the involvement of gamma rhythm in memory encoding and retrieval (Colgin & Moser, 2010; Hasselmo et al., 1996; Montgomery & Buzsáki, 2007). Research studies with humans and primates have shown that increased gamma power in the hippocampus during encoding of words or stimuli results in better recall rates (Sederberg et al., 2007; Sederberg et al., 2007b). Similarly, the synchronization of gamma between regions, such as the entorhinal cortex and the hippocampus, during the encoding is critical for a successful recall (Fell et al., 2001). Further studies have shown increased gamma power or gamma CA3-CA1 coherence in rats during successful retrieval of a piece of memory needed to make a decision (Johnson & Redish, 2007; Montgomery & Buzsáki, 2007). It is suggested that the slow gamma band supports memory retrieval, while the fast gamma band supports memory encoding (Colgin et al., 2009; Colgin & Moser, 2010).

Additionally, it is supported that the emotional component of memories is connected with the gamma activity (Headley & Paré, 2013). Previous electro- or magnetic encephalogram (EEG or MEG) studies from participants, that were shown pictures with human faces, demonstrated enhanced gamma in the amygdala and cortex particularly when a face had a fearful but not a neutral expression (Keil et al., 2001; Luo et al., 2007, 2009; Senkowski et al., 2011). Gamma oscillations exhibit alterations in their synchronicity & theta modulation in affective disorders. Previous studies with human participants have shown that gamma rhythm synchronicity increases in the hippocampus during anxiogenic tasks (Khemka et al., 2017). *In vitro* studies have demonstrated that endocrine stress response factors, such as corticosterone and corticotropin-releasing factor (CRF), increase the gamma power in the vHP (Çalışkan et al., 2015b). On the other hand, animal studies have shown decreased anxiety accompanied by *ex vivo* decreased power of pharmacologically KA-induced gamma in the vHP (Albrecht et al., 2013). Therefore, gamma synchronicity and power in different brain regions and study models are associated with emotional processing.

1.4 Animal models

1.4.1 The GAD65 knock-out (KO) mouse

1.4.1.1 GABA synthesis

Gamma-aminobutyric acid (GABA) is the main inhibitory neurotransmitter in the mammalian central nervous system. It has a crucial role in generating distinct network oscillations and is implicated in many neuropsychiatric disorders (Benes & Berretta, 2001). GABA is synthesized from glutamate by two glutamic acid decarboxylase isoforms, GAD67 and GAD65. GAD67 isoform is crucial during development, acts as a trophic factor, is located in the cytosol, and synthesizes 90% of GABA. In contrast, GAD65 synthesizes 10% of basal levels of GABA, is situated in axon terminals, and is found at high levels in an apo-enzyme form. It is involved in the fine-tuning of GABAergic transmission, used as a buffer to increase inhibition in highly activating situations. Thus, GAD65 is responsible for on-demand GABA production, vesicular GABA release, and activity-dependent phasic inhibition (Soghomonian & Martin, 1998).

Interfering with GAD67 in early stages, such as knocking out the GAD1 gene, results in meager survival of the GAD67 KO mice due to serious cleft palate, which indicates the importance of GAD67 during development (Asada et al., 1997). However, GAD65 KO mice survive and display a postnatal deficit in GABA synthesis and susceptibility to stress. Early studies showed that GAD65 KO mice do not exhibit changes in GABA levels in the hippocampus, cerebellum, cortex (Asada et al., 1996; Kash et al., 1997), but the cofactor pyridoxal 5 phosphate-inducible apo-enzyme reservoir is significantly decreased. However, other studies showed that GAD65 KO mice exhibit GABA levels alterations (Stork et al., 2000) since there is no GABA increase in the first two months after birth, as it occurs in the amygdala, the hypothalamus, and the parietal cortex of GAD65 +/+ mice. Additionally, there is a 50% reduced expression of GABA-positive cells and a 50% decrease of the neuropeptide Y (NPY) in the hippocampi of GAD65 KO mice (Qi et al., 2018). Nevertheless, GABA-A receptors remain unaffected, without changes in their density or affinity (Kash et al., 1999).

1.4.1.2 Behavioral profile

GAD65 KO mice exhibit frequent seizures and emotional processing deficits. In particular, they show increased anxiety, assessed in the open field and the elevated zero maze tests (Kash et al., 1999). In line, they exhibit increased anxiety in a light/dark avoidance test and altered responsiveness to the anxiolytic drugs diazepam and pentobarbital (Kash et al., 1999; Stork et al., 2000). They show reduced inter-male aggression and reduced immobility in the forced-swim test (Stork et al., 2000). Fear memory formation is also affected, with overgeneralization of cued long-term fear memory and reduction in theta amygdala-hippocampal (LA-CA1) synchronization (Bergado-Acosta et al., 2008). Likewise, fear extinction is impaired after cued FC but connected with increased LA-CA1 theta frequency synchronization (Sangha et al., 2009).

Furthermore, circadian rhythm affects conditioned fear in GAD65 KO mice. Specifically, reduction in freezing and increased hyperactivity were observed in GAD65 KO mice, when FC training and retrieval were tested at the beginning of the active phase. At the same time, hippocampal subregions, the amygdala, and the medial hypothalamus showed increased activity, assessed by c-Fos expression (Bergado-Acosta et al., 2014).

Last, GAD65 KO mice show spontaneous seizures (Stork et al., 2000) after fear or mild stress and seizure susceptibility after picrotoxin (Asada et al., 1996). During epileptic attacks, areas active in GAD65 KO mice involve the DG, the CA3 region, the amygdala, and the EC (Kash et al., 1997). In addition to the emotional deficits, GAD65 KO mice show cognitive deficits, such as impaired spatial learning acquisition (Qi et al., 2018).

Taken together, increased anxiety, altered responsiveness to anxiolytics, hyperarousal, fear generalization, extinction deficits, and hyperactivity of the amygdala, observed in the GAD65 KO mice, recapitulate traits of PTSD and fulfill face and predictive validity criteria to be used to study this disorder (Kumar et al., 2013).

1.4.2 The Fmr1 knock-out mouse: an animal model of Fragile X Syndrome

Fragile X Syndrome (FXS) is a neurodevelopmental disorder and the most common inherited form of intellectual impairment and autism, with a prevalence of 1:7.000 males and 1:11.000 females (Hunter et al., 2014). From early on, the affected individuals exhibit neurological symptoms, such as hypotonia, which later develop into motor and cognitive delays. Except for the characteristic

physical features, they demonstrate social anxiety, sensory hypersensitivity, seizures, and impulsivity. FXS is caused by mutations in the promoter region of the Fragile X mental retardation (Fmr1) gene, which is located in the X chromosome. Multiplications of the CGG triplet more than 200 times lead to the complete absence of the Fragile X mental retardation protein (FMRP) (Hagerman et al., 2017). FMRP is implicated in the translational regulation of proteins located in the postsynaptic compartment of neurons, including activation proteins of metabotropic glutamate receptors (mGluR) and potassium channels (Bear et al., 2004; Brown et al., 2010; Deng et al., 2013; Richter et al., 2015). Therefore, its absence results in disturbances in axonal development, synapse formation, plasticity, and excitation-inhibition balance (Bassell & Warren, 2008; Hagerman et al., 2017).

A very commonly used animal model to study the pathogenesis of the FXS is the Fmr1 knock-out (KO) mouse. Fmr1 KO mice lack the FMRP and display a similar phenotype to FXS patients, such as hyperactivity, cognitive impairments, seizures, and sensitivity to auditory stimuli (Bakker et al., 1994; Kooy, 2003). An anxiety phenotype is also reported in many studies, even though there is no consensus, due to difficulties in the behavioral interpretations (Santos et al., 2014). Similarly, deficits in the hippocampus-dependent learning have been observed, with Fmr1 KO mice exhibiting less freezing in both cued and contextual FC (Guo et al., 2011).

Additionally, the Fmr1 KO mice display a range of electrophysiological alterations. Firstly, they exhibit gamma range oscillopathy in the cortex (Lovelace et al., 2020) and the hippocampus. In particular, freely behaving Fmr1 KO mice show increased hippocampal gamma coherence and interneuronal hypersynchronization, implying local network impairments (Arbab et al., 2018). Furthermore, in the CA1 region, altered theta-gamma coupling (Radwan et al., 2016) and hyperactive pyramidal cells in awake and sleep are observed, possibly due to increased gamma power (Boone et al., 2018). Similar findings are observed in the FXS patients, including increased gamma power and reduced gamma synchrony after auditory stimuli, correlated with social and sensory deficits (Wang et al., 2017). Last, changes in synaptic plasticity are reported, including an LTD increase in the SC-CA1 synapse (Huber et al., 2002) and an LTP decrease in the cortex (Koga et al., 2015).

Among the molecular changes that result from the FMRP loss, there are reported alterations in receptors that trigger distinct signaling pathways. For example, the mGluR group 1 ($mGluR_{1/5}$)

pathway is hyperactive, leading to enhanced protein synthesis and LTD (Bear et al., 2004; Huber et al., 2002). The muscarinic receptors type 4 (M4) and type 1 (M1) are increased in the hippocampus (Thomson et al., 2017). Furthermore, the cortical kainic ionotropic glutamate receptors (KA) show aberrant function, with reduced synaptic levels but an overall unchanged expression (Qiu et al., 2018). GABA signaling is affected, including deficiencies in the GABA-A and GABA-B receptor subunits or changes in the equilibrium of the glutamatergic neurotransmission, which leads to excitation-inhibition disbalance (Kang et al., 2017; Martin et al., 2014; Paluszkiewicz et al., 2011).

Interestingly, manipulating these signaling pathways alters the electrophysiological and behavioral impairments observed in the Fmr1 KO mice. For instance, a genetic decrease of mGluR5 expression reverses epilepsy, sensory hypersensitivity, learning, and plasticity deficits (Dölen et al., 2007). In line, pharmacological blockage of M1 reduces seizures and repetitive anxiety-related behaviors (Veeraragavan et al., 2011). On the other hand, even though M1 and M4 are excessively expressed, their upregulation or enhanced translation reverses observed symptomatology, such as the increased LTD, the seizures, and the general unregulated protein synthesis (Thomson et al., 2017). Additionally, the behavioral deficits in anxiety and exploration of the Fmr1 KO mice are improved after knocking-in in the human FMRP, even though with new phenotypic alterations (Peier et al., 2000).

1.5 Aims

The thesis contains four main studies.

STUDY 1 presents an electrophysiological characterization of GAD65 KO mice. GAD65 KO mice exhibit reduced GABA synthesis, emotional memory deficits, and increased anxiety (Asada et al., 1996; Bergado-Acosta et al., 2008; Kash et al., 1999; Stork et al., 2000), resembling traits of PTSD and supporting existing literature about the implication of GABArgic system in PTSD and anxiety (Colic et al., 2018; Feusner et al., 2001; Vaiva et al., 2004, 2006). Amygdala is a central component in the pathophysiology of the GAD65 KO mice (Müller et al., 2015), but the contribution of the ventral hippocampus (vHP), a structure with a differential role in anxiety and emotional memories (Ciocchi et al., 2015; Kjelstrup et al., 2002), is still not completely understood. Interestingly, the vHP exhibits robust oscillatory activity implicated in memory formation and anxiety (Girardeau et

al., 2014; Joo & Frank, 2018; Khemka et al., 2017), which critically depends on the interaction of pyramidal cells and interneurons. Therefore, I hypothesized that GAD65-dependent excitation/inhibition imbalance would lead to electrophysiological alterations that could subsequently underlie the anxiety phenotype and the emotional memory processing deficits of the animal model. To this extent, *in vitro* spontaneous SW-R and CCh-induced gamma oscillations were described in the vHP of GAD65 KO mice.

STUDY 2 follows up on findings from STUDY 1 that indicated an inconclusive excitability status in the CA1 region of the vHP, with enhanced ripples but decreased SW incidence. Previous studies (Behrens et al., 2005; Suh et al., 2013; Zeng et al., 2001) have demonstrated that plasticity and excitability in the hippocampus were associated with changes in SW incidence. Thus, I hypothesized that the reduced CA1 SW incidence, observed in the GAD65 KO mice, could result from a decrease in the baseline synaptic excitability or plasticity in the CA1 region. To this extent, the SC-CA1 synapse, the main input to the CA1 region, was examined. Additionally, to identify whether the excitation/inhibition balance in the CA1 region was associated with alterations at the cellular level, the intrinsic and synaptic properties of the CA1 pyramidal cells were assessed. Last, I asked whether the electrophysiological findings of the global GAD65 KO mouse model were primarily connected with the GABA deficiency in the vHP or occurred after a developmental reconfiguration of the hippocampal circuit. To clarify this question, GAD65 expression was locally reduced in the vHP, as previously described (Tripathi et al., 2021), and the network oscillations in the CA1 and CA3 areas were described.

STUDY 3 describes behavioral correlates of ventral hippocampal SW-R connected with fear memory and its persistence. SW-R occur during quiet immobility and slow-wave sleep, with an important role in memory processes, particularly memory consolidation and retrieval (Buzsáki, 2015; Jai & Frank, 2015; Joo & Frank, 2018; O'Neill et al., 2006; Pfeiffer & Foster, 2013). Interrupting the SW-R during these processes results in memory formation deficits (Ego-Stengel & Wilson, 2010; Girardeau et al., 2009; Jadhav et al., 2012). However, it is not clear whether SW-R carry information regarding the content of these experiences. To approach this question, I investigated the development of fear memories in wild-type C57BL/6 mice that underwent a hippocampus-dependent memory task, a contextual fear conditioning paradigm. To determine whether SW-R convey information regarding the contextual adversity, the paradigm involved

increasing shock intensity levels. Additionally, to understand whether the (re)consolidation of a recent fear memory would be differentially represented from the (re)consolidation of its extinction, I assessed the SW-R at two different time points, after the training session and at the end of the extinction phase.

STUDY 4 focuses on the Fmr1 KO mouse, an animal model of FXS. Fmr1 KO mice exhibit a similar phenotype to human patients, including cognitive impairments and anxiety (Bakker et al., 1994; Kooy, 2003; Santos et al., 2014). Electrophysiological alterations, such as gamma range oscillopathy, have been observed in both patients and animals (Arbab et al., 2018; Lovelace et al., 2020; Radwan et al., 2016; Wang et al., 2017). Additionally, molecular changes, in particular, overexpression of M1 and M4 muscarinic cholinergic receptors (Thomson et al., 2017), hyperactive glutamatergic signaling, mediated by $mGluR_{1/5}$ and KA receptors (Bear et al., 2004; Huber et al., 2002; Qiu et al., 2018), compromised GABAergic signaling, and GAD65/67 decrease (Kang et al., 2017; Martin et al., 2014; Nomura, 2021; Paluszkiewicz et al., 2011) have been implicated in the pathogenesis of the model. However, a direct link between these pathways and the electrophysiological alterations is not clearly defined. Interestingly, agonists of cholinergic and glutamatergic receptors can induce inhibition-dependent gamma oscillations *in vitro* (Fisahn et al., 1998; Traub et al., 2003; Pálhalmi et al., 2004). Therefore, using the *in vitro* approach, I hypothesized that over-excitation of these signaling pathways would reveal electrophysiological alterations. To this extent, three types of pharmacologically-induced gamma oscillations (KA, CCh, DHPG) were characterized in the vHP.

CHAPTER 2. METHODS

2.1 Hippocampal network oscillations in GAD65 KO mice - STUDY 1

2.1.1 Animals

Animals were bred in our animal facility at the Institute of Biology, Otto-von-Guericke University Magdeburg, and standard pellet food and water ab libitum. Room temperature was stable at about 21 °C, humidity at 50 - 60% with inverted light/dark cycle with 12h dark phase (7.00 am - 7.00 pm) and 12 h light phase (07.00 pm - 07.00 am). In the summertime zone, the cycle was shifted by 1 hour. In the transition between the two phases, there was a 30 min dim light phase. Weaning was done in P28. Male and female mice were kept separately, in groups of 2-6 littermates, in long type 2 cages (Techniplast GmbH and Bioscape GmbH, Germany) with standard bedding material. Experiments were carried out when animals were between 2-5 months. For unbiased observations, the animals were selected blindly. All behavioral experiments were performed during the daytime, between 09.00 am - 01.00 pm. The state's authorities for animal experimentation approved animal housing and all experiments (Landesverwaltungsamt Sachsen Anhalt: Permission No. 42502-2-1177/ - 1516 - UniMD).

Male GAD65 constitutive knock-out (KO) mice and wild-type (WT) littermates were used for *in vitro* or *ex vivo* electrophysiology, a contextual fear conditioning task, and subsequent immunohistochemistry. GAD65 KO mice were developed by (Asada et al., 1996) and then kept breeding in our animal facility using heterozygous pairs after crossing KO mice with C57BL/6. Genotyping was performed in our facility using the PCR method (detailed information in Appendix A.6).

2.1.2 Behavior- contextual fear conditioning paradigm

For the investigation of contextual fear memory, mice were placed in a fear conditioning (FC) apparatus (TSE, Bad Homburg, Germany). The apparatus contained a soundproof chamber with a metallic grid floor that delivered the electrical stimuli. The mouse behavior was monitored, and the freezing behavior was captured by a photo beam device (TSE, Bad Homburg, Germany). The protocol was adapted from (Çalışkan et al., 2016). Nineteen male animals, 10 GAD65 KO and 9 WT, aged 2-5 months old, underwent a contextual FC paradigm that contained five extinction (E) and one spontaneous recovery (SR) sessions. Each session occurred one day after the previous session, except the SR that occurred two weeks later. In detail, mice were single caged 2 days before the start of the experiment. Then, two habituation sessions of 6 min were followed by a training session of 6 min, where mice received grid electric shock with three shocks (0.4 mA, 1 s; ISI 20 s). The training session included 2 min free exploration, three one-second-shocks with 20 sec intershock interval, and 2 min again of free exploration. Then, in the same training context, five extinction sessions of 10 min duration occurred, followed by the two-minute SR session. Ninety minutes after the end of the behavioral paradigm, the animals were either perfused and their brains were processed for c-Fos immunostaining or prepared for acute slice electrophysiology (Fig. 2.1). The FC apparatus were cleaned with 70% ethanol before each session.

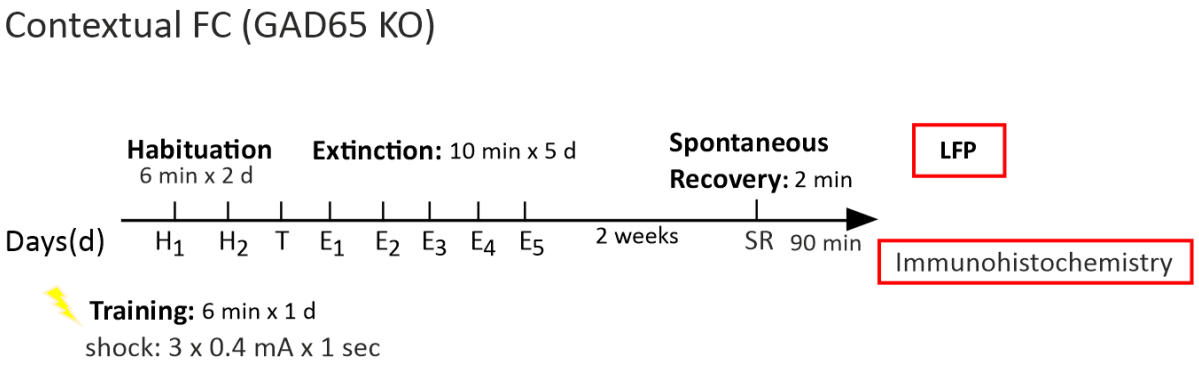

Fig. 2.1: Contextual fear conditioning protocol for GAD65 KO mice. *The mice underwent two habituation sessions before the training in the same context. During the training session, they received mild shock three times, followed by five extinction sessions of 10 min per day. Two weeks later, the mice were placed again in the training context for 2 min to assess a potential spontaneous recovery of the fear memory, after it has been extinguished. After a waiting time of 90 min, the mice were either perfused for c-Fos immunohistochemistry or prepared for acute slice LFP electrophysiology. H: habituation; T: training; E: extinction; SR: spontaneous recovery; LFP: local field potential.*

2.1.3 Slice electrophysiology

2.1.3.1 Acute slice preparation

Mice under isoflurane anesthesia were decapitated, their brains were quickly removed and placed in ice-cold (-4 °C) artificial cerebrospinal fluid (aCSF) solution. The aCSF composed of (mM): NaCl, 129; NaH_2PO_4, 1.25; glucose, 10; $MgCl_2$, 1; $CaCl_2$, 2; KCl, 3; $NaHCO_3$, 21; diluted in double distilled (Millipore) water with an osmolarity of ~300 mOsm and saturated with 95% O_2 / 5% CO_2 for at least 30 min and obtained pH≈7.4. Using a manual vibratome (Campden Instruments or Model 1000, The Vibratome Company, St. Louis, USA), horizontal slices of 400 µm thickness were obtained containing the ventral to intermediate hippocampus. The cut had an angle of ~12° in the anterior-posterior direction to preserve the connections between the hippocampus and the entorhinal cortex (Boulton et al., 1992) and between the CA3 and CA1 subregions (Mizunuma et al., 2014). The slices were immediately transferred to an interface chamber perfused with carbogenated aCSF solution at a rate of ~2 ml/min and recovered for at least 1.5 h at 32 °C.

2.1.3.2 Extracellular local field potential recordings

Local field potential (LFP) recordings were performed in an interface chamber at 32 °C ± 1 °C or 36 °C ± 1 °C for SW-R and gamma oscillations, respectively. With the guidance of a stereomicroscope (Stemi 2000, Zeiss), borosilicate glass electrodes with ~1 MΩ resistance, when filled with aCSF, were inserted ~80 µm deep into the s.p. of areas CA3 and CA1 of the hippocampus. SW-R occurred spontaneously (Çalışkan et al., 2016; Maier et al., 2003), whereas gamma oscillations were pharmacologically induced by adding 5 µM Carbachol for at least 45 min (Fisahn et al., 1998) and by increasing the temperature of the aCSF solution and the incubation chamber to 36 °C (Fig. 2.2).

The LFP signals were amplified and low-pass filtered at 3 kHz using either a custom-made extracellular amplifier or a commercial device (EXT-02F - Extracellular Amplifier; npi Electronic GmbH, Tamm, Germany). The data were sampled at 5 kHz rate using a digitizer unit (CED-Micro1401; Cambridge Electronic Design, Cambridge, UK) and the corresponding software (Spike2.8; Cambridge Electronic Design) and were stored on a hard disc for offline analysis.

2.1.4 Immunohistochemistry

To quantify the activated cells during the last session of the behavior paradigm, immunohistochemistry for the immediate early gene c-Fos was performed. Ninety minutes after the behavior paradigm, mice were anesthetized via intraperitoneal (i.p.) injections of ketamine (80 mg/ml)/ xyzaline (6 mg/ml) mixture (approx. 1 mg/kg mouse body weight; Sigma-Aldrich, Seelze, Germany). Then, they were transcardially perfused with 50 ml phosphate buffer (PBS) pH=7.4, followed by 100 ml 4% paraformaldehyde (PFA) in PBS. The brains were removed, placed in 4% PFA, and stayed overnight in 4 °C. The following day, the brains were submerged in a sucrose-based cryoprotection solution (30% PBS) for two days. Then, the brains were snap-frozen using dry ice and stored in a -20 °C freezer. Horizontal sections of 30 µm thickness were obtained with a cryostat (Leica CM 1950, Leica Microsystems) at -18 °C and stored in wells with sodium azide (0.02% in PBS) solution.

Sections floating in the solution were washed three times with PBS, and 10% normal donkey serum in 1x PBS with 0.5% Triton X (400 µl per well) was applied to block unrelated sites. The primary antibody anti-cFos (Cell Signaling #2250, Frankfurt am Main, Germany) was applied at dilution 1:1000 and incubated overnight at 4 °C. Besides, some sections were used as negative control and received no primary antibody solution. The next day, sections were washed out three times with PBS. Then, the secondary antibody, biotinylated rabbit anti-goat (1:200 in PB-Triton X (0.2%); Vector Laboratories, USA), conjugated with streptavidin Cy2 (dilution at 1:1000 in PB; Jackson ImmunoResearch Labs, UK) was applied for 1 h. Sections were washed out three times with PBS, and DAPI (1:100 in PB) was applied for ~30 sec to stain the cell nuclei. One more PBS wash-out followed, and finally, slices were mounted on glass slides and fixed with coverslips using Immu-Mount™. Dried slides were observed under an epifluorescent microscope (Leica Microsystems, Germany), and images were stored using the LAS AF software (Leica). c-Fos$^+$ cells were manually counted in the different strata of CA3 and CA1 regions of the ventral hippocampus using the ImageJ software (National Institutes of Health).

2.1.5 Drug application

For induction of gamma oscillations, the cholinergic agonist carbachol (CCh [5 µM]; TOCRIS, Bristol, UK) was applied. CCh had been previously aliquoted with double distilled water in higher concentration stocks and stored in a -20 °C freezer. Shortly before the experiment, stock solutions

were thawed and diluted in their final concentration in the aCSF solution and perfused with a flow rate of ~2 ml/min.

2.1.6 Data analysis

2.1.6.1 Sharp wave-ripple

Two minutes of artifact-free LFP signal was analyzed offline using custom-made MATLAB scripts (MathWorks, Natick, MA, USA; main scripts written by Dr. Anton Rösler & Dr. Jan-Oliver Hollnagel). To describe the SW-R, the following parameters were used: the sharp wave (SW) incidence, the SW area under the curve (AUC), the ripple frequency, and the ripple amplitude. The SW, slow component of the SW-R event, was isolated using low–pass filter at 45 Hz (FFT filter, cut frequency: 45 Hz). Two inclusion criteria were considered for the analysis: SW events higher than 3 times the standard deviation (SD) of the filtered signal and with a minimum interevent interval of 100 ms. The SW incidence was measured as the counts of detected events per second. The SW AUC was calculated using trapezoidal numerical integration of the signal above the mean of the data. Then, to define the ripples, the fast component of the SW-R, each SW event was identified, and the signal of 125 ms with center at the SW peak was band-pass filtered at 120-300 Hz (FFT filter). The ripple amplitude was calculated using triple-point-minimax-determination from a signal of 15 ms before and 10 ms after the peak of the SW event. The ripple frequency was calculated within each SW-R event using the time between the troughs of successive ripples. The data were considered only when the ripple amplitudes were higher than 3 times the SD of the filtered signal (120-300 Hz) and when the difference between the falling and rising component of a ripple was lower than 75%.

To describe the signal-to-noise ratio (signal/noise), I employed the following analysis: The noise level was calculated by the decomposition of the detected SW peak (trough) distribution using a bivariate Gaussian mixture distribution model (MATLAB statistics toolbox: gmddistribution class). The most prominent distribution was assumed to follow a gaussian distribution. Then, the confidence levels were tested, using 2-20 times the SD above the mean of the noise distribution in four hundred steps. The signal-to-noise ratio was defined as follows: the signal was calculated as the mean peak value of all the values higher than the tested confidence level to the power of two (power of signal with SW peaks). The noise was calculated as the mean peak value of all the

values lower than the tested confidence level to the power of two (power of the signal without the SW events) (Çalışkan et al., 2016).

To compare the similarity of the signal between the areas CA3 and CA1, as well as their temporal relationship, I assessed the following parameters: SW waveform correlation of all SW events, SW waveform correlation of the connected SW events, SW propagation failure from CA3 to CA1, and SW peak correlation. Connected SW events were defined as the first SW events that occurred in the CA1 area in time between two consecutive SW events that occurred in the CA3 region. From the calculated time distance of the connected events, time distance distributions were formed. Only the connected events with distance below the 0.05 level of the cumulative density function of the time distance distribution were included in the analysis. Then, event trains were formed, and each train was convolved by a gaussian function with a SD of 2 ms (95% of the area within the duration of 8 ms). For all the detected event times of the CA3 and CA1 areas and only the connected events, the event trains were cross-correlated, and the global maximum coefficient was identified. The SW peak correlation was calculated from the peak values of only the related events (the zero-lag of the normalized covariance function). The propagation failure was calculated as the ratio of the connected SW events occurring in the CA1 area to the globally detected events in CA3.

2.1.6.2 Gamma oscillations

The electrophysiological signal was recorded and analyzed offline using Spike2.8 software (Cambridge Electronic Design) and custom-made MATLAB scripts (MathWorks, Natick, MA, USA). Artifact-free data of two-minute duration were analyzed using the Fast Fourier Transformation with a frequency resolution of 1.221 Hz. For the description of the gamma oscillations, the variables peak frequency (frequency with the highest power), integrated power (20-80 Hz), and peak power were acquired from the power spectrum analysis (Fig. 2.2d). The auto-correlation of the signal in the CA3 or CA1 regions was the value at the 2nd positive peak of the auto-correlogram (Fig. 2.2d). The cross-correlation value between the signals recorded in CA3 and CA1 regions was the peak value closest to the time 0 s of the correlogram. Slices that showed gamma oscillations with peak power lower than 10 μV^2 and peak frequency lower than 20 Hz were excluded from the analysis.

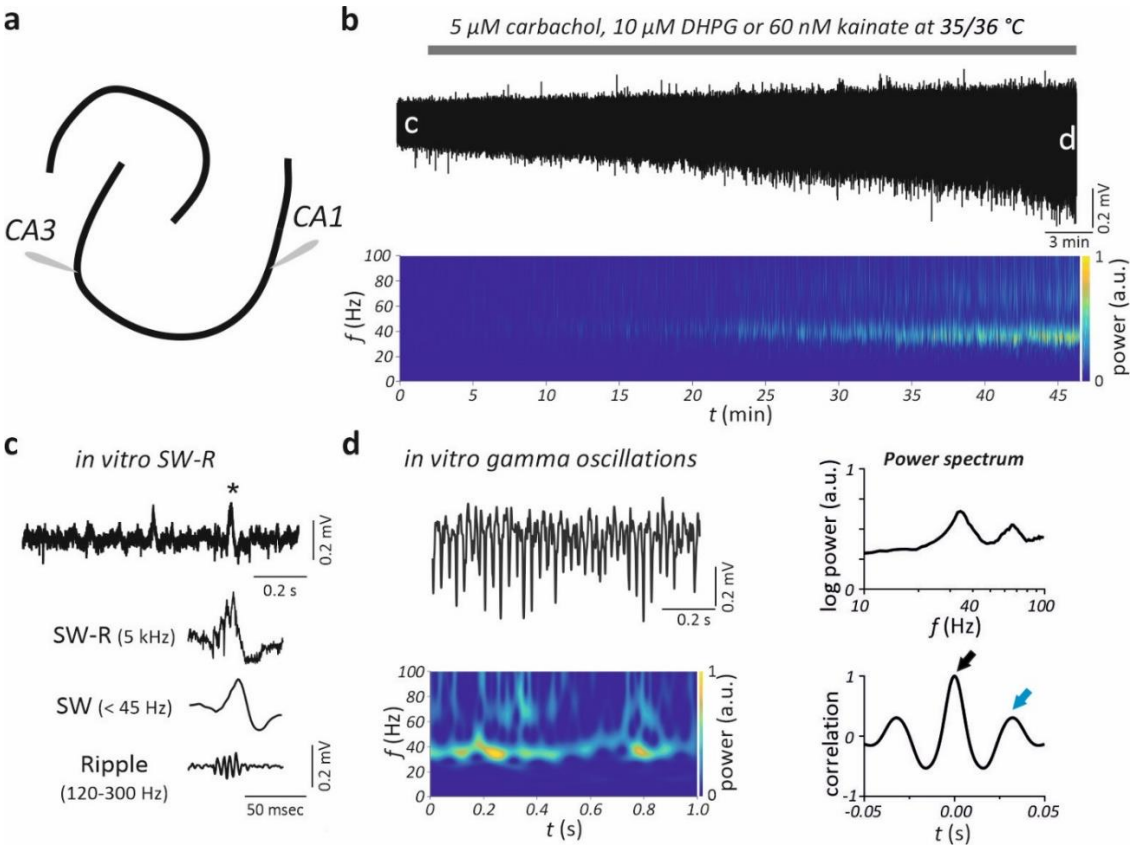

***Fig. 2.2: Extracellular local field potential (LFP) recordings and in vitro oscillations**. **(a)** Scheme illustrating a ventral hippocampal slice and two recording electrodes, in the regions CA3 and CA1. **(b)** Example of a ~45 min LFP recording from the CA3 region. For the induction of gamma rhythm, carbachol was used in STUDY 1 and one of the three drugs carbachol, DHPG or kainate was used in STUDY 4. Note the increasing amplitude of the signal after the drug administration as well as the corresponding spectrogram below exhibiting the increasing power in the gamma frequency range of ~40 Hz. **(c)** Representative trace of SW-R recorded in the CA3 region at the beginning of the recording in (b). Below, a SW-R trace (indicated by an asterisk) in higher resolution demonstrating an unfiltered SW-R trace of 5 kHz sampling rate, a low-pass filtered trace (<45 Hz) illustrating the sharp wave component, and a band-pass filtered trace (120-300 Hz), illustrating the ripple component. **(d)** Trace of the pharmacologically-induced gamma oscillations at the end of the recording in (b). Below, the corresponding power spectrum demonstrating a prominent frequency of ~40 Hz. Right up, the corresponding power spectrum in log power (in arbitrary units-a.u) and frequency in log scale. Below, an example graph of waveform correlation analysis. The second peak (black arrow) indicates the CA3-CA1 cross-correlation coefficient, while the third peak (blue arrow) indicates the CA3 or CA1 auto-correlation coefficient. DHPG: (RS)-3,5-dihydroxyphenylglycine.*

2.1.7 Statistical analysis

Statistical comparison was performed using GraphPad Prism (version 9.1.2; GraphPad Software, CA, USA). For the data distribution definition, the Shapiro-Wilk normality test was first used. For comparison of two groups, Student's t-test or Mann-Whitney U test was used when the data were normally distributed or skewed, respectively. Due to the variable nature of the data, power log

transformation was applied to statistically compare gamma oscillation power. The Chi-Square (χ^2) test was used to assess the likelihood of RED events.

For the statistical analysis of the behavioral experiments, two-way repeated-measures (RM) ANOVA, followed by post-hoc Sidak's test, was performed. Additionally, the sessions were analyzed in two minutes bins. Only the first two minutes of the extinction sessions were used to include information specific to the memory retrieval/consolidation due to the habituation possibly occurring in the ten minutes course of the entire extinction session. The number of animals (N) and the number of slices (n) are indicated in the legend of each figure. Data are presented as mean ± standard error of the mean (SEM). Differences were considered statistically significant when at least $p \leq 0.05$ (*).

2.2 Cellular and network correlates of altered SW-R in GAD65 KO mice - STUDY 2

2.2.1 Animals

General conditions and GAD65 mouse line are described in section 2.1.1. The wild-type (WT) C57BL/6 mice were purchased from M&B Taconic and bred in the animal facility of our Institute. Male C57BL/6 were used for sterotactic viral injections and subsequent slice LFP electrophysiology. The state's authorities for animal experimentation approved animal housing and all experiments (Landesverwaltungsamt Sachsen Anhalt: Permission No. 42502-2-1177/ -1516 - UniMD).

2.2.2 Slice electrophysiology

Acute slice preparation was performed as described in section 2.1.3.

2.2.2.1 LFP recordings

The extracellular local field potential (LFP) recordings were performed in an interface chamber at 32 °C ± 1 °C with the guidance of a stereomicroscope (Stemi 2000, Zeiss) borosilicate glass electrodes with ~1 MΩ resistance, when filled with aCSF, were inserted ~80 µm deep in the ventral to the intermediate hippocampus. The spontaneous SW-R activity (Çalışkan et al., 2016;

Maier et al., 2003) was captured by inserting the recording electrodes into the s.p. of areas CA3 and CA1.

To capture the synaptic plasticity and excitability of the Schaffer-collateral (SC) - CA1 synapse, a recording electrode was inserted in the s.r. of the CA1 region, and a stimulation electrode was placed in the s.r. of CA3 region to activate SC fibers. Upon stabilization of the responses, 12 current stimuli with intensities between 5 and 100 μA were incrementally applied to obtain an input-output (I-O) curve. The stimulus which produced a response with ~40% of the maximum amplitude was kept as stimulation intensity for the paired-pulse (PP) and long-term potentiation (LTP) experiments. The short-term plasticity was assessed by applying PP stimuli of increasing distances ranging between 10 and 500 msec. To describe the long-term plasticity, high-frequency stimulation (HFS), consisting of two 100 Hz train pulses of 1 sec with a 20 msec interval between them, was used. Subsequently, the fiber volley (fv) and the field postsynaptic excitatory potential (fEPSP) of the responses in the CA1 area were analyzed. The synaptic fatigue was calculated as the fEPSP responses during the first HFS train.

The LFP signals were amplified and low-pass filtered at 3 kHz using either a custom-made extracellular amplifier or a commercial device (EXT-02F, Extracellular Amplifier; npi Electronic GmbH, Tamm, Germany). The data were sampled at a minimum 5 kHz rate using a digitizer unit (CED-Mikro1401; Cambridge Electronic Design, Cambridge, UK) and the corresponding software (Spike2.8; Cambridge Electronic Design) and were stored on a hard disc for offline analysis.

2.2.2.2 Patch-clamp electrophysiology

Slices were first incubated for at least 1.5 h in an interface chamber and then transferred to a submerged chamber with continuous perfusion of standard carbogenated aCSF of 2 ml/min flow and 32 °C chamber temperature. Borosilicate glass pipettes (GC150T-10, Clark Electromedical Instruments, Pangbourne, UK) pulled with a pipette puller had about 4-5 MΩ resistance, after filling with intracellular solution (composition see below). The electrodes were inserted in area CA1 of the ventral hippocampus and patched the soma of the pyramidal-shaped cells of s.p., guided by a differential interference-contrast microscope (Zeiss, Oberkochen, Germany) connected to a digital camera (Kappa, Gleichen, Germany). The signals were amplified using a patch-clamp amplifier (EPC-9, Heka, Lamprecht, Germany) and recording software (Pulse, HEKA,

Lamprecht, Germany). Data were low-pass filtered at 3 kHz and sampled at minimally 5 kHz. Liquid junction potentials were not corrected.

For current-clamp mode, pipettes were filled with an intracellular solution of the following composition (mM): K-gluconate, 95; K_3- citrate, 20; NaCl, 10; HEPES, 10; $MgCl_2$, 1; $CaCl_2$, 0.1; EGTA, 5, MgATP, 3; NaGTP, 0.5; adjusted at 7.2 with KOH. Once a stable membrane seal was achieved, cells were current-clamped with zero current. An input-output current-voltage curve (I-V curve) was created by injecting current pulses to each patched cell and recording the membrane potential (Pulse, HEKA). The current pulses ranged from -125 pA to 150 pA, with 1-sec duration and incrementally increasing steps of 25 pA, with an interval of 3 sec.

Inhibitory postsynaptic currents (IPSCs) were recorded under voltage-clamp conditions. Micropipettes were filled with intracellular solution of the following composition (in mM): Cs-gluconate, 120; NaCl, 10; HEPES, 10; $MgCl_2$, 1; $CaCl_2$, 0.1; EGTA, 5; MgATP, 3; NaGTP, 0.5; adjusted at 7.25 with CsOH). Cells were clamped at a holding potential of 0 mV in the presence of glutamate receptors blockers (see drug application below), and 5 min sweeps were recorded and saved on the computer hard disc for offline analysis.

2.2.2.3 Intracellular recordings during SW-R

A combination of LFP and patch-clamp electrophysiology was performed in a separate set of experiments. Slices were kept for at least 2 h in an interface chamber and transferred to a submerged chamber for the recording. The submerged chamber was equipped with a wire net on its base to allow superfusion of both sides of the slice, and the aCSF had a flow of 5-6 ml/min (Hájos et al., 2009; Maier et al., 2009). This way, sufficient oxygenation was provided to the slices to facilitate SW-R network activity. An electrode was inserted in the area CA3 to record extracellularly spontaneous SW-R, as described above. A second electrode with an intracellular solution suitable for whole-cell (see above) was inserted in area CA1 to record from individual pyramidal cells postsynaptic currents. The perfusion solution contained no glutamate receptor blocker. To record the compound inhibitory & excitatory postsynaptic currents (cIPSCs & cEPSCs) CA1 pyramidal cells were voltage-clamped at 0 mV and -70 mV, respectively (Maier et al., 2011). Signals were captured as described above and stored on a hard disc for offline analysis.

2.2.3 Drug application

For blocking glutamate receptors, 10 µM 6-cyano-7-nitroquinoxoxaline-2,3-dione (DNQX; TOCRIS, Bristol, UK) and 50 µM d,l-2-Amino-5-phosphonopentanoic acid (AP5; TOCRIS) were applied. All drugs had been previously aliquoted in higher concentration stocks; DNQX had been aliquoted in dimethyl sulfoxide (DMSO; Final Concentration: 0.01%) (Merck KGaA, Darmstadt, Germany) whereas AP5 in double distilled water. AP5 stocks were stored in a -20 °C freezer, whereas DNQX was stored at 4 °C. Shortly before the experiment, stock solutions were thawed and diluted in their final concentration in the aCSF solution and perfused with a flow rate of ~2 ml/min.

2.2.4 Stereotactic surgeries and viral injection

C57BL/6 male mice were anesthetized, inhaling 5% isofluorane in a mixture of O_2/N_2O, and placed in a motorized stereotactic apparatus (Robot Stereotax, Neurostar). After anesthesia induction, the isoflurane concentration was decreased to 2% until the end of the experiment. The mice were positioned on a warming pad (~35 °C), the head was gently fixed, the eyes were covered with a dry protection ointment (Bepanthen, Bayer), the skin on the head midline was incised, and the skull was revealed and cleaned with saline 0.9%. Bregma and lambda raphes were visually defined and manually set on the computer system (Stereodrive, Neurostar). Then, a motorized micro drill was guided above the area of interest, and a craniotomy of about 5 mm depth on each side was made. A motorized pump from the same robotic system holding a 10 µL NanoFil microsyringe (World Precision Instruments, Berlin, Germany) was guided to the specific brain coordinates. To reach the DG-CA3 area of the vHP, the needle was inserted (according to “The mouse Brain”, Franklin & Paxinos, 2008) anteroposteriorly (AP): -3.0 mm and mediolaterally (ML): +/- 2.5 mm from bregma and dorsoventrally (DV): 3.2 mm from the brain surface. To reach the ventral CA1 subregion, the following coordinates were used; anteroposterior (AP): -3.3 mm and mediolateral (ML): +/- 3.2 mm from bregma and dorsoventral (DV): 3.7 mm from the brain surface. The mice received microinjections with lentiviruses transfected with plasmids that contained either a shGAD65 RNA to impede GAD65 expression (Rehberg et al., 2014) or a random sequence as a control (Thiere et al., 2016) (more details in Appendix A.5).

About 1.5 µL of lentiviral solution was injected in each hemisphere with a flow rate of 0.1 µl/min. After the solution ejection, the needle stayed on site for about 10 min to avoid mechanical solution spread when withdrawing it. Then, the needle was slowly retracted, and the same

procedure was followed for the other hemisphere. At the end of the injections, the skin was sutured with sterile surgical stitches, and Xylocaine® gel 2% (Aspen) was applied for postsurgical anesthesia. Shortly after ending isoflurane administration, the mice recovered and were placed in individual cages. Ten to fourteen days later, the mice were killed, and acute slices for LFP electrophysiology were obtained. After electrophysiology, the slices were placed under the fluorescent microscope to confirm the injection site by observing the GFP fluorescence. Additionally, the part of the slices containing the hippocampus was kept at -20 °C for western blotting to verify the GAD65 enzyme expression.

2.2.5 Data analysis

2.2.5.1 Sharp wave-ripple analysis

As described in section 2.1.6.

2.2.5.2 LFP-synaptic plasticity analysis

The responses were analyzed offline with the help of custom-made scripts in Spike2 and MATLAB. The fv amplitude and the fEPSP slope were analyzed from the I-O curves. The fEPSP slope (V/s) was calculated by dividing the amplitude value between 10-90% of the maximum amplitude by time. PP ratio was calculated by dividing the fEPSP slope of the second response by the first. For the LTP analysis, the fEPSP slope values were calculated and were normalized to the average of the last 10 min of baseline fEPSP (Ivens et al., 2019; Papatheodoropoulos & Kostopoulos, 2000a). For the synaptic fatigue, fEPSP slope values within the first HFS train were calculated and normalized to the first fEPSP response.

2.2.5.3 Patch-clamp analysis

Only recordings with a stable seal for at least 15 min were kept for analysis. At current-clamp mode, the injecting current and voltage response relationship (I-V curve) was analyzed offline using the software FitMaster (HEKA, Lambrecht, Germany) and OriginPro (OriginLab, Northhampton, MA, USA). The resting membrane potential (Vm) was determined as the cell's potential when injecting zero current. The neuronal input resistance (R_{IN}) was calculated as the slope from a linear regression analysis fit to the I-V curve around the resting Vm, which constitutes the most linear part of the curve.

To create a current-frequency curve (I-f curve), I calculated the number of action potentials (AP) on each current injection step. The suprathreshold membrane properties and the AP kinetics were based on the analysis of the first AP that arose at the rheobase current injection. The rheobase was calculated as the linear fit in the I-f curve and by interpolating the current step that induced one AP.

The AP threshold was calculated from the first peak of the third derivative of the AP trace, and the maximum steepness of the AP rising phase was calculated from the peak of the first derivative of the AP trace (Henze & Buzsáki, 2001). The AP amplitude was calculated as the voltage distance from the threshold to the peak of the AP.

In voltage-clamp mode, cells were held at 0 mV, and the recorded currents were stored for offline analysis. The spontaneous inhibitory postsynaptic currents (sIPSC) were detected using the software Mini-Analysis (Synaptosoft Inc, NJ, USA). The frequency was calculated from the interevent interval and the amplitude as the distance from the baseline to the peak of the event. The sIPSc kinetics rise and decay were calculated as follows: the rise time of IPSCs was defined from the values between 10 and 90% of the peak amplitude, and the decay time was fitted to a mono-exponential function. Cumulative histograms were calculated from recordings of a 1-minute duration that contained exactly 150 events.

2.2.5.4 Analysis of intracellular recordings during SW-R

Two-minute artifact-free data were used for analysis. Waveform averages of cIPScs or cEPSCs relating to SW-R peaks were calculated using Spike2 software (Spike2.8; Cambridge Electronic Design). The SW-R peaks were identified by setting a threshold of 0.06 mV (± 0.01) mV amplitude in the LFP signal and manually excluding false-positive occurrences. The intracellular signal was low-pass filtered (Butterworth 45 Hz) with DC-remove at 2 Hz. The postsynaptic events that occurred in a time window of 0.03-0.15 sec after the peak of each SW-R event were included in the waveform average. From the waveform, the following parameters were measured; the amplitude, the AUC, the slope of rising phase, and the decay phase between 10% and 90% of the peak amplitude.

2.2.6 Statistical analysis

In addition to section 2.1.7, for the statistical analysis of the I-O curves, PPR ratios and synaptic fatigue two-way RM ANOVA was performed, followed by post-hoc Sidak's test or multiple Mann-Whitney tests. For the statistical comparison of the LTP responses, the average value of the normalized fEPSP slopes at the last 10 min of the recording (30-40 min after the HFS) was measured. Kolmogorov-Smirnoff (OriginPro 2019, OriginLab Corporation, Northhampton, MA, USA) was used to compare cumulative probability curves.

2.3 Behavioral correlates of SW-R - STUDY 3

2.3.1 Animals

General conditions as described in section 2.1.1. All experiments of this study were approved by the state's authorities for animal experimentation (Landesverwaltungsamt Sachsen-Anhalt: Permission No. 42502-2-1295/- 1563/- 1628 - UniMD).

2.3.2 Behavior - contextual fear conditioning paradigm

The protocol was adapted from (Çalışkan et al., 2016). In total, 69 C57BL/6 male mice, 2-4 months old, underwent a contextual FC paradigm, followed by one (re)consolidation (E1.1) or five extinction (E) sessions. Each session occurred one day after the previous (Fig. 2.3). In detail, mice were single-caged 3-4 days before the start of the experiment, and they underwent two habituation sessions before the training. During the training session, they were divided into three groups, each receiving grid electric shock of different intensity. Specifically, after two minutes of exploration, the low-intensity group received one electrical stimulus (0.3 mA, 1 s), the mild-intensity group received three stimuli (0.4 mA, 1 s; interstimulus interval (ISI) 20 s), whereas the high-intensity group received three stronger stimuli (0.5 mA, 2 s; ISI 20 s). The mice stayed in the apparatus for a total of 6 min and then were placed back in their home cages. An additional group of mice, used as control, underwent the same protocol without any electric shock. Post-training, the mice were further divided into E1 and E5 groups. The E1 group underwent only one two-minute retrieval session in the training context, then killed, and acute LFP electrophysiology was performed. On the other hand, the E5 group underwent five ten-minute extinction sessions and

was then prepared for LFP electrophysiology. The slice preparation took place ninety minutes after the end of the behavioral paradigm.

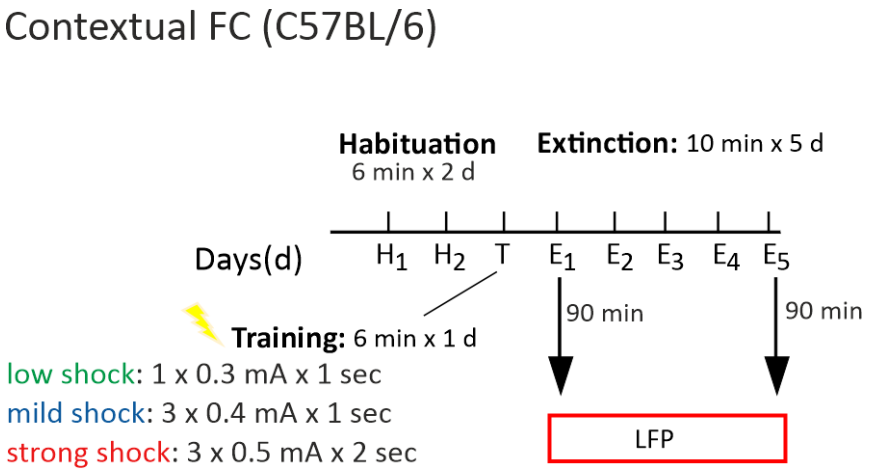

Fig. 2.3: Contextual fear conditioning and extinction protocol for C57BL/6 mice. *Mice underwent two habituation sessions before training in the same context. During the training session, they were divided into three groups, each receiving different shock intensity, indicated by different color. In addition, a control mice group followed the same protocol, but did not receive electric shock during the training session. Then, the mice were further divided into E1 and E5 groups. The E1 group underwent, only one two-minute retrieval session in the training context and then mice were prepared for acute slice electrophysiology. On the other hand, the E5 group underwent five ten-minute extinction sessions followed by LFP electrophysiology ninety minutes later. H: habituation; T: training; E: extinction; Numbers' subscripts indicate the session order; LFP: local field potential.*

2.3.3 Data & statistical analysis

In addition to the description in section 2.1.7, for three or more groups one-way ANOVA or Kruskal-Wallis was used followed by post-hoc Tukey's test or Dunn's test, respectively. Pearson's or Spearman's r was used for the correlation analysis accordingly, after assessing the normality of the data.

2.4 Signaling pathways involved in the gamma oscillopathy of FXS - STUDY 4

2.4.1 Animals

General conditions as described in section 2.1.1. Fmr1 KO mice were purchased from Jackson laboratories (JAX stock #003024; Bakker et al., 1994) and kept breeding in pairs of heterozygous females (X^*/X) and KO males (X^*/Y) in our animal facility. Genotyping was performed in our facility

using the PCR method (detailed information in appendix A.6). Male Fmr1 KO mice and WT littermates were weaned at P21 and used for *in vitro* electrophysiology at 28-32 days. All experiments for this study were approved by the state's authorities for animal experimentation (Landesverwaltungsamt Sachsen-Anhalt: Permission No. 42502-2-1009-UniMD).

2.4.2 LFP electrophysiology and drug application

Slice preparation and LFP electrophysiology were performed as described in section 2.1.3. For induction of gamma oscillations, 5 µM CCh (TOCRIS, Bristol, UK), or 60 nM ionotropic GluR agonist kainic acid (KA; TOCRIS) or 10 µM $mGluR_{1/5}$ agonist Dihydroxyphenylglycine (DHPG; TOCRIS) were used. All drugs had been previously aliquoted in higher concentration stocks in double distilled water and stored in -20 °C freezers. Shortly before the experiment, stock solutions were thawed and diluted in their final concentration in the aCSF solution and perfused with a flow rate of ~2 ml/min.

2.4.3 Data analysis

Electrophysiological signals were recorded from the ventral CA3 region and analyzed offline using Spike2.8 software and custom-made MATLAB scripts (written by Dr. Oliver Hollnagel). Artifact-free data of two-minute duration were analyzed using the Fast Fourier Transformation with a frequency resolution of 1.221 Hz. For description of the oscillation, the estimates peak frequency (frequency with the highest power), integrated power (20-80 Hz), and half-band width (HBW) were acquired from power spectrum analysis. The HBW was defined as the frequency at half of the maximum power. The autocorrelation of the signal was the value at the 2^{nd} positive peak of the auto-correlogram (Fig. 2.2d), while the time constant (Tau) was defined as the decaying exponential fit to the peaks of the auto-correlogram. The slices that showed gamma oscillations with maximum power lower than 10 μV^2 and maximum frequency lower than 20 Hz were excluded from the analysis. Statistical analysis was performed as described in section 2.1.7.

CHAPTER 3. RESULTS

3.1 Hippocampal network oscillations in GAD65 KO mice - STUDY 1

GAD65 KO mice exhibit reduced GABA synthesis and behavioral deficits, including fear memory extinction impairments, increased anxiety, and stress-induced epilepsy (Asada et al., 1996; Bergado-Acosta et al., 2008; Kash et al., 1999; Stork et al., 2000). Amygdala is a key player in the pathophysiology of the model (Müller et al., 2015), but the role of the vHP, a region with a differential role in anxiety and emotional memories, remains elusive. Interestingly, the vHP exhibits robust oscillatory activity implicated in memory formation and anxiety, which critically depends on the interaction of pyramidal cells and interneurons (as described in section 1.3). Therefore, I used the network oscillations as a read-out to study the effect of GAD65-dependent excitation/inhibition imbalance on the stress susceptibility phenotype the animal model exhibits. To this extent, LFP electrophysiology was performed and *in vitro* oscillations in the CA3 and CA1 regions of the vHP were recorded.

3.1.1 Enhanced gamma oscillations in the vHP of GAD65 KO mice

For gamma oscillatory activity to emerge, the slices were incubated with 5 µM CCh for at least 45 min at 36 °C. In the CA3 subregion, the gamma oscillations exhibited increased gamma peak frequency (Fig. 3.1c; Student's two-tailed t-test; $T(31) = 3.274$, $p = 0.0026$) in GAD65 KO compared to WT mice. On the contrary, the integrated power (20-80 Hz) (Fig. 3.1d; Student's two-tailed t-test; $T(31) = 1.627$, $p = 0.1139$), the peak power (Fig. 3.1e; Student's two-tailed t-test; $T(31) = 0.992$, $p = 0.3289$) and the waveform auto-correlation (Fig. 3.1f; Student's two-tailed t-test; $T(26) = 1.128$, $p = 0.2698$) remained unaltered. Furthermore, in the CA1 subregion, the gamma peak frequency was increased (Fig. 3.1g; Student's two-tailed t-test; $T(31) = 2.469$, $p = 0.0193$) in GAD65 KO compared to WT mice, whereas there were no differences in the integrated power (20-80 Hz) (Fig. 3.1h; Student's two-tailed t-test; $T(31) = 0.8202$, $p = 0.4184$), the peak power (Fig. 3.1i; Student's two-tailed t-test; $T(31) = 0.4397$, $p = 0.6632$) and the waveform auto-correlation

(Fig. 3.1j; Student's two-tailed t-test; T(26) = 0.087, p = 0.9313). Similarly, cross-correlation analysis of the waveforms between CA3 and CA1 subregions showed no differences between the groups (Fig. 3.1k; Student's two-tailed t-test; T(26) = 1.34, p = 0.1917). Interestingly, GAD65 KO mice were more likely to develop recurrent epileptiform discharges (REDs) compared to WT (Fig. 3.2; Chi-Square test; χ^2 (1, 59) = 5.4289; p = 0.019).

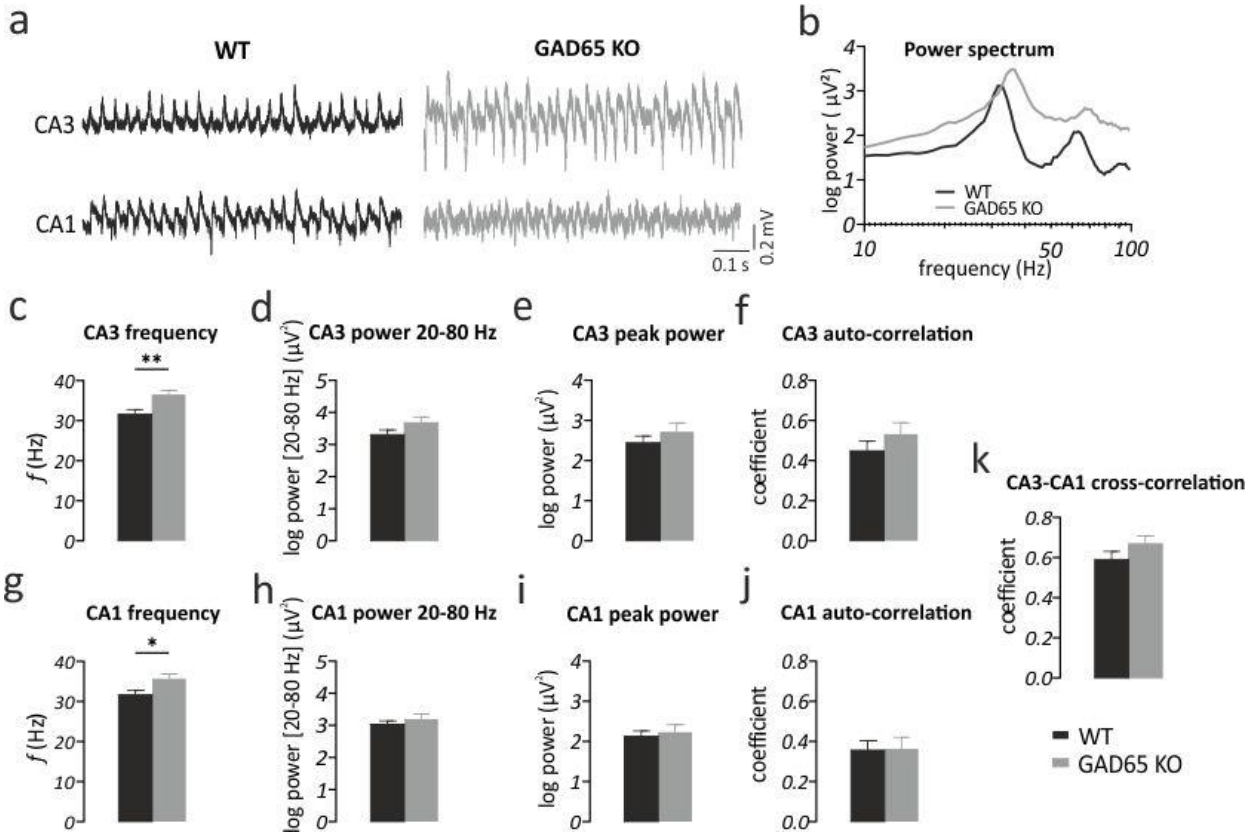

Fig. 3.1: Altered CCh-induced gamma oscillations in the CA3 and CA1 areas of the vHP in GAD65 KO mice. ***(a)*** *Representative traces of gamma oscillations recorded in the CA3 and CA1 regions of the vHP.* ***(b)*** *Corresponding spectrogram highlighting the higher frequency (f) of GAD65 KO mice (frequency is on a log scale) and a tendency for increased power. Summary graphs demonstrating in CA3 region* ***(c)*** *increased gamma frequency of GAD65 KO compared to WT,* ***(d)*** *unaltered CA3 integrated power (20-80 Hz),* ***(e)*** *peak power and* ***(f)*** *waveform auto-correlation. In the CA1 region, summary graphs illustrating* ***(g)*** *increased frequency in GAD65 KO mice, but* ***(h)*** *unaltered integrated power (20-80 Hz),* ***(i)*** *peak power and* ***(j)*** *waveform auto-correlation between the genotypes. Last,* ***(k)*** *cross-correlation between the CA3 and CA1 subregions showed no differences between the groups. Statistical comparison was performed using Student's two-tailed t-test. *p < 0.05. Data are given as mean ± SEM. WT: N = 5 mice, n = 16 slices, GAD65 KO: N = 5 mice, n = 17 slices. For correlations (**f, j, k**,): WT: N = 5 mice, n = 16 slices, GAD65KO: N = 4 mice, n = 12 slices.*

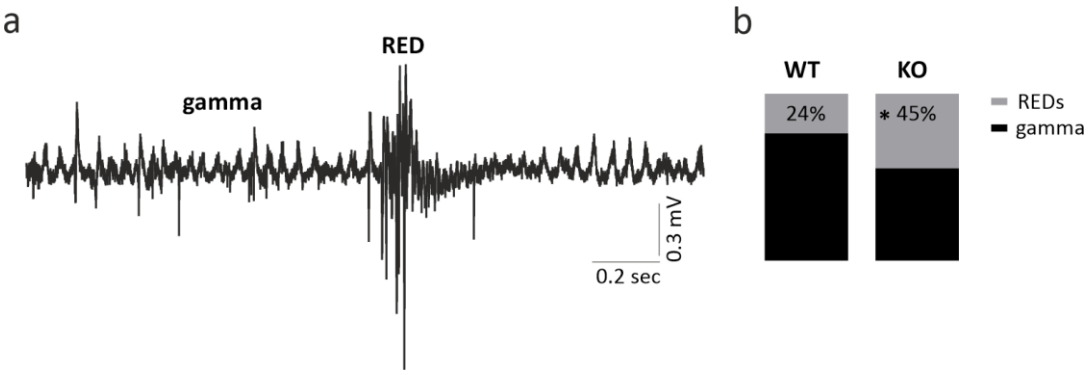

Fig. 3.2: Recurrent epileptiform discharges in hippocampal slices of GAD65 KO mice. (a) *Representative trace of CCh-induced gamma oscillation that exhibits REDs events after 5 µM CCh administration. Note the high magnitude of the REDs and the recovery period until gamma rhythm is formed again.* ***(b)*** *Graph showing the increased proportion of slices that developed REDs in GAD65 KO mice compared to WT. Statistical comparison was performed using the Chi-Square test. *p < 0.05. WT: N = 5 mice, n = 21 total slices, REDs = 5 slices; GAD65 KO: N = 7 mice, n = 38 total slices, n = 21 REDs slices.*

3.1.2 Altered SW-R activity in the vHP of GAD65 KO mice

3.1.2.1 Enhanced CA3 SW-R and decreased SW incidence in the CA1 region

To characterize the spontaneous network activity in the stress susceptible GAD65 KO mice, I performed LFP recordings, and analyzed the local SW-R activity in CA3 and CA1 regions of the vHP. In the CA3 region, the ripple amplitude (Fig. 3.3d; Mann-Whitney U test; $p < 0.05$) and the AUC (Fig. 3.3f; Mann-Whitney U test; $p < 0.05$) were significantly increased in GAD65 KO mice compared to WT. On the contrary, the signal-to-noise ratio (Fig. 3.3b; Mann-Whitney U test; $p = 0.1086$), the SW incidence (Fig. 3.3c; Mann-Whitney U test; $p = 0.34$) and the ripple frequency (Fig. 3.3e; Student's two-tailed t-test; $T(72) = 0.1563$, $p = 0.8$) showed no changes. Furthermore, in the CA1 region, the SW incidence (Fig. 3.3h; Student's two-tailed t-test; $T(72) = 3.678$, $p < 0.001$) was decreased in GAD65 KO compared to WT mice, while the AUC (Fig. 3.3k; Mann-Whitney U test; $p = 0.08$) showed only a trend for decrease. The ripple frequency (Fig. 3.3j; Student's two-tailed t-test; $T(72) = 3.277$, $p < 0.01$) was increased in GAD65 KO mice compared to WT, whereas the signal-to-noise ratio (Fig. 3.3g; Mann-Whitney U test; $p = 0.3863$) and the ripple amplitude (Fig. 3.3i; Mann-Whitney U test; $p = 0.31$) showed no differences between the genotypes. Therefore, these data show enhanced SW-R network activity in the CA3 region and decreased SW activity in the CA1 region in GAD65 KO mice compared to WT, which might lead to or be a consequence of propagation deficits or hippocampal synaptic excitability in GAD65 KO mice.

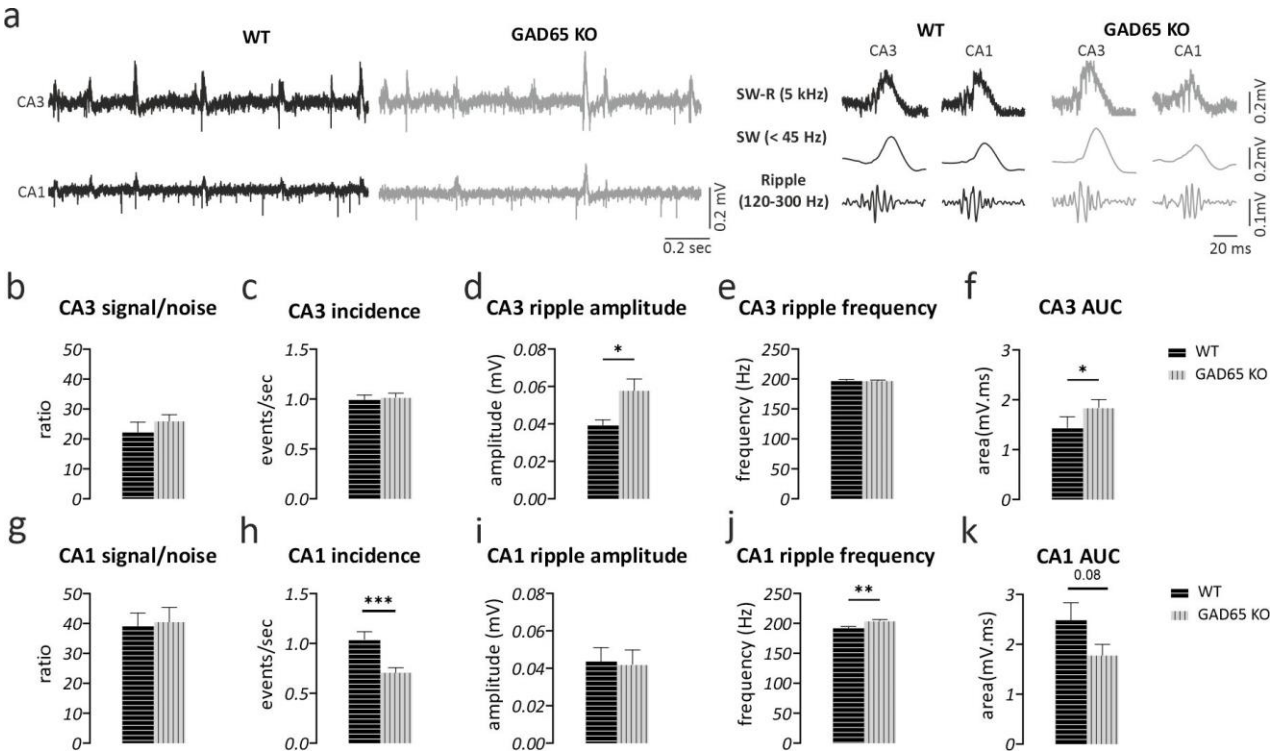

***Fig. 3.3: Altered spontaneous SW-R in the CA3 and CA1 regions of the vHP in GAD65 KO mice**. **(a)** Representative traces of SW-R recorded in the CA3 and CA1 areas. Note the enhanced SW-R in the CA3 and the decreased number of SW-R events in the CA1 region. On the right, SW-R traces of sampling rate 5 kHz are low-pass filtered (<45 Hz), illustrating the sharp wave component or band-pass filtered (120-300 Hz), revealing the ripple component. Statistical comparison of SW-R properties in the CA3 region are shown in panels **(b-f)**. SW-R showed no significant alterations in **(b)** signal-to-noise ratio, **(c)** SW incidence and **(e)** ripple frequency, but a significant increase in **(d)** ripple amplitude and **(f)** AUC in GAD65 KO compared to WT mice. On the other hand, analysis of SW-R in CA1 (panels **g**-**k**) revealed unaltered **(g)** signal-to-noise ratio and **(i)** ripple amplitude, but a prominent decrease in **(h)** SW incidence, a trend for a reduced **(k)** AUC and significant increase in **(j)** ripple frequency in GAD65 KO mice compared to WT mice. Statistical comparison was performed using Student´s two-tailed t-test for **e**, **h**, **j** and Mann-Whitney U test for **b-d**, **f**, **g**, **I**, **k**. Data are given as mean ± SEM. *p < 0.05, **p < 0.01, ***p < 0.001. WT: N = 6 mice, n = 27 slices, GAD65 KO: N = 10 mice, n = 47 slices. AUC: area under the curve.*

3.1.2.2 Hippocampal CA3-CA1 interactions during SW-R in GAD65 KO mice

It has been previously shown that SW-R propagate from CA3 to CA1 region (Both et al., 2008; Chrobak & Buzsáki, 1996). The LFP network interactions along the CA3-CA1 axis during SW-R were analyzed in GAD65 KO and WT mice. Specifically, the SW-R propagation along the CA3-CA1 axis, the waveform correlation of low pass-filtered SW signal, and the peak amplitude correlation of SW in the CA3 and CA1 regions were assessed. The waveform correlation of all SW, between CA3 and CA1 and the correlation of the connected SW (SW occurring in CA1 in a specific time window after CA3) showed no alterations between the groups (All SW: Fig. 3.4b; Mann-Whitney U test; p = 0.67, only connected SW: Fig. 3.4c; Mann-Whitney U test; p = 0.57). Similarly, the coherence of

the SW signal in the CA3 and CA1 regions (correlation of the peak SW amplitudes) remained unaltered (Fig. 3.4d; Mann-Whitney U test; p = 0.9). Interestingly, the SW-R propagation showed a strong trend for increased failure in GAD65 KO mice compared to WT mice (Fig. 3.4a; Student's one-tailed t-test; T(73) = 1.583, p = 0.058).

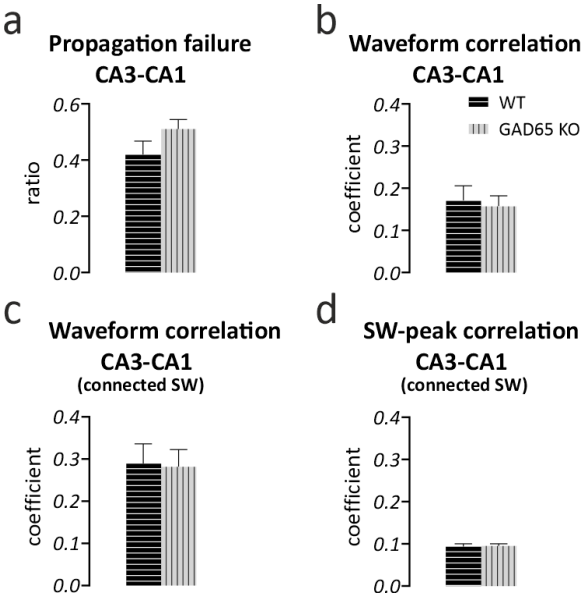

Fig. 3.4: Unaltered CA3-CA1 network interactions during SW-R in the vHP of GAD65 KO mice. *Summary plots illustrating **(a)** a strong trend for increased propagation failure along the CA3-CA1 axis in GAD65 KO compared to WT but **(b)** unaltered waveform correlation of all detected SW-R events, **(c)** unaltered waveform correlation of connected CA3-CA1 SW-R events and **(d)** unaltered SW-peak amplitude correlation between the groups. Statistical comparison was performed using Student´s one-tailed t-test for **a** and Mann-Whitney U test for **b**, **c**, **d**. Data are given as mean ± SEM. WT: N = 6 mice, n = 30 slices, GAD65 KO: N = 10 mice, n = 45 slices.*

3.1.3 Examination of contextual fear memory and its persistence in GAD65 KO mice

GAD65 KO naïve mice exhibited enhanced SW-R in the CA3 and decreased incidence in the CA1, accompanied by a strong trend for propagation failure. To assess if the PTSD-like phenotype these mice exhibit would also be represented in the SW-R properties, I designed a fear conditioning (FC) paradigm. Previous studies have used FC behavioral paradigms on this animal model and have revealed cued but not contextual fear memory persistence (Sangha et al., 2009). However, that contextual FC paradigm had a short extinction protocol, and I postulated that a more extended protocol would better assess the fear memory persistence. For this reason, a prolonged paradigm was used, based on (Çalışkan et al., 2016), which contained five extinction sessions and one additional re-exposure session (spontaneous recovery - SR). This way, fear memory was assessed at a remote time point, expressed in freezing terms, and subsequently, the electrophysiological correlates from acute brain slices were estimated.

3.1.3.1 Freezing levels during contextual FC and re-exposure in GAD65 KO mice

GAD65 KO mice increased their freezing during the first two minutes of extinction 1 (E1.1) session and decreased their freezing rapidly after. On the other hand, WT mice showed increased freezing immediately after the shock delivery (T3) and gradually reduced it until the end of the daily extinction sessions (Fig. 3.5Aa; two-way RM ANOVA; effect of genotype $F(1, 17) = 9.393$, $p = 0.007$; post-hoc for T3, $p = 0.0114$; for E2.1, $p = 0.0177$). Within session analysis revealed a constant decrease in freezing behavior of GAD65 KO mice compared to WT. During the extinction sessions there are evident effects of session and genotype between GAD65 KO and WT mice (Fig. 3.5Ab-f; two-way RM ANOVA; effect of genotype for E1: $F(1, 17) = 47.38$, $p < 0.0001$; E2: $F = 42.73$, $p < 0.0001$; E3: $F = 4.049$, $p = 0.063$; E4: $F = 18.33$, $p < 0.0001$; E5: $F = 14.84$, $p = 0.0013$). In particular, GAD65 KO showed decreased freezing levels in most of the sessions, which was more prominent after the second minute of each session (bins 2-5), while in the E3 session, they showed only a trend. These data suggest that GAD65 KO mice successfully retrieved the fear memory, as shown in E1.1, but only shortly. For the rest of the paradigm, GAD65 KO did not retain the acquired fear-context association, indicating a potential contextual fear memory deficit.

In addition, to assess if a different number of hippocampal cells was activated during the last session of the behavioral paradigm (SR), c-Fos expression was estimated using immunohistochemistry. The signal analysis showed that the number of c-Fos$^+$ neurons remained unchanged in both CA3 (Fig. 3.5Ba; Mann-Whitney U test; $p = 0.4914$) and CA1 subregions (Fig. 3.5Bb; Mann-Whitney U test; $p = 0.829$).

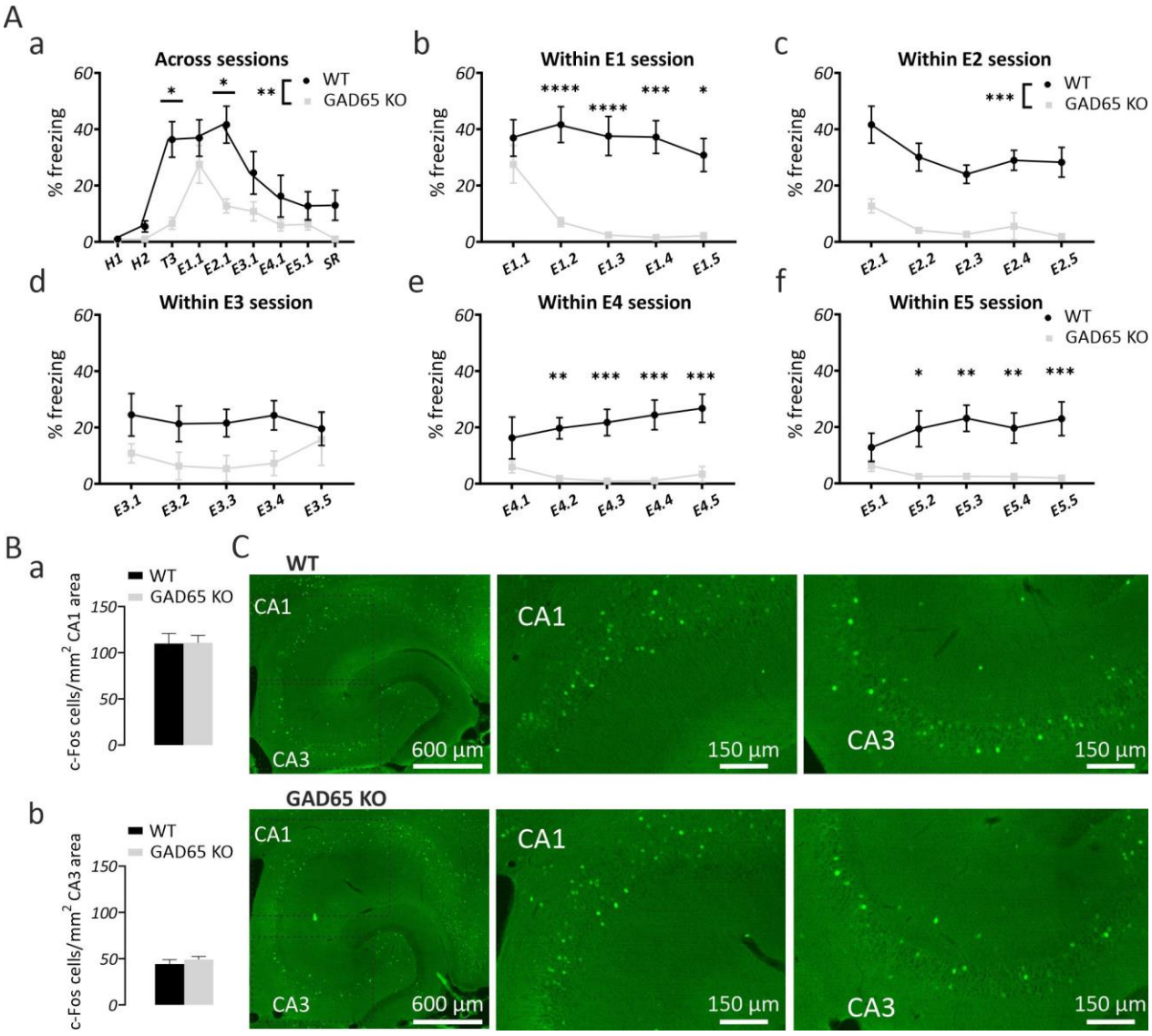

Fig. 3.5: Freezing levels during contextual FC and c-Fos expression in GAD65 KO mice. (Aa) *Graph illustrating the freezing time of GAD65 KO and WT mice across the FC paradigm. Both genotypes showed low freezing levels during habituation, which increased after the shock delivery (T3) and the retrieval session (E1.1). Upon the end of the extinction series, freezing levels were decreased without a re-activation during the spontaneous recovery (SR) session. Strikingly, GAD65 KO mice showed persistently lower freezing than the WT mice, except during the E1.1 session.* ***(Ab-e)*** *Graphs demonstrating inter-session freezing levels of GAD65 KO and WT mice during extinction. Each extinction session lasted in total 10 min, and data are presented in 2-min bins.* ***(Ab)*** *During E1.1, both genotypes displayed comparable freezing levels, but after E1.2, they differentiated with GAD65 KO mice showing constant low freezing.* ***(Ac)*** *Similarly, in the E2 session, GAD65 KO mice showed decreased freezing compared to WT.* ***(Ad)*** *In the E3 session, mice showed no significant differences but a trend for decreased freezing in GAD65 KO mice compared to WT. Last,* ***(Ae)*** *during E4 and* ***(Af)*** *E5 sessions, both genotypes showed similar freezing in the first bin, followed by close to zero values for GAD65 KO and freezing at ˜20% of the total time for the WT.* ***(Ba)*** *Number of c-Fos⁺ cells in the CA3 area and* ***(Bb)*** *CA1 area was comparable between the genotypes.* ***(C)*** *Representative microscopic images showing comparable c-Fos expression in the vHP of GAD65 KO and WT mice after the SR session. H1: Habituation session 1; H2: Habituation session 2; T3: Last 2 min of the training session (after the shock delivery); E1-E5: extinction sessions 1-5; In each extinction session, a second number indicates*

*the 2-min bin interval; SR: spontaneous recovery session. Statistical comparison was performed using two-way RM ANOVA and post-hoc Sidak's test for **Aa-f** and Mann-Whitney for **Ba-b**. Data are given as mean ± SEM. WT: N = 9 mice, GAD65 KO: N = 10 mice.*

3.1.3.2 Altered hippocampal SW-R in GAD65 KO mice after contextual FC

After the end of the behavioral paradigm, LFP recordings *ex vivo* in horizontal brain slices were performed, and the spontaneous SW-R in areas CA3 and CA1 in the vHP were measured. In the CA3 region, SW-R were enhanced showing increased SW incidence (Fig. 3.6c; Student's one-tailed t-test; T(49) = 2.18, p = 0.0341) and AUC (Fig. 3.6f; Mann-Whitney U test; p = 0.0049) in GAD65 KO mice compared to WT mice. However, the signal-to-noise ratio (Fig. 3.6b; Mann-Whitney U test; p = 0.4122), the ripple amplitude (Fig. 3.6d; Mann-Whitney U test; p = 0.2853), and the ripple frequency (Fig. 3.6e; Mann-Whitney U test; p = 0.8876) were unaltered between the genotypes. In contrast to the CA3 subregion and similar to the findings from naive mice, SW-R incidence in the CA1 subregion was significantly decreased in GAD65 KO mice compared to WT mice (Fig. 3.6h; Student's one-tailed t-test; T(49) = 2.060, p = 0.0447). Assessment of the signal-to-noise ratio (Fig. 3.6g; Mann-Whitney U test; p = 0.2050), ripple amplitude (Fig. 3.6i; Mann-Whitney U test; p = 0.1265), ripple frequency (Fig. 3.6j; Student's one-tailed t-test; T(49) = 0.3914, p = 0.6972) and AUC (Fig. 3.6k; Mann-Whitney U test; p = 0.6172) revealed no changes between the genotypes. Furthermore, examination of CA3-CA1 interactions during SW-R revealed significantly higher propagation failure rates in GAD65 KO mice than in WT mice (Fig. 3.7a; Student's one-tailed t-test; T(39) = 2.116, p = 0.0407). In addition, waveform correlation analysis of the low pass-filtered SW signal between the two regions showed no alterations when comparing all events in both regions (Fig. 3.7b; Mann-Whitney U test; p = 0.8051), nor upon the comparison of only the connected events (Fig. 3.7c; Mann-Whitney U test; p = 0.995). Similarly, the correlation of SW-peak amplitude in the CA3 and CA1 subregions showed no changes between the genotypes (Fig. 3.7d; Mann-Whitney U test; p = 0.6918).

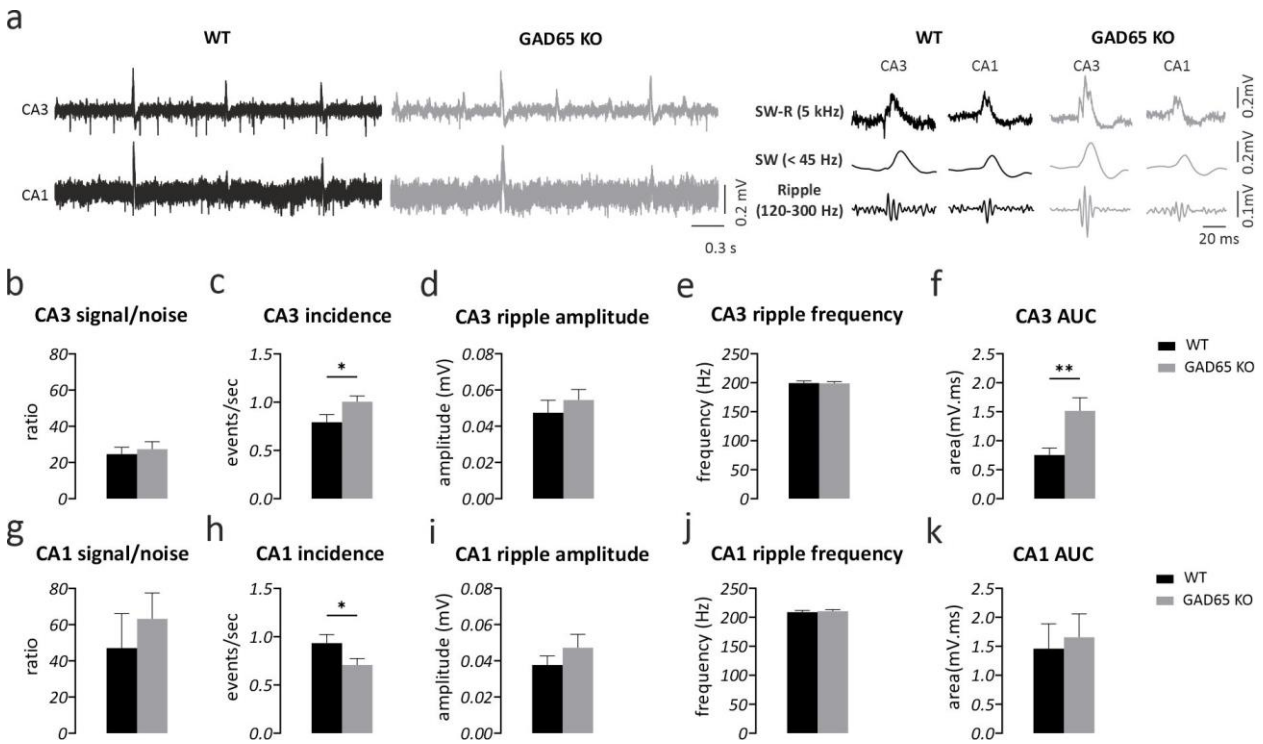

Fig. 3.6: Altered SW-R in CA3 and CA1 regions of the vHP in GAD65 KO mice after contextual re-exposure. ***(a)*** *Representative traces of SW-R recorded in the CA3 and CA1 of the vHP of GAD65 KO and WT mice. Note the enhanced SW-R in the CA3 and the decreased SW-R events in the CA1. On the right, SW-R traces of sampling rate 5 kHz are low-pass filtered (<45 Hz), illustrating the sharp wave component, or band-pass filtered (120-300 Hz), illustrating the ripple component. Summary graphs exhibiting* ***(b)*** *unaltered signal-to-noise rate,* ***(c)*** *increased incidence,* ***(d)*** *unaltered ripple amplitude and* ***(e)*** *ripple frequency, and* ***(f)*** *increased AUC in the CA3 region of GAD65 KO mice compared to WT. Comparison of SW-R in the CA1 region revealed* ***(h)*** *decreased SW incidence in GAD65 KO compared to WT mice but unaltered* ***(g)*** *signal-to-noise ratio,* ***(i)*** *ripple amplitude* ***(j)*** *ripple frequency, and* ***(k)*** *AUC. Statistical comparison was performed using Student's t-test for* ***c***, ***h***, ***j,*** *and Mann-Whitney for* ***b***, ***d***, ***e***, ***f***, ***g***, ***i***, ***k***. *Data are given as mean ± SEM. WT: N = 4 mice, n = 22 slices; GAD65 KO: N = 5 mice, n = 29 slices. For* ***a***, ***f***: *WT: N = 4 mice, n = 18 slices; GAD65 KO: N = 5 mice, n = 23 slices. *p < 0.05, **p < 0.01. AUC: area under the curve.*

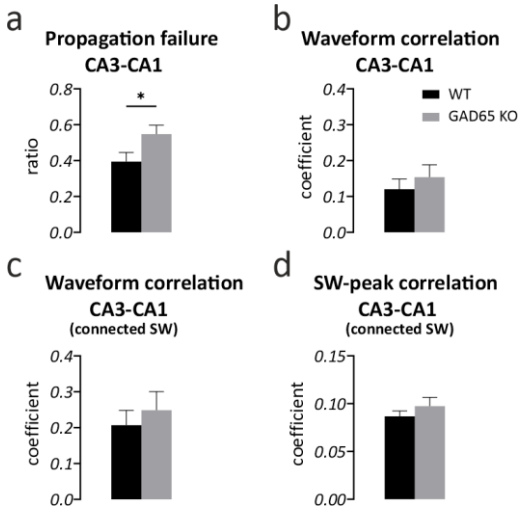

Fig. 3.7: Altered CA3-CA1 interactions during SW-R in GAD65 KO mice after contextual re-exposure. *Summary graphs illustrating* ***(a)*** *increased propagation failure in GAD65 KO compared to WT mice, but unaltered waveform correlation of* ***(b)*** *all detected SW-R events,* ***(c)*** *of the connected CA3-CA1 SW-R events and* ***(d)*** *unchanged SW-peak amplitude correlation between the groups. Statistical comparison was performed using Student's t-test for* ***a*** *and Mann-Whitney for* ***b***, ***c***, ***d***. *Data are given as mean ± SEM. WT: N = 4 mice, n = 18 slices; GAD65 KO: N = 5 mice, n = 23 slices. *p < 0.05.*

3.2 Cellular and network correlates of altered SW-R in GAD65 KO mice - STUDY 2

In Study 1, the *in vitro* SW-R in the CA3 and CA1 regions of the vHP in GAD65 KO mice were examined. Naïve GAD65 KO mice exhibited enhanced SW-R properties (ripple amplitude and AUC) in the CA3 area and reduced SW-R incidence in the CA1 region. The same direction of findings followed after FC, with a prominent SW-R propagation failure from the CA3 to CA1 region. The enhanced SW-R in the CA3 area would imply increased excitability of the network, in line with the GABA deficiency of the animal model. However, the reduced CA1 incidence would suggest the opposite. Previous studies (Behrens et al., 2005; Suh et al., 2013; Zeng et al., 2001) demonstrated that enhancements in plasticity and excitability in the hippocampus were associated with changes in SW incidence, such as occurrence of SW-R in the CA3 area after LTP induction in the mossy fibers-CA3 synapse. Thus, I hypothesized that the reduced CA1 SW incidence, observed in GAD65 KO mice, could be due to a decrease in the baseline synaptic excitability or plasticity in the CA1 region. For this reason, the field excitatory postsynaptic potentials (fEPSP) in the CA3-CA1 synapse via stimulation of the Schaffer collaterals (SC) was assessed. Additionally, to investigate if the excitation/inhibition balance in the CA1 region was associated with alterations at the cellular level, I performed patch-clamp electrophysiology and investigated the intrinsic and synaptic properties of CA1 pyramidal cells.

3.2.1 Unaltered excitability and plasticity at the SC-CA1 synapse

To describe the synaptic efficacy and excitability, an input-output curve was generated from the voltage responses and the current stimuli in the range of 5-100 μA. Analysis of the fiber volley (fv) amplitude (Fig. 3.8d; two-way RM ANOVA/Mixed-effects analysis; $F(1,24) = 0.1125$, $p = 0.7402$), the fEPSP slope (Fig. 3.8e; two-way RM ANOVA; $F(1,24) = 0.9854$, $p = 0.3308$) and the average in all intensities of the ratio between the fEPSP value and the corresponding fv value (Fig. 3.8f; Mann-Whitney U test; $p = 0.1005$) revealed no differences between the groups. Furthermore, to assess a potential change in the short-term plasticity, paired pulses of increasing stimulation intervals (10 to 500 ms) were applied, and the fEPSP responses were recorded and calculated as ratios (PPR). The PPR analysis revealed no genotype effect (Fig. 3.8g; two-way RM ANOVA; $F(1,24)$

= 0.009, p = 0.923). Similarly, two high-frequency stimulation trains (HFS) of 100 Hz were applied after a stable baseline to assess the long-term plasticity. The calculation of the fEPSP responses, 30 to 40 min after the HFS, normalized to the baseline, remained unaltered between the groups (Fig. 3.8j; Mann-Whitney U test; p = 0.55). Examination of the synaptic fatigue, calculated as the fEPSP responses within the first HFS, showed no differences between the groups (Fig. 3.8i; multiple Mann-Whitney U tests; p > 0.05). These results demonstrate an unaffected SC-CA1 baseline excitability, synaptic efficacy, and short- and long-term plasticity in GAD65KO compared to WT mice.

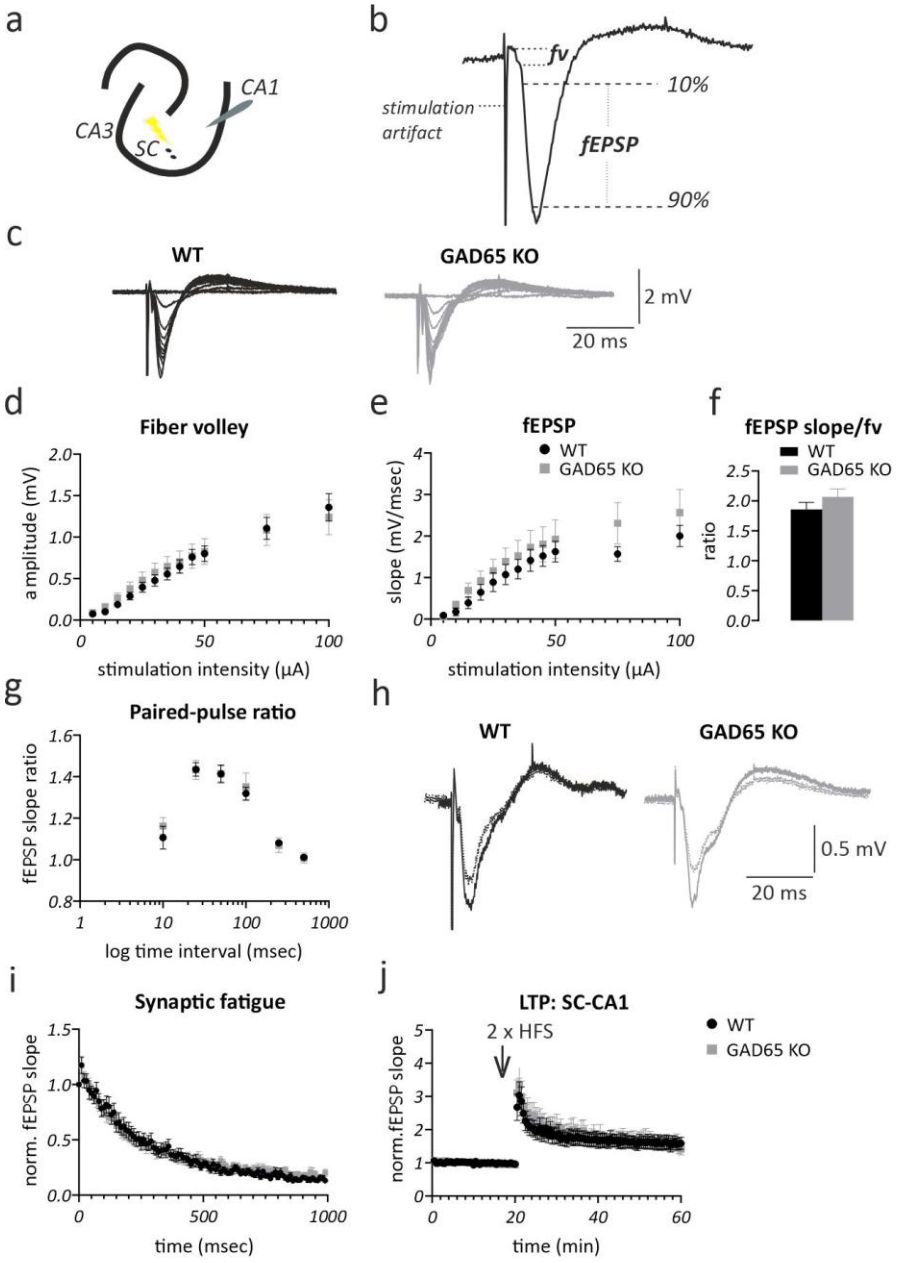

Fig. 3.8: Unaltered baseline excitability, short- and long-term plasticity at the SC-CA1 synapse of GAD65 KO mice. (a) *Sketch illustrating the location of the stimulating electrode at the SC and the recording electrode at the s.r. of the CA1 area.* ***(b)*** *Example of a recorded response that consists of the stimulation artifact, the fiber volley (fv), and the fEPSP. The fEPSP slope was calculated as the value between 10% and 90% of the maximum amplitude divided by time.* ***(c)*** *Merged traces of fEPSP in response to stimulation intensities between 5 and 100 µA. Summary graphs indicating unaltered* ***(d)*** *fv amplitude and* ***(e)*** *fEPSP slopes in response to incremental increases of stimulation intensity.* ***(f)*** *Graph of the fEPSP ratios by the corresponding fv showing unaltered synaptic efficacy in the SC-CA1 synapse between the genotypes.* ***(g)*** *Paired-pulse ratio summary graph of fEPSP slope ratios in stimulus intervals of 10-500 ms illustrating no difference between the genotypes.* ***(h)*** *Traces of baseline (dashed) and fEPSP responses 40 min after LTP induction in WT and GAD65 KO. Summary plots illustrating no changes* ***(i)*** *in the synaptic fatigue within the first HFS train (values normalized to the first fEPSP response) and* ***(j)*** *in the LTP induction of SC-CA1 synapse (fEPSP responses normalized to the baseline). High-frequency stimulation (HFS): two times 100 Hz bursts of 1 sec. Statistical comparison was performed using two-way RM ANOVA/mixed effects for* ***d, e, h****, Mann Whitney U test for* ***f*** *and* ***j****, and multiple Mann- Whitney tests for* ***i****. Data are given as mean ± SEM. WT: N = 7 mice, n = 16 slices; GAD65 KO: N = 4 mice, n = 10 slices.*

3.2.2 Mild reduction in CA1 pyramidal neurons intrinsic excitability of GAD65 KO mice

To assess the intrinsic excitability of CA1 pyramidal neurons, I performed patch-clamp electrophysiology and examined the subthreshold and suprathreshold membrane properties. The analysis showed that the resting membrane potential (Fig. 3.9c; Mann-Whitney U test; $p = 0.08$) had a hyperpolarizing trend in GAD65KO compared to WT mice. In line, action potential (AP) threshold was increased in GAD65KO compared to WT mice (Fig. 3.9f; Student's two-tailed t-test; $T(29) = 2.268$, $p = 0.031$). On the contrary, input resistance (Fig. 3.9d; Mann-Whitney U test; $p > 0.99$), the membrane potential responses after current pulse injection depicted as input-output curve (Fig. 3.9b; multiple unpaired t-tests; $p > 0.05$) and the rheobase (Fig. 3.9i; Student's two-tailed t-test; $T(29) = 1.583$, $p = 0.1243$) remained unaltered between the genotypes. Additionally, AP amplitude (Fig. 3.2g; Mann-Whitney U test; $p = 0.4173$), 1st AP maximum rising slope (Fig. 3.9h; Mann-Whitney U test; $p = 0.5453$) and firing frequency in response to increasing current steps (Fig. 3.9e; multiple unpaired t-tests; $p > 0.05$) showed no significant differences between genotypes. These data suggest a minor decrease in the intrinsic excitability of CA1 pyramidal cells in GAD65 KO compared to WT mice.

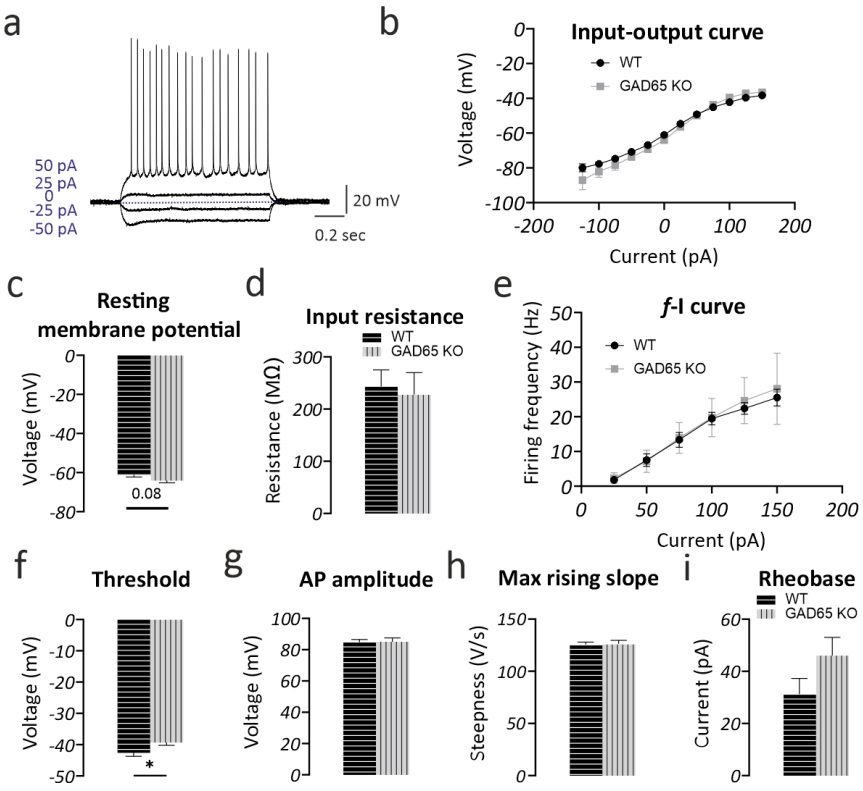

Fig. 3.9: Intrinsic properties of CA1 pyramidal cells in the vHP of GAD65 KO mice. (a) *Voltage responses (output) of a current-clamped neuron after current injection steps (input). Current amplitude is indicated in purple color.* ***(b)*** *Summary graph illustrating that Input-output curve (voltage in response to current steps) was not different between the genotypes. Analysis of subthreshold properties revealed a tendency for increased* ***(c)*** *resting membrane potential but* ***(d)*** *unaltered input resistance in GAD65 KO mice compared to WT mice. Analysis of suprathreshold properties indicated* ***(e)*** *I-f curve showing unaltered AP firing frequency in response to current steps,* ***(f)*** *increased threshold for action potential (AP) generation,* ***(g)*** *unaltered AP amplitude,* ***(h)*** *unaltered maximum steepness of AP rising phase and* ***(i)*** *unaltered rheobase between the genotypes. Statistical comparison was performed using Student's t-test for* ***f, b****, Mann-Whitney U test for* ***c, d, g, h*** *& multiple unpaired t-tests for* ***b, e****. WT: N = 8 mice, n = 15 cells; GAD65 KO: N = 9 mice, n = 16 cells. Data are given as mean ± SEM. *p < 0.05. f-I curve: firing frequency vs. current.*

3.2.3 Mild increase in the IPSC on CA1 pyramidal neurons of GAD65 KO mice

To investigate if the changes of CA1 pyramidal cell intrinsic properties are synaptically driven, I examined the synaptic properties of CA1 pyramidal cells. For this, the patch-clamp technique was used and the spontaneous postsynaptic inhibitory currents (sIPSC) were measured, which represent the inhibitory input to CA1 pyramidal cells. The inhibitory postsynaptic currents of the local circuits were isolated by blocking the glutamatergic receptors, and the IPSC-events occurring during a 5-minute recording were analyzed. Analysis showed that the sIPSC amplitude (Fig. 3.10b; Student's two-tailed t-test; T(19) = 0.1858, p = 0.8546), sIPSC frequency (Fig. 3.10c; Mann-

Whitney U test; p = 0.2872) and sIPSC kinetics; rise- (Fig. 3.10d; Student's two-tailed t-test; T(19) = 0.8401, p = 0.4113) and decay-time (Fig. 3.10e; Student's two-tailed t-test; T(19) = 0.0005207, p = 0.9996) remained unaltered. However, examining the cumulative distribution of 150 events per cell occurring within 60 sec, the distribution of frequency (Fig. 3.10g; Kolmogorov-Smirnov test; p < 0.00001) was altered significantly between the groups, while the amplitude (Fig. 3.10f; Kolmogorov-Smirnov test; p = 0.309) remained unchanged. Specifically, the frequency distribution of GAD65 KO mice was shifted to the right compared to the WT mice supporting the trend found in the average frequency values for increased frequency in naïve GAD65 KO mice.

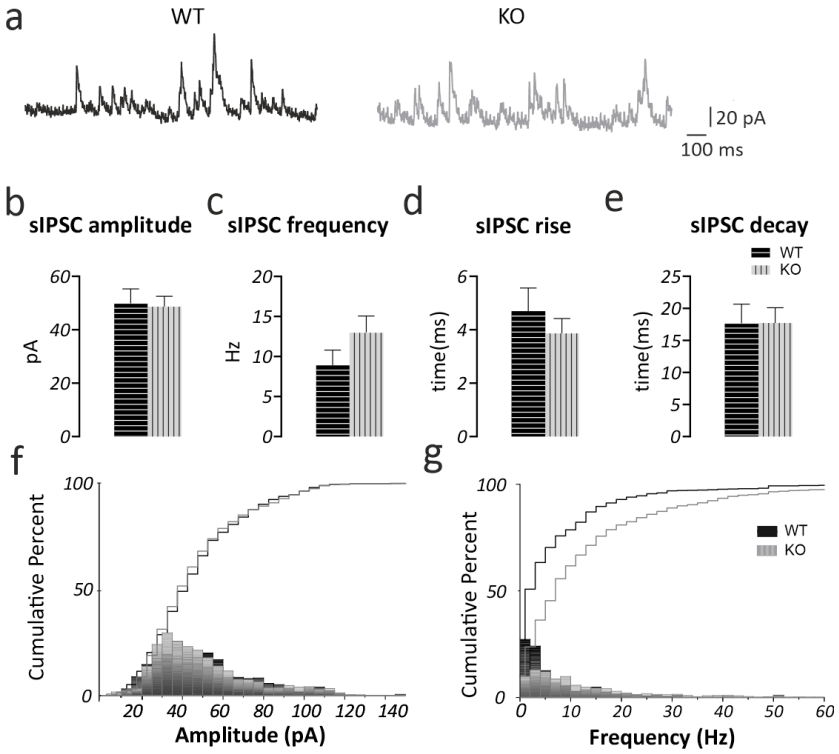

Fig. 3.10: Spontaneous inhibitory postsynaptic currents on CA1 pyramidal neurons. (a) *Representative traces of voltage-clamped CA1 pyramidal neurons at 0 mV. Summary graphs illustrating that* ***(b)*** *the amplitude and* ***(c)*** *frequency, as well as the kinetics of sIPSC* ***(d)*** *rise- and* ***(e)*** *decay-phase did not show any differences between the genotypes. Histograms of cumulative distributions illustrating* ***(f)*** *the amplitude and* ***(g)*** *frequency of 150 events per cell occurring in 60 sec. Note the right shift in the frequency curve of GAD65 KO mice compared to WT mice. Statistical comparison was performed using Student's t-test for* ***b****,* ***d****,* ***e****, Mann-Whitney for* ***c*** *& Kolmogorov-Smirnov for* ***f****,* ***g****. Data are given as mean ± SEM. WT: N = 4 mice, n = 7 cells, GAD65 KO: N = 5 mice, n = 14 cells.*

3.2.4 Compound postsynaptic currents on CA1 pyramidal cells during SW-R

It has been shown that changes in the SW-R properties might be associated with altered excitation-inhibition (E/I) balance, specifically during SW-R (Maier et al., 2012). To assess this, I performed simultaneous patch-clamp and extracellular LFP recordings. The compound postsynaptic activity in the CA1 pyramidal cells in relation to the LFP SW-R event originating from the CA3 area was assessed. The intracellular pipette contained a Cs-based solution, while the LFP pipette standard aCSF solution. Single CA1 pyramidal cells were voltage-clamped at the reversal potential of excitatory postsynaptic receptors (~0 mV) to record the compound (c) IPSC and at the reversal potential of fast GABAergic chloride channels (-70 mV) to record compound (c) EPSC. This approach allowed to assess excitatory and inhibitory input converging onto single pyramidal cells in an intact hippocampal CA3-CA1 network able to produce oscillatory activity and spontaneously occurring SW-R without any pharmacological blocker. The amplitude (Fig. 3.11c; Mann-Whitney U test; $p = 0.8683$), AUC (Fig. 3.11d; Mann-Whitney U test; $p = 0.6098$), rise (Fig. 3.11e; Mann-Whitney U test; $p = 0.4611$) and decay slopes (Fig. 3.11f; Mann-Whitney U test; $p = 0.6047$) of the average cIPSCs arising within 0.15 sec after a SW-R peak were comparable between GAD65 KO and WT mice. Similarly, the average cEPSC amplitude (Fig. 3.11g; Mann-Whitney U test; $p = 0.3434$), AUC (Fig. 3.11h; Student's two-tailed t-test; $T(10) = 1.23$, $p = 0.2470$), rise (Fig. 3.11i; Mann-Whitney U test; $p = 0.2677$) and decay slope (Fig. 3.11j; Mann-Whitney U test, $p = 0.999$) exhibited no significant differences between the groups.

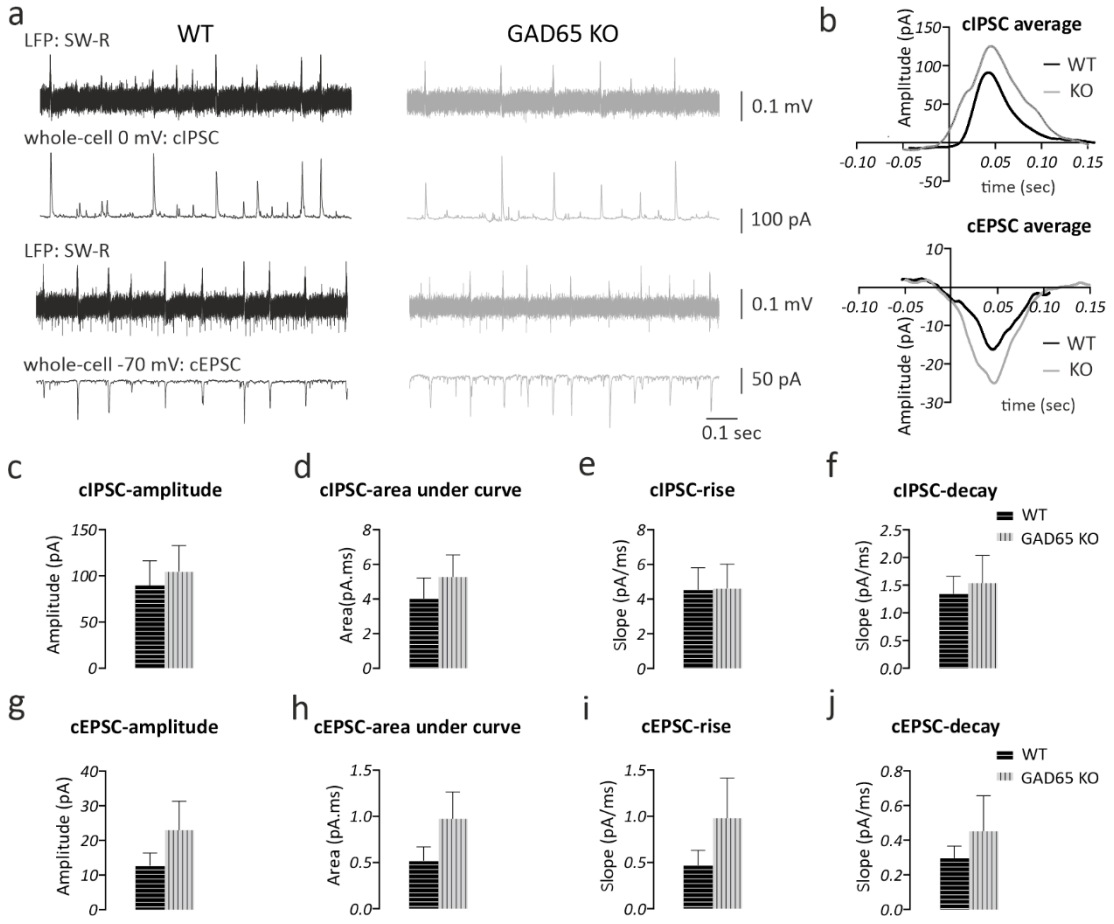

Fig. 3.11: Compound postsynaptic currents on CA1 pyramidal cells driven by SW-R events. (a) *Representative traces of SW-R, recorded in the CA3 region of the vHP and cIPSC or cEPSC, recorded from CA1 pyramidal cells in GAD65 KO and WT mice. Note the increased amplitude of cI/EPSC events that occurred in time with SW-R and the smaller amplitude cI/EPSC that occurred irrespectively of a SW-R event.* ***(b)*** *Example graphs illustrating the waveform average of cIPSC or cEPSC events that occurred 0.03-0.15 sec after a SW-R event. Note a trend for increased amplitude of compound postsynaptic currents in GAD65 KO mice compared to control. Summary graphs illustrating unchanged* ***(c)*** *cIPSC amplitude,* ***(d)*** *AUC,* ***(e)*** *rise, and* ***(f)*** *decay slope between the genotypes. Similarly, cEPSC* ***(g)*** *amplitude,* ***(h)*** *AUC,* ***(i)*** *rise, and* ***(j)*** *decay slope showed no significant differences between the genotypes. Note a trend for increased cEPSC magnitude and slower rise of GAD65 KO mice compared to WT. Statistical comparison was performed using Student's t-test for* ***h*** *and Mann-Whitney for* ***c***-***g***, ***i***, ***j***. *Data are given as mean ± SEM. For cEPSC WT: N = 5 mice, n = 5 cells, KO: N = 7 mice, n = 7 cells; for cIPSC WT: N = 6 mice, n = 11 cells, KO: N = 8 mice, n = 15 cells.*

3.2.5 Increasing specificity of the GAD65 KO model: local GAD65 decrease in the vHP

Previously, the *in vitro* electrophysiological profile of GAD65 KO mice, such as oscillatory activity, synaptic plasticity, and excitability, were described with focus on CA3-CA1 interactions. To understand whether local GABAergic changes in the vHP have a critical role on the observed phenotype in global GAD65 KO mice, I carried out two local knock-down (KD) experiments targeting either the CA1 or the DG-CA3 areas of the vHP. A lentiviral construct was injected intracranially in the hippocampi of C57BL/6 male mice. The construct contained GAD65 shRNA, which reduced GAD65 translation (Tripathi et al., 2021), or a random shRNA sequence as a control.

3.2.5.1 Unaltered SW-R after local GAD65 decrease in the vDG-vCA3 circuit

Two weeks after local vCA3-vDG injections, the mouse brains were prepared for slice electrophysiology, and the LFP network oscillations in CA3 and CA1 of vHP were investigated. The spontaneous SW-R in the CA1 and CA3 subregions of the vHP did not differ between the GAD65 KD and control group. Specifically, in the CA3 region, the signal-to-noise ratio (Fig. 3.12b; Mann-Whitney U test; $p = 0.81$), SW incidence (Fig. 3.12c; Student's two-tailed t-test; $T(65) = 0.3585$, $p = 0.7212$), ripple amplitude (Fig. 3.12d; Mann-Whitney U test; $p = 0.7201$), ripple frequency (Fig. 3.12e; Student's two-tailed t-test; $T(65) = 0.1745$, $p = 0.862$) and AUC (Fig. 3.12f; Mann-Whitney U test; $p = 0.7581$) remained unaltered between the groups. Similarly, in the CA1 subregion, signal-to-noise ratio (Fig. 3.12g; Mann-Whitney U test; $p = 0.8671$), SW incidence (Fig. 3.12h; Student's two-tailed t-test; $T(65) = 0.1231$, $p = 0.9024$), ripple amplitude (Fig. 3.12i; Mann-Whitney U test; $p = 0.1592$), ripple frequency (Fig. 3.12j; Student's two-tailed t-test; $T(65) = 1.682$, $p = 0.0974$) and AUC (Fig. 3.12k; Mann-Whitney U test; $p = 0.9950$) showed no differences between the groups. Investigating the CA3-CA1 network interactions during SW-R, similar propagation rates were observed between the groups (Fig. 3.13a; Student's two-tailed t-test; $T(59) = 1.818$, $p = 0.0741$). Furthermore, the waveform correlation of all SW events between CA3 and CA1 regions (Fig. 3.13b; Mann-Whitney U test; $p = 0.5263$) and of the connected SW events (observation of SW-R in CA1 in a certain time window after CA3) (Fig. 3.13c; Mann-Whitney U test; $p = 0.3621$) did not show any alterations. Similarly, SW-peak amplitude correlation (Fig. 3.13d; Mann-Whitney U test; $p = 0.1894$) showed no differences between the groups. These

results indicate a potential secondary role of the CA3 region in the SW-R changes observed in the global GAD65 KO model.

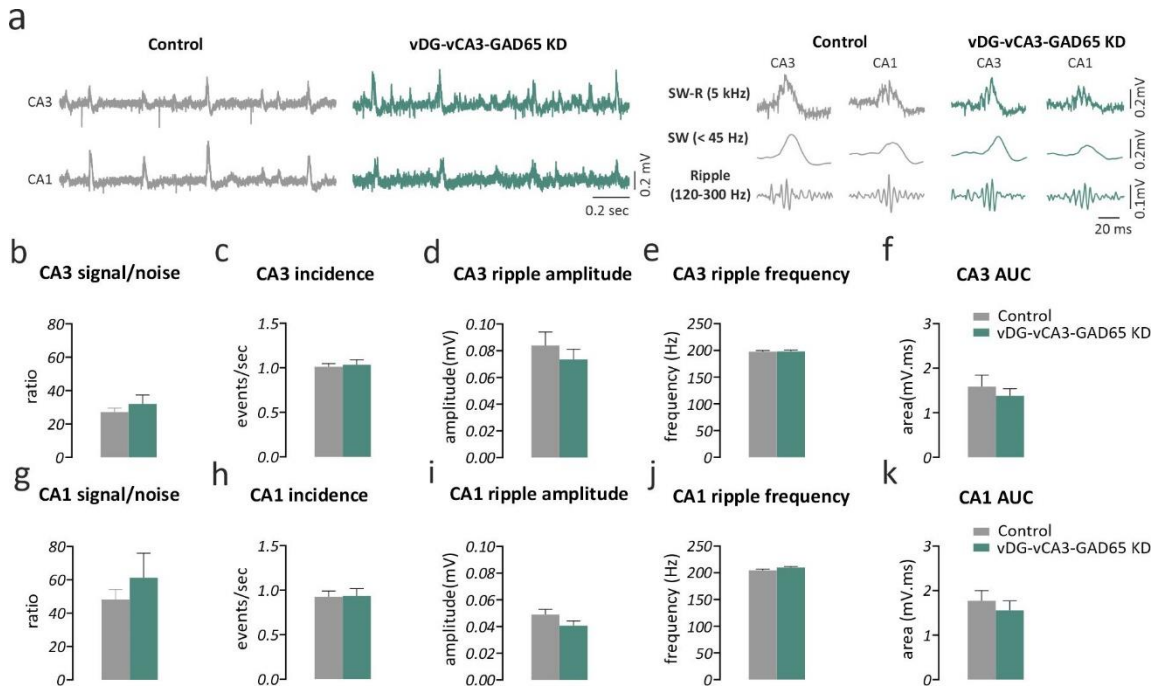

Fig. 3.12: Unaltered SW-R in CA3 and CA1 regions of the vHP upon local DG-CA3 GAD65 reduction. (a) *Representative traces of SW-R recorded in the CA3 and CA1 of the vHP in vDG-vCA3 GAD65 KD and WT mice. On the right, SW-R traces of sampling rate 5 kHz are low-pass filtered (<45 Hz), illustrating the sharp wave component or band-pass filtered (120-300 Hz), illustrating the ripple component. Summary graphs demonstrating unaltered* ***(b)*** *signal-to-noise ratio,* ***(c)*** *SW incidence,* ***(d)*** *ripple amplitude,* ***(e)*** *ripple frequency, and* ***(f)*** *AUC in the CA3 region. Similarly, SW-R in the CA1 region showed no differences between the groups in* ***(g)*** *signal-to-noise ratio,* ***(h)*** *incidence,* ***(i)*** *ripple amplitude,* ***(j)*** *ripple frequency, and* ***(k)*** *AUC. Statistical comparison was performed using Student's t-test for* ***c, e, h, j*** *and Mann-Whitney for* ***b, d, f, g, i, k****. Data are given as mean ± SEM. *p < 0.05. Control: N = 12 mice, n = 38 slices, vDG-vCA3-GAD65KD: N = 11 mice, n = 29 slices. Control: random shRNA. AUC: area under the curve.*

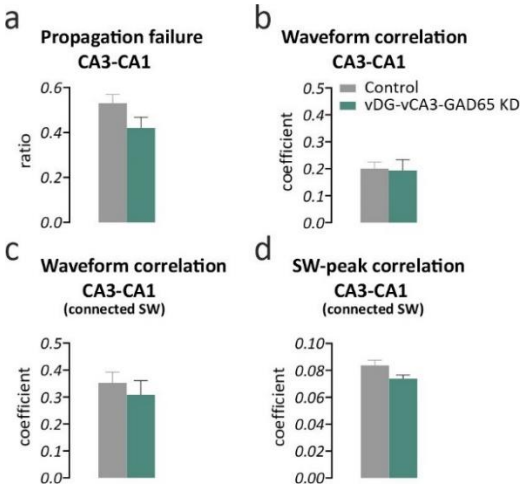

Fig. 3.13: Unaltered CA3-CA1 network interactions during SW-R upon local DG-CA3 GAD65 reduction. *Summary plots illustrating unaltered* ***(a)*** *SW-R propagation failure along the CA3-CA1 axis,* ***(b)*** *unaltered waveform correlation of all detected SW-R events* ***(c)*** *unaltered waveform correlation of connected CA3-CA1 SW-R events and* ***(d)*** *unaltered SW-peak amplitude correlation between the groups. Statistical comparison was performed using Student's t-test for* ***a*** *and Mann-Whitney for* ***b****,* ***c****,* ***d****. Data are given as mean ± SEM. control: N = 12 mice, n = 38 slices control; vDG-vCA3-GAD65KD: N = 11 mice, n = 29 slices.*

3.2.5.2 CA1-specific alterations in SW-R upon local GAD65 decrease in the vCA1

Two weeks after injections, LFP recordings were performed in slices containing the vHP with GAD65 KD in the vCA1 and in control slices. Analysis of the spontaneous SW-R showed in the CA3 subregion, a trend for increased SW incidence (Fig. 3.14c; Student's one-tailed t-test; $T(48) = 1.845$, $p = 0.0713$) and frequency of ripples (Fig. 3.14e; Student's one-tailed t-test; $T(48) = 1.985$, $p = 0.0529$). However, no alterations in the signal-to-noise ratio (Fig. 3.14a; Mann-Whitney U test; $p = 0.341$), ripple amplitude (Fig. 3.14d; Mann-Whitney U test; $p = 0.4644$) and AUC (Fig. 3.14f; Mann-Whitney U test; $p = 0.2736$) were evident. On the other hand, in the CA1 subregion, ripple amplitude (Fig. 3.14i; Mann-Whitney U test; $p = 0.0245$) and ripple frequency (Fig. 3.14j; Student's one-tailed t-test; $T(48) = 2.229$, $p = 0.0305$) were significantly decreased in the vCA1-GAD65 KD compared to the control mice, whereas no alterations in the signal-to-noise ratio (Fig. 3.14g; Mann-Whitney U test; $p = 0.223$), SW incidence (Fig. 3.14h; Mann-Whitney U test; $p = 0.515$.) and AUC (Fig. 3.14k; Mann-Whitney U test; $p = 0.2014$) were evident. Additionally, no changes in the propagation failure rates between the groups were observed (Fig. 3.15a; Mann-Whitney U test; $p = 0.8777$). The correlation analysis of the signal between CA3 and CA1 region showed a trend for increased correlation of vCA1-GAD65 KD mice when all SW events in CA3 & CA1 regions (Fig. 3.15b; Mann-Whitney U test; $p = 0.0820$) or only the connected SW events were compared (Fig. 3.15c; Mann-Whitney U test; $p = 0.0729$). However, SW-peak amplitude correlation of CA3 and CA1 events showed no changes between the genotypes (Fig. 3.15d; Mann-Whitney U test; $p = 0.4252$). These results exhibit specifically diminished ripple characteristics in the CA1 area of the vHP upon local GAD65 reduction in this region.

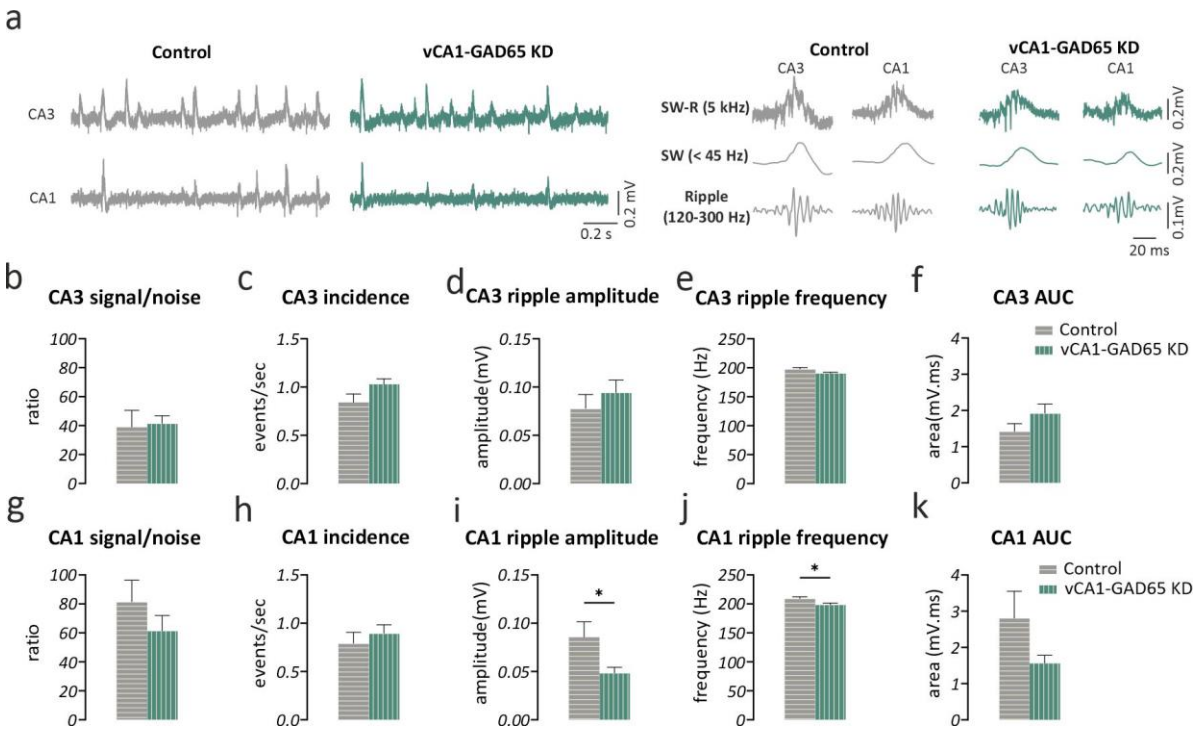

Fig. 3.14: SW-R in the CA3 and CA1 regions of the vHP upon local CA1 GAD65 reduction. (a) *Representative traces of SW-R recorded in the CA3 and CA1 of vHP of vCA1-GAD65 KD and control mice. Note the decreased SW-R in the CA1 region. On the right, SW-R traces of sampling rate 5 kHz are low-pass filtered (<45 Hz), illustrating the sharp wave component or band-pass filtered (120-300 Hz), illustrating the ripple component. Summary graphs demonstrating unaltered* ***(b)*** *signal-to-noise ratio,* ***(c)*** *incidence,* ***(d)*** *ripple amplitude,* ***(e)*** *ripple frequency, and* ***(f)*** *AUC in the CA3 region. In the CA1 region* ***(g)*** *signal-to-noise ratio,* ***(h)*** *incidence and* ***(k)*** *AUC remained unaltered, but* ***(i)*** *ripple amplitude and* ***(j)*** *ripple frequency decreased in vCA1 GAD65 KD mice compared to control. Statistical comparison was performed using Student's t-test for* ***c***, ***e***, ***j,*** *and Mann-Whitney for* ***b***, ***d***, ***f***, ***g***, ***h***, ***i***, ***k****. Data are given as mean ± SEM. *p < 0.05. Control: N = 3 mice, n = 18 slices; vCA1-GAD65 KD: N = 5 mice, n = 32 slices; for* ***b***, ***g*** *control: N = 3 mice, n = 21 slices; vCA1-GAD65 KD: N = 5 mice, n = 33 slices. AUC: area under the curve.*

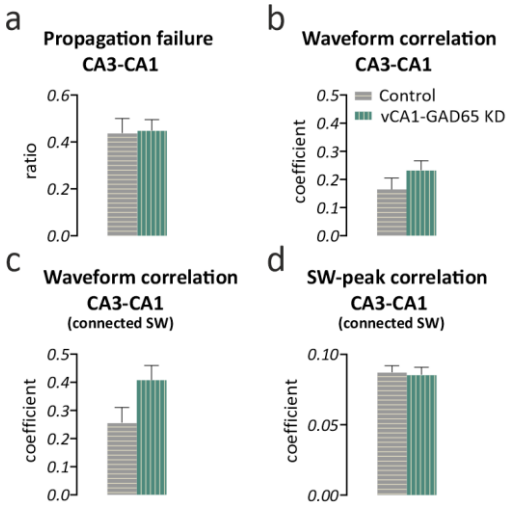

Fig. 3.15: Unaltered CA3-CA1 network interactions during SW-R in the vHP upon local CA1 GAD65 reduction. *Summary plots illustrating unaltered* ***(a)*** *SW-R propagation failure along the CA3-CA1 axis,* ***(b)*** *unaltered waveform correlation of all detected SW-R events* ***(c)*** *unaltered waveform correlation of connected CA3-CA1 SW-R events and* ***(d)*** *unaltered SW-peak amplitude correlation between the groups. Statistical comparison was performed using Mann-Whitney U test for all. Data are given as mean ± SEM. control: N = 3 mice, n = 21 slices; vCA1-GAD65 KD: N = 5 mice, n = 33 slices.*

3.3 Behavioral correlates of SW-R - STUDY 3

SW-R are observed in the hippocampus during consummatory behaviors and slow-wave sleep and are associated with memory consolidation and retrieval (Buzsáki, 2015; Jai & Frank, 2015; Joo & Frank, 2018; O'Neill et al., 2006; Pfeiffer & Foster, 2013). The consolidation process is crucial for the transition of recently experienced events into long-lasting memories that will be retrieved for successful future decisions. Disruption of SW-R during these processes eliminates memory formation of recent events (Ego-Stengel & Wilson, 2010; Girardeau et al., 2009; Jadhav et al., 2012). However, do SW-R carry information regarding the content of the experiences? To investigate this question in a healthy system, I used wild-type C57BL/6 mice that underwent a hippocampus-dependent memory task, a contextual fear conditioning paradigm. Precisely, to determine whether SW-R convey information regarding the contextual adversity, I introduced three electrical stimuli in the paradigm with different intensities (low: 1 x 0.3 mA x 1 sec; mild: 3 x 0.4 mA x 1 sec; high: 3 x 0.5 mA x 2 sec). Additionally, to understand whether the (re)consolidation of a recent fear memory would be differentially represented from the (re)consolidation of its extinction, I stopped the paradigm after the first two minutes of extinction session 1 (E1.1) or after five ten-minute extinction sessions (until E5). Then, the freezing levels during the FC paradigm were assessed, and slice LFP electrophysiology was performed.

3.3.1 Freezing levels during contextual FC and extinction

Behavioral analysis showed increased freezing time in the E1 session between all shock intensities and the control (no electrical shock) animals, which decreased to the control levels upon five days of the fear extinction paradigm. Specifically, the low shock group, mild shock group, and high shock group decreased their freezing to control levels after E2, E3, and E4, respectively. Significant effect of shock was evident (Fig. 3.16a; two-way RM ANOVA; effect of shock $F(3, 31) = 3.098$, $p = 0.041$; effect of session $F(4.030, 124.9) = 31.57$, $p < 0.0001$; shock x session interaction $F(21, 217) = 2.504$; $p = 0.0005$). Post-hoc analysis showed significant differences in the freezing levels between control and shocked groups in several sessions (Session E1; low shock vs. control: $p = 0.023$; mild shock vs. control: $p = 0.009$; high shock vs. control: $p = 0.01$, Session E2; high shock vs. control: $p = 0.029$ and mild shock vs. control: $p = 0.027$, Session E3; high shock vs. control: $p = 0.045$). Furthermore, the extinction rate, which was defined as the difference in freezing time

between E5 and E1 normalized to the freezing in E1, was significantly different between low shock and control mice, as well as mild shock and control mice (Fig. 3.16b; one-way ANOVA; shock effect $F(3, 31) = 5.427$, $p = 0.0041$). Post-hoc analysis showed an overall decrease in freezing in all shock groups in E5 compared to E1, with the mild shock group exhibiting the highest decrease and, therefore, the best extinction rate. In more detail, the effect was obvious between mild shock vs. control mice ($p = 0.0027$) & low shock vs. control mice ($p = 0.0338$), but with a trend in high shock vs. control mice ($p = 0.0546$). In line, the extinction rates within the high shock group exhibited high heterogeneity (Fig. 3.16b; Student's one sample t-test; $T(9) = 2.785$; $p = 0.0212$). Thus, these data show comparable freezing levels of all shock groups in E1 and E5, but uneven progress across the extinction phase and a high variation inside the high shock group.

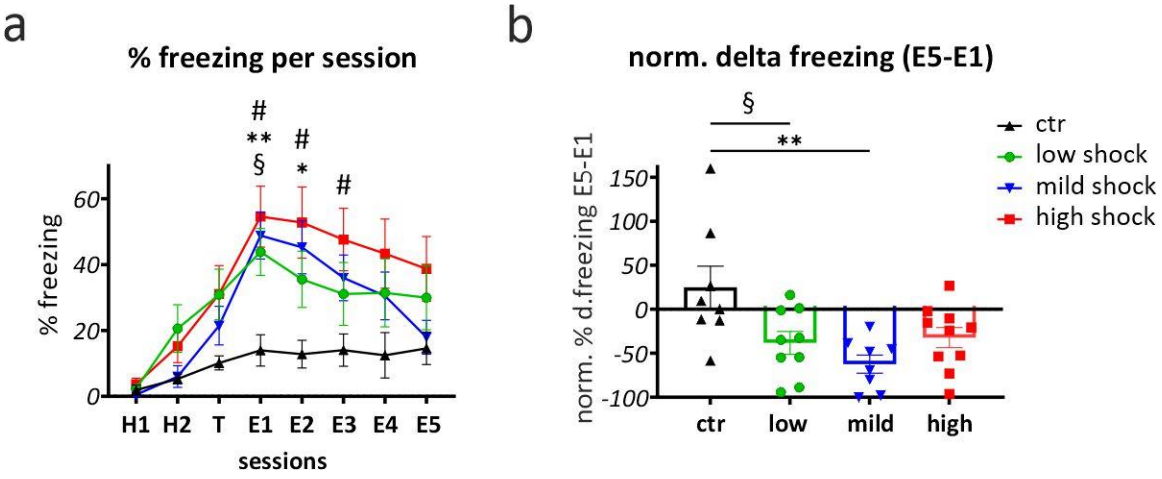

Fig. 3.16: Freezing levels during contextual fear conditioning and extinction in C57BL/6 mice. (a) *Freezing levels across all sessions of a contextual FC and extinction paradigm. Mice that received shock increased their freezing rate significantly compared to control (no shock) mice and showed extinction after E2, E3, or E4 according to the intensity of the shock, with the high shocked mice to extinguish the fear memory fully last. Specifically, in E1, all shock groups had significantly higher freezing than control animals. The freezing levels at the end of the paradigm (E5) were comparable in all groups.* ***(b)*** *Summary graph with individual animal values illustrating the fear memory extinction rate, defined as the freezing levels at E1 that were subtracted from the freezing levels at E5 and normalized to E1 freezing levels. Only the low and mild shock groups showed a significant decrease in freezing between the post-training (E1) and at the end of the paradigm (E5) compared to control. H1-H2: Habituation sessions 1 & 2; T: last 2 min of the training session; E1-E5: first 2 min of each extinction session 1-5. Statistical comparison was performed using two-way RM ANOVA for panel* ***a*** *and ordinary one-way ANOVA for panel* ***b*** *followed by post-hoc Tukey's test. Data are given as mean ± SEM. control (ctr): N = 8 mice; low shock group: N = 9 mice; mild shock group: N = 8 mice; high shock group: N = 10 mice. § $p < 0.05$: low shock vs. control; *$p < 0.05$, **$p < 0.01$: mild shock vs. control; # $p < 0.05$: high shock vs. control.*

3.3.2 Local SW-R properties in CA3 and CA1 of the ventral hippocampus after E1.1

After the session E1.1 of the contextual FC, mice were killed and the brains were prepared for slice electrophysiology and recordings of hippocampal SW-R in areas CA3 and CA1. In CA3 region, shock intensity had an overall effect on signal-to-noise ratio (Fig. 3.17b; Kruskal-Wallis; $p = 0.0001$, post-hoc control vs. low shock group: $p = 0.0008$; low shock vs. mild shock group: $p = 0.0004$) and on ripple frequency (Fig. 3.17e; one-way ANOVA; $F(3,30) = 9.746$, $p = 0.0001$, post hoc: high shock vs. control $p = 0.0002$; mild shock vs. high shock: $p = 0.0007$). On the contrary, the SW incidence (Fig. 3.17c; one-way ANOVA; $F(3, 30) = 0.8412$, $p = 0.4821$), ripple amplitude (Fig. 3.17d; one-way ANOVA; $F(3, 30) = 0.8412$, $p = 0.4821$), and AUC (Fig. 3.17f; one-way ANOVA; $F(3, 30) = 0.3460$, $p = 0.7922$) remained unaltered among the groups. Of note, in the CA1 region, significant effect of shock was observed on SW incidence (Fig. 3.17h; one-way ANOVA; $F(3, 30) = 4.116$, $p = 0.0147$), while post-hoc analysis revealed significant higher incidence in high compared to mild ($p = 0.0157$) and to low ($p = 0.0439$) shock groups. At the same time, shock intensity had a significant effect on ripple amplitude (Fig. 3.17i; one-way ANOVA; $F(3, 30) = 4.871$, $p = 0.0071$), while post-hoc analysis showed higher ripple amplitude in high shock group compared to control ($p = 0.0145$) and to low shock group ($p = 0.01$). Furthermore, significant shock effect was observed on ripple frequency (Fig. 3.17j; one-way ANOVA; $F(3, 30) = 7.766$, $p = 0.0006$) with post-hoc test revealing higher ripple frequency in high shock compared to mild shock group ($p = 0.0045$) and to control ($p = 0.0037$). In line, higher ripple frequency was observed in low shock compared to control ($p = 0.0234$) and to mild shock ($p = 0.0278$). Last, signal-to-noise ratio (Fig. 3.17g; Kruskal-Wallis; $p = 0.1389$) and AUC (Fig. 3.17k; one-way ANOVA; $F(3, 30) = 1.798$, $p = 0.1688$) remained unaltered. To sum up, there was a differential enhancement of SW-R in the high shock group, particularly in the CA1 region.

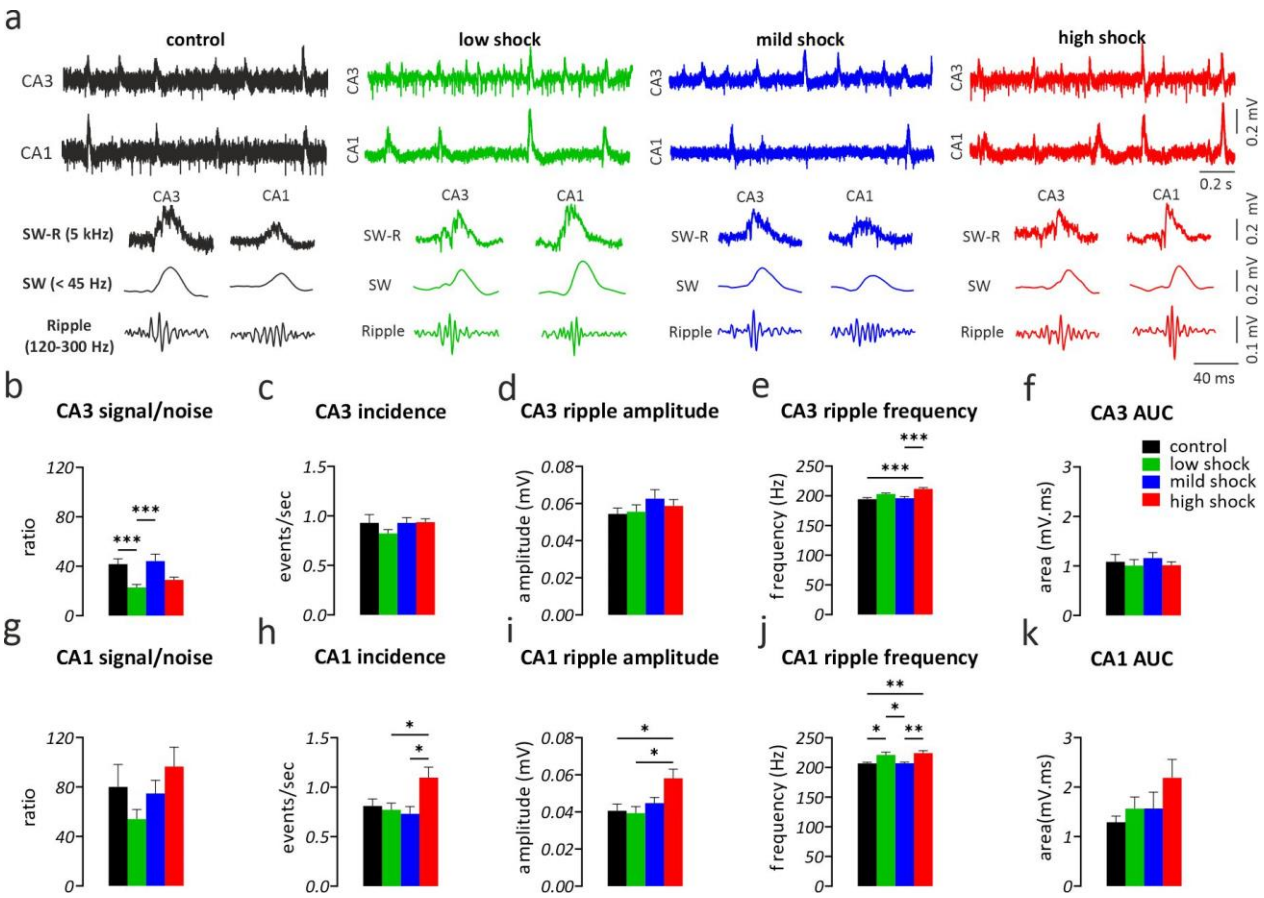

Fig. 3.17: Altered SW-R in CA3 and CA1 regions of C57BL/6 mice after E1.1 in a shock-intensity manner*. **(a)** Representative traces of SW-R recorded in the CA3 and CA1 of the vHP. Note the enhanced CA1 SW-R events in high shock animals (red). Below, SW-R traces of sampling rate 5 kHz are low-pass filtered (<45 Hz), illustrating the sharp wave component or band-pass filtered (120-300 Hz), illustrating the ripple component. Statistical comparison of SW-R properties in the CA3 region are shown in panels **(b-f)**. Shock intensity had an overall effect on **(b)** signal-to-noise ratio and **(e)** ripple frequency, whereas **(c)** incidence, **(d)** ripple amplitude and **(f)** AUC remained unaltered among the groups. Statistical comparison of SW-R properties in the CA1 region are shown in panels **(g-k)**. **(g)** Signal-to-noise ratio of low-pass filtered LFP signal and **(k)** AUC were similar among the groups. However, shock intensity had significant effect on **(h)** SW incidence, **(i)** ripple amplitude and **(j)** ripple frequency. Statistical comparison was performed using one-way ANOVA followed by post-hoc Tukey's test for panels **c-f, h-k** and Kruskal-Wallis followed by post-hoc Dunn's test for panels **b, g.** Data are given as mean ± SEM. *p < 0.05, **p < 0.01, ***p < 0.001. control: N = 9 mice, n = 39 slices; low shock: N = 8 mice, n = 35 slices; mild shock: N = 9 mice, n = 39 slices; high shock: N = 8 mice, n = 32 slices. AUC: area under the curve.*

3.3.3 Hippocampal CA3-CA1 interactions during SW-R after E1.1

As the next step, distinct properties indicative of the CA3-CA1 interaction during SW-R were analyzed, including the SW-R propagation along the CA3-CA1 axis, the waveform correlation of low pass-filtered SW signal, and the peak amplitude correlation of SW in the CA3 and CA1 regions. The analysis showed an overall effect of shock intensity on the SW propagation rate from CA3 to

CA1 (Fig. 3.18a; one-way ANOVA; F(3, 122) = 3.64, p = 0.0148; post-hoc low vs. high shock group p = 0.0073), on waveform correlation of all SW (Fig. 3.18b; Kruskal-Wallis; p = 0.0083; post-hoc low shock vs. control: p = 0.0132, low shock vs. high shock group: p = 0.0249) between CA3 and CA1 and on waveform correlation of connected SW (SW occurring in the CA1 in a certain time window after CA3) (Fig. 3.18c; Kruskal-Wallis; p = 0.0245; post-hoc control vs. low shock group: p = 0.0228). However, shock intensity did not affect the correlation of the SW peak amplitudes between areas CA3 and CA1 among the groups (Fig. 3.18d; Kruskal-Wallis; p = 0.1257). Therefore, in the high shock group, a differentially increased CA3-CA1 propagation rate and waveform correlation were observed, in line with the enhanced SW-R in CA1 region.

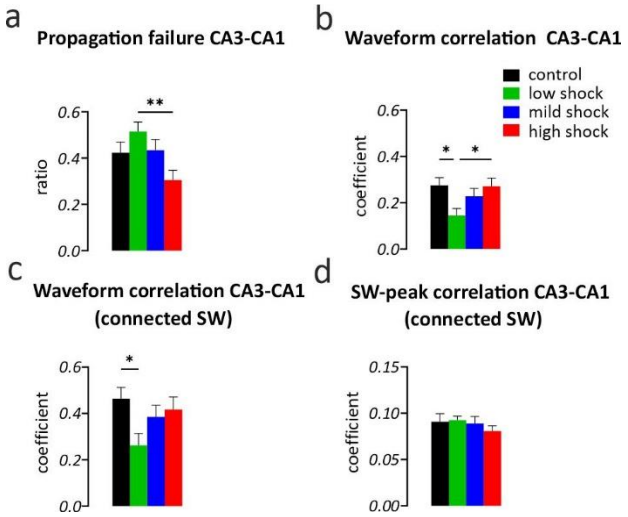

Fig. 3.18: Altered CA3-CA1 network interactions during SW-R in the vHP of C57BL/6 mice after E1.1 in a shock-intensity manner. *Summary graphs illustrating* ***(a)*** *decreased SW-R propagation failure along the CA3-CA1 axis in high shock compared to low shock mice,* ***(b)*** *decreased waveform correlation of all detected SW-R events in low shock compared to control and high shock mice,* ***(c)*** *decreased waveform correlation of connected CA3-CA1 SW-R events between low shock and control mice, but* ***(d)*** *unaltered SW-peak amplitude correlation among the groups.* *Statistical comparison was performed using one-way ANOVA and post-hoc Tukey's test for* ***a*** *and Kruskal-Wallis and post-hoc Dunn's test for* ***b***, ***c***, ***d***. *Data are given as mean ± SEM. *p < 0.05, **p < 0.01. control: N = 9 mice, n = 32 slices; low shock: N = 8 mice, n = 31 slices; mild shock: N = 9 mice, n*

3.3.4 Local SW-R properties in CA3 and CA1 of the vHP after fear memory extinction (E5)

Furthermore, to identify possible changes in the network oscillations after fear memory extinction, the SW-R properties after the E5 session were assessed. The LFP signal in areas CA3 and CA1 did not change, as shown after fear memory retrieval (section 3.3.2). Specifically, in the CA3 region, the signal-to-noise ratio (Fig. 3.19b; Kruskal-Wallis; p = 0.8292), SW incidence (Fig. 3.19c; Kruskal-Wallis; p = 0.4817), ripple amplitude (Fig. 3.19d; Kruskal-Wallis; p = 0.4415), ripple frequency (Fig. 3.19e; one-way ANOVA; F(3, 31) = 2.228, p = 0.1047) and AUC (Fig. 3.19f; Kruskal-Wallis; p = 0.1175), remained unaltered among the groups. In the CA1 region, shock intensity had

an overall effect on signal-to-noise ratio (Fig. 3.19g; Kruskal-Wallis; p = 0.0219, post-hoc mild shock vs. high shock group: p = 0.0242) and AUC (Fig. 3.19k; one-way ANOVA; F(3, 31) = 4.3, p = 0.012, post-hoc mild shock vs. high shock group: p = 0.0137). SW incidence showed no differences among the groups (Fig. 3.19h; one-way ANOVA showed a general effect; F(3, 31) = 3.032, p = 0.044, but no post-hoc group differences). Furthermore, ripple amplitude (Fig. 3.19i; one-way ANOVA; F(3, 31) = 0.7473, p = 0.5322) and ripple frequency (Fig. 3.19j; Kruskal-Wallis; p = 0.0718) remained unaltered among the groups. Thus, after E5, the SW-R differences observed after E1 were normalized.

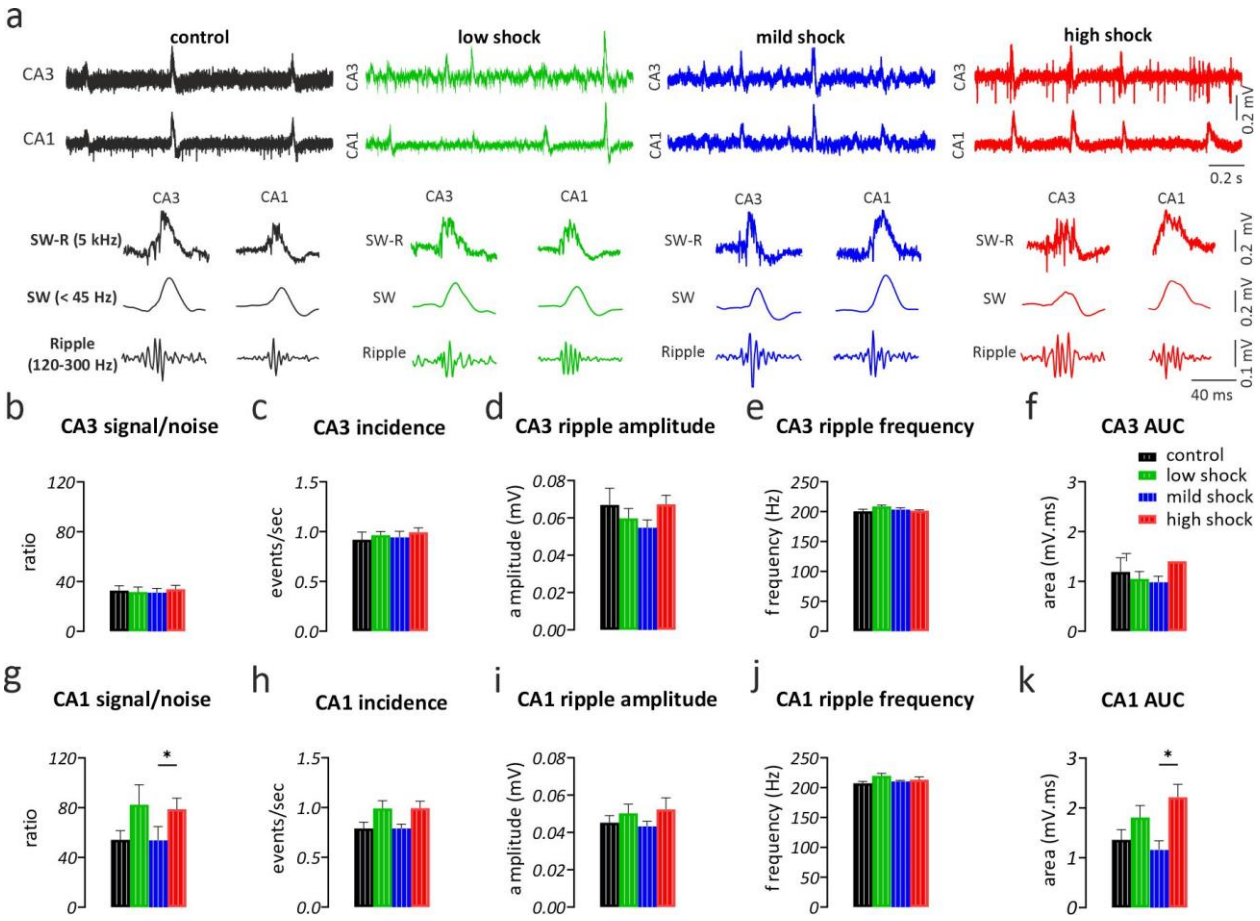

Fig. 3.19: SW-R in the CA3 and CA1 regions of C57BL/6 mice after contextual fear conditioning and extinction (E5). (a) *Representative traces of SW-R recorded in the CA3 and CA1 of the vHP. Below, SW-R traces of sampling rate 5 kHz are low-pass filtered (<45 Hz), illustrating the sharp wave component or band-pass filtered (120-300 Hz), illustrating the ripple component. Statistical comparison of SW-R properties in the CA3 region are shown in panels* ***(b-f).*** *Shock intensity did not affect* ***(b)*** *signal-to-noise ratio,* ***(c)*** *incidence,* ***(d)*** *ripple amplitude,* ***(e)*** *ripple frequency, and* ***(f)*** *AUC. Statistical comparison of SW-R properties in the CA1 region are shown in panels* ***(g-k)****.* ***(g)*** *Signal-to-noise ratio was increased in high shock compared to mild shock group, while* ***(h)*** *incidence,* ***(i)*** *ripple amplitude, and* ***(j)*** *ripple frequency showed no differences among the groups. Last,* ***(k)*** *AUC was increased in high shock compared to mild shock group. Statistical comparison was performed using one-way ANOVA followed by post-hoc Tukey's test for* ***e****,* ***h****,* ***i****,* ***k*** *and*

*Kruskal-Wallis followed by post-hoc Dunn's test for **b**, **c**, **d**, **f**, **g**, **j**. Data are given as mean ± SEM. *p < 0.05. Control: N = 8 mice, n = 38 slices; low shock: N = 9 mice, n = 32 slices; mild shock: N = 8 mice, n = 38 slices; high shock: N = 10 mice, n = 42 slices. AUC: area under the curve.*

3.3.5 Hippocampal CA3-CA1 interactions during SW-R after fear memory extinction (E5)

After the last extinction session (E5), the SW-R interactions along the CA3-CA1 axis were investigated, as explained in section 3.3.3. Interestingly, the changes in SW propagation along the CA3-CA1 axis, found after the fear memory retrieval session (E1.1) were not present after E5. This finding aligns well with the unaffected CA1 SW incidence values after E5 session (Fig. 3.19h). Specifically, shock intensity had no effect on propagation rates (Fig. 3.20a; Kruskal-Wallis; p = 0.4447), on waveform correlation of all SW (Fig. 3.20b; Kruskal-Wallis; p = 0.2739) between CA3 and CA1, on waveform correlation of connected SW (SW occurring in CA1 in a certain time window after CA3) (Fig. 3.20c; Kruskal-Wallis; p = 0.1593) and lastly no effect on the correlation of the SW peak amplitude between areas CA3 and CA1 among the groups (Fig. 3.20d; Kruskal-Wallis; p = 0.7039). Therefore, the CA3-CA1 network interactions during SW-R after E5 were unaltered.

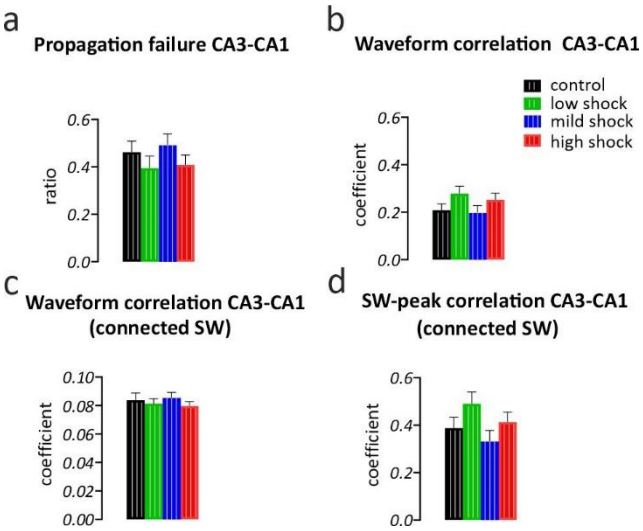

Fig. 3.20: Unaltered CA3-CA1 network interactions during SW-R in the vHP of C57BL/6 mice after fear memory extinction (E5). *Summary graphs illustrating no effect of shock intensity on **(a)** SW-R propagation failure along the CA3-CA1 axis, **(b)** on the waveform correlation of all detected SW-R events, **(c)** on the waveform correlation of connected CA3-CA1 SW-R events **(d)** nor on the SW-peak amplitude correlation among the groups. Statistical comparison was performed using Kruskal-Wallis and post-hoc Dunn's test. Data are given as mean ± SEM. *p < 0.05, control: N = 9 mice, n = 30 slices; low shock: N = 9 mice, n = 30 slices; mild shock: N = 8 mice, n = 31 slices; high shock group: N = 10 mice, n = 42 slices.*

3.3.6 Correlating freezing behavior and hippocampal SW-R properties

Behavior analysis (section 3.3.1) during the contextual FC and extinction paradigm revealed that mice within each shock group exhibited smaller or higher variability in their freezing time during E1.1, E5, and between E1 and E5 sessions (Fig. 3.16). For this reason, I postulated that the individual differences within each group could be depicted on their SW-R properties. Therefore, a correlation study was performed between the freezing time and the SW-R properties of each mouse after E1.1 and after E5. The analysis showed that only the high shock group mice and only after the E5 session had a negative correlation between freezing and CA1 incidence (Fig. 3.21f; Pearson r; p = 0.024). Therefore, high shocked group showed higher CA1 incidence when freezing levels were lower in E5.

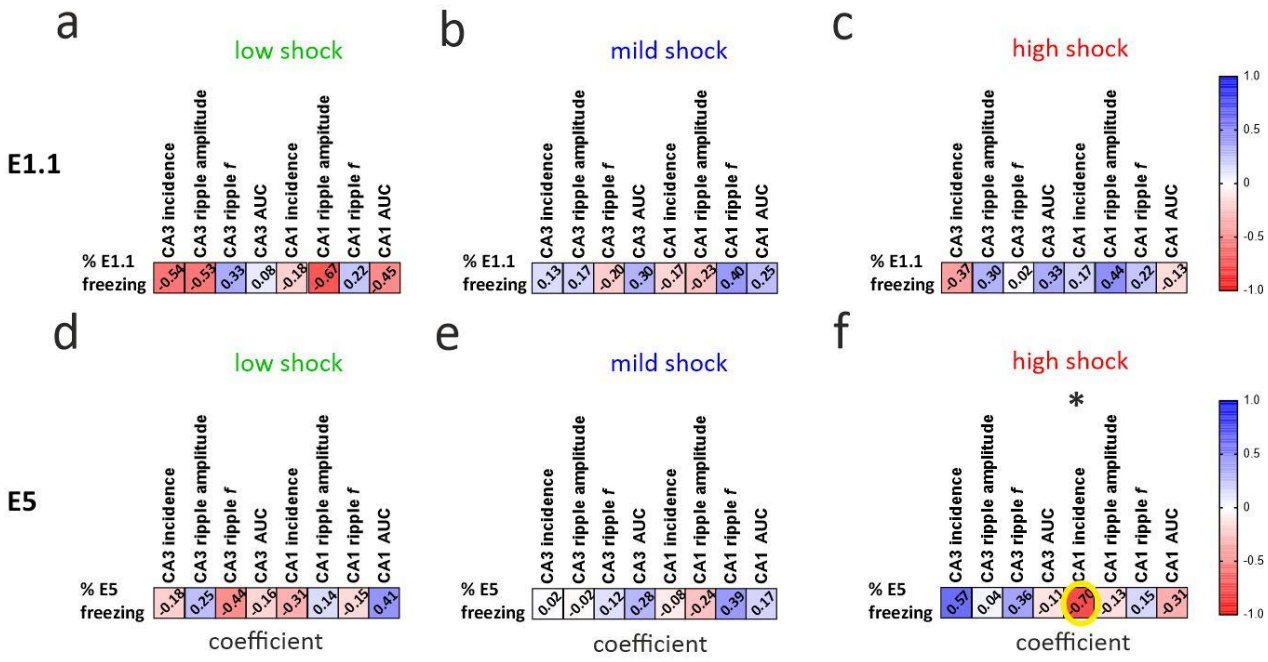

Fig. 3.21: Correlation of freezing time and SW-R properties of CA3 and CA1 after E1.1 and E5 in C57BL/6 mice. *Correlation of freezing time during E1.1 and SW incidence, ripple amplitude, ripple frequency and AUC in CA3 and CA1 region after E1.1 are shown in panels **a**-**c**. No significant findings were revealed in **(a)** low shock group, **(b)** mild shock group nor **(c)** high shock group animals. Similarly, analysis of freezing in E5 and SW-R properties after E5 showed no significant observations in **(d)** low shock and **(b)** mild shock groups. However, **(f)** CA1 incidence was negatively correlated with the freezing time in high shock group. Statistical comparison was performed by using Pearson r. *p < 0.05. For graphs **a**-**c**: low shock: N = 8 mice; mild shock: N = 9 mice; high shock: N = 8 mice. For graphs **d**-**f**: low shock: N = 9 mice; mild shock: N = 8 mice; high shock: N = 10 mice. AUC: area under the curve.*

3.4 Signaling pathways involved in the gamma oscillopathy of Fragile X syndrome - STUDY 4

Fmr1 KO mice exhibit similar clinical manifestations to human patients, such as cognitive impairments, anxiety, and sensory hypersensitivity (Bakker et al., 1994; Kooy, 2003; Santos et al., 2014). Common electrophysiological alterations have been observed in both patients and animals, such as gamma range oscillopathy (Arbab et al., 2018; Lovelace et al., 2020; Radwan et al., 2016; Wang et al., 2017). In the pathogenesis of the model, molecular changes have been implicated, including overexpression of M1 and M4 muscarinic cholinergic receptors (Thomson et al., 2017), hyperactive glutamatergic signaling, mediated by $mGluR_{1/5}$ and KA receptors (Bear et al., 2004; Huber et al., 2002; Qiu et al., 2018). Additionally, deficient GABAegic signaling is reported, including changes in GABA receptors subunits and GAD65/67 protein expression (D'Hulst et al., 2009; Kang et al., 2017; Olmos-Serrano et al., 2010; Paluszkiewicz et al., 2011). However, a direct connection between these pathways and the electrophysiological alterations is not fully understood. Interestingly, agonists of cholinergic and glutamatergic receptors can induce inhibition-dependent gamma oscillations *in vitro* (Fisahn et al., 1998, 2004; Pálhalmi et al., 2004; Traub et al., 2003). To this extent, using the *in vitro* model, I hypothesized that over-excitation of these signaling pathways would reveal electrophysiological alterations. For this reason, CCh, a muscarinic cholinergic receptor agonist; KA, a glutamatergic receptor agonist; and DHPG, a $mGluR_{1/5}$ agonist were used to generate slow gamma oscillations in the CA3 region of the vHP.

3.4.1 Enhanced CCh-induced gamma oscillations in the CA3 of Fmr1 KO mice

The involvement of the cholinergic pathway in the Fmr1 oscillopathy was assessed by administering the cholinergic agonist CCh via bath application in the brain slices containing the vHP for ~45 min. The gamma oscillations arising in the CA3 subregion of vHP in Fmr1 KO mice and WT littermates were analyzed. A prominent increase in the integrated gamma power (20-80 Hz) in the Fmr1 KO compared to the WT mice was evident (Fig. 3.22d; Student's two-tailed t-test; $T(57) = 4.055$, $p = 0.0002$). However, analysis of gamma peak frequency (Fig. 3.22e; Mann-Whitney U test, $p = 0.1463$), the half-band width (Fig. 3.22f; Mann-Whitney U test, $p = 0.7477$),

the decay constant gamma auto-correlation fit (Tau) (Fig. 3.22g; Mann-Whitney U test, p = 0.5094) and the auto-correlation (2nd peak value) of local gamma oscillations (Fig. 3.22c,h; Mann-Whitney U test; p = 0.4535) revealed no alterations.

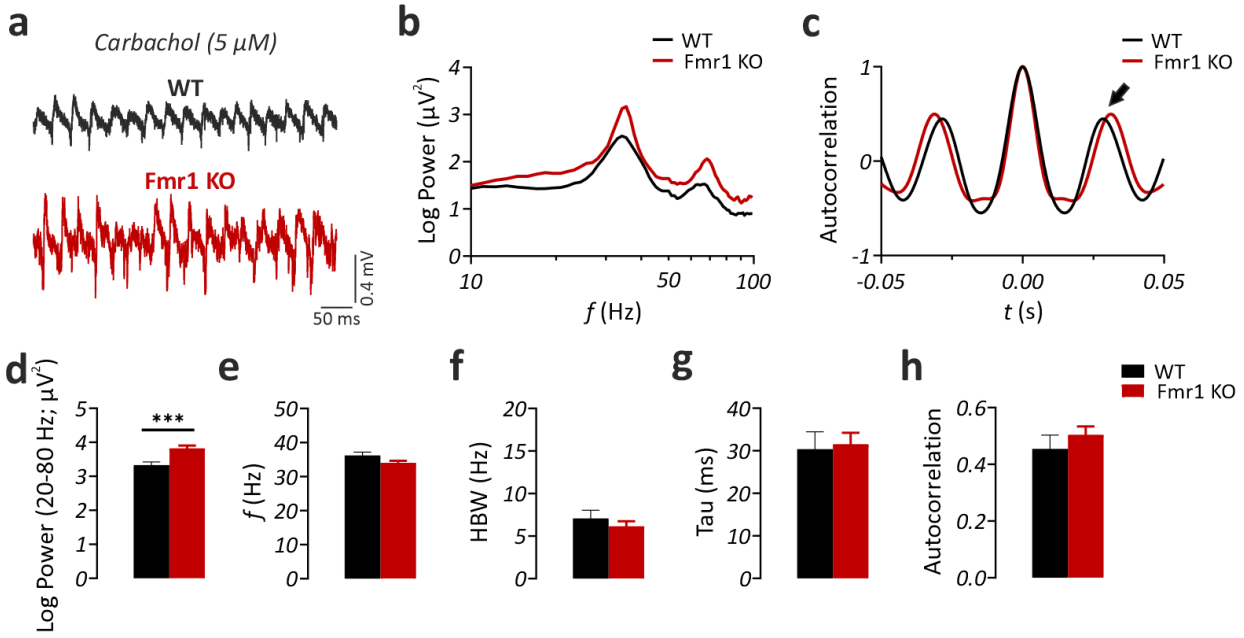

Fig. 3.22: Enhanced CCh-induced gamma oscillation power in the CA3 area of the vHP in Fmr1 KO mice. ***(a)*** *Representative traces of pharmacologically induced gamma oscillations using the cholinergic agonist carbachol (CCh, 5 µM).* ***(b)*** *Corresponding graph of power spectrum analysis showing an increase in the power of gamma-range oscillations (20-80 Hz) without any change in the peak frequency (f) of the LFP signal (f is shown on a logarithmic scale).* ***(c)*** *Example auto-correlogram showing similar coefficients in both genotypes. The 2nd positive peak value (indicated by the arrow) was measured for statistical comparison. On the bottom row, summary plots illustrating a significant increase in the* ***(d)*** *integrated gamma power (20-80 Hz), but no significant alterations in* ***(e)*** *the gamma peak f,* ***(f)*** *the half-band width (HBW),* ***(g)*** *time constant (Tau) of the decaying exponential fit to the peaks of the auto-correlation nor in* ***(h)*** *the 2nd peak value of the auto-correlogram. Statistical comparison was performed using Student´s two-tailed t-test for* ***d*** *and Mann-Whitney U test for* ***e, f, g,*** *and* ***h****. Data are given as mean ± SEM. ***p < 0.001. WT: N = 8 mice, n = 24 slices, Fmr1 KO: N = 11 mice, n = 35 slices for* ***d, e;*** *WT: N = 8 mice, n = 18 slices, Fmr1 KO: N = 11 mice, n = 30 slices for* ***f, g, h.***

3.4.2 Enhanced DHPG-induced gamma oscillations in the CA3 of Fmr1 KO mice

Previous studies have shown that mGluR signaling is also implicated in the Fmr1 KO mice pathophysiology (Dölen et al., 2007; Michalon et al., 2012). Additionally, agonists of the mGluR pathway have been previously used to induce *in vitro* hippocampal oscillations in the gamma frequency range (Gillies et al., 2002; Pálhalmi et al., 2004). Therefore, the $mGluR_{1/5}$ agonist DHPG (10 µM) was applied via bath-perfusion in slices containing the vHP from Fmr1 KO mice and *in vitro* gamma oscillations in the CA3 subregion were recorded. Power spectrum analysis revealed

significantly increased gamma integrated power [20-80 Hz] of the Fmr1 KO mice compared to WT (Fig. 3.23d; Student's two-tailed t-test; T(46) = 2.179, p = 0.0345). On the contrary, peak frequency (Fig. 3.23e; Student's two-tailed t-test; T(46) = 0.8122, p = 0.4209), HBW (Fig. 3.23f; Mann-Whitney U test, p = 0.4876), Tau (Fig. 3.23g; Mann-Whitney U test, p = 0.7788) and gamma auto-correlation (Fig. 3.23c,h; Student's two-tailed t-test; T(30) = 0.6405, p = 0.5267) exhibited no differences between the genotypes.

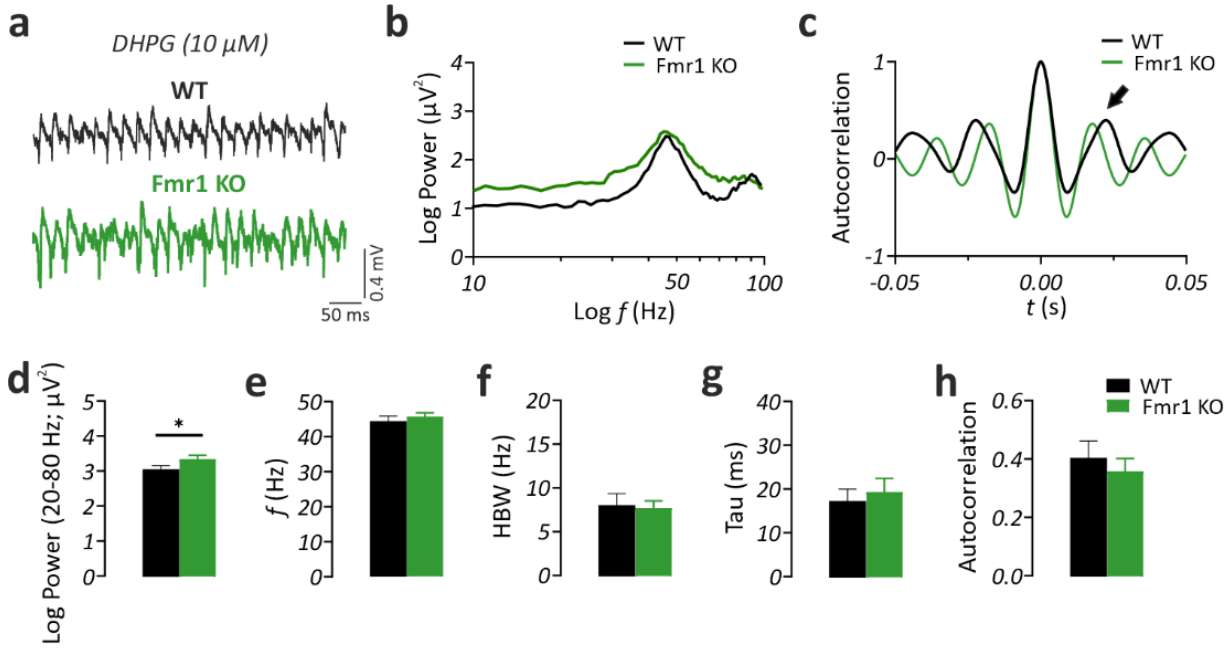

Fig. 3.23: Enhanced DHPG-induced gamma oscillation power in the CA3 area of the vHP in Fmr1 KO mice. ***(a)*** *Representative traces of pharmacologically induced gamma oscillations using the mGluR agonist DHPG (10 µM).* ***(b)*** *Corresponding graph of power spectrum analysis showing an increase in the power of gamma-range oscillations (20-80 Hz) without any change in the peak frequency (f) of the LFP signal (f is shown in logarithmic scale).* ***(c)*** *Example auto-correlogram showing similar coefficients in both genotypes. The 2nd positive peak value (indicated by the arrow) was measured for statistical comparison. On the bottom row, summary plots illustrating a significant increase in* ***(d)*** *the integrated gamma power (20-80 Hz), but no significant alterations* ***(e)*** *in the gamma peak f,* ***(f)*** *half-band width (HBW),* ***(g)*** *time constant (Tau) of the decaying exponential fit to the peaks of the auto-correlation nor in the* ***(h)*** *2nd peak value of the auto-correlogram. Statistical comparison was performed using Student´s two-tailed t-test for* ***c, d, e, h*** *and Mann-Whitney U test for* ***f*** *and* ***g****. Data are given as mean ± SEM. *p < 0.05. WT: N = 9 mice, n = 22 slices, Fmr1 KO: N = 8 mice, n = 26 slices for* ***d, e****; WT: N = 7 mice, n = 14 slices, Fmr1 KO: N = 7 mice, n = 18 slices for* ***f, g, h****.*

3.4.3 Decreased synchronization of KA-induced gamma oscillations in Fmr1 KO mice

Kainic acid (KA), a KA receptor agonist, is commonly used to pharmacologically induce *in vitro* fast oscillations in the gamma range (Bartos et al., 2007). To assess its implication in the Fmr1 KO

oscillopathy, I perfused hippocampal slices with 60 nM KA and recorded ~45 min later the network activity in the CA3 subregion. The analysis revealed that the peak frequency of gamma oscillations of Fmr1 KO mice was significantly increased compared to the WT (Fig. 3.24e; Student's two-tailed t-test; T(59) = 2.009, p = 0.0491) with the same trend for the HBW (Fig. 3.24f; Mann-Whitney U test; p = 0.0598). Additionally, the time constant (Tau) of the decaying exponential fit to the peaks of the auto-correlation was significantly decreased (Fig. 3.24g; Student's two-tailed t-test; T(50) = 3.056, p = 0.0036) accompanied with a trend for decreased auto-correlation (Fig. 3.24c,h; Student's two-tailed t-test; T(50) = 2.001, p = 0.0508) in Fmr1 KO mice compared to WT. On the contrary, integrated power [20-80 Hz] of KA-induced gamma oscillations was comparable between the genotypes (Fig. 3.24b,d; Mann-Whitney U test, p = 0.0959).

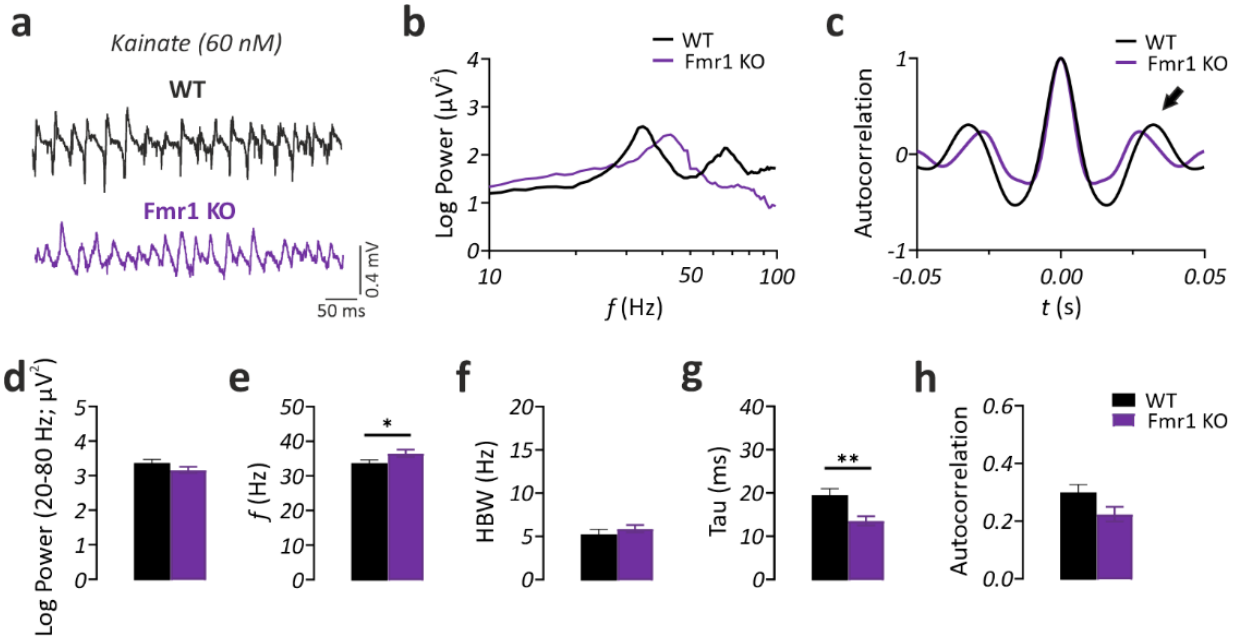

Fig. 3.24: Decreased synchronization and increased frequency of KA-induced gamma oscillations in the CA3 area of the vHP in Fmr1 KO mice. (a) *Representative traces of gamma oscillations in Fmr1 KO and WT mice.* ***(b)*** *Corresponding graph of power spectrum analysis showing a right shift in the peak frequency (f) (f is shown in logarithmic scale) without any change in the power of the oscillation.* ***(c)*** *Corresponding auto-correlogram showing a slight medial shift and a decrease trend in the 2nd positive peak value (indicated by the arrow). Summary plots illustrating a significant increase in* ***(e)*** *the gamma peak f and a decrease in the* ***(g)*** *time constant (Tau) of the decaying exponential fit to the peaks of the auto-correlation, with no significant alterations in* ***(d)*** *the integrated gamma power (20-80 Hz),* ***(f)*** *half-band width (HBW), and* ***(h)*** *2nd peak value of the auto-correlogram. Statistical comparison was performed using Student´s t-test for* ***e, g, h*** *and Mann-Whitney U test for* ***d*** *and* ***f****. Data are given as mean ± SEM. *p < 0.05. WT: N = 7 mice, n = 31 slices; Fmr1 KO: N = 7 mice, n = 30 slices for* ***d, e****; WT: N = 7 mice, n = 29 slices; Fmr1 KO: N = 7 mice, n = 23 slices for* ***f, g, h****.*

CHAPTER 4. DISCUSSION

4.1 Hippocampal network oscillations in GAD65 KO mice - STUDY 1

Previous studies in patients and animal models have implicated the GABAergic system in anxiety disorders and PTSD (Möhler, 2012). For example, blockage of GABA-A receptors in the amygdala inhibited fear extinction in rats after cued FC (Lin et al., 2009). Low GABA plasma levels after an acute severe traumatic experience (car accident) were associated with a higher probability of individuals developing PTSD (Vaiva et al., 2004, 2006). Polymorphisms of the GABA-A receptor subunit gene have been connected with increased severity of PTSD symptomatology in patients (Feusner et al., 2001), while a GAD2 gene polymorphism modulated GABA/glutamate balance and harm avoidance behavior (Colic et al., 2018). GAD65 KO mice exhibit reduced GABA synthesis, increased anxiety, and emotional processing deficits (Bergado-Acosta et al., 2008; Kash et al., 1999; Sangha et al., 2009; Stork et al., 2000) and have been used as an animal model in the investigation of GABAergic system's role in PTSD and anxiety traits. Amygdala is a structure involved in anxiety and PTSD (Adhikari, 2014; Nuss, 2015; Shin et al., 2006) and has a critical role in the pathophysiology of GAD65 KO mice (Müller et al., 2015). The present study describes the contribution of the vHP, a region involved in the formation of emotional memories and anxiety (Ciocchi et al., 2015; Kjelstrup et al., 2002) that exhibits behavior-relevant network activity patterns.

To this extent, hippocampal SW-R and CCh-induced gamma oscillations in the areas CA3 and CA1 were described *in vitro*, which demonstrate similar characteristics as *in vivo* (Butler & Paulsen, 2015; Hájos & Paulsen, 2009). As main findings, ripples and gamma oscillations were enhanced in GAD65 KO mice, with increased RED occurrence. Specifically, in the CA3 region, the ripple amplitude and the AUC were increased as well as the ripple frequency in the CA1 region. However, SW incidence was reduced in the CA1 region with a trend for a CA3-to-CA1 propagation

deficit, which was more prominent after mice underwent a contextual fear conditioning paradigm.

Gamma oscillations

Gamma oscillations were induced by bath application of the cholinergic agonist CCh, which pharmacologically mimics the physiological medial septal cholinergic projections (Vandecasteele et al., 2014). Naïve GAD65 KO mice, with no prior behavioral manipulation, exhibited enhanced gamma frequency in the CA3 and CA1 areas of the vHP. Under physiological conditions, in isolated hippocampal preparation, the CA3 area, due to its recurrent excitatory network, is supported to be the gamma generator of a slow rhythm, which propagates to CA1 (Colgin et al., 2009; Hájos & Paulsen, 2009). During gamma rhythm, INs receive higher excitatory input than pyramidal cells, probably from the local circuit (Hájos & Paulsen, 2009). In GAD65 KO mice, GABA synthesis is reduced, and thus excitation/inhibition imbalance could explain the network hyper-excitability. In line, previous studies intervening with GABAergic transmission by deleting the GABA-A R delta subunit showed increases in CCh-induced oscillation frequency in the CA3 area (Mann & Mody, 2010). Of note, the more prominent REDs activity in GAD65 KO mice would also support a hyperactive state. Therefore, increased gamma frequency could be related to an increase in the excitability of the local CA3 network.

The emergence of epileptiform activity in GAD65 KO mice aligns with the phenotypic observation of stress-induced seizures. Additionally, the increased gamma frequency found in the stress-susceptible GAD65 KO mice is in line with a previous study where acute administration of high concentrations of the stress hormone CORT increased the frequency of the CA3 CCh-induced gamma (Weiss et al., 2008). However, no effect on gamma power was found, contrary to enhanced ACh-induced gamma power after acute stress in slice preparations (Çalışkan et al., 2015b) or decreased power of KA-induced gamma after behavioral stress (Albrecht et al., 2013). This difference might imply that naive GAD65 KO mice do not show altered gamma power, which could be revealed after stress administration in these mice. Therefore, considering previous studies that showed an effect of stress on gamma oscillations, this study suggests that a stress predisposition in animals could also be represented by altered gamma frequency.

Sharp wave-ripples

Investigation of the spontaneous SW-R that arise in the vHP of naïve GAD65 KO mice revealed enhanced ripple components, with increased frequency in the CA1 region and increased amplitude in the CA3 region. Ripples arise from a reciprocal and feedback interaction between local perisomatic INs and pyramidal cells (Buzsáki et al., 1983, 1992; Csicsvari et al., 1999; English et al., 2014; Schomburg et al., 2012; Stark et al., 2014). Therefore, faster CA1 ripple oscillations could imply faster kinetics of interneurons, in line with the increased frequency of the gamma rhythm in this model. This aligns with the findings from STUDY 2, where a strong trend for increased IPSC frequency on pyramidal cells is found. Increased CA3 ripple amplitude would suggest synchronized firing of a larger pyramidal cell population, indicating higher excitability in the CA3 circuit, in line with the GABA deficiency of the model. Similarly, the increased AUC found in the CA3 region would suggest higher recruitment of CA3 pyramidal cells in the recurrent collateral network population and increased excitability.

Furthermore, a surprising effect is observed in the CA1 region, where SW incidence and AUC are decreased, whereas gamma and ripple frequency are increased. Since the SW component reflects the excitatory afferents from the CA3 region, these findings would indicate a potential propagation blockade from CA3 to CA1 (Both et al., 2008) and a decrease in the excitability of the CA1 region. This is also observed in previous studies with animal models of different disorders. For example, in animal models of schizophrenia, a decrease in SW incidence is related to decreases in synaptic plasticity or decreased hippocampal excitability (Suh et al., 2013). Excitability and plasticity of the network seem to be interconnected, since increased excitability can arise from a rearrangement in the plasticity properties towards increased potentiation and decreased depression (Zeng et al., 2001). LTP induction is also supported as a generation mechanism of SW-R (Behrens et al., 2005). In line, LTP induction in SC-CA1 synapse results in increased incidence and amplitude of SW (Buzsáki, 1984). For this reason, STUDY 2 assessed properties of the SC-CA1 synapse, the major connection from CA3 to CA1 area. However, as main findings, no differences in excitability and plasticity of the SC-CA1 synapse were found, explained in detail in the next section.

An alternative source of decreased excitability in the CA1 region could arise from intrinsic CA1 pyramidal cell mechanisms that could prolong the hyperpolarization state of pyramidal cells, such

as enhanced activation of GABA-B-related K^+ channels (Buzsáki, 2015; English et al., 2014). To test this assumption, STUDY 2 also investigates the intrinsic CA1 pyramidal cell properties and identifies mild hyperpolarization of these cells, described more extensively below.

Furthermore, chronic CORT injections in rats decreased GAD65 expression in the hippocampus (Lussier et al., 2013), whereas CORT bath perfusion in slices of WT rodents affected SW-R occurrence. Therefore, the effects of CORT on the SW-R could be relatable with the findings in the GAD65 KO mice for two reasons. Firstly, because of the reduced GAD65 expression and secondly due to the phenotypic stress susceptibility of this model. Specifically, bath administration of high CORT concentrations in hippocampal slices decreases SW incidence in CA1 (Çalışkan et al., 2015b; Weiss et al., 2008), while low CORT increases incidence (Weiss et al., 2008). This is in line with the decreased CA1 SW incidence in the GAD65 KO mice, which would imply that their baseline stress levels are already heightened. The fact that the CA3 region shows an opposite phenotype would suggest differentiated underlying mechanisms. Therefore, STUDY 2 investigated whether GAD65-dependent GABA deficiency differentially affects CA3 and CA1 regions by limiting the GAD65 expression locally in these areas. As main findings, local DG-CA3 GAD65 reduction does not affect SW-R, but local CA1 reduction weakens CA1 ripples, as detailed below.

The electrophysiological phenotype of GAD65 KO mice after an episode of fear exposure (FC paradigm) showed amplification of the existing CA3 and CA1 properties. The SW-R characteristics after the FC resembled the baseline phenotype of the naïve GAD65 KO with an exaggeration in the CA3-CA1 dichotomy. In particular, CA3 SW-R were enhanced with increased incidence and AUC, while CA1 SW-R were attenuated with decreased incidence and a CA3-to-CA1 propagation deficit. These data would suggest a prominent genetic predisposition of the GAD65 KO mice to demonstrate enhanced SW-R in the CA3 network and decreased incidence in the CA1 network maintained throughout the FC paradigm. Thus, they would indicate GAD65-dependent excitation/inhibition alterations in the CA3 and CA1 networks that shape the electrophysiological features of the model, in line with the critical role of inhibition in the formation of network oscillations.

During the contextual FC, GAD65 KO and WT mice learned the context-shock association, expressed by increased freezing levels at the retrieval session (E1.1), and successfully

extinguished the fear memory by the end of the extinction protocol. However, in the intermediate extinction sessions, GAD65 KO mice showed steadily lower freezing levels than WT mice, indicating a rapid extinction of contextual fear memory. In line, reduced GABAergic tone has been previously connected with enhanced fear memory extinction (Makkar et al., 2010). Alternatively, it would be plausible to assume that after the E1 extinction session, the context was not perceived as a clear threat but rather as an ambiguous environment, making the highly anxious GAD65 KO mice exhibit an alert behavior and higher activity. This view is supported by other studies, where increased locomotion of GAD65 KO mice in tasks, such as forced-swim test, is attributed to the elevated psychomotor activity due to the stressful situation (Müller et al., 2015; Stork et al., 2000).

At first sight, these findings might seem contradictory to previous reports of this animal model displaying no contextual inter-session fear memory impairments (Sangha et al., 2009). However, Sangha and co-workers investigated fast extinction with a protocol in which extinction sessions took place within the same day. Consequently, the reminiscent fear memory from one day to the next and the involvement of sleep-associated SW-R activity during extinction consolidation were not assessed in that paradigm. In the current study, it was hypothesized that overnight sessions would affect more contextual memory, as previously seen (Çalışkan et al., 2016), due to the consolidation phases during sleep. Therefore, the current experimental layout was chosen specifically to address the role of the consolidation process and eventually the SW-R in the fear memory extinction in these animals. To this extent, after this paradigm, GAD65 KO mice surprisingly extinguished the fear memory faster than WT, which can be directly connected to the consolidation phases attributed to the presence of SW-R. This finding is aligned with the function of SW-R in memory consolidation (Ego-Stengel & Wilson, 2010; Girardeau et al., 2009; Jadhav et al., 2012).

The next question that arises is whether the particular characteristics of the SW-R found in GAD65 KO mice can mediate the enhanced fear memory extinction. Specifically, is increased CA3 SW incidence and AUC as well as with the decreased CA1 SW incidence implicated in the behavioral phenotype of GAD65 KO mice? Previous studies have revealed enhanced CA1 SW incidence and CA3-CA1 propagation of SW events in a genetic mouse model with enhanced GABAergic tonus that showed a profoundly retarded extinction of contextual fear memories (Çalışkan et al., 2016).

This aligns well with the rather opposite findings observed in GAD65 KO mice with reduced GABAergic tonus, reduced CA1 SW incidence and SW propagation along the CA3-CA1 axis and a rather accelerated extinction of contextual fear memories. However, because decreased SW-R CA1 incidence and enhanced CA3 properties were also present in naïve GAD65 KO mice, it would be difficult to conclude whether the genetic predisposition and GABA baseline decrease or the network dynamics after the FC was more critical in shaping the SW-R. For this reason, STUDY 3 explored the SW-R in the vHP of WT mice that underwent a stressful experience and its extinction. STUDY 3 demonstrated an effect of shock intensity on SW-R after fear memory (re)consolidation but not after fear memory extinction that are discussed extensively below.

In total, the findings from GAD65 KO mice after an FC paradigm that included overnight consolidation phases showed facilitation of fear memory extinction. Thus, they would indicate a role of GAD65-dependent GABA in the extinction of contextual FC, which is facilitated by the consolidation process, mediated by SW-R. However, it should be pointed out that even though GAD65 KO mice showed decreased freezing, suggesting enhanced extinction of the imminent threat, this could also indicate a fast decrease of the clarity of the fearful representation and its replacement with vague anxiety. Last, more experiments would be necessary to determine if enhanced CA3 area or decreased CA1 area SW-R have a critical role in the behavioral phenotype or they represent the predisposition of the animal independent of the learning process.

Furthermore, to determine a putative role of GAD65-dependent activation of distinct neuronal assemblies during the contextual fear re-exposure, I assessed the immediate early gene c-Fos activation. Analysis revealed unaltered c-Fos expression in the CA areas of the HP, a region critical for contextual FC tasks (Kjelstrup et al., 2002; Zhang et al., 2014). Previous observations in GAD65 KO mice have indicated hyperactivity of structures, such as the amygdala after cued FC, but unaltered c-Fos expression in the CA areas (Bergado-Acosta et al., 2014). Therefore, these results indicate that contextual fear re-exposure is not represented in the total number of activated assemblies in the CA3 and CA1 of the vHP. Even though this finding suggests similar cellular activation patterns between the genotypes, it does not exclude a potential differentiation in the composition of the assemblies, such as the number of inhibitory and excitatory cells that participate.

In conclusion, naïve GAD65 KO mice displayed increased peak frequency of both CCh-induced gamma and ripple oscillations in the CA3 and CA1 areas of the vHP along with decreased CA1 SW incidence. These alterations implicate the vHP in the pathophysiology of GAD65 KO mice and support existing literature about the contribution of the vHP in anxiety and emotional processing (Ciocchi et al., 2015; Kjelstrup et al., 2002) and the involvement of a compromised GABAergic system in neuropsychiatric disorders (Möhler, 2012). Last, the differential excitability status between CA3 and CA1 areas found in GAD65 KO mice with the propagation deficit of SW-R from CA3 to CA1 could potentially reflect an enhanced filter function to the hyper-excitability of the network. To investigate the excitability of the CA1 network, STUDY 2 follows and describes different network and cellular parameters.

4.2 Cellular and network correlates of altered SW-R in GAD65 KO mice - STUDY 2

STUDY 2 examined parameters that might underlie the network oscillation changes found in the vHP of GAD65 KO mice. Specifically, STUDY 1 demonstrated enhanced ripple components in both CA3 and CA1 regions, with particular increased SW AUC in the CA3 area and reduced SW incidence in the CA1 area. These findings maintained a similar direction after mice underwent a contextual FC paradigm, with an apparent SW-R propagation failure from the CA3 to CA1 region. The enhanced SW-R in the CA3 area would imply increased excitability of the local network, aligned with the GABA deficiency of the animal model, but the reduced CA1 incidence would suggest the opposite. Previous literature (Behrens et al., 2005; Schlingloff et al., 2014; Zeng et al., 2001) proposed that changes in the plasticity of the hippocampus could affect its excitability and, therefore, the SW-R generation. Thus, I hypothesized that the reduced CA1 SW incidence, observed in GAD65 KO mice, could be due to a decrease in the baseline synaptic excitability or plasticity in the CA1 region. For this reason, synaptic transmission and plasticity of the SC-CA1 synapse, which is the primary synaptic connection between CA3 and CA1, were examined. Additionally, to investigate if the excitation/inhibition balance in the CA1 region was associated with alterations at the cellular level, I investigated the intrinsic and synaptic properties of CA1 pyramidal cells.

Last, to explore whether the vHP was critically involved in the electrophysiological phenotype of the general GAD65 KO mice, mice with local GAD65 decrease in the CA1 or DG-CA3 regions were characterized. This experiment would potentially distinguish between a primary role of the intra-hippocampal circuit in the oscillatory alterations of GAD65 KO mice and a secondary role that could occur after a developmental reconfiguration of the hippocampal circuit in response to general GABA deficiency.

Network plasticity and excitability

In the current study, fEPSP and fv responses of the SC-CA1 synapse via stimulation of the SC were assessed. Firstly, fEPSP values to incrementally increasing stimuli (I-O curve) that indicate postsynaptic excitability showed no differences between the groups. Similarly, fv values, a parameter of presynaptic response to stimuli and the measure of synaptic efficacy, defined as the fEPSP to fv ratio, remained unaltered. fEPSP responses in paired pulses that describe short-term plasticity and during and after HFS, a description of synaptic fatigue and long-term plasticity, respectively, remained unaltered between the groups. Therefore, the examination of the SC-CA1 synapse could not explain the alteration in the CA1 SW incidence found in GAD65 KO mice and indicates that the oscillatory changes are not an outcome of plasticity modifications in this synapse.

Previous studies have connected LTP differences in the hippocampus with neuropsychiatric diseases, which could be relevant for GAD65 KO mice and their stress susceptibility phenotype. For example, Suh et al., 2013 showed enhanced LTP *in vivo* in the dHP in a mouse model of schizophrenia that connects the cognitive deficits of the disease with temporal lobe dysfunction, including the hippocampus. Other studies pointed out a connection between acute or chronic stress and enhanced LTP in the vHP. Specifically, rats socially isolated with increased risk for anxiety and post-traumatic stress exhibited increased SC-CA1 synaptic excitability in ventral hippocampal slices (Almonte et al., 2017). Additional *ex vivo* studies showed increased LTP after juvenile or acute stress in the CA1 of vHP slices (Grigoryan & Segal, 2016; Ivens et al., 2019; Maggio & Segal, 2007a, 2011). Such studies could be relevant to the stress susceptibility of the GAD65 KO mouse and would indicate a potential enhancement in the LTP of the vHP and its implication in the pathophysiology.

Even though the baseline response of the SC-CA1 synapse was found unaltered in naïve GAD65 KO mice, it could be possible that it would reveal alterations after a mildly stressful experience. It should be mentioned that the heightened anxiety of GAD65 KO mice is an innate characteristic that did not occur after learning or an induced stressful experience. For this reason, it would be essential to examine this synapse after a stress protocol and importantly identify interactions of such intervention, since stress itself modulates GABAergic functions (Albrecht et al., 2016, 2017, 2020; Sangha et al., 2012).

Intrinsic and synaptic properties

Intrinsic neuronal properties might underlie changes in the SW-R generation (Buzsáki, 2015). For this reason, the patch-clamp technique was used, and the subthreshold and suprathreshold membrane properties of CA1 pyramidal cells were assessed. As main observations, the resting membrane potential had a hyperpolarization tendency, and the action potential (AP) threshold was increased in GAD65 KO compared to WT mice. These results indicate a mild reduction in the CA1 pyramidal cell excitability, which could partially explain the decrease in the CA1 SW incidence. However, other excitability measures, such as firing frequency and membrane voltage responses to depolarizing current steps, remained unaltered, making a conclusion about neuronal excitability more complex. In addition, taking into account that GAD65-mediated GABA synthesis might be involved not only in phasic (Tian et al., 1999) but also in tonic inhibition (Stork et al., 2000), it would be expected that membrane potential and conductance would be affected in the direction of hyperexcitability, given the GABA deficiency. Thus, it would be interesting to further investigate neuronal excitability and membrane permeability determinants, such as distribution and activation status of membrane channels. Additionally, the number and activity of neurotransmitter receptors might also play a role in determining the neuron's membrane potential and excitability (Dunn & Kaczorowski, 2019). It would be plausible to assume that GAD65 KO mice, given the GABA deficiency, might regulate the GABAergic receptors through homeostatic mechanisms (Roth & Draguhn, 2012). Yet, the postsynaptic GABA-A receptors did not show affinity or density alterations in this animal model (Kash et al., 1999).

To determine if the trend in a more hyperpolarizing state of CA1 pyramidal neurons are synaptically driven, I investigated their inhibitory current inputs. The spontaneous postsynaptic inhibitory currents (sIPSC), which reflect the GABA release and represent the GABAergic synaptic

transmission, were measured. It was observed that, on average, the amplitude and frequency of the sIPSC were unaltered. These findings align with previous observations that baseline inhibitory synaptic signaling is intact (Song et al., 2011; Tian et al., 1999) and evoked IPSC are decreased (Tian et al., 1999), in accordance with the role of GAD65 being at the terminals of the neurons and activated in higher GABA demands (Soghomonian & Martin, 1998).

Interestingly, I also observed that the frequency distribution of the sIPSCs revealed a bigger proportion of fast occurring currents in GAD65 KO mice than in WT. This would indicate a mild increase in inhibitory transmission and could partially explain the hyperpolarizing trend of CA1 pyramidal neurons and the faster CA1 gamma rhythm and ripples. To justify such observation, an assumption of a different effect of GABA deficiency on IN types would be plausible. In favor of this argument, it has been shown that GAD65 is not equally present in ventral CA1 interneurons but mostly in cholecystokinin (CCK^+) and substantially less in PV^+ IN (Nagode et al., 2014; Nguyen et al., 2014). Furthermore, it would be plausible to assume that because sIPSC measures are from a somatic patch-clamp, perisomatic IN would contribute more to the IPSC than distal innervating IN. Therefore, perisomatic IN, such as PV^+ BC, might be potentially less affected by the GABAergic dysfunction. An alternative possibility would be that PV^+ BC might still be very excitable due to their gap junctions, which are not reported in other IN types (Fujuda & Kosaka, 2000). To conclude about such alterations, more studies regarding IN subpopulations in the GAD65 KO mice should be conducted.

Investigating the inhibitory synaptic input onto the CA1 pyramidal cells independent of the LFP dynamics could not give time-specific information regarding the synaptic activity during the SW-R. Considering that SW-R propagate from CA3 to CA1 (Both et al., 2008; Maier et al., 2003), I assumed that the SW-R in the CA3 region would trigger synaptic currents in the CA1 pyramidal cells. Therefore, to identify whether the SW-R-driven excitation/inhibition (E/I) balance in the CA1 region was changed, I assessed the compound postsynaptic activity on the CA1 pyramidal cells with reference to the timing of SW-R events occurring in the CA3. On average, the cIPSCs and cEPSCs arising shortly after a SW-R peak were comparable between GAD65 KO and WT mice. Therefore, reduced CA1 SW-R incidence and CA1 pyramidal cell excitability could not be explained by altered synaptic drive from the CA3 region and cannot explain the CA3-CA1 propagation deficits. However, striking studies have indicated that pyramidal cells that participate in the SW-

R events have distinct properties from non- participants (Bähner et al., 2011), such as altered E/I balance towards excitation in the cells participating in a SW-R event (Ishikawa & Ikegaya, 2020; Mizunuma et al., 2014). Therefore, it would be essential to further investigate the E/I ratio in CA1 pyramidal cells-participants that fire during a SW-R event.

In total, in search of a cellular mechanism that could underlie the electrophysiological alterations found in GAD65 KO mice, these results show mild hyperpolarization of the CA1 pyramidal cells and an increased trend for inhibitory currents. These changes could contribute to a less excitable local CA1 network and thus decreased CA1 SW incidence. Last, the tendency for increased sIPSC frequency could point in the direction of faster ripples and gamma oscillations.

Local GAD65 decrease in the vHP

To understand whether the electrophysiological phenotype of GAD65 KO mice resulted from an intra-hippocampal mechanism or as a developmental reconfiguration of the hippocampal circuit under GABA deficiency, I created two local knock-down models, reducing the GAD65 expression either in the ventral CA1 or DG-CA3 regions. I asked whether local GAD65 deficiency in these subregions would differentially affect the network activity and potentially the anxiety and fear in these mice compared to the global GAD65 KO model.

Previous studies have indicated differential roles of the intra-hippocampal circuit subregions in behavior. Lesion studies have reported an essential function of the ventral CA3 region in retrieving contextual FC, whereas ventral CA1 was involved in trace FC (Hunsaker & Kesner, 2008; Rogers et al., 2006; Weeden et al., 2015). Furthermore, enhancing ventral DG activity had a differential anxiolytic role (Kheirbek et al., 2013), while decreasing the GABA levels increased anxiety (Tripathi et al., 2021). Different studies observed segregation of information processing within the hippocampus, with DG-CA3 subregions involved in anxiety and CA1 in fear (Engin et al., 2016). Furthermore, GAD65 expression is modulated by stressful experiences differentially in the hippocampus. For example, previous studies have shown a reduction in GAD65 gene expression of DG and CA1 after the extinction of a new fear memory attributed to contextual fear learning (Sangha et al., 2012). In line, a GAD65 expression decrease was observed in the ventral CA1 after combined juvenile/adult stress (Albrecht et al., 2020). To this extent, limiting the GABA deficiency locally in CA1 or DG-CA3 regions of the vHP, the anatomical specificity of the GAD65 deficiency was increased. C57BL/6 mice were intracranially injected with a lentiviral construct

carrying GAD65 shRNA (Tripathi et al., 2021). Of note, the ratio of inhibitory/pyramidal cells in the hippocampus is about 6%, and even small changes in the number or function of INs would critically affect the microcircuits (Czéh et al., 2013).

As main findings, local GAD65 reduction in the DG-CA3 region of the vHP did not reveal any differences in the SW-R properties. This observation seems peculiar since the CA3 region is proposed to be the SW initiator, and thus compromising the inhibitory system would be expected to cause network imbalance. However, the interneuron networks and their interactions with pyramidal cells are complex (Kullmann, 2011; Maccaferri & Lacaille, 2003) and seem sufficient to compensate for the local GAD65 decrease. On the other hand, upon local GAD65 reduction in the CA1 region, mice exhibited decreased ripple amplitude and frequency in the CA1 subregion, indicating decreased excitability and slower inhibitory kinetics. This finding aligns with a potential decrease in the functionality of the INs that critically shape the fast oscillations, and thus the INs kinetics and the ripple rhythm is slower. However, the opposite is found in the global GAD65 KO that showed enhanced ripple components. The divergence between the acute KD and global KO models could emerge from systemic changes of the GAD65 KO model. Such changes could include alterations in additional brain regions and a reconfiguration of the hippocampal microcircuits as a result. In support, previous studies have indicated increased amygdala activity in GAD65 KO mice after fear memory tasks (Bergado-Acosta et al., 2014). Other studies, indicated GAD65 polymorphisms in the ACC being involved in anxiety traits (Colic et al., 2018). In addition, communication between regions and specifically synchronization between amygdala and hippocampus has been altered in GAD65 KO mice during retrieval and extinction of FC tasks (Bergado-Acosta et al., 2008; Sangha et al., 2009) suggesting impairments in amygdalo-hippocampal interactions during emotional processing. Therefore, these results indicate that the pathophysiology of the GAD65 KO model is more complex than a deficit attributed to one brain region and a combination of factors results in the modulation of the neural circuits and the mediation of behavioral outcomes.

Concluding, genetic variations in the GABAergic transmission have been implicated in anxiety and stress responding (Colic et al., 2018; Feusner et al., 2001; Möhler, 2012) along with distinct modulation of GAD65 expression in different hippocampal regions (Sangha et al., 2012)and amygdala after stressful experience (Bergado-Acosta et al., 2008; Sangha et al., 2012). The

present study shows alterations in the network oscillations of the vHP in GAD65 KO mice, indicating network activity changes in a compromised GABAergic system that also exhibits emotional processing deficits. In search of the critical mechanisms that might underlie such alterations, local GAD65 decrease in CA1 and DG-CA3 regions was induced, which revealed distinct electrophysiological phenotype compared to global GAD65 KO mice. The discrepancies might be a result of a general reorganization of the system that involves dysregulation of allostatic mechanisms that balance excitation/inhibition (Albrecht et al., 2020), as well as other brain regions of emotional regulation, such as the amygdala, ACC, and their communication. Therefore, these data indicate that the formation of the network oscillations in GAD65 KO mice is the outcome of abnormal postnatal GABA development (Stork et al., 2000) and not a direct effect of the local GABA reduction. Last, even though the local GABA reduction models did not replicate the electrophysiological findings of the KO, they would suggest that the CA1 area is more sensitive to GAD65 deficiency than CA3 and indicate a critical role of GAD65 for the local CA1 interneurons in shaping the ripples.

4.3 Behavioral correlates of SW-R - STUDY 3

STUDY 3 described behavioral correlates of ventral hippocampal SW-R in regard to contextual fear memory and its persistence. Previous studies have indicated the role of SW-R in memory consolidation and retrieval (Buzsáki, 2015; Jai & Frank, 2015; Joo & Frank, 2018; O'Neill et al., 2006; Pfeiffer & Foster, 2013). The development of SW-R is essential for the memory formation of recent events as well as contextual emotional memories (Ego-Stengel & Wilson, 2010; Girardeau et al., 2009, 2017; Jadhav et al., 2012). However, it is not fully understood whether SW-R carry information regarding the content of these experiences and how they affect the emotional memory specificity and persistence. Therefore, I investigated whether the adversity of the environment would be mapped in the SW-R properties and lead to salient fear memories that would be specific and robustly stored as long-term memories. To this extent, e*x vivo* SW-R were examined in the vHP of wild-type mice that went through a contextual FC with increasing levels of shock intensity.

The FC paradigm contained three different levels of shock intensities, from low, mild to high, with an additional control group that received no shock at all. As main findings, mice of all groups

learned the fear association, as exhibited by their increased freezing levels in session E1.1 (fear retrieval), and extinguished the fear memory by decreasing their freezing levels upon the end of the protocol (E5). However, shock intensity had an effect on the extinction curves with high shocked group to extinguish the fear memory slower than the other groups. Additionally, the high shock group exhibited intragroup heterogeneity regarding their extinction rate along the course of the extinction phase. Interestingly, in session E1.1, all groups exhibited comparable freezing levels in response to gradually increasing shock intensities. However, it would be intuitively expected that freezing time would increase proportionally to shock intensity, as others have previously reported (Merino et al., 2000). A potential reason would be the differences in the protocols, such as that study was done in rats with large steps among the shock intensities (0.2, 0.4 mV, and 1 mV). Alternatively, in the current protocol, an upper limit in the freezing in E1.1 could indicate a plateau in the freezing responses for contextual fear freezing. This point has been previously observed in cued FC paradigms after overtraining protocols (Laxmi et al., 2003). In line, previous studies reported generally low to middle-level freezing after contextual FC compared with cued FC (Çalışkan et al., 2016).

The intragroup variability of high shock animals could indicate a difficulty extinguishing the contextual fear memory of high adversity, and thus part develops PTSD characteristics. In line, previous studies found generalization of fear after increasing adversity of the US (Laxmi et al., 2003) or extinction deficits (Golub et al., 2009), both being traits of PTSD. To further support this assumption, it would be essential to test the freezing responses in a prolonged extinction phase that would include more extinction sessions. This way, all animals would have more time to potentially reach freezing levels comparable to control.

Examining the LFP signal in the CA3 and CA1 regions after E1.1, which corresponds to fear memory retrieval or re-consolidation process, SW-R properties were selectively enhanced in the high shock group and primarily in the CA1 region, accompanied by CA3-CA1 propagation facilitation. Interestingly, SW-R properties after E5, which represents the retrieval of the extinction, were principally normalized. This could be supported by a shift in the hippocampus's role in extinction to other regions, such as the mPFC, which significantly increase their activation at this stage (Mamiya et al., 2009). Therefore, the selective enhancement of SW-R in the high shock group

might indicate a role in representing the intensive training and, consequently, the fear memory salience in session E1.

Generally, it is well supported that SW-R mediate learning and consolidation of recent memories (Ego-Stengel & Wilson, 2010; Girardeau et al., 2009; Wang et al., 2015), and it could be assumed that the observed SW-R changes are a reflection of the most recent memory encoding event. However, in this experimental setting, this is not obvious, since SW-R did not change in the mild and low shock groups compared to control, even though their fear memory association was successful, as indicated by their freezing behavior in the retrieval session E1.1. To support such statement, more studies would be essential to investigate the network circuits after the training without further exposure to the fear context. For example, investigation of the SW-R 12 h and 24 h after the training would be indicative time points, as long-term memory consolidation that requires new protein synthesis takes place 12 h after acquisition (Karunakaran et al., 2016). In the present study, to assess also the behavioral readout, I examined the SW-R after an additional exposure to the context (E1.1), which eventually represents an additional memory process step.

Alternatively, enhanced SW-R in E1.1 only in the high shock group could imply that more adverse experiences would need more effort to extinguish. Thus, the recruitment of SW-R might be a mechanism to support extinction, in line with previous studies reporting decreased extinction of contextual fear memory after CA1 SW-R reduction (Polepalli et al., 2017). This proposal could also explain the negative correlation in E5 between CA1 SW incidence and freezing level, suggesting that persistence of an increased SW propensity in some mice under high-intensity training was associated with poor performance in the extinction.

In total, the enhanced SW-R observed in the high shock group only after fear memory retrieval could potentially represent the adversity of the emotional experience recall, which normalizes after fear memory extinguishes. However, an alternative role of SW-R is possible and would suggest a connection between decreased CA1 SW incidence and extinction deficits. The last view can be compared with the findings from STUDY 1 in GAD65 KO mice, where decreased CA1 SW incidence is observed in mice either naïve or after a stressful memory task, indicating a potential role of decreased CA1 SW incidence in the predisposition of the animal for PTSD-related behaviors. Of note, the behavior of GAD65 KO mice contains two intermingling components, the freezing, which is a measure of the fear response, and the fear memory association and the

anxiety traits. These two components contradict each other since anxiety could underlie an elevated psychomotor activity (Müller et al., 2015) and, therefore, their discrimination would require a more complex experimental design. Nevertheless, the current study suggests that SW-R can map properties of the adversity of an environment with a potential contribution of CA1 SW in the contextual fear memory extinction.

4.4 Signaling pathways involved in the gamma oscillopathy of Fragile X syndrome - STUDY 4

STUDY 4 examined the gamma oscillations in Fmr1 KO mice, a mouse model of FXS that exhibits electrophysiological alterations in the gamma range and changes in the ACh- and mGluR-signaling. Gamma oscillations were investigated in an *in vitro* model by pharmacological activation of the M1, mGlu, or KA receptors (Fisahn et al., 1998; Pálhalmi et al., 2004; Traub et al., 2003). Upon activation of M1 or $mGLuR_{1/5}$ pathways, gamma power was increased, whereas, upon excitation of KAR, gamma frequency was increased, but synchronization was decreased. These data provide evidence that the molecular alterations of these glutamatergic and cholinergic receptors through their aberrant signaling might be directly involved in the oscillopathy of Fmr1 KO mice and potentially in the manifestations of the syndrome.

Firstly, a significant increase in the power of CCh- induced gamma rhythm was found in Fmr1 KO mice. Previous studies have shown that ACh metabolism is unaffected in Fmr1 KO mice (Scremin et al., 2015), which suggest that the availability of the ligand was not the reason for the gamma enhancement. However, it has been shown that M1 receptors are overexpressed (Thomson et al., 2017) with a downstream effect on the hippocampal LTD (Volk et al., 2007). Therefore, activation of the pathologically upregulated M1 receptors might contribute to the gamma oscillopathy of Fmr1 KO mice.

Similar to CCh, DHPG also induced gamma oscillations with increased power in Fmr1 KO mice compared to WT. This finding conforms to previous studies with a direct link between the aberrant mGluR signaling and the gamma oscillopathy (Arbab et al., 2018; Dölen et al., 2007; Dölen & Bear, 2008). Of note, the increased peak frequency of the DHPG-induced gamma is in accordance with previous studies and independent of the genotype (Pálhalmi et al., 2004).

M1 and mGluR pathways are essentially independent mechanisms to induce gamma rhythm. CCh-gamma are not affected by mGluR blockers, even though DHPG might also tonically activate M1 (Pálhalmi et al., 2004). However, they have a common approach to induce LTD in Fmr1 KO mice, mediated by the FMRP (Huber et al., 2002; Volk et al., 2007; Zhang et al., 2009). Additionally, from this *in vitro* study, both CCh and DHPG increased the gamma power, in line with previous *in vivo* studies. Specifically, gamma oscillations recorded from parietal, frontal, or temporal cortices showed increased gamma power in Fmr1 KO mice (Jonak et al., 2020; Lovelace et al., 2018, 2020; Pirbhoy et al., 2020; Wen et al., 2019; Wong et al., 2020). EEG recordings from FXS patients detected enhanced gamma power, which was correlated with the severity of the clinical manifestations (Ethridge et al., 2017, 2019; Wang et al., 2017).

Gamma rhythm induction by using the agonist KA did not affect the power of the oscillation, as observed after the administration of CCh or DHPG. Instead, it increased the frequency and decreased synchronization of gamma rhythm in Fmr1 KO mice compared to the WT. In support, reduced gamma synchrony was observed in the auditory cortex of Fmr1 KO mice (Lovelace et al., 2020). Further studies showed reduced KAR synaptic expression and function in the insular cortex, with KA-dependent synaptic currents of faster kinetics but low efficacy (Qiu et al., 2018). Therefore, even though KA-mediated excitation contributes less to the total postsynaptic excitatory currents, KAR changes in Fmr1 KO mice could considerably add to its symptomatology (Koga et al., 2012).

Gamma oscillations arise from an interaction between interneurons and pyramidal cells (Hájos & Paulsen, 2009; Wang & Buzsáki, 1996; Whittington et al., 2000). Both inhibition and excitation are essential for pharmacologically-induced gamma generation, but substantial differences exist. For example, blocking $GABA_A$ transmission, all three (CCh-, DHPG- and KA-induced) gamma oscillation types are abolished (Fisahn et al., 1998, 2004; Pálhalmi et al., 2004). However, modifying the kinetics of the inhibitory transmission, such as using drugs that prolong the IPSC, DHPG- and KA-gamma show decreased frequency, while there is no effect on CCh-gamma frequency (Fisahn et al., 2004; Pálhalmi et al., 2004). Additionally, blocking the AMPAR-dependent glutamatergic neurotransmission, DHPG- and CCh- gamma are abolished (Pálhalmi et al., 2004) but not KA-gamma oscillations (Fisahn et al., 2004). Considering this, the AMPA-dependent gamma

oscillations of this study showed increased power in Fmr1 KO mice, while the inhibition-driven KA-gamma showed alterations in the frequency and synchronization domain.

Interneurons, especially PV^+ basket cells, are crucial for gamma rhythm generation, and importantly, they pace the gamma oscillation frequency (Buzsáki & Wang, 2012). Therefore, the changes observed regarding the KA-induced gamma frequency and synchronization would suggest potential alterations in this interneuron type. Indeed, previous studies have reported decreased PV^+ IN in the neocortex and impaired functionality of PV^+ and their perineuronal networks of Fmr1 KO mice (Lee et al., 2019; Lovelace et al., 2020; Wen et al., 2019). Interestingly, PV^+ IN deficits can lead to asynchronous gamma rhythm, but also to increased power of the rhythm, indicating that enhanced power might correspond to abnormal underlying networks (Guyon et al., 2021).

The increased power of CCh- and DHPG-induced gamma found in this study would suggest a more extensive accumulation of postsynaptic inhibitory currents, which could arise from an elevated excitatory input to the interneurons (Butler et al., 2016; Oren & Paulsen, 2010). However, due to the compromised GABAergic signaling of Fmr1 KO mice (Nomura, 2021; Olmos-Serrano et al., 2010; Paluszkiewicz et al., 2011), the net effect could direct towards excitation. In support, previous studies have shown that in Fmr1 KO mice, hippocampal pyramidal neurons exhibit excitation/inhibition disbalance in favor of excitation. Specifically, in hippocampal slices, responses of CA3 and CA1 pyramidal cells to high-frequency stimulation were increased, while short-term depression was reduced (Deng et al., 2011). Furthermore, neuronal hyperexcitability has been observed in cortical areas, such as the somatosensory cortex of Fmr1 KO mice, which was dependent on the sleep-wakefulness state (Gonçalves et al., 2013). Therefore, the increased power of the CCh-DHPD gamma might be an indication of an abnormal underlying network, also indicated by the correlation between the cognitive severity of the syndrome and the CA3-origin gamma oscillation dominance (Dvorak et al., 2018; Radwan et al., 2016; Talbot et al., 2018).

Overall, this study directly involves M1, mGlu, and KA receptors in the gamma oscillopathy and bridges molecular alterations and electrophysiological manifestations of Fmr1 KO model and FXS. It also supports that the *in vitro* approach could be used as a proxy to investigate underlying pathophysiological mechanisms and have clinical relevance. Last, it suggests a connection between Fmr1 KO and GAD65 KO mice, animal models that exhibit common phenotypical

characteristics, such as seizures and anxiety, excitation/inhibition imbalance, and electrophysiological alterations in the gamma range.

4.5 Conclusions and Outlook

This thesis studied the involvement of hippocampal network oscillations in anxiety and learned fear and investigated their cellular and behavioral correlates.

The first study assessed the *in vitro* ventral hippocampal network activity and the contribution of the GAD65-dependent GABA deficiency in anxiety and PTSD, using as an animal model the GAD65 KO mouse that exhibits emotional processing deficits. Main findings included enhanced gamma and ripple oscillations, indicating a hyperexcitable network state, in line with the GABA deficiency of the model, but also indicating enhancement of the inhibitory kinetics. For this reason, kinetics and properties of the GABA receptors would be interesting to examine in this animal model in the future. Furthermore, enhancement of the IN kinetics would imply an enhancement in the GABAergic transmission that would seem counterintuitive in an animal model of GABA deficiency. Therefore, it would be interesting to assess in future studies whether distinct IN types are differentially affected. For example, perisomatic INs (PV^+ and axo-axonic) that determine the synchronicity of the pyramidal firing and set the pace of the rhythm. In total, enhanced gamma oscillations and ripples in the vHP of GAD65 KO mice indicate a potential contribution of augmented fast oscillations in the predisposition for anxiety and stress susceptibility in this animal model and support current literature about the involvement of the GABAergic system in these neuropsychiatric conditions.

Previous studies have revealed altered power of pharamacologically-induced gamma oscillations after stress (Albrecht et al., 2013; Çalışkan et al., 2015b), which was not found in naïve but stress-susceptible GAD65 KO mice. Therefore, it would be interesting to assess further how acute and chronic stress change the oscillatory phenotype of the GAD65 KO mouse, as it has been previously shown for the theta rhythm. Such studies reported *in vivo* hippocampal-amygdalar theta synchrony upon retrieval of fearful memories (Seidenbecher et al., 2003). Also, in GAD65 KO mice, fear memory deficits, including overgeneralization or extinction impairments, are connected with alterations in the theta synchronization between the amygdala and hippocampus (Bergado-

Acosta et al., 2008; Sangha et al., 2009), which can subsequently modify the gamma rhythm (Bragin et al., 1995).

GAD65 KO mice, after a contextual FC, reduced very fast their freezing behavior and not gradually, as happened with WT mice. To distinguish between facilitation of fear memory extinction and a potential elevated psychomotor activity due to the stressful situation and increased anxiety (Müller et al., 2015), it would be interesting to examine the animal behavior in more detail. In this study, additional observations on behavior that exhibit defense, such as flight, were not distinct (Laxmi et al., 2003). Therefore, using machine learning methods (Luxem et al., 2020) that can categorize the animal motions into clusters could help identify motifs of neuropsychiatric conditions, such as stereotypies or panic-like patterns.

Examination of the baseline excitability and plasticity of the SC-CA1 synapse, a major synaptic input to CA1 pyramidal cells that could underlie changes in the CA1 SW incidence of the GAD65 KO mice, revealed no differences between the genotypes. However, the CA1 region also receives input from other regions, such as directly from the EC through the temporoammonic path (Neves et al., 2008). Thus, exploration of this synapse in future studies could add information about the excitability and plasticity in the CA1 area. Besides, it would be interesting to investigate how different LTP induction protocols would affect plasticity in GAD65 KO mice. For example, previous studies have shown that HFS- and TBS-induced LTP are regulated differentially by the GABA inhibitory tone (Gong et al., 2009; Percelay et al., 2021).

Furthermore, previous studies have shown plastic effects on intrinsic excitability. For example, neurons related to emotional responses, such as hypothalamic neurons, increased their excitability after stress in terms of firing frequency and R_{in} (Matovic et al., 2020). Considering that GAD65 KO mice have susceptibility to stress, it would be interesting to assess the intrinsic neuronal properties in the vHP after applying a stress paradigm.

CA1 pyramidal cells exhibited altered intrinsic properties with mild hyperpolarization and a trend for increased inhibitory currents, which could partially explain the enhanced fast ripples and gamma, as well as the decrease in CA1 SW incidence. Examination of excitation/inhibition balance in CA1 triggered by CA3 SW-R did not demonstrate differences in the CA1 currents during SW-R. Further studies would be required to differentially examine the properties and currents between

pyramidal cells participants and non-participants in SW-R events (Bähner et al., 2011; Ishikawa & Ikegaya, 2020; Mizunuma et al., 2014). The current study focused on the CA1 area to explain the inconsistency of the excitability status arising from enhanced fast oscillation but SW reduced incidence. However, it would be interesting to examine the CA3 area and identify cellular excitability measures that could underlie the enhanced network oscillations in the region.

In search of critical mechanisms that might underlie the electrophysiological alterations of GAD65 KO mice, a local GAD65 decrease in the ventral CA1 and DG-CA3 regions was induced. Upon local GAD65 reduction in the CA3 area, SW-R revealed no alterations, while after local reduction in the CA1 area, CA1 ripple components were differentially decreased, consistent with an impairment in the GABAergic system to pace the fast oscillations. However, the KD models did not replicate the electrophysiological phenotype of GAD65 KO mice. This finding would indicate a potential reorganization of the hippocampal circuits as a result of the general GABAergic dysfunction in GAD65 KO mice, which could also include dysregulation of allostatic mechanisms that balance excitation/inhibition and modifications in regions of emotional regulation, such as the amygdala, ACC, and their communication, as previously described. Nevertheless, behavioral characterization of mice after local GAD65 decrease in the ventral CA1 area could reveal an effect of decreased CA1 ripples in anxiety and fear memory formation.

The examination of GAD65 KO mice after contextual FC could not demonstrate whether SW-R represent fear learning and its extinction or traits of the model. Subsequent assessment of SW-R in WT C57BL/6 mice showed a putative differential function of SW-R. In particular, enhanced SW-R were present only after the retrieval of adverse learning with the suggestion that increased CA1 SW incidence would facilitate extinction. A more timely-detailed investigation of SW-R properties during distinct phases of contextual fear memories would be necessary to support this conclusion.

In total, this study used the ventral hippocampal network oscillations as proxies to describe anxiety and fear memories employing different animal models that exhibit learning and emotional processing deficits.

Firstly, it could demonstrate altered oscillations in the vHP of GAD56 KO mice, supporting previous studies about the involvement of a compromised GABAergic system in anxiety and stress susceptibility. In this model, both CA3 and CA1 areas of the vHP showed enhanced gamma

oscillations and ripples, with dissociation in the sharp-wave characteristics between CA3 and CA1 regions that was more prominent after a stressful experience that contained contextual fear conditioning and its extinction. Therefore, these findings indicate enhanced fast oscillations as correlates of stress susceptibility upon GAD65-dependent GABA deficiency. Interestingly, after local GAD65 reduction in the vHP, the electrophysiological phenotype was not replicated, implying systemic changes and reconfiguration of the hippocampal circuits upon abnormal postnatal GABA development. The compromised GABAergic system of the GAD65 KO mice would suggest excitation/inhibition imbalance in favour of excitation, consistent with the higher likelihood of developing RED and the enhanced SW components in the CA3 area. In search of mechanisms to explain the decreased SW incidence in the CA1 region, cellular investigation showed a tendency for hyperpolarizing membrane potential of CA1 pyramidal cells that tend to receive higher frequency inhibitory currents.

Furthermore, this study suggests that enhanced SW-R might represent adversity of a fearful experience, with a possibility to facilitate the extinction of the fear memory. On the other hand, it suggests that a decrease in the SW incidence might be connected with a predisposition to develop stress susceptibility, as observed in GAD65 KO mice and in the WT mice that were trained with high adversity.

Last, this study connected reported molecular deficits with the gamma oscillopathy of Fmr1 KO mice, by pharmacological hyperactivation of M1, mGlu, and KA receptors. Fmr1 KO mice, an animal model of FXS, exhibits excitation/inhibition imbalance and recapitulates manifestations of the FXS, such as intellectual disability and social deficits, including anxiety. Thus, it reveals a direct implication of glutamatergic and muscarinergic pathways in the pathophysiology of Fmr1 KO mice and possibly in the syndrome.

APPENDIX

A.1 Characterization of beta/gamma oscillations in GAD65 KO mice with focus on sex differences

Anxiety disorders and related traits, such as amplification of perceived danger and approach-avoidance conflict, have greater incidence in women (Bandelow & Michaelis, 2015). Previous studies have implicated cortical GABAergic transmission in such behaviors. Specifically, a prominent single nucleotide polymorphism change in the GAD2 gene, which encodes GAD65 enzyme, in the ACC of women modulated GABA/glutamate rate and harm avoidance behavior (Colic et al., 2018). Additionally, sex hormones modify GABA synthesis (Davis et al., 1999; Seney et al., 2013) and GAD65 mRNA (Ikeda et al., 2015). The vHP and ACC are brain regions involved in anxiety (Bush et al., 2000; Jimenez, 2018; Jovanovic & Ressler, 2010; Kheirbek & Hen, 2011), and they exhibit behavior-relevant fast oscillatory activity in the beta/gamma range, which is shaped by GABAergic transmission *in vivo* and *in vitro* (Whittington et al., 1995, 2000).

Therefore, to investigate the GAD2-dependent neurobiological basis of sex differences in anxiety-like behaviors, I used the GAD65 KO mouse, a model of decreased GABA synthesis and increased anxiety and stress susceptibility. I hypothesized that the network activity in anxiety-related areas would represent potential sex differences. To this extent, the oscillatory activity in the ACC and vHP were characterized in male, female GAD65 KO mice, and WT littermates. In addition to the investigation of gamma oscillations in the vHP of male GAD65 KO mice (STUDY 1), vHP gamma oscillations of both sexes are described in this section.

A.1.1 Enhanced fast beta/gamma oscillations in the ACC of GAD65 KO mice

Fast oscillations in the range of beta/gamma in slices containing the dorsal ACC from female and male GAD65 KO and WT mice were characterized. The oscillations were induced by co-perfusion of carbachol (CCh, 50 µM) and kainate (KA, 0.8 µM), as described previously (Steullet et al., 2014). The analysis was divided into two frequency ranges, beta range (10-25 Hz) and slow gamma range (25-45 Hz). The peak frequency of the oscillation in the beta range (Fig. A.1c; two-way ANOVA, effect of genotype $F(1, 22) = 0.0002$, $p = 0.98$; effect of sex $F(1, 22) = 0.41$) and slow gamma range

(Fig. A.1f; two-way ANOVA; effect of genotype F(1, 22) = 0.17, p = 0.68; effect of sex F(1, 22) = 2.29, p = 0.143) remained unaltered among the groups. However, the peak power (Fig. A.1d; two-way ANOVA; effect of genotype F(1, 22) = 8.372, p = 0.0084) and integrated power (Fig. A.1e; two-way ANOVA; effect of genotype F(1, 22) = 10.64, p = 0.0036) in the slower frequency range showed a significant genotype effect. Similarly, in the faster frequency range (26-45 Hz) the peak power (Fig. A.1g; two-way ANOVA; effect of genotype F(1, 22) = 3.361, p = 0.08) showed a trend for a genotype effect, while the integrated power showed a clear genotype effect (Fig. A.1h; two-way ANOVA; effect of genotype F(1, 22) = 4.659, p = 0.0421). These results indicate that increased power of cortical oscillations recorded in dACC might be associated with the phenotype of GAD65 KO mice independent of sex.

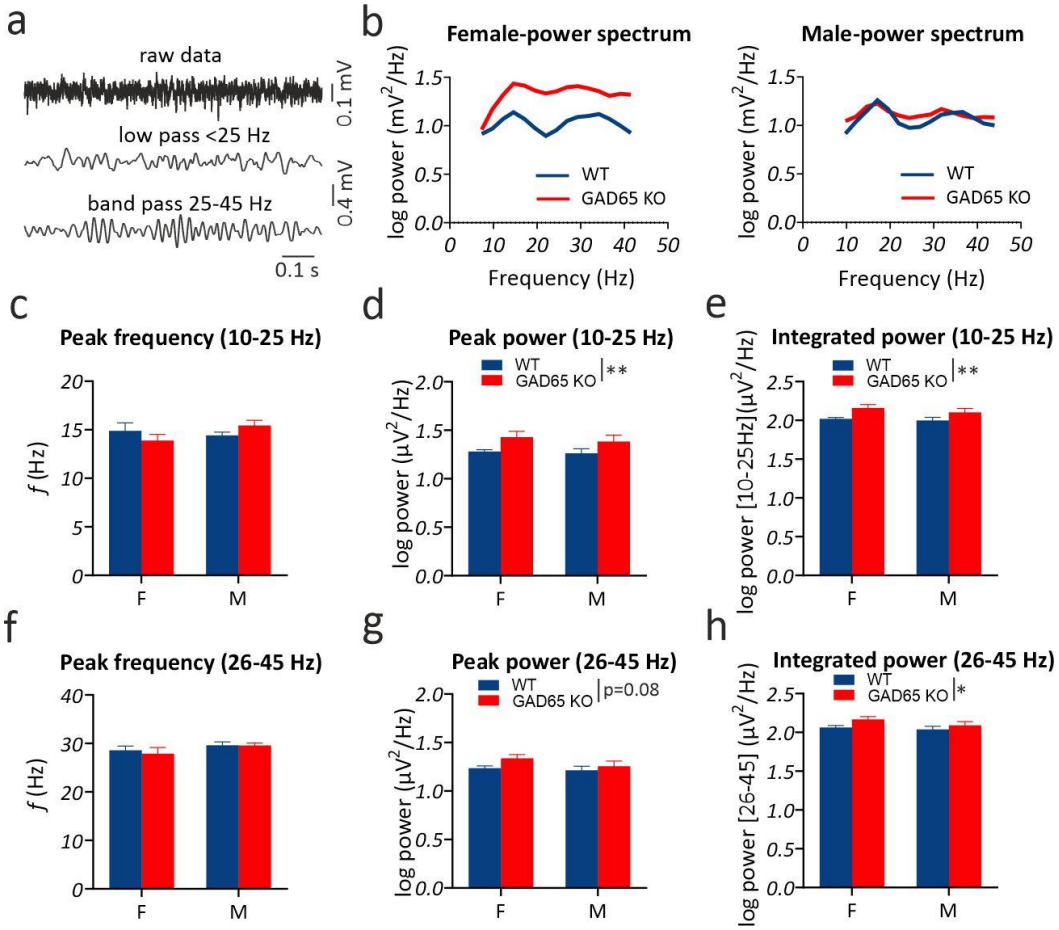

Fig. A.1: CCh- and KA-induced fast oscillations in the ACC of male and female GAD65 KO mice. (a) *Example traces of unprocessed raw data (5 kHz), low-pass filtered (<25 Hz), and band-pass filtered (25-45 Hz) in vitro beta/gamma oscillations.* ***(b)*** *Representative power spectra of female (F) and male (M) mice showing two main peak frequencies in the LFP signal; around 15 Hz and around 35 Hz. Summary graphs illustrating*

(c) *no differences in peak frequency, but prominent genotype effect for* ***(d)*** *peak power and* ***(e)*** *integrated power in the range of 10-15 Hz. In the range of 26-45 Hz* ***(f)*** *peak frequency and* ***(g)*** *peak power showed no alteration, whereas* ***(h)*** *integrated power showed a general genotype effect. Statistical comparison was performed by using two-way ANOVA. Data are given as mean ± SEM. *p < 0.05, **p < 0.01. Female WT: N = 8 mice, n = 47 slices, GAD65 KO: N= 6 mice, n= 36 slices; Male WT: N = 6 mice, n = 29 slices, GAD65 KO: N = 6 mice, n = 30 slices; F: female, M: male.*

A.1.2 Altered gamma oscillations in the vHP of GAD65 KO mice in a sex-dependent manner

In addition to the study of gamma oscillations in male GAD65 KO mice (STUDY 1 - section 3.1.1), female GAD65 KO and WT littermates were investigated. In the CA3 subregion, the peak gamma frequency (Fig. A.2e; Student's two-tailed t-test; T(39) = 0.2351, p = 0.8153), integrated power (20-80 Hz) (Fig. A.2f; Student's two-tailed t-test; T(39) = 0.9702, p = 0.3379), peak power (Fig. A.2g; Student's two-tailed t-test; T(39) = 1.458, p = 0.1528) and waveform auto-correlation (Fig. A.2h; Student's two-tailed t-test; T(39) = 1.531, p = 0.134) showed no differences between the genotypes. Similarly, in the CA1 subregion, gamma frequency (Fig. A.2i; Student's two-tailed t-test; T(39) = 0.173, p = 0.863), integrated power (Fig. A.2j; Student's two-tailed t-test; T(39) = 0.0732, p = 0.942), peak power (Fig. A.2k; Student's two-tailed t-test; T(39) = 0.6173, p = 0.5406) and waveform auto-correlation (Fig. A.2l; Student's two-tailed t-test; T(39) = 0.04907, p = 0.9611) remained unaltered between the genotypes in the female mice. The CA3-CA1 waveform cross-correlation revealed no difference within the female group (Fig. A.2o; Student's two-tailed t-test; T(39) = 0.6442, p = 0.5232). These data reveal no differences in the CCh-induced gamma oscillations of female GAD65 KO mice. However, male GAD65 KO mice showed enhanced frequency compared to WT, which implies a sex effect in the gamma oscillations of GAD65 KO mice. For a better overview, Fig. A.2 contains the results from the male study (section 3.1.1), as well.

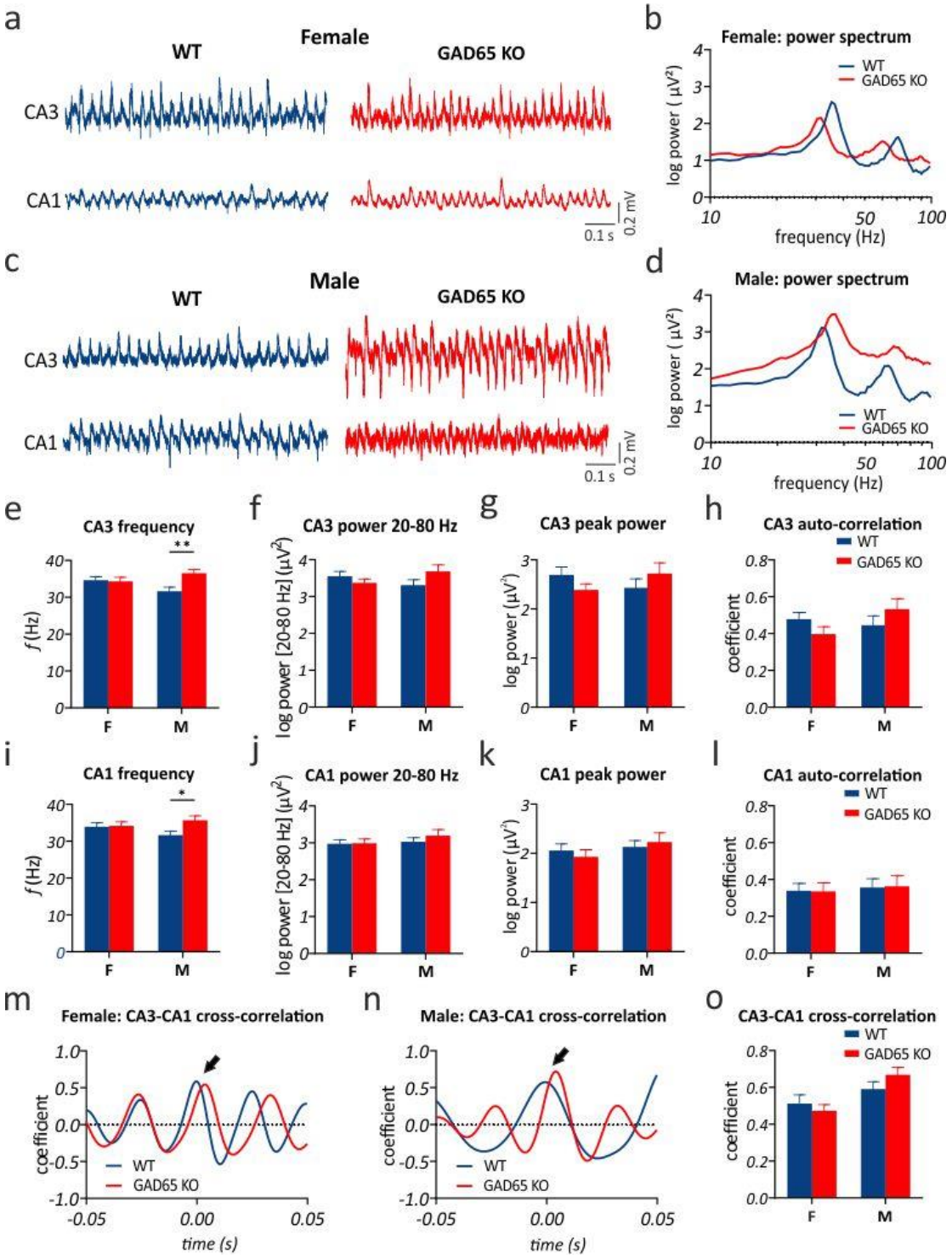

Fig. A.2: CCh-induced gamma oscillations in the vHP of male and female GAD65 KO mice. (a, c) *Representative traces of gamma oscillations recorded from the CA3 and CA1 regions of GAD65 KO and WT mice.* ***(b, d)*** *Corresponding spectrograms highlighting the higher frequency (f) of male GAD65 KO mice. In the CA3 region, summary graphs demonstrating,* ***(e)*** *increased gamma frequency only in male GAD65 KO compared to WT,* ***(f)*** *unaltered integrated power (20-80 Hz),* ***(g)*** *peak power, and* ***(h)*** *waveform auto-correlation. In the CA1 region, summary graphs illustrating* ***(i)*** *increased frequency in male GAD65 KO compared to male WT mice, but no differences in* ***(j)*** *integrated power (20-80 Hz),* ***(k)*** *peak power, and* ***(h)***

waveform auto-correlation between the sexes and the genotypes. ***(m, n)*** *Example CA3-CA1 waveform cross-correlograms and* ***(o)*** *summary graph showing no differences within sex between GAD65 KO and WT mice. Statistical comparison was performed using Student's t-test within sex. *p ≤ 0.05. Data are given as mean ± SEM. Female (F): WT N = 5 mice, n = 23 slices, GAD65 KO N = 5 mice, n = 18 slices; Male (M) WT: N = 5 mice, n = 16 slices, GAD65 KO: N = 5 mice, n = 17 slices. For correlations (**j, k, l**): Male WT: N = 5 mice, n = 16 slices, GAD65 KO: N = 4 mice, n = 12 slices.*

In conclusion, this study showed increased power of CCh- and KA-induced fast oscillations in the ACC in a genotype but not sex-dependent manner. This would suggest that increased fast oscillation power in the ACC could be a correlate of anxiety-like behavior independent of the sex. On the other hand, CCh-induced gamma oscillations in the CA3 and CA1 subregions of the vHP showed increased frequency only in the male GAD65 KO mice compared to WT, supporting sex differences in the expression of anxiety-like behavior.

A.1.3 Supplementary methods for ACC slice electrophysiology

Coronal slices of 400 µm that contained the ACC were obtained from GAD65 KO mice and WT littermates from both sexes. They were rapidly transferred to an interface chamber and incubated at 32 °C for 1 h in standard aCSF. After incubation, a modified aCSF was perfused containing 50 µM CCh, 0.8 µM KA and increased K^+ (5 mM) (Steullet et al., 2014). Fast oscillations in the beta/gamma-band range were induced after about 45 min. The LFP activity was recorded by placing one recording electrode on each hemisphere in layer 5 of dorsal ACC (dACC). Artifact-free data of two-minute duration were analyzed using the Fast Fourier Transformation with a frequency resolution of 2.441 Hz. Power spectrum analysis revealed peaks in two frequency ranges, 10-25 Hz and 26-45 Hz. Peak power, frequency, and integrated power were calculated in these frequency bands, 10-25 Hz and 26-45 Hz, corresponding to beta and gamma rhythm, respectively. For statistical comparison, only signals with peak power higher than 5 μV^2 and peak frequency higher than 10 Hz were included.

A.2 Investigation of additional behaviors during contextual FC in GAD65 KO mice

GAD65 KO mice showed decreased freezing levels during the contextual FC, interpreted as impaired learning capacity. This contrasts with previous studies that exhibited no contextual fear memory deficits in this animal model (Sangha et al., 2009). Additionally, it has been shown that GAD65 KO mice have a tendency for flight responses instead of freezing to demonstrate their fear (Bergado-Acosta et al., 2014; Stork et al., 2003). To test this, I investigated additional parameters

that could shed light on the differential fear expression of the mice. Other behaviors, such as rearing, grooming, general immobility, and ratios of immobility and freezing at the retrieval session (E1.1), the end of the extinction phase (E5.1), and the contextual re-exposure session (SR) were monitored. Total inactivity (Fig. A.3a; two-way RM ANOVA; effect of session $F(2, 34) = 3.570$, $p = 0.0391$), rearing (Fig. A.3b; two-way RM ANOVA; effect of session $F(2, 34) = 6.435$, $p = 0.0043$), and grooming (Fig. A.3c; two-way RM ANOVA; effect of session $F(2, 34) = 20.29$, $p < 0.0001$) showed only a session but not a genotype effect. The extinction ratio, defined as the subtraction of the freezing rates between E5.2 and E1.1 (Fig. A.3d; Mann Whitney U test, $p = 0.8416$) and SR and E1.1 (Fig. A.3e; Mann Whitney U test, $p = 0.0109$), indicated higher extinction in the GAD65 KO mice, as their freezing time fell to very low levels at the end of the paradigm. Flight responses were not detected, whereas jumping, startle, and tail rattling were barely observed. These results indicate a complex phenotype of the GAD65 KO mice, with equal inactivity levels with WT mice, but not freezing, which is defined as a rigid posture for more than 1 sec.

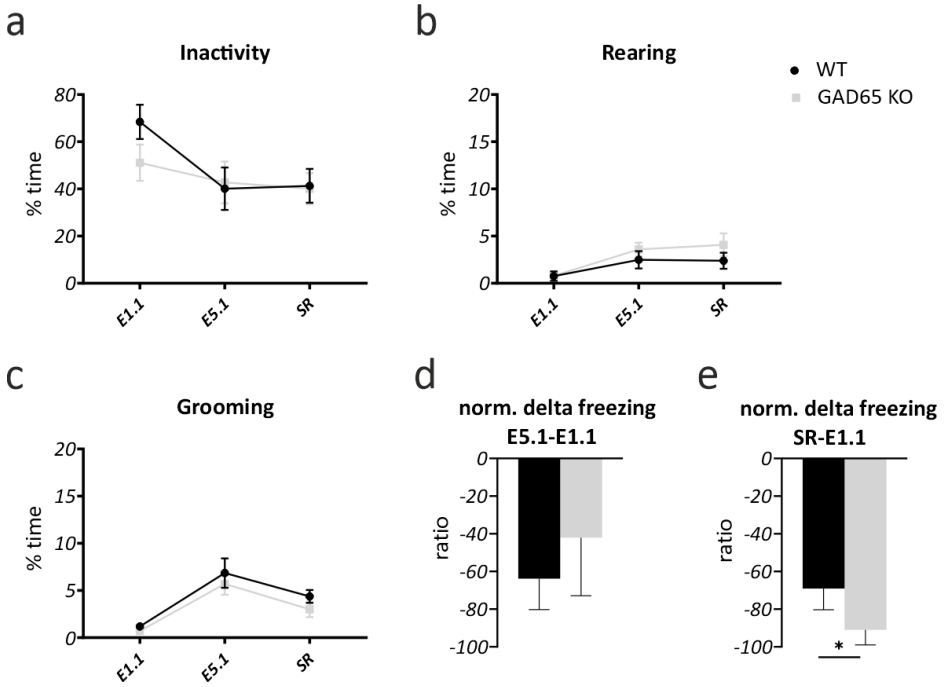

Fig. A.3: Behaviors of GAD65 KO mice during contextual FC. (a) *Total inactivity time,* ***(b)*** *occurrence of rearing and* ***(c)*** *grooming behaviors across the paradigm showed no differences in GAD65 KO mice compared to WT. (d) Norm. extinction rate at E5.1 was comparable between the groups, while (e) norm. extinction rate at SR was higher in GAD65 KO mice. E1.1: first two minutes of extinction session 1; E5.1: first two minutes of extinction session 5; SR: spontaneous recovery session. Statistical comparison was performed using two-way RM ANOVA and post-hoc Sidak's test for* ***a, b, c,*** *and Mann Whitney for* ***d*** *and* ***e****. Data are given as mean ± SEM. *p < 0.05. WT: N = 9 mice, GAD65 KO: N = 10 mice.*

A.3 Total numbers of C57BL/6 mice during contextual FC (Supplementary to Fig. 3.16)

In section 3.3.1, to statistically compare the groups in subsequent sessions, I used mice that participated in the whole paradigm (E5 group). However, the SW-R characterization after E1.1 included mice that performed the paradigm until E1.1 and for this reason the animal numbers until E5 decreased. Merging all groups, the freezing phenotype was similar: freezing increased after shock delivery (T.3) or during E1.1 and reached levels comparable to control upon E5.1. Additionally, the extinction curve retained a shock intensity-dependent manner (Fig. A.5; Mixed-effects model; effect of shock $F(3, 65) = 8.033$, $p = 0.0001$). Notably, the low shock group exhibited relatively high baseline freezing levels, but they successfully learned the fear association and its extinction.

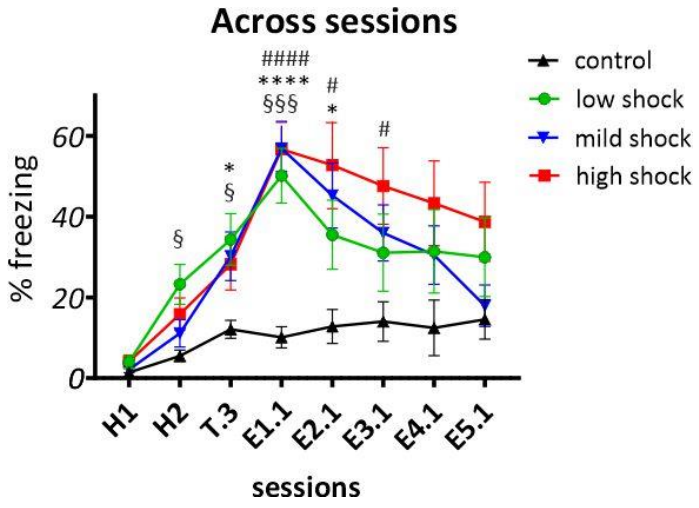

Fig. A.4: Freezing during contextual FC and extinction in C57BL/6 mice (merged number of animals: E1 and E5 groups). *Freezing levels across all sessions of a contextual FC and extinction paradigm. Mice that received shock increased their freezing rate significantly compared to control mice and showed extinction at the end of the paradigm. H1-H2: Habituation sessions 1 & 2; T.3: last 2 min of the training session; E1.1-E5.1: first 2 min of each extinction session 1-5. Statistical comparison was performed using mixed-effects model followed by post-hoc Tukey's test. Data are given as mean ± SEM. For sessions H1-E1.1: control: N=17; low shock: N = 17 mice; mild shock: N = 17 mice; high shock: N = 18 mice. For sessions E2.1-E5.1: control: N=8 low shock: N = 9 mice; mild shock: N = 8 mice; high shock: N = 10 mice. § $p < 0.05$, §§§ $p < 0.001$: low shock vs. control; * $p < 0.05$, **** $p < 0.0001$: mild shock vs. control; # $p < 0.05$, #### $p < 0.0001$: high shock vs. control.*

A.4 Inter-session freezing of C57BL/6 mice during contextual FC extinction

Analysis within each extinction session revealed a shock intensity effect for sessions E1, E2, and E3 (Fig. A.5a-e; two-way RM ANOVA; effect of shock intensity for E1: $F(3, 31) = 3.703$, $p = 0.0219$; E2: $F = 3.271$, $p = 0.0342$; E3: $F = 2.448$, $p = 0.0823$; E4: $F = 2.834$, $p = 0.0543$; E5: $F = 1.974$, $p = 0.1383$). In particular, within extinction session E1, all shock groups increased their freezing levels

compared to control, steadily decreasing upon the end of the session. In session E2, only mild and high shock groups showed increased freezing during the first 2-min bin compared to control. In the first minutes of E3, only the high shock group showed increased freezing compared to control, while during sessions E4 and E5, all mice groups exhibited comparable freezing levels. Thus, these data show comparable freezing levels of all shock groups during fear memory retrieval (E1.1 session) with successful extinction (E5 session), with a slower extinction curve for the high shock group.

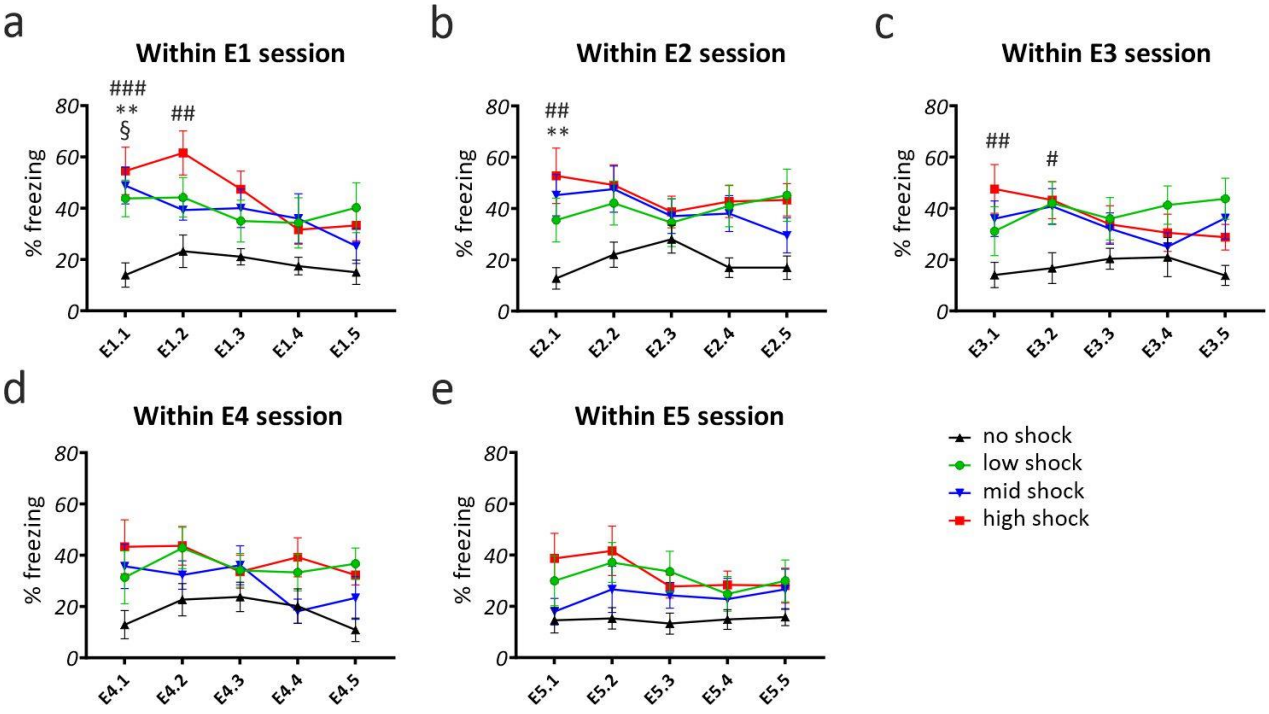

Fig. A.5: Inter-session freezing levels of C57BL/6 mice during extinction. *Each extinction session lasted in total 10 min, and data are presented in 2-min bins.* ***(a)*** *Within extinction session E1, all shock groups increased their freezing levels compared to control, gradually decreasing upon the end of the session.* ***(b)*** *In the first 2-min bin of E2, mild and high shock groups showed increased freezing compared to control, which gradually decreased upon the end of the session.* ***(c)*** *In the first minutes of E3, only the high shock group showed increased freezing compared to control, while during* ***(d)*** *E4 and* ***(e)*** *E5 sessions, the freezing levels of all shock groups were comparable to control's. E1-5: extinction sessions 1-5. The number after the dot illustrates the 2-min bin. Statistical comparison was performed using two-way RM ANOVA followed by post-hoc Tukey's test. Data are given as mean ± SEM. control: N=8 mice; low shock: N = 9 mice; mild shock: N = 8 mice; high shock: N = 10 mice. Significant difference is indicated with § for low shock vs. control, * for mild shock vs. control, and # for high shock vs. control (§, #: p < 0.05; ##, **: p < 0.01; ###: p < 0.001).*

A.5 Lentiviral constructs, GFP expression and western blotting

The oligonucleotide sequence 5' - GCATGCTTCCTACCTCTTTCA-3' was used to generate shRNA hairpin constructs to impede the GAD65 expression (Rehberg et al., 2014) while a random

sequence 5’ - TCGTCATGACGTGCATAGG -3’ (Thiere et al., 2016) was used as a control. shRNA constructs were cloned into the pll3.7 vector under the U6 promoter (Rubinson et al., 2003). HEK293T cells were used for the generation of lentiviral particles. The QuickTiter™ Lentivirus Kit (Cell Biolabs, USA) was employed to estimate the viral titer. Production of both experimental and control vectors was done in parallel.

To verify the correct injection sites for the local GAD65 reduction in the ventral DG-CA3 or CA1 regions, GFP and GAD65 expression was assessed. Only the slices with GFP fluorescence under the microscope and decreased GAD65 expression were used for statistical analysis.

Western blotting was performed by Miguel del Angel, Stork Lab, OvGU Magdeburg, Germany. After the electrophysiological experiment of GAD65 KD animals, slices of 400 µm containing only the ventral hippocampus were stored in a -20 °C freezer. To quantify the GAD65 protein content, slices were mechanically homogenized in cold Lysis buffer of the following composition: 1% Laurylmaltoside, 1% NP-40, 1 mM Na_3VO_4, 2 mM EDTA, 50 mM Tris-HCl pH 8.0, 150 mM NaCl, 0.5% deoxycholate, 1 mM NaF 1 mM AEBSF protease inhibitor (Thermo Scientific, cat. No. 78431), 1 µM Pepstatin A (Thermo Scientific, cat. No. 78436) and 1 tablet of Pierce protease inhibitor (Thermo Scientific, cat. No. A32963). Samples were incubated for 10 minutes and then centrifuged at 13.000 g. The supernatant was collected, and protein concentration was quantified using the RC DC Protein assay Kit II from Biorad, cat. No. 5000122. Then, samples were prepared for immunoblot analysis, in 4X Sample buffer containing 40% glycerol, 240 mM Tris HCl pH 6.8, 8% SDS, 0.04% Bromophenol blue, and 5% mercaptoethanol, and then heated at 95 °C for 5 minutes. 20 µg of each sample was loaded in an SDS Bis-Acrylamide gel for electrophoresis. Proteins were transferred to FL- PVDF membranes (Millipore, cat. No. IPFL00010) and probed with primary antibodies; anti-GFP (abcam, ab6673, 1:2000) in anti-Gad65 (abcam, ab26113, 1:1000) and anti-α tubulin (Sigma, T6199). Primary antibodies were detected using the near-infrared labeled secondary antibodies IRDye 800CW & IRDye 680CW (Licor, 1:10,000). Imaging was performed using the Odyssey Imaging System (LI-COR), and the protein signal was quantified in the Image Studio software (LI-COR).

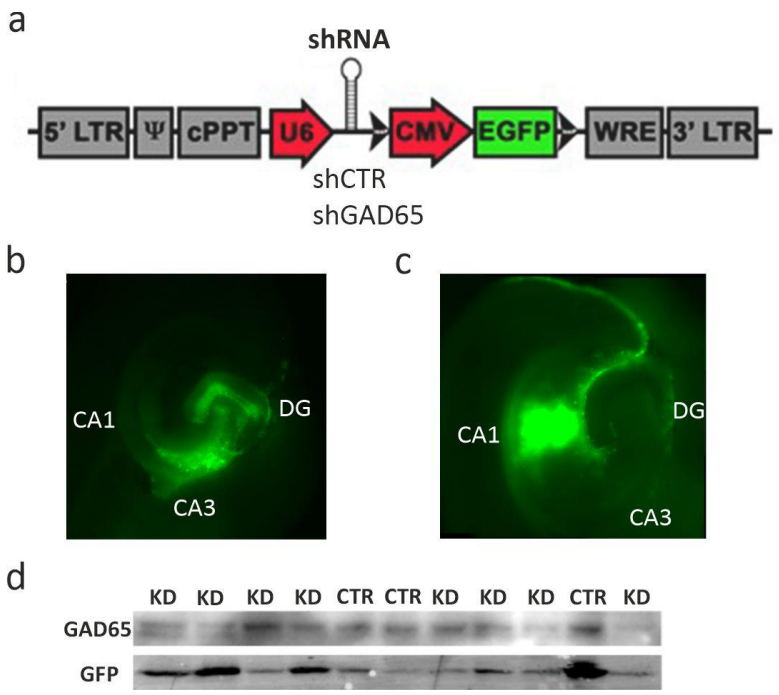

Fig. A.6: GFP and GAD65 expression after viral injections in the vHP. (a) *Lentiviral construct containing shRNA for GAD65 or a random sequence (CTR). The lentiviral construct contained either a shGAD65 RNA for knocking down the GAD65 expression or a random shRNA for the control group. Horizontal brain slices containing the hippocampus under the fluorescent microscope with a* ***(a)*** *representative example of GFP expression in the vCA3-DG and* ***(b)*** *vCA1 after injection of GFP-tagged lentivirus.* ***(c)*** *An additional verification was performed using westerns blotting for GFP & GAD65 protein detection, isolating the HP from the slices after the electrophysiological recordings. CMV: cytomegalovirus promoter; cPPT: central polypurine tract; EGFP: enhanced green fluorescence protein; LTR: long terminal repeat; Ψ: psi packaging element; U6: U6 promoter; WRE: woodchuck hepatitis virus posttranscriptional regulatory element. (****(a)*** *Reproduced from Tripathi et al.,* [*2021*] *with permission from Elsevier).*

A.6 Genotyping of transgenic mouse lines using the PCR method

Ear biopsies were taken from the mice after weaning. The tissues were lyzed with protein kinase K (10 mg/ml, Carl Roth GmbH, Karlsruhe, Germany) and PCR direct lysis buffer (Peqlab, Erlangen, Germany) and incubated at 55 °C overnight. After digestion, the kinase K was heat inactivated at 85 °C for 45 min and the samples were stored at -20 °C until further process. For genotyping, allele-specific primers designed to target the transgenes or the wild-type (WT) allele were used (see tables T.1 and T.4). After the PCR reaction, the products were placed in agarose gels that contained the DNA marker EtBr. After the electrophoresis, the DNA fragments were visualized under ultraviolet light and compared with the size of the standard DNA ladder. For the GAD65 mouse line, the size of the WT fragment is 90 bp, while the transgene fragment 160 bp. For the Fmr1 mouse line, the WT fragment is 131 bp, while the transgene 300 bp.

PCR protocol for genotyping the GAD65 mouse line

Table T.1: Primers

Primer Name	Sequence
G65 S3	GGG AAG CCA GCG GAG GGC GG (forward-both genotypes)
Rnco3	GGC TGC TAA AGC GCA TGC TC (transgene)
G65 A3	CCC ATT TAC CTG TTG CGT GCA G (reverse-wild-type allele)

Table T.2: Master Mix

1 µl 10x Cl buffer (with magnesium)
1 µl dNTPs
2 µl Q-solution
0.3 µl Primer G65 S3 (10 µM)
0.7 µl Primer Rnco3 (10 µM)
2.94 µl H_2O
0.06 µl DREAM Taq polymerase (5 U/µl)

Table T.3: PCR repetitions program

Phase	Duration	Temperature	Repetitions
Inital denaturation	5 min	95 °C	1
Denaturation	20 s	94 °C	35
Annealiation + extension	90 s	68 °C	35
Final extension	7 s	72 °C	1
Cooling & storage	∞	4 °C	1

PCR protocol for genotyping the Fmr1 mouse line

Table T.4: Primers

Primer Name	Sequence
FreX oIMR 6734	TGT GAT AGA ATA TGC AGC ATG TGA (wild type)

FreX oIMR 6735	CTT CTG GCA CCT CCA GCT T (common)
FreX oIMR 2060	CAC GAG ACT AGT GAG ACG TG (mutant)

Table T.5: Master Mix

1.0 µl 10x DreamTaq green buffer
0.8 µl dNTP's (2.5 mM)
0.5 µl Primer oIMR 6734 (10 mM)
0.5 µl Primer oIMR 6745 (10 mM)
0.5 µl Primer oIMR 2060 (10 mM)
5.65 µl ddH_2O
0.05 µl DreamTaq polymerase

Table T.6: PCR repetitions program

Phase	Duration	Temperature	Repetitions
Inital denaturation	3 min	94 °C	1
Denaturation	30 sec	94 °C	35
Annealiation	15 sec	62 °C	35
Extension	30 sec	72 °C	35
Final extension	7 min	72 °C	1
Cooling & storage	∞	4 °C	1

A.7 Supplement to the statistical analysis

Table T.7: ANOVA results relevant to Fig. 3.5

ANOVA table **Fig. 3.5a**	**F (DFn, DFd)**	**P value**
session x genotype	F (8, 136) = 4.381	P < 0.0001
session	F (4.482, 76.19) = 19.70	P < 0.0001
genotype	F (1, 17) = 9.393	P = 0.0070
animal	F (17, 136) = 6.589	P < 0.0001
ANOVA table for **Fig. 3.5b**	**F (DFn, DFd)**	**P value**
Interaction	F (4, 68) = 3.417	P = 0.0132
sex	F (4, 68) = 4.103	P = 0.0049
genotype	F (1, 17) = 47.38	P < 0.0001
ANOVA table for **Fig. 3.5c**	**F (DFn, DFd)**	**P value**
Interaction	F (4, 68) = 0.5063	P = 0.7312
sex	F (4, 68) = 7.053	P < 0.0001
genotype	F (1, 17) = 42.73	P < 0.0001

ANOVA table for **Fig. 3.5d**	**F (DFn, DFd)**	**P value**
Interaction	F (4, 68) = 0.8778	P = 0.4819
sex	F (4, 68) = 0.4942	P = 0.7400
genotype	F (1, 17) = 4.049	P = 0.0603
ANOVA table for **Fig. 3.5e**	**F (DFn, DFd)**	**P value**
Interaction	F (4, 68) = 2.794	P = 0.0329
sex	F (4, 68) = 1,176	P = 0.3292
genotype	F (1, 17) = 18,33	P = 0.0005
ANOVA table for **Fig. 3.5f**	**F (DFn, DFd)**	**P value**
Interaction	F (4, 68) = 2.602	P = 0.0435
sex	F (4, 68) = 0.5303	P = 0.7139
genotype	F (1, 17) = 14.84	P = 0.0013

Table T.8: Mixed-effects results relevant to Fig. 3.8

Mixed effects (type III) **Fig. 3.8d**	**F (DFn, DFd)**	**P value**
stimulus	F (11, 263) = 72.49	P < 0.0001
genotype	F (1, 24) = 0.1125	P = 0.7402
stimulus x genotype	F (11, 263) = 0.4946	P = 0.9059
ANOVA table for **Fig. 3.8e**	**F (DFn, DFd)**	**P value**
stimulus x genotype	F (11, 264) = 0.7137	P = 0.7251
stimulus	F (2.560, 61.45) = 38.16	P < 0.0001
genotype	F (1, 24) = 0.9854	P = 0.3308
animal	F (24, 264) = 24.76	P < 0.0001
ANOVA table for **Fig. 3.8g**	**F (DFn, DFd)**	**P value**
stimulus x genotype	F (5, 120) = 0.09488	P = 0.9929
stimulus	F (3.242, 77.81) = 54.16	P < 0.0001
genotype	F (1, 24) = 0.009513	P = 0.9231
animal	F (24, 120) = 2.156	P = 0.0036

Multiple Mann-Whitney test results relevant to Fig. 3.8i

P value	**Mean rank of WT**	**Mean rank of GAD65**	**Mean rank diff.**	**Mann-Whitney U**	**q value**
>0,999999	12,00	12,00	0,000	65,00	>0,999999
0,879260	11,77	12,30	-0,5308	62,00	>0,999999
0,738062	11,54	12,60	-1,062	59,00	>0,999999
0,879260	12,23	11,70	0,5308	62,00	>0,999999
0,692607	11,46	12,70	-1,238	58,00	>0,999999
0,879260	11,77	12,30	-0,5308	62,00	>0,999999
>0,999999	12,00	12,00	0,000	65,00	>0,999999
0,409952	13,08	10,60	2,477	51,00	>0,999999
0,831546	12,31	11,60	0,7077	61,00	>0,999999
0,831546	12,31	11,60	0,7077	61,00	>0,999999
0,975772	12,08	11,90	0,1769	64,00	>0,999999
0,409952	13,08	10,60	2,477	51,00	>0,999999
0,784444	12,38	11,50	0,8846	60,00	>0,999999
0,831546	12,31	11,60	0,7077	61,00	>0,999999
0,927375	12,15	11,80	0,3538	63,00	>0,999999

0,879260	11,77	12,30	-0,5308	62,00	>0,999999
0,927375	11,85	12,20	-0,3538	63,00	>0,999999
0,831546	12,31	11,60	0,7077	61,00	>0,999999
0,784444	12,38	11,50	0,8846	60,00	>0,999999
0,831546	12,31	11,60	0,7077	61,00	>0,999999
0,975772	12,08	11,90	0,1769	64,00	>0,999999
0,975772	12,08	11,90	0,1769	64,00	>0,999999
>0,999999	12,00	12,00	0,000	65,00	>0,999999
0,879260	11,77	12,30	-0,5308	62,00	>0,999999
0,975772	12,08	11,90	0,1769	64,00	>0,999999
0,784444	11,62	12,50	-0,8846	60,00	>0,999999
0,975772	11,92	12,10	-0,1769	64,00	>0,999999
0,738062	12,46	11,40	1,062	59,00	>0,999999
0,927375	11,85	12,20	-0,3538	63,00	>0,999999
0,831546	12,31	11,60	0,7077	61,00	>0,999999
0,975772	11,92	12,10	-0,1769	64,00	>0,999999
0,927375	12,15	11,80	0,3538	63,00	>0,999999
>0,999999	12,00	12,00	0,000	65,00	>0,999999
0,831546	11,69	12,40	-0,7077	61,00	>0,999999
0,784444	11,62	12,50	-0,8846	60,00	>0,999999
>0,999999	12,00	12,00	0,000	65,00	>0,999999
0,927375	12,15	11,80	0,3538	63,00	>0,999999
0,975772	11,92	12,10	-0,1769	64,00	>0,999999
0,927375	11,85	12,20	-0,3538	63,00	>0,999999
0,975772	11,92	12,10	-0,1769	64,00	>0,999999
0,784444	12,38	11,50	0,8846	60,00	>0,999999
0,738062	12,46	11,40	1,062	59,00	>0,999999
0,831546	12,31	11,60	0,7077	61,00	>0,999999
0,692607	12,54	11,30	1,238	58,00	>0,999999
0,784444	11,62	12,50	-0,8846	60,00	>0,999999
0,375819	10,85	13,50	-2,654	50,00	>0,999999
0,604913	11,31	12,90	-1,592	56,00	>0,999999
0,562933	11,23	13,00	-1,769	55,00	>0,999999
0,445810	11,00	13,30	-2,300	52,00	>0,999999
0,343409	10,77	13,60	-2,831	49,00	>0,999999
0,975772	12,08	11,90	0,1769	64,00	>0,999999
0,648162	11,38	12,80	-1,415	57,00	>0,999999
0,692607	11,46	12,70	-1,238	58,00	>0,999999
0,208044	10,38	14,10	-3,715	44,00	>0,999999
0,975772	11,92	12,10	-0,1769	64,00	>0,999999
0,343409	10,77	13,60	-2,831	49,00	>0,999999
0,692607	12,54	11,30	1,238	58,00	>0,999999
0,049329	9,538	15,20	-5,662	33,00	>0,999999
0,445810	11,00	13,30	-2,300	52,00	>0,999999
0,088294	9,846	14,80	-4,954	37,00	>0,999999
0,409952	10,92	13,40	-2,477	51,00	>0,999999
0,312788	10,69	13,70	-3,008	48,00	>0,999999

0,312788	10,69	13,70	-3,008	48,00	>0,999999
0,927375	12,15	11,80	0,3538	63,00	>0,999999
0,604913	11,31	12,90	-1,592	56,00	>0,999999
0,522375	11,15	13,10	-1,946	54,00	>0,999999
0,692607	12,54	11,30	1,238	58,00	>0,999999
0,130554	10,08	14,50	-4,423	40,00	>0,999999
0,975772	11,92	12,10	-0,1769	64,00	>0,999999
0,784444	11,62	12,50	-0,8846	60,00	>0,999999
0,483290	11,08	13,20	-2,123	53,00	>0,999999
0,231578	10,46	14,00	-3,538	45,00	>0,999999
0,483290	11,08	13,20	-2,123	53,00	>0,999999
0,049329	9,538	15,20	-5,662	33,00	>0,999999
0,522375	11,15	13,10	-1,946	54,00	>0,999999
0,522375	11,15	13,10	-1,946	54,00	>0,999999
0,343409	10,77	13,60	-2,831	49,00	>0,999999
0,130554	10,08	14,50	-4,423	40,00	>0,999999
0,445810	11,00	13,30	-2,300	52,00	>0,999999
0,375819	10,85	13,50	-2,654	50,00	>0,999999
0,604913	11,31	12,90	-1,592	56,00	>0,999999
0,562933	11,23	13,00	-1,769	55,00	>0,999999
0,409952	10,92	13,40	-2,477	51,00	>0,999999
0,088294	9,846	14,80	-4,954	37,00	>0,999999
0,101012	9,923	14,70	-4,777	38,00	>0,999999
0,409952	10,92	13,40	-2,477	51,00	>0,999999
0,101012	9,923	14,70	-4,777	38,00	>0,999999
0,166064	10,23	14,30	-4,069	42,00	>0,999999
0,088294	9,846	14,80	-4,954	37,00	>0,999999
0,312788	10,69	13,70	-3,008	48,00	>0,999999
0,343409	10,77	13,60	-2,831	49,00	>0,999999
0,283929	10,62	13,80	-3,185	47,00	>0,999999
0,208044	10,38	14,10	-3,715	44,00	>0,999999
0,283929	10,62	13,80	-3,185	47,00	>0,999999

Table T.9: Multiple unpaired t-test results relevant to Fig. 3.9

Results for **Fig. 3.9b**							
P value	**Mean of WT**	**Mean of KO**	**Difference**	**SE of difference**	**t ratio**	**df**	**q value**
0.297878	-79.94	-87.08	7.136	6.459	1.105	9	0.520990
0.360861	-77.74	-82.11	4.369	4.635	0.9425	15	0.520990
0.400699	-74.73	-78.41	3.687	4.263	0.8649	15	0.520990
0.227303	-70.77	-73.70	2.934	2.377	1.234	28	0.520990
0.217694	-66.83	-69.27	2.431	1.929	1.260	29	0.520990
0.087090	-61.08	-64.04	2.957	1.670	1.771	29	0.520990
0.397610	-54.65	-56.44	1.791	2.086	0.8586	29	0.520990
0.781111	-49.20	-49.86	0.6619	2.360	0.2805	29	0.788922
0.452059	-45.10	-43.68	-1.416	1.858	0.7623	29	0.520990

0.116931	-42.25	-39.51	-2.734	1.692	1.616	29	0.520990
0.188228	-39.67	-37.09	-2.574	1.904	1.351	26	0.520990
0.472846	-38.30	-36.57	-1.733	2.364	0.7333	18	0.520990
Results for **Fig. 3.9e**							
P value	**Mean of WT**	**Mean of KO**	**Difference**	**SE of difference**	**t ratio**	**df**	**q value**
0.792184	1.800	2.294	-0.4941	1.859	0.2658	30	0.971202
0.925827	7.533	7.176	0.3569	3.801	0.09388	30	0.971202
0.915842	13.33	13.88	-0.5490	5.152	0.1066	30	0.971202
0.961586	19.47	19.76	-0.2980	6.137	0.04857	30	0.971202
0.772280	22.38	24.65	-2.262	7.743	0.2922	28	0.971202
0.849185	25.50	28.08	-2.577	13.37	0.1928	19	0.971202

Table T.10: ANOVA results relevant to Fig. 3.16a

ANOVA table	**F (DFn, DFd)**	**P value**
session x shock	F (21, 217) = 2.504	P = 0.0005
session	F (4.030, 124.9) = 31.57	P < 0.0001
shock	F (3, 31) = 3.098	P = 0.0410
animal	F (31, 217) = 13.95	P < 0.0001

Table T.11: ANOVA results relevant to Fig. A.1

ANOVA table for **Fig. A.1c**	**F (DFn, DFd)**	**P value**
Interaction	F (1, 22) = 2.342	P = 0.1402
sex	F (1, 22) = 0.7041	P = 0.4104
genotype	F (1, 22) = 0.0002825	P = 0.9867
ANOVA table for **Fig. A.1d**	**F (DFn, DFd)**	**P value**
Interaction	F (1, 22) = 0.07943	P = 0.7807
sex	F (1, 22) = 0.4637	P = 0.5030
genotype	F (1, 22) = 8.372	P = 0.0084
ANOVA table for **Fig. A.1e**	**F (DFn, DFd)**	**P value**
Interaction	F (1, 22) = 0.2548	P = 0.6187
sex	F (1, 22) = 1.035	P = 0.3201
genotype	F (1, 22) = 10.64	P = 0.0036
ANOVA table for **Fig. A.1f**	**F (DFn, DFd)**	**P value**
Interaction	F (1, 22) = 0.1407	P = 0.7112
sex	F (1, 22) = 2.299	P = 0.1437
genotype	F (1, 22) = 0.1710	P = 0.6832
ANOVA table for **Fig. A.1g**	**F (DFn, DFd)**	**P value**
Interaction	F (1, 22) = 0.5918	P = 0.4499
sex	F (1, 22) = 1.739	P = 0.2008
genotype	F (1, 22) = 3.361	P = 0.0803
ANOVA table for **Fig. A.1h**	**F (DFn, DFd)**	**P value**
Interaction	F (1, 22) = 0.5328	P = 0.4731
sex	F (1, 22) = 1.935	P = 0.1781
genotype	F (1, 22) = 4.659	P = 0.0421

Table T.12: ANOVA results relevant to Fig. A.3

ANOVA table for **Fig. A.3a**	**F (DFn, DFd)**	**P value**
Interaction	F (2, 34) = 0.8563	P = 0.4337
sex	F (2, 34) = 3.570	P = 0.0391
genotype	F (1, 17) = 0.7843	P = 0.3882
ANOVA table for **Fig. A.3b**	**F (DFn, DFd)**	**P value**
Interaction	F (2, 34) = 0.6057	P = 0.5515
sex	F (2, 34) = 6.435	P = 0.0043
genotype	F (1, 17) = 1.580	P = 0.2258
ANOVA table for **Fig. A.3c**	**F (DFn, DFd)**	**P value**
Interaction	F (2, 34) = 0.1532	P = 0.8586
sex	F (2, 34) = 20.29	P < 0.0001
genotype	F (1, 17) = 1.374	P = 0.2574

Table T.13: ANOVA results relevant to Fig. A.4

ANOVA table	**F (DFn, DFd)**	**P value**
session x shock	F (21, 319) = 5.233	P < 0.0001
session	F (3.754, 171.1) = 61.08	P < 0.0001
shock	F (3, 65) = 8.033	P = 0.0001

Table T.14: ANOVA results relevant to Fig. A.5

ANOVA table for **Fig. A.5a**	**F (DFn, DFd)**	**P value**
session x shock	F (12, 124) = 2.286	P = 0.0116
session	F (4, 124) = 7.439	P < 0.0001
shock	F (3, 31) = 3.703	P = 0.0219
animal	F (31, 124) = 9.443	P < 0.0001
ANOVA table for **Fig. A.5b**	**F (DFn, DFd)**	**P value**
session x shock	F (12, 128) = 1.563	P = 0.1104
session	F (4, 128) = 1.193	P = 0.3169
shock	F (3, 32) = 2.977	P = 0.0461
animal	F (32, 128) = 8.917	P < 0.0001
ANOVA table for **Fig. A.5c**	**F (DFn, DFd)**	**P value**
session x shock	F (12, 128) = 2.207	P = 0.0149
session	F (4, 128) = 1.490	P = 0.2090
shock	F (3, 32) = 2.343	P = 0.0916
animal	F (32, 128) = 10.50	P < 0.0001
ANOVA table for **Fig. A.5d**	**F (DFn, DFd)**	**P value**
session x shock	F (12, 128) = 1.221	P = 0.2754
session	F (4, 128) = 2.432	P = 0.0508
shock	F (3, 32) = 2.649	P = 0.0656
animal	F (32, 128) = 6.969	P < 0.0001
ANOVA table for **Fig. A.5e**	**F (DFn, DFd)**	**P value**
session x shock	F (12, 128) = 0.8101	P = 0.6396
session	F (4, 128) = 1.456	P = 0.2196
shock	F (3, 32) = 1.779	P = 0.1710
animal	F (32, 128) = 8.532	P < 0.0001

A.8 Chemicals

4', 6-diamidino-2-phenylindole dihydrochloride (DAPI)	Life Technologies, Darmstadt, DE
Agarose	Carl Roth, Karlsruhe, DE
AP5	TOCRIS, Bristol, UK
Carbachol	TOCRIS, Bristol, UK
DHPG	TOCRIS, Bristol, UK
Dimethyl dicarbonat (DMDC)	Sigma-Aldrich, Seelze, DE
Dimethylsulfoxid (DMSO)	Merck KGaA, Darmstadt, DE
di-Nucleotide-Tri-Phosphate (dNTPs)	Thermo Scientific , St. Leon-Roth, DE
DirectPCR lysis reagent	Peqlab, Erlangen, DE
DNQX	TOCRIS, Bristol, UK
Donkey serum	Vector laboratories, Burlingame, USA
Ethanol 96%	Carl Roth, Karlsruhe, DE
Ethidium bromide	Carl Roth, Karlsruhe, DE
Eye ointment	Bepanthen, DE
Immu-Mount™	Thermo Scientific, DE
Isoflurane	Nicholas Piramal limited, UK
Kainic acid	TOCRIS, Bristol, UK
KCl	Carl Roth, Karlsruhe, DE
Ketamine/ Xylazine	Sigma-Aldrich, Seelze, DE
KH_2PO_4	Sigma-Aldrich, Seelze, DE
Methylbutane	Carl Roth, Karlsruhe, DE
Na_2HPO_4	Sigma-Aldrich, Seelze, DE
Na_2HPO_4 x $2H_2O$	Carl Roth, Karlsruhe, DE
NaCl	Carl Roth, Karlsruhe, DE
$NaHCO_3$	Carl Roth, Karlsruhe, DE
NaOH	Carl Roth, Karlsruhe, DE
Oligonucleotide (dT)18 primer	Ambion/Life Technologies, Darmstadt, DE
Paladur resin	Heraeus Kulzer GmbH, Wehrheim, DE
Paraformaldehyde	Carl Roth, Karlsruhe, DE
Pentobarbital	Sigma-Aldrich, Seelze, DE
Poly-L-Lysine 1%	Sigma-Aldrich, Seelze, DE
Primer for genotyping PCRs	Life Technologies, Darmstadt, DE
Proteinase K	Carl Roth, Karlsruhe, DE
RNAse Zap	Life Technologies, Darmstadt, DE
Sodium Thiosulfate	Sigma-Aldrich, Seelze, DE
ß-Mercaptoethanol	Serra, Heidelberg, DE
Sucrose	Sigma-Aldrich, Seelze, DE

SuperaseIN	Ambion/Life Technologies, Darmstadt, DE
TissueTek	Leica, Nussloch, DENetherlands
Triton X	Sigma-Aldrich, Seelze, DE

A.9 Consummables and instruments

Animal care

Macrolon standard cages (type II long)	Techniplast GmbH, Hohenpeissenberg & Bioscape, Castrop-Rauxel, DE
Food pellets	Ssniff R/M-H V-1534, Ssniff spezialdiaten, Soest, DE

Behavioral test systems

TSE Fear Conditioning System	TSE, Bad Homburg, DE

Stereotactic surgery

motorized stereotactic apparatus	Robot Stereotax, Neurostar
NanoFil microsyringe	World Precision Instruments, Berlin, DE
Surgical instruments	Carl Roth, Karlsruhe, Germany
Non-absorbable suture material	5-0/PS3, Perma-Hand. silk suture
5% isoflurane in O_2/N_2O mixture	Rothacher Medical GmbH., Switzerland

Electrophysiology-Tissue preparation

Vibratome	Model 752; Campden Instruments LTD,
Water bath	Lauda Dr. R. Wobser, Lauda-Königshof, DE
Patch clamp amplifier	EP-9, HEKA Electronik GmbH, Reutlingen, DE
Extracellular amplifier - EXT-02F	npi Electronic GmbH, Tamm, DE
Digitizer/acquisition unit	CED-Mikro1401; Cambridge Electronic Design,
Stereomicroscope	Carl Zeiss Microscopy, LLC, NY,USA
Micromanipulators	Märzhäuser Wetzlar GmbH, Wetzlar, DE

Software

Anymaze Video tracking system	Stoelting Co., Wood Dale, IL, USA
Corel draw 2020	Corel GmbH, Munich, DE
Microsoft office	Mircosoft, Redmond, WA, USA
FITMaster	HEKA Electronik GmbH, Reutlingen, DE
Graphpad Prism	GraphPad Software, San Diego, CA, USA
Mini analysis 6.0	Synaptosoft Inc., NJ, USA

LAS AF	Leica Microsystems, Nussloch, DE
ImageJ	National Institutes of Health
Matlab 2018a	The MathWorks, Inc., Natick, MA, USA
Mendeley	Mendeley Ltd, London, UK
OriginPro 2019	OriginLab Corporation, Northhampton, MA, USA
Pulse	HEKA Electronik GmbH, Reutlingen, DE
Spike 2	CED, Cambridge, UK
Freezers and fridges	
Liebherr KU 2407	Liebherr Hausgerate, Ochsenhausen, DE
Liebherr GU 4506	Liebherr Hausgerate, Ochsenhausen, DE
Sanyo Ultra Low	Ewald Innovationstechnik, Bad Nenndorf, DE
Gel electrophoresis	
AGT3 & Maxi-VG	VWR International, DE
InGenius LHR	Syngene, Cambridge, UK
FL- PVDF membranes	Merck KGaA, Darmstadt, Germany
Odyssey Imaging System	LI-COR GmbH, Bad Homburg, DE
Image Studio software (quantification)	LI-COR GmbH, Bad Homburg, DE
Glass ware	
Glass bottles	Carl Roth, Karlsruhe, DE
Beaker	Carl Roth, Karlsruhe, DE
Graduated cylinder	Carl Roth, Karlsruhe, DE
Staining cuvettes	Carl Roth, Karlsruhe, DE
Slide holder	Carl Roth, Karlsruhe, DE
Object slide box	Carl Roth, Karlsruhe, DE
Membrane slides 1.0 PEN	Carl Zeiss, Jena, DE
Plastic ware	
Micro-Amp Fast Reaction Tubes	Life Technologies, Darmstadt, DE
Micro-Amp Optical Adhesive Film	Life Technologies, Darmstadt, DE
Micor-Amp Fast Optical 96-well plate	Life Technologies, Darmstadt, DE
Micro-Amp 8-cap strips	Life Technologies, Darmstadt, DE
Pipettes & pipette tips	Brand, Wertheim, DE
Cryostat	
Leica CM 1950	Leica Microsystems, Nussloch, DE

Antibodies

primary

anti-cfos	Cell Signaling #2250, Frankfurt am Main, DE
anti-GFP	abcam, Cambridge,UK
anti-Gad65	abcam, Cambridge,UK
anti-α tubulin	Sigma-Aldrich, Seelze, DE

secondary

IRDye 800CW	Licor, Bad Homburg, DE
IRDye 680CW	Licor, Bad Homburg, DE
anti-goat	Vector Laboratories, USA
streptavidin Cy2	Jackson ImmunoResearch Labs, UK

Kits and assays

Dream Taq polymerase	Thermo Scientific , St. Leon-Roth, DE
RC DC Protein assay Kit II	Biorad, Feldkirchen, DE
QuickTiter™ Lentivirus Titer Kit	Cell Biolabs, USA

Magnet stirrer

IKA RET basic	IKA-Werke, Staufen, DE
magnetic stir bar	Brand, Wertheim, DE

Autoclave

Systec DB-23 & VA120	Systec Labortechnik, Wettenberg, DE

Scale-Sartorius TE 2101	Sartorius AG, Gottingen, DE
Centrifuge-Heraeus Pico 17	Thermo Scientific, DE
Vortexer-VWR Lab dancer S40	VWR International, Darmstadt, DE
Sonicator	VWR International, Darmstadt, DE

Solutions & Buffers

AEBSF protease inhibitor	Thermo Scientific, DE
Pepstatin A	Thermo Scientific, DE
Pierce protease inhibitor	Thermo Scientific, DE

Lysis buffer

1% Laurylmaltoside, 1% NP-40, 1 mM Na_3VO_4, 2 mM EDTA, 50 mM Tris-HCl pH 8.0, 150 mM NaCl, 0.5% deoxycholate, 1 mM NaF 1 mM AEBSF protease inhibitor, 1 µM Pepstatin A 1 tablet of Pierce protease inhibitor.

Sample buffer (western blotting)

40% glycerol, 240 mM Tris HCl pH 6.8, 8% SDS, 0.04% Bromophenol blue, and 5% mercaptoethanol.

10x Phosphate buffer

saline (PBS); 11.5 g Na_2HPO x H2O; 2.0 g KH_2PO_4; 80.0 g NaCl; 2.0 g KCl; in ca. 900 ml double-distilled H_20; pH ~ 7.4; total 1 L.

4 % Paraformaldehyde (PFA)

40 g PFA were diluted in ca. 700 ml double-distilled water, stirring on a heating plate and adding 500 µl NaOH (5 M) for better solving. After cooling down for 1 h in ice, the solution was filtrated, and 100 ml 10x PBS were added. The pH was adjusted in ~ 7.4, and total volume was 1 L, by adding double-distilled H_20.

0.9 % Saline

Autoclaved solution of 4.5 g NaCl in 500 ml double-distilled H_20.

30 % Sucrose

For a solution of total volume 100 mL, 30 g sucrose were diluted in ca. 80 ml double-distilled H_20 and 10 ml PBS (10x).

REFERENCES

Adhikari, A. (2014). Distributed circuits underlying anxiety. *Frontiers in Behavioral Neuroscience*, *8*(APR), 1–6. https://doi.org/10.3389/fnbeh.2014.00112

Adhikari, A., Topiwala, M. A., & Gordon, J. A. (2010). Synchronized Activity between the Ventral Hippocampus and the Medial Prefrontal Cortex during Anxiety. *Neuron*, *65*(2), 257–269. https://doi.org/10.1016/j.neuron.2009.12.002

Adhikari, A., Topiwala, M. A., & Gordon, J. A. (2011). Single units in the medial prefrontal cortex with anxiety-related firing patterns are preferentially influenced by ventral hippocampal activity. *Neuron*, *71*(5), 898–910. https://doi.org/10.1016/j.neuron.2011.07.027

Adolphs, R. (2013). The biology of fear. *Current Biology*, *23*(2), R79–R93. https://doi.org/10.1016/j.cub.2012.11.055

Adrian, E. D. (1942). Olfactory reactions in the brain of the hedgehog. *The Journal of Physiology*, *100*(4), 459–473. https://doi.org/10.1113/jphysiol.1942.sp003955

Albrecht, A., Çalışkan, G., Oitzl, M. S., Heinemann, U., & Stork, O. (2013). Long-Lasting Increase of Corticosterone After Fear Memory Reactivation: Anxiolytic Effects and Network Activity Modulation in the Ventral Hippocampus. *Neuropsychopharmacology*, *38*(3), 386–394. https://doi.org/10.1038/npp.2012.192

Albrecht, A., Ivens, S., Papageorgiou, I. E., Çalışkan, G., Saiepour, N., Br??ck, W., Richter-Levin, G., Heinemann, U., & Stork, O. (2016). Shifts in excitatory/inhibitory balance by juvenile stress: A role for neuron-astrocyte interaction in the dentate gyrus. *Glia*, *64*(6), 911–922. https://doi.org/10.1002/glia.22970

Albrecht, A., Müller, I., Ardi, Z., Çalışkan, G., Gruber, D., Ivens, S., Segal, M., Behr, J., Heinemann, U., Stork, O., & Richter-Levin, G. (2017). Neurobiological consequences of juvenile stress: A GABAergic perspective on risk and resilience. *Neuroscience and Biobehavioral Reviews*, *74*(January), 21–43. https://doi.org/10.1016/j.neubiorev.2017.01.005

Albrecht, A., Segal, M., & Stork, O. (2020). Allostatic gene regulation of inhibitory synaptic factors in the rat ventral hippocampus in a juvenile/adult stress model of psychopathology. *European Journal of Neuroscience*, *December*, 1–12. https://doi.org/10.1111/ejn.15091

Almonte, A. G., Ewin, S. E., Mauterer, M. I., Morgan, J. W., Carter, E. S., & Weiner, J. L. (2017). Enhanced ventral hippocampal synaptic transmission and impaired synaptic plasticity in a rodent model of alcohol addiction vulnerability. *Scientific Reports*, *7*(1), 1–14. https://doi.org/10.1038/s41598-017-12531-z

Amaral, D. G., & Witter, M. P. (1989). The three-dimensional organization of the hippocampal formation: a review of anatomical data. *Neuroscience*, *31*(3), 571–591.

Anastasiades, P. G., & Carter, A. G. (2021). Circuit organization of the rodent medial prefrontal cortex. *Trends in Neurosciences*, *44*(7), 550–563. https://doi.org/10.1016/j.tins.2021.03.006

Arbab, T., Battaglia, F. P., Pennartz, C. M. A., & Bosman, C. A. (2018). Abnormal hippocampal theta and gamma hypersynchrony produces network and spike timing disturbances in the Fmr1-KO mouse model of Fragile X syndrome. *Neurobiology of Disease*, *114*(February), 65–73. https://doi.org/10.1016/j.nbd.2018.02.011

Asada, H., Kawamura, Y., Maruyama, K., Kume, H., Ding, R. G., Ji, F. Y., Kanbara, N., Kuzume, H., Sanbo, M., Yagi, T., & Obata, K. (1996a). Mice lacking the 65 kDa isoform of glutamic acid decarboxylase (GAD65) maintain normal levels of GAD67 and GABA in their brains but are susceptible to seizures. *Biochemical and Biophysical Research Communications*, *229*(3), 891–895. https://doi.org/10.1006/bbrc.1996.1898

Asada, H., Kawamura, Y., Maruyama, K., Kume, H., Ding, R. G., Kanbara, N., Kuzume, H., Sanbo, M., Yagi, T., & Obata, K. (1997). Cleft palate and decreased brain γ-aminobutyric acid in mice lacking the 67-kDa isoform of glutamic acid decarboxylase. *Proceedings of the National Academy of Sciences of the United States of America*, *94*(12), 6496–6499. https://doi.org/10.1073/pnas.94.12.6496

Asada, H., Kawamura, Y., Maruyama, K., Kume, H., Ding, R., Ji, F. Y., Kanbara, N., Kuzume, H., Sanbo, M., Yagi, T., & Obata, K. (1996b). Mice Lacking the 65 kDa Isoform of Glutamic Acid Decarboxylase (GAD65) Maintain Normal

Levels of GAD67 and GABA in Their Brains but Are Susceptible to Seizures central nervous system (1) and is synthesized from glutamic acid by glutamic acid decarboxy. *Biochemical and Biophysical Research Communications*, *229*, 891–895.

Bähner, F., Weiss, E. K., Birke, G., Maier, N., Schmitz, D., Rudolph, U., Frotscher, M., Traub, R. D., Both, M., & Draguhn, A. (2011). Cellular correlate of assembly formation in oscillating hippocampal networks in vitro. *Proceedings of the National Academy of Sciences of the United States of America*, *108*(35). https://doi.org/10.1073/pnas.1103546108

Bakker, C. E., Verheij, C., Willemsen, R., van der Helm, R., Oerlemans, F., Vermey, M., Bygrave, A., Hoogeveen, A. T., Oostra, B. A., Reyniers, E., De Boule, K., D'Hooge, R., Cras, P., van Velzen, D., Nagels, G., Martin, J. J., De Deyn, P. P., Darby, J. K., & Willems, P. J. (1994). Fmr1 knockout mice: A model to study fragile X mental retardation. *Cell*, *78*(1), 23–33. https://doi.org/10.1016/0092-8674(94)90569-X

Bandelow, B., & Michaelis, S. (2015). Epidemiology of anxiety disorders in the 21st century. *Dialogues in Clinical Neuroscience*, *17*(3), 327–335. https://doi.org/10.1016/j.siny.2015.10.004

Bannerman, D. M., Grubb, M., Deacon, R. M. J., Yee, B. K., Feldon, J., & Rawlins, J. N. P. (2003). Ventral hippocampal lesion affect anxiety but not spatial learning. *Behavioural Brain Research*, *139*, 197–213.

Bannerman, D. M., Rawlins, J. N. P., McHugh, S. B., Deacon, R. M. J., Yee, B. K., Bast, T., Zhang, W. N., Pothuizen, H. H. J., & Feldon, J. (2004). Regional dissociations within the hippocampus - Memory and anxiety. *Neuroscience and Biobehavioral Reviews*, *28*(3), 273–283. https://doi.org/10.1016/j.neubiorev.2004.03.004

Bannerman, D. M., Sprengel, R., Sanderson, D. J., McHugh, S. B., Rawlins, J. N. P., Monyer, H., & Seeburg, P. H. (2014). Hippocampal synaptic plasticity, spatial memory and anxiety. *Nature Reviews Neuroscience*, *15*(3), 181–192. https://doi.org/10.1038/nrn3677

Barbano, A. C., van der Mei, W. F., deRoon-Cassini, T. A., Grauer, E., Lowe, S. R., Matsuoka, Y. J., O'Donnell, M., Olff, M., Qi, W., Ratanatharathorn, A., Schnyder, U., Seedat, S., Kessler, R. C., Koenen, K. C., & Shalev, A. Y. (2019). Differentiating PTSD from anxiety and depression: Lessons from the ICD-11 PTSD diagnostic criteria. *Depression and Anxiety*, *36*(6), 490–498. https://doi.org/10.1002/da.22881

Bartos, M., Vida, I., & Jonas, P. (2007). Synaptic mechanisms of synchronized gamma oscillations in inhibitory interneuron networks. *Nature Reviews Neuroscience*, *8*(1), 45–56. https://doi.org/10.1038/nrn2044

Bassell, G. J., & Warren, S. T. (2008). Fragile X Syndrome: Loss of Local mRNA Regulation Alters Synaptic Development and Function. *Neuron*, *60*(2), 201–214. https://doi.org/10.1016/j.neuron.2008.10.004

Bast, T., Wilson, L. A., Witter, M. P., & Morris, R. G. M. (2009). From rapid place learning to behavioral performance: A key role for the intermediate hippocampus. *PLoS Biology*, *7*(4), 0730–0746. https://doi.org/10.1371/journal.pbio.1000089

Bear, M. F., Huber, K. M., & Warren, S. T. (2004). The mGluR theory of fragile X mental retardation. *Trends in Neurosciences*, *27*(7), 370–377. https://doi.org/10.1016/j.tins.2004.04.009

Behrens, C. J., van den Boom, L. P., de Hoz, L., Friedman, A., & Heinemann, U. (2005). Induction of sharp wave–ripple complexes in vitro and reorganization of hippocampal networks. *Nature Neuroscience*, *8*(11), 1560–1567. https://doi.org/10.1038/nn1571

Behrens, C. J., Van Den Boom, L. P., & Heinemann, U. (2007). Effects of the GABAA receptor antagonists bicuculline and gabazine on stimulus-induced sharp wave-ripple complexes in adult rat hippocampus in vitro. *European Journal of Neuroscience*, *25*(7), 2170–2181. https://doi.org/10.1111/j.1460-9568.2007.05462.x

Benes, F. M., & Berretta, S. (2001). GABAergic interneurons: Implications for understanding schizophrenia and bipolar disorder. *Neuropsychopharmacology*, *25*(1), 1–27. https://doi.org/10.1016/S0893-133X(01)00225-1

Bereza, B. G., Machado, M., & Einarson, T. R. (2009). Systematic review and quality assessment of economic evaluations and quality-of-life studies related to generalized anxiety disorder. *Clinical Therapeutics*, *31*(6), 1279–1308. https://doi.org/10.1016/j.clinthera.2009.06.004

Bergado-Acosta, J. R., Müller, I., Richter-Levin, G., & Stork, O. (2014). The GABA-synthetic enzyme GAD65 controls circadian activation of conditioned fear pathways. *Behavioural Brain Research*, *260*, 92–100. https://doi.org/10.1016/j.bbr.2013.11.042

Bergado-Acosta, J. R., Sangha, S., Narayanan, R. T., Obata, K., Pape, H. C., & Stork, O. (2008). Critical role of the 65-kDa isoform of glutamic acid decarboxylase in consolidation and generalization of Pavlovian fear memory. *Learn. Mem*, *15*, 163–171. https://doi.org/10.1101/lm.705408

Berke, J. D., Okatan, M., Skurski, J., & Eichenbaum, H. B. (2004). Oscillatory entrainment of striatal neurons in freely moving rats. *Neuron*, *43*(6), 883–896. https://doi.org/10.1016/j.neuron.2004.08.035

Blanchard, D. C., Griebel, G., Pobbe, R., & Blanchard, R. J. (2011). Risk assessment as an evolved threat detection and analysis process. *Neuroscience and Biobehavioral Reviews*, *35*(4), 991–998. https://doi.org/10.1016/j.neubiorev.2010.10.016

Bliss, T. V. P., & Lomo, T. (1973). Long-Lasting Potentiation of Synaptic transmission in the Dentate Area of the Anaesthetized Rabbit following Stimulation of the Perforant Path. *Journal of Physiology*, *232*, 331–356.

Boone, C. E., Davoudi, H., Harrold, J. B., & Foster, D. J. (2018). Abnormal Sleep Architecture and Hippocampal Circuit Dysfunction in a Mouse Model of Fragile X Syndrome. *Neuroscience*, *384*, 275–289. https://doi.org/10.1016/j.neuroscience.2018.05.012

Both, M., Bähner, F., Von Bohlen Und Halbach, O., & Draguhn, A. (2008). Propagation of specific network patterns through the mouse hippocampus. *Hippocampus*, *18*(9), 899–908. https://doi.org/10.1002/hipo.20446

Boulton, C. L., v. Haebler, D., & Heinemann, U. (1992). Tracing of axonal connections by rhodamine-dextran-amine in the rat hippocampal-entorhinal cortex slice preparation. *Hippocampus*, *2*(2), 99–106. https://doi.org/10.1002/hipo.450020203

Bouton, M. E., Westbrook, R. F., Corcoran, K. A., & Maren, S. (2006). Contextual and Temporal Modulation of Extinction: Behavioral and Biological Mechanisms. *Biological Psychiatry*, *60*(4), 352–360. https://doi.org/10.1016/j.biopsych.2005.12.015

Bragin, A., Engel, J., Wilson, C. L., Fried, I., & Buzsáki, G. (1999). High-frequency oscillations in human brain. *Hippocampus*, *9*(2), 137–142. https://doi.org/10.1002/(SICI)1098-1063(1999)9:2<137::AID-HIPO5>3.0.CO;2-0

Bragin, A., Jandó, G., Nádasdy, Z., Hetke, J., Wise, K., & Buzsáki, G. (1995). Gamma (40-100 Hz) oscillation in the hippocampus of the behaving rat. *Journal of Neuroscience*, *15*(1 I), 47–60. https://doi.org/10.1523/jneurosci.15-01-00047.1995

Brown, M. R., Kronengold, J., Gazula, V. R., Chen, Y., Strumbos, J. G., Sigworth, F. J., Navaratnam, D., & Kaczmarek, L. K. (2010). Fragile X mental retardation protein controls gating of the sodium-activated potassium channel Slack. *Nature Neuroscience*, *13*(7), 819–821. https://doi.org/10.1038/nn.2563

Burgess, N., Maguire, E. A., & O'Keefe, J. (2002). The human hippocampus and spatial and episodic memory. *Neuron*, *35*(4), 625–641. https://doi.org/10.1016/S0896-6273(02)00830-9

Bush, G., Luu, P., & Posner, M. I. (2000). Cognitive and emotional influences in anterior cingulate cortex. *Trends in Cognitive Sciences*, *4*(6), 215–222. https://doi.org/10.1016/S1364-6613(00)01483-2

Butler, J. L., Mendonça, P. R. F., Robinson, H. P. C., & Paulsen, O. (2016). Intrinsic cornu ammonis area 1 theta-nested gamma oscillations induced by optogenetic theta frequency stimulation. *Journal of Neuroscience*, *36*(15), 4155–4169. https://doi.org/10.1523/JNEUROSCI.3150-15.2016

Butler, J. L., & Paulsen, O. (2015). Hippocampal network oscillations - recent insights from in vitro experiments. *Current Opinion in Neurobiology*, *31*, 40–44. https://doi.org/10.1016/j.conb.2014.07.025

Buzsáki, G. (1984). Long-term changes of hippocampal sharp-waves following high frequency afferent activation. *Brain Research*, *300*(1), 179–182. https://doi.org/10.1016/0006-8993(84)91356-8

Buzsáki, G. (1989). TWO-STAGE MODEL OF MEMORY TRACE FORMATION : *Neuroscience*, *31*(3), 551–570.

Buzsáki, G. (2005). Theta rhythm of navigation: Link between path integration and landmark navigation, episodic and semantic memory. *Hippocampus*, *15*(7), 827–840. https://doi.org/10.1002/hipo.20113

Buzsáki, G. (2006). Rhythms of the Brain. In *Oxford University Press*.

Buzsáki, G. (2015). Hippocampal sharp wave-ripple: A cognitive biomarker for episodic memory and planning. *Hippocampus*, *25*(10), 1073–1188. https://doi.org/10.1002/hipo.22488

Buzsáki, G., Anastassiou, C. A., & Koch, C. (2012). The origin of extracellular fields and currents-EEG, ECoG, LFP and spikes. *Nature Reviews Neuroscience*, *13*(6), 407–420. https://doi.org/10.1038/nrn3241

Buzsáki, G., & Draguhn, A. (2004). Neuronal Oscillations in Cortical Networks. *Science*, *304*(June), 1926–1929. http://science.sciencemag.org/

Buzsáki, G., Horváth, Z., Urioste, R., Hetke, J., & Wise, K. (1992). High-frequency network oscillation in the hippocampus. *Science*, *256*(5059), 1025–1027. https://doi.org/10.1126/science.1589772

Buzsáki, G., Leung, L. S., & Vanderwolf, C. H. (1983). Cellular Bases of Hippocampal EEG in the Behaving Rat. *Brain Research Reviews*, *6*, 139–171.

Buzsáki, G., & Wang, X.-J. (2012). Mechanisms of Gamma Oscillations. *Annual Review of Neuroscience*, *March*, 203–225. https://doi.org/10.1146/annurev-neuro-062111-150444

Cahill, L., & McGaugh, J. L. (1998). Mechanisms of emotional arousal and lasting declarative memory. *Trends in Neurosciences*, *21*(7), 294–299. https://doi.org/10.1016/S0166-2236(97)01214-9

Calandreau, L., Desgranges, B., Jaffard, R., & Desmedt, A. (2010). Switching from contextual to tone fear conditioning and vice versa: The key role of the glutamatergic hippocampal-lateral septal neurotransmission. *Learning and Memory*, *17*(9), 440–443. https://doi.org/10.1101/lm.1859810

Calhoon, G. G., & Tye, K. M. (2015). Resolving the neural circuits of anxiety. *Nature Neuroscience*, *18*(10), 1394–1404. https://doi.org/10.1038/nn.4101

Çalışkan, G., Müller, I., Semtner, M., Winkelmann, A., Raza, A. S., Hollnagel, J. O., Rösler, A., Heinemann, U., Stork, O., & Meier, J. C. (2016). Identification of Parvalbumin Interneurons as Cellular Substrate of Fear Memory Persistence. *Cerebral Cortex*, *26*(5), 2325–2340. https://doi.org/10.1093/cercor/bhw001

Çalışkan, G., Schulz, S. B., Gruber, D., Behr, J., Heinemann, U., & Gerevich, Z. (2015). Corticosterone and corticotropin-releasing factor acutely facilitate gamma oscillations in the hippocampus in vitro. *European Journal of Neuroscience*, *41*(1), 31–44. https://doi.org/10.1111/ejn.12750

Çalışkan, G., & Stork, O. (2018). Hippocampal network oscillations at the interplay between innate anxiety and learned fear. *Psychopharmacology*, *236*(1), 321–338. https://doi.org/10.1007/s00213-018-5109-z

Carr, M. F., Jadhav, S. P., & Frank, L. M. (2011). Hippocampal replay in the awake state: A potential substrate for memory consolidation and retrieval. *Nature Neuroscience*, *14*(2), 147–153. https://doi.org/10.1038/nn.2732

Cenquizca, L. A., & Swanson, L. W. (2007). Spatial organization of direct hippocampal field CA1 axonal projections to the rest of the cerebral cortex. *Brain Research Reviews*, *56*(1), 1–26. https://doi.org/10.1016/j.brainresrev.2007.05.002

Chrobak, J. J., & Buzsáki, G. (1996). High-frequency oscillations in the output networks of the hippocampal-entorhinal axis of the freely behaving rat. *Journal of Neuroscience*, *16*(9), 3056–3066. https://doi.org/10.1523/jneurosci.16-09-03056.1996

Ciocchi, S., Passecker, J., Malagon-Vina, H., Mikus, N., & Klausberger, T. (2015). Selective information routing by ventral hippocampal CA1 projection neurons. *Science*, *348*(6234), 560–563. https://doi.org/10.1126/science.aaa3245

Citri, A., & Malenka, R. C. (2008). Synaptic plasticity: Multiple forms, functions, and mechanisms. *Neuropsychopharmacology*, *33*(1), 18–41. https://doi.org/10.1038/sj.npp.1301559

Colbert, C., & Levy, W. (1992). Electrophysiological and pharmacological characterization of perforant path synapses in CA1: Mediation by glutamate receptors. *Journal of Neurophysiology*, *68*, 1–8. https://doi.org/10.1152/jn.1992.68.1.1

Colgin, L. L., Denninger, T., Fyhn, M., Hafting, T., Bonnevie, T., Jensen, O., Moser, M. B., & Moser, E. I. (2009). Frequency of gamma oscillations routes flow of information in the hippocampus. *Nature*, *462*(7271), 353–357. https://doi.org/10.1038/nature08573

Colgin, L. L., Kubota, D., Brucher, F. A., Jia, Y., Branyan, E., Gall, C. M., & Lynch, G. (2004). Spontaneous waves in the dentate gyrus of slices from the ventral hippocampus. *Journal of Neurophysiology*, *92*(6), 3385–3398. https://doi.org/10.1152/jn.00478.2004

Colgin, L. L., & Moser, E. I. (2010). Gamma oscillations in the hippocampus. *Physiology*, *25*(5), 319–329. https://doi.org/10.1152/physiol.00021.2010

Colic, L., Li, M., Demenescu, L. R., Li, S., Müller, I., Richter, A., Behnisch, G., Seidenbecher, C. I., Speck, O., Schott, B. H., Stork, O., & Walter, M. (2018). GAD65 promoter polymorphism rs2236418 modulates harm avoidance in women via inhibition/excitation balance in the rostral ACC. *Journal of Neuroscience*, *38*(22), 5067–5077. https://doi.org/10.1523/JNEUROSCI.1985-17.2018

Collins, D. R., Pelletier, J. G., & Paré, D. (2001). Slow and fast (gamma) neuronal oscillations in the perirhinal cortex and lateral amygdala. *Journal of Neurophysiology*, *85*(4), 1661–1672. https://doi.org/10.1152/jn.2001.85.4.1661

Csicsvari, J., Hirase, H., Czurkó, A., Mamiya, A., & Buzsáki, G. (1999). Oscillatory coupling of hippocampal pyramidal cells and interneurons in the behaving rat. *Journal of Neuroscience*, *19*(1), 274–287. https://doi.org/10.1523/jneurosci.19-01-00274.1999

Csicsvari, J., Hirase, H., Mamiya, A., & Buzsáki, G. (2000). Ensemble patterns of hippocampal CA3-CA1 neurons during sharp wave-associated population events. *Neuron*, *28*(2), 585–594. https://doi.org/10.1016/S0896-6273(00)00135-5

Czéh, B., Ábrahám, H., Tahtakran, S., Houser, C. R., & Seress, L. (2013). Number and regional distribution of GAD65 mRNA-expressing interneurons in the rat hippocampal formation. *Acta Biologica Hungarica*, *64*(4), 395–413. https://doi.org/10.1556/ABiol.64.2013.4.1

D'Hulst, C., Heulens, I., Brouwer, J. R., Willemsen, R., De Geest, N., Reeve, S. P., De Deyn, P. P., Hassan, B. A., & Kooy, R. F. (2009). Expression of the GABAergic system in animal models for fragile X syndrome and fragile X associated tremor/ataxia syndrome (FXTAS). *Brain Research*, *1253*, 176–183. https://doi.org/10.1016/j.brainres.2008.11.075

Davis, A. M., Ward, S. C., Selmanoff, M., Herbison, A. E., & McCarthy, M. M. (1999). Developmental sex differences in amino acid neurotransmitter levels in hypothalamic and limbic areas of rat brain. *Neuroscience*, *90*(4), 1471–1482. https://doi.org/10.1016/S0306-4522(98)00511-9

Davis, M. (1992). The role of the amygdala in fear and anxiety. *Annual Review of Neuroscience*, *15*, 353–375. https://doi.org/10.1146/annurev.ne.15.030192.002033

Davis, M. (1997). Neurobiology of fear responses: The role of the amygdala. *Journal of Neuropsychiatry and Clinical Neurosciences*, *9*(3), 382–402. https://doi.org/10.1176/jnp.9.3.382

Davis, M., Walker, D. L., Miles, L., & Grillon, C. (2010). Phasic vs sustained fear in rats and humans: Role of the extended amygdala in fear vs anxiety. *Neuropsychopharmacology*, *35*(1), 105–135. https://doi.org/10.1038/npp.2009.109

Deng, P. Y., Rotman, Z., Blundon, J. A., Cho, Y., Cui, J., Cavalli, V., Zakharenko, S. S., & Klyachko, V. A. (2013). FMRP Regulates Neurotransmitter Release and Synaptic Information Transmission by Modulating Action Potential Duration via BK Channels. *Neuron*, *77*(4), 696–711. https://doi.org/10.1016/j.neuron.2012.12.018

Deng, P. Y., Sojka, D., & Klyachko, V. A. (2011). Abnormal presynaptic short-term plasticity and information processing in a mouse model of fragile X syndrome. *Journal of Neuroscience*, *31*(30), 10971–10982. https://doi.org/10.1523/JNEUROSCI.2021-11.2011

Diamond, D. M., Catherine Bennett, M., Stevens, K. E., Wilson, R. L., & Rose, G. M. (1990). Exposure to a novel environment interferes with the induction of hippocampal primed burst potentiation in the behaving rat. *Psychobiology*, *18*(3), 273–281. https://doi.org/10.3758/BF03327243

Diba, K., & Buzsáki, G. (2007). Forward and reverse hippocampal place-cell sequences during ripples. *Nature Neuroscience*, *10*(10), 1241–1242. https://doi.org/10.1038/nn1961

Dölen, G., & Bear, M. F. (2008). Role for metabotropic glutamate receptor 5 (mGluR5) in the pathogenesis of fragile X syndrome. *Journal of Physiology*, *586*(6), 1503–1508. https://doi.org/10.1113/jphysiol.2008.150722

Dölen, G., Osterweil, E., Rao, B. S. S., Smith, G. B., Auerbach, B. D., Chattarji, S., & Bear, M. F. (2007). Correction of Fragile X Syndrome in Mice. *Neuron*, *56*(6), 955–962. https://doi.org/10.1016/j.neuron.2007.12.001

Dragoi, G., & Tonegawa, S. (2011). Preplay of future place cell sequences by hippocampal cellular assemblies. *Nature*, *469*(7330), 397–401. https://doi.org/10.1038/nature09633

Draguhn, A., Traub, R. D., Schmitz, D., & Jefferys, J. G. R. (1998). Electrical coupling underlies high-frequency oscillations in the hippocampus in vitro. *Nature*, *394*, 189–192. http://proquest.umi.com/pqdweb?did=31963288&Fmt=7&clientId=75702&RQT=309&VName=PQD

Dunn, A. R., & Kaczorowski, C. C. (2019). Regulation of intrinsic excitability: Roles for learning and memory, aging and Alzheimer's disease, and genetic diversity. *Neurobiology of Learning and Memory*, *164*, 1–27. https://doi.org/10.1016/j.nlm.2019.107069

Ego-Stengel, V., & Wilson, M. A. (2010). Disruption of ripple-associated hippocampal activity during rest impairs spatial learning in the rat. *Hippocampus*, *20*(1), 1–10. https://doi.org/10.1002/hipo.20707

Eichenbaum, H., Otto, T., & Cohen, N. J. (1992). The hippocampus-what does it do? *Behavioral and Neural Biology*, *57*(1), 2–36. https://doi.org/10.1016/0163-1047(92)90724-I

Elfant, D., Pál, B. Z., Emptage, N., & Capogna, M. (2008). Specific inhibitory synapses shift the balance from feedforward to feedback inhibition of hippocampal CA1 pyramidal cells. *European Journal of Neuroscience*, *27*(1), 104–113. https://doi.org/10.1111/j.1460-9568.2007.06001.x

Ellender, T. J., Nissen, W., Colgin, L. L., Mann, E. O., & Paulsen, O. (2010). Priming of hippocampal population bursts by individual perisomatic- targeting interneurons. *Journal of Neuroscience*, *30*(17), 5979–5991. https://doi.org/10.1523/JNEUROSCI.3962-09.2010

Empson, R. M., & Heinemann, U. (1995). Perforant path connections to area CA1 are predominantly inhibitory in the rat hippocampal-entorhinal cortex combined slice preparation. *Hippocampus*, *5*(2), 104–107. https://doi.org/10.1002/hipo.450050203

Engin, E., Smith, K. S., Gao, Y., Nagy, D., Foster, R. A., Tsvetkov, E., Keist, R., Crestani, F., Fritschy, J.-M., Bolshakov, V. Y., Hajos, M., Heldt, S. A., & Rudolph, U. (2016). Modulation of anxiety and fear via distinct intrahippocampal circuits. *ELife*, *5*, 1–23. https://doi.org/10.7554/elife.14120

English, D. F., Peyrache, A., Stark, E., Roux, L., Vallentin, D., Long, M. A., & Buzsáki, G. (2014). Excitation and inhibition compete to control spiking during hippocampal ripples: Intracellular study in behaving mice. *Journal of Neuroscience*, *34*(49), 16509–16517. https://doi.org/10.1523/JNEUROSCI.2600-14.2014

Ethridge, L. E., De Stefano, L. A., Schmitt, L. M., Woodruff, N. E., Brown, K. L., Tran, M., Wang, J., Pedapati, E. V., Erickson, C. A., & Sweeney, J. A. (2019). Auditory EEG Biomarkers in Fragile X Syndrome: Clinical Relevance. *Frontiers in Integrative Neuroscience*, *13*(October), 1–16. https://doi.org/10.3389/fnint.2019.00060

Ethridge, L. E., White, S. P., Mosconi, M. W., Wang, J., Pedapati, E. V., Erickson, C. A., Byerly, M. J., & Sweeney, J. A. (2017). Neural synchronization deficits linked to cortical hyper-excitability and auditory hypersensitivity in fragile X syndrome. *Molecular Autism*, *8*(1), 1–11. https://doi.org/10.1186/s13229-017-0140-1

Fanselow, M. S. (1986). Associative vs topographical accounts of the immediate shock-freezing deficit in rats: Implications for the response selection rules governing species-specific defensive reactions. *Learning and Motivation*, *17*(1), 16–39. https://doi.org/10.1016/0023-9690(86)90018-4

Fanselow, M. S., & Dong, H. W. (2010). Are the Dorsal and Ventral Hippocampus Functionally Distinct Structures? *Neuron*, *65*(1), 7–19. https://doi.org/10.1016/j.neuron.2009.11.031

Felix-Ortiz, A. C., Beyeler, A., Seo, C., Leppla, C. A., Wildes, C. P., & Tye, K. M. (2013). BLA to vHPC inputs modulate anxiety-related behaviors. *Neuron*, *79*(4), 658–664. https://doi.org/10.1016/j.neuron.2013.06.016

Fell, J., Klaver, P., Lehnertz, K., Grunwald, T., Schaller, C., Elger, C. E., & Fernández, G. (2001). Human memory formation is accompanied by rhinal-hippocampal coupling and decoupling. *Nature Neuroscience*, *4*(12), 1259–1264. https://doi.org/10.1038/nn759

Feusner, J., Ritchie, T., Lawford, B., Young, R. M. D., Kann, B., & Noble, E. P. (2001). GABAA receptor β3 subunit gene and psychiatric morbidity in a post-traumatic stress disorder population. *Psychiatry Research*, *104*(2), 109–117. https://doi.org/10.1016/S0165-1781(01)00296-7

Fisahn, A., Contractor, A., Traub, R. D., Buhl, E. H., Heinemann, S. F., & McBain, C. J. (2004). Distinct roles for the

kainate receptor subunits GluR5 and GluR6 in kainate-induced hippocampal gamma oscillations. *Journal of Neuroscience*, *24*(43), 9658–9668. https://doi.org/10.1523/JNEUROSCI.2973-04.2004

Fisahn, A., Pike, F. G., Buhl, E. H., & Paulsen, O. (1998). Cholinergic induction of network oscillations at 40 Hz in the hippocampus in vitro. *Nature*, *394*(6689), 186–189. https://doi.org/10.1038/28179

Foster, D. J. (2017). Replay Comes of Age. *Annual Review of Neuroscience*, *40*, 581–602. https://doi.org/10.1146/annurev-neuro-072116-031538

Freemon, F. R., McNew, J. J., & Adey, W. R. (1969). Sleep of unrestrained chimpanzee: Cortical and subcortical recordings. *Experimental Neurology*, *25*(1), 129–137. https://doi.org/10.1016/0014-4886(69)90076-4

Freemon, F. R., & Walter, R. D. (1970). Electrical activity of human limbic system during sleep. *Comprehensive Psychiatry*, *11*(6), 544–551. https://doi.org/10.1016/0010-440X(70)90017-9

Fries, P., Reynolds, J. H., Rorie, A. E., & Desimone, R. (2001). Modulation of oscillatory neuronal synchronization by selective visual attention. *Science*, *291*(5508), 1560–1563. https://doi.org/10.1126/science.1055465

Gillies, M. J., Traub, R. D., LeBeau, F. E. N., Davies, C. H., Gloveli, T., Buhl, E. H., & Whittington, M. A. (2002). A model of atropine-resistant theta oscillations in rat hippocampal area CA1. *Journal of Physiology*, *543*(3), 779–793. https://doi.org/10.1113/jphysiol.2002.024588

Girardeau, G., Benchenane, K., Wiener, S. I., Buzsáki, G., & Zugaro, M. B. (2009). Selective suppression of hippocampal ripples impairs spatial memory. *Nature Neuroscience*, *12*(10), 1222–1223. https://doi.org/10.1038/nn.2384

Girardeau, G., Cei, A., & Zugaro, M. (2014). Learning-induced plasticity regulates hippocampal sharp wave-ripple drive. *Journal of Neuroscience*, *34*(15), 5176–5183. https://doi.org/10.1523/JNEUROSCI.4288-13.2014

Girardeau, G., Inema, I., & Buzsáki, G. (2017). Reactivations of emotional memory in the hippocampus-amygdala system during sleep. *Nature Neuroscience*, *20*(11), 1634–1642. https://doi.org/10.1038/nn.4637

Golub, Y., Mauch, C. P., Dahlhoff, M., & Wotjak, C. T. (2009). Consequences of extinction training on associative and non-associative fear in a mouse model of Posttraumatic Stress Disorder (PTSD). *Behavioural Brain Research*, *205*(2), 544–549. https://doi.org/10.1016/j.bbr.2009.08.019

Gonçalves, J. T., Anstey, J. E., Golshani, P., & Portera-Cailliau, C. (2013). Circuit level defects in the developing neocortex of Fragile X mice. *Nature Neuroscience*, *16*(7), 903–909. https://doi.org/10.1038/nn.3415

Gong, N., Li, Y., Cai, G. Q., Niu, R. F., Fang, Q., Wu, K., Chen, Z., Lin, L. N., Xu, L., Fei, J., & Xu, T. Le. (2009). GABA transporter-1 activity modulates hippocampal theta oscillation and theta burst stimulation-induced long-term potentiation. *Journal of Neuroscience*, *29*(50), 15836–15845. https://doi.org/10.1523/JNEUROSCI.4643-09.2009

Gray, C. M. (1994). Synchronous oscillations in neuronal systems: Mechanisms and functions. *Journal of Computational Neuroscience*, *1*(1–2), 11–38. https://doi.org/10.1007/BF00962716

Gray, C. M., Konig, P., Engel, A. K., & Singer, W. (1989). *Cortex Exhibit Inter-Columnar Global Stimulus Properties*. *338*(March).

Gray, J. A., & McNaughton, N. (1982). The Neuropsychology of Anxiety. *Oxford University Press*, *33*. https://doi.org/10.1017/S0140525X00013170

Grigoryan, G., & Segal, M. (2016). Lasting Differential Effects on Plasticity Induced by Prenatal Stress in Dorsal and Ventral Hippocampus. *Neural Plasticity*, *2016*. https://doi.org/10.1155/2016/2540462

Guo, W., Allan, A. M., Zong, R., Zhang, L., Johnson, E. B., Schaller, E. G., Murthy, A. C., Goggin, S. L., Eisch, A. J., Oostra, B. A., Nelson, D. L., Jin, P., & Zhao, X. (2011). Ablation of Fmrp in adult neural stem cells disrupts hippocampus-dependent learning. *Nature Medicine*, *17*(5), 559–565. https://doi.org/10.1038/nm.2336

Guyon, N., Zacharias, L. R., de Oliveira, E. F., Kim, H., Leite, J. P., Lopes-Aguiar, C., & Carlén, M. (2021). Network asynchrony underlying increased broadband gamma power. *Journal of Neuroscience*, *41*(13), 2944–2963. https://doi.org/10.1523/JNEUROSCI.2250-20.2021

Hagerman, R. J., Berry-Kravis, E., Hazlett, H. C., Bailey, D. B., Moine, H., Kooy, R. F., Tassone, F., Gantois, I., Sonenberg, N., Mandel, J. L., & Hagerman, P. J. (2017). Fragile X syndrome. *Nature Reviews. Disease Primers*, *3*, 17065. https://doi.org/10.1038/nrdp.2017.65

Hájos, N., Ellender, T. J., Zemankovics, R., Mann, E. O., Exley, R., Cragg, S. J., Freund, T. F., & Paulsen, O. (2009). Maintaining network activity in submerged hippocampal slices: Importance of oxygen supply. *European Journal of Neuroscience*, *29*(2), 319–327. https://doi.org/10.1111/j.1460-9568.2008.06577.x

Hájos, N., & Mody, I. (2009). Establishing a physiological environment for visualized in vitro brain slice recordings by increasing oxygen supply and modifying aCSF content. *Journal of Neuroscience Methods*, *183*(2), 107–113. https://doi.org/10.1016/j.jneumeth.2009.06.005

Hájos, N., & Paulsen, O. (2009a). Network mechanisms of gamma oscillations in the CA3 region of the hippocampus. *Neural Networks*, *22*(8), 1113–1119. https://doi.org/10.1016/j.neunet.2009.07.024

Hájos, N., & Paulsen, O. (2009b). Network mechanisms of gamma oscillations in the CA3 region of the hippocampus. *Neural Networks*, *22*(8), 1113–1119. https://doi.org/10.1016/j.neunet.2009.07.024

Hartse, K. M., Eisenhart, S. F., Bergmann, B. M., & Rechtschaffen, A. (1979). Ventral hippocampus spikes during sleep, wakefulness, and arousal in the cat. *Sleep*, *1*(3), 231–246. https://doi.org/10.1093/sleep/1.3.231

Hasselmo, M. E., Wyble, B. P., & Wallenstein, G. V. (1996). Encoding and retrieval of episodic memories: Role of cholinergic and GABAergic modulation in the hippocampus. *Hippocampus*, *6*(6), 693–708. https://doi.org/10.1002/(SICI)1098-1063(1996)6:6<693::AID-HIPO12>3.0.CO;2-W

Headley, D. B., & Paré, D. (2013). In sync: Gamma oscillations and emotional memory. *Frontiers in Behavioral Neuroscience*, *7*(NOV), 1–12. https://doi.org/10.3389/fnbeh.2013.00170

Hebb, D. O. (1949). The Organization of Behavior; A Neuropsychological Theory. *Wiley, New York*.

Henze, D. A., & Buzsáki, G. (2001). Action potential threshold of hippocampal pyramidal cells in vivo is increased by recent spiking activity. *Neuroscience*, *105*(1), 121–130. https://doi.org/10.1016/S0306-4522(01)00167-1

Hirsh, R. (1974). The hippocampus and contextual retrieval of information from memory: A theory. *Behavioral Biology*, *12*(4), 421–444. https://doi.org/10.1016/S0091-6773(74)92231-7

Hofer, K. T., Kandrács, Á., Ulbert, I., Pál, I., Szabó, C., Héja, L., & Wittner, L. (2015). The hippocampal CA3 region can generate two distinct types of sharp wave-ripple complexes, in vitro. *Hippocampus*, *25*(2), 169–186. https://doi.org/10.1002/hipo.22361

Hoover, W. B., & Vertes, R. P. (2007). Anatomical analysis of afferent projections to the medial prefrontal cortex in the rat. *Brain Structure and Function*, *212*(2), 149–179. https://doi.org/10.1007/s00429-007-0150-4

Huber, K. M., Gallagher, S. M., Warren, S. T., & Bear, M. F. (2002). Altered synaptic plasticity in a mouse model of fragile X mental retardation. *Proceedings of the National Academy of Sciences of the United States of America*, *99*(11), 7746–7750. https://doi.org/10.1073/pnas.122205699

Huff, M. L., Emmons, E. B., Narayanan, N. S., & LaLumiere, R. T. (2016). Basolateral amygdala projections to ventral hippocampus modulate the consolidation of footshock, but not contextual, learning in rats. *Learning and Memory*, *23*(2), 51–60. https://doi.org/10.1101/lm.039909.115

Hunsaker, M. R., & Kesner, R. P. (2008). Evaluating the differential roles of the dorsal dentate gyrus, dorsal CA3, and dorsal CA1 during a temporal ordering for spatial locations task. *Hippocampus*, *18*(9), 955–964. https://doi.org/10.1002/hipo.20455

Hunt, D. L., Linaro, D., Si, B., Romani, S., & Spruston, N. (2018). A novel pyramidal cell type promotes sharp-wave synchronization in the hippocampus. In *Nature Neuroscience* (Vol. 21, Issue 7). https://doi.org/10.1038/s41593-018-0172-7

Hunter, J., Rivero-Arias, O., Angelov, A., Kim, E., Fotheringham, I., & Leal, J. (2014). Epidemiology of fragile X syndrome: A systematic review and meta-analysis. *American Journal of Medical Genetics, Part A*, *164*(7), 1648–1658. https://doi.org/10.1002/ajmg.a.36511

Ikeda, T., Makino, Y., & Yamada, M. K. (2015). 17α-Estradiol is generated locally in the male rat brain and can regulate GAD65 expression and anxiety. *Neuropharmacology*, *90*, 9–14. https://doi.org/10.1016/j.neuropharm.2014.10.019

Imbrosci, B., Nitzan, N., McKenzie, S., Donoso, J. R., Swaminathan, A., Böhm, C., Maier, N., & Schmitz, D. (2021). Subiculum as a generator of sharp wave-ripples in the rodent hippocampus. *Cell Reports*, *35*(3).

https://doi.org/10.1016/j.celrep.2021.109021

Ishikawa, T., & Ikegaya, Y. (2020). Locally sequential synaptic reactivation during hippocampal ripples. *Science Advances*, *6*(7), 1–11. https://doi.org/10.1126/sciadv.aay1492

Ivens, S., Çalışkan, G., Papageorgiou, I. E., Cesetti, T., Malich, A., Kann, O., Heinemann, U., Stork, O., & Albrecht, A. (2019). Persistent increase in ventral hippocampal long-term potentiation by juvenile stress: A role for astrocytic glutamine synthetase. *Glia*, *67*(12), 2279–2293. https://doi.org/10.1002/glia.23683

Jackson, J., Goutagny, R., & Williams, S. (2011). Fast and slow gamma rhythms are intrinsically and independently generated in the subiculum. *Journal of Neuroscience*, *31*(34), 12104–12117. https://doi.org/10.1523/JNEUROSCI.1370-11.2011

Jadhav, S. P., Kemere, C., German, P. W., & Frank, L. M. (2012). Awake hippocampal sharp-wave ripples support spatial memory. *Science*, *336*(6087), 1454–1458. https://doi.org/10.1126/science.1217230

Jai, Y. Y., & Frank, L. M. (2015). Hippocampal-cortical interaction in decision making. *Neurobiology of Learning and Memory*, *117*, 34–41. https://doi.org/10.1016/j.nlm.2014.02.002

Janak, P. H., & Tye, K. M. (2015). From circuits to behaviour in the amygdala. *Nature*, *517*(7534), 284–292. https://doi.org/10.1038/nature14188

Jimenez, J. C. (2018). The Role of the Ventral Hippocampus in Anxiety-Related Behavior. *Thesis*.

Joëls, M. (2006). Corticosteroid effects in the brain: U-shape it. *Trends in Pharmacological Sciences*, *27*(5), 244–250. https://doi.org/10.1016/j.tips.2006.03.007

Johnson, A., & Redish, A. D. (2007). Neural ensembles in CA3 transiently encode paths forward of the animal at a decision point. *Journal of Neuroscience*, *27*(45), 12176–12189. https://doi.org/10.1523/JNEUROSCI.3761-07.2007

Jonak, C. R., Lovelace, J. W., Ethell, I. M., Razak, K. A., & Binder, D. K. (2020). Multielectrode array analysis of EEG biomarkers in a mouse model of Fragile X Syndrome. *Neurobiology of Disease*, *138*(November 2019). https://doi.org/10.1016/j.nbd.2020.104794

Joo, H. R., & Frank, L. M. (2018). The hippocampal sharp wave–ripple in memory retrieval for immediate use and consolidation. *Nature Reviews Neuroscience*, *19*(12), 744–757. https://doi.org/10.1038/s41583-018-0077-1

Jovanovic, T., & Ressler, K. J. (2010). How the neurocircuitry and genetics of fear inhibition may inform our understanding of PTSD. *American Journal of Psychiatry*, *167*(6), 648–662. https://doi.org/10.1176/appi.ajp.2009.09071074

Kahana, M. J., Seelig, D., & Madsen, J. R. (2001). Theta returns. *Current Opinion in Neurobiology*, *11*(6), 739–744. https://doi.org/10.1016/S0959-4388(01)00278-1

Kang, J. Y., Chadchankar, J., Vien, T. N., Mighdoll, M. I., Hyde, T. M., Mather, R. J., Deeb, T. Z., Pangalos, M. N., Brandon, N. J., Dunlop, J., & Moss, S. J. (2017). Deficits in the activity of presynaptic-aminobutyric acid type B receptors contribute to altered neuronal excitability in fragile X syndrome. *Journal of Biological Chemistry*, *292*(16), 6621–6632. https://doi.org/10.1074/jbc.M116.772541

Karunakaran, S., Chowdhury, A., Donato, F., Quairiaux, C., Michel, C. M., & Caroni, P. (2016). PV plasticity sustained through D1/5 dopamine signaling required for long-term memory consolidation. *Nature Neuroscience*, *19*(3), 454–464. https://doi.org/10.1038/nn.4231

Kash, S. F., Johnson, R. S., Tecott, L. H., Noebels, J. L., Mayfield, R. D., Hanahan, D., & Baekkeskov, S. (1997). Epilepsy in mice deficient in the 65-kDa isoform of glutamic acid decarboxylase. *Proceedings of the National Academy of Sciences of the United States of America*, *94*(25), 14060–14065. https://doi.org/10.1073/pnas.94.25.14060

Kash, S. F., Tecott, L. H., Hodge, C., & Baekkeskov, S. (1999). Increased anxiety and altered responses to anxiolytics in mice deficient in the 65-kDa isoform of glutamic acid decarboxylase. *Proceedings of the National Academy of Sciences of the United States of America*, *96*(4), 1698–1703. https://doi.org/10.1073/pnas.96.4.1698

Keil, A., Müller, M. M., Gruber, T., Wienbruch, C., Stolarova, M., & Elbert, T. (2001). Effects of emotional arousal in the cerebral hemispheres: A study of oscillatory brain activity and event-related potentials. *Clinical Neurophysiology*, *112*(11), 2057–2068. https://doi.org/10.1016/S1388-2457(01)00654-X

Kessler, R. C., Chiu, W. T., Demler, O., & Walters, E. E. (2005). Prevalence, Severity, and Comorbidity of 12-Month DSM-IV Disorders in the National Comorbidity Survey Replication. *Archives of General Psychiatry*, *62*(6), 617–627. https://doi.org/10.1001/archpsyc.62.6.617

Kheirbek, M. A., Drew, L. J., Burghardt, N. S., Costantini, D. O., Tannenholz, L., Ahmari, S. E., Zeng, H., Fenton, A. A., & Henl, R. (2013). Differential control of learning and anxiety along the dorsoventral axis of the dentate gyrus. *Neuron*, *77*(5), 955–968. https://doi.org/10.1016/j.neuron.2012.12.038

Kheirbek, M. A., & Hen, R. (2011). Dorsal vs Ventral Hippocampal Neurogenesis: Implications for Cognition and Mood. *Neuropsychopharmacology*, *36*(1), 373–374. https://doi.org/10.1038/npp.2010.148

Khemka, S., Barnes, G., Dolan, R. J., & Bach, D. R. (2017). Dissecting the Function of Hippocampal Oscillations in a Human Anxiety Model. *The Journal of Neuroscience*, *37*(29), 6869–6876. https://doi.org/10.1523/JNEUROSCI.1834-16.2017

Khodagholy, D., Gelinas, J. N., & Buzsáki, G. (2017). Learning-enhanced coupling between ripple oscillations in association cortices and hippocampus. *Science*, *358*(6361), 369–372. https://doi.org/10.1126/science.aan6203

Kishi, T., Tsumori, T., Ono, K., Yokota, S., Ishino, H., & Yasui, Y. (2000). Topographical organization of projections from the subiculum to the hypothalamus in the rat. *Journal of Comparative Neurology*, *419*(2), 205–222. https://doi.org/https://doi.org/10.1002/(SICI)1096-9861(20000403)419:2<205::AID-CNE5>3.0.CO;2-0

Kjelstrup, K. B., Solstad, T., Brun, V. H., Hafting, T., Leutgeb, S., Witter, M. P., Moser, E. I., & Moser, M.-B. (2008). Finite scale of spatial representation in the hippocampus. *Science*, *321*(5885), 140–143. https://doi.org/10.1126/science.1157086

Kjelstrup, K. G., Tuvnes, F. A., Steffenach, H.-A., Murison, R., Moser, E. I., & Moser, M.-B. (2002). Reduced fear expression after lesions of the ventral hippocampus. *Proceedings of the National Academy of Sciences*, *99*(16), 10825–10830. https://doi.org/10.1073/pnas.152112399

Koga, K., Liu, M. G., Qiu, S., Song, Q., O'Den, G., Chen, T., & Zhuo, M. (2015). Impaired presynaptic long-term potentiation in the anterior cingulate cortex of Fmr1 knock-out mice. *Journal of Neuroscience*, *35*(5), 2033–2043. https://doi.org/10.1523/JNEUROSCI.2644-14.2015

Koga, K., Sim, S. E., Chen, T., Wu, L. J., Kaang, B. K., & Zhuo, M. (2012). Kainate receptor-mediated synaptic transmissions in the adult rodent insular cortex. *Journal of Neurophysiology*, *108*(7), 1988–1998. https://doi.org/10.1152/jn.00453.2012

König, P., Engel, A. K., & Singer, W. (1995). Relation between oscillatory activity and long-range synchronization in cat visual cortex. *Proceedings of the National Academy of Sciences of the United States of America*, *92*(1), 290–294. https://doi.org/10.1073/pnas.92.1.290

Kooy, R. F. (2003). Of mice and the fragile X syndrome. *Trends in Genetics*, *19*(3), 148–154. https://doi.org/10.1016/S0168-9525(03)00017-9

Kouvaros, S., & Papatheodoropoulos, C. (2017). Prominent differences in sharp waves, ripples and complex spike bursts between the dorsal and the ventral rat hippocampus. *Neuroscience*, *352*, 131–143. https://doi.org/10.1016/j.neuroscience.2017.03.050

Kubota, D., Colgin, L. L., Casale, M., Brucher, F. A., & Lynch, G. (2003). Endogenous waves in hippocampal slices. *Journal of Neurophysiology*, *89*(1), 81–89. https://doi.org/10.1152/jn.00542.2002

Kullmann, D. M. (2011). Interneuron networks in the hippocampus. *Current Opinion in Neurobiology*, *21*(5), 709–716. https://doi.org/10.1016/j.conb.2011.05.006

Kumar, V., Bhat, Z. A., & Kumar, D. (2013). Animal models of anxiety: A comprehensive review. *Journal of Pharmacological and Toxicological Methods*, *68*(2), 175–183. https://doi.org/10.1016/j.vascn.2013.05.003

Langille, J. J., & Brown, R. E. (2018). The synaptic theory of memory: A historical survey and reconciliation of recent opposition. *Frontiers in Systems Neuroscience*, *12*(October), 1–15. https://doi.org/10.3389/fnsys.2018.00052

Laurent, G. (2002). Olfactory network dynamics and the coding of multidimensional signals. *Nature Reviews Neuroscience*, *3*(11), 884–895. https://doi.org/10.1038/nrn964

Laxmi, T. R., Stork, O., & Pape, H. C. (2003). Generalisation of conditioned fear and its behavioural expression in mice.

Behavioural Brain Research, *145*(1–2), 89–98. https://doi.org/10.1016/S0166-4328(03)00101-3

Lee, F. H. F., Lai, T. K. Y., Su, P., & Liu, F. (2019). Altered cortical Cytoarchitecture in the Fmr1 knockout mouse. *Molecular Brain*, *12*(1), 1–12. https://doi.org/10.1186/s13041-019-0478-8

Likhtik, E., Stujenske, J. M., A Topiwala, M., Harris, A. Z., & Gordon, J. A. (2014). Prefrontal entrainment of amygdala activity signals safety in learned fear and innate anxiety. *Nature Neuroscience*, *17*(1), 106–113. https://doi.org/10.1038/nn.3582

Lin, H. C., Mao, S. C., & Gean, P. W. (2009). Block of γ-Aminobutyric Acid-A Receptor Insertion in the Amygdala Impairs Extinction of Conditioned Fear. *Biological Psychiatry*, *66*(7), 665–673. https://doi.org/10.1016/j.biopsych.2009.04.003

Llinas, R., & Ribary, U. (1993). Coherent 40-Hz oscillation characterizes dream state in humans. *Proceedings of the National Academy of Sciences of the United States of America*, *90*(5), 2078–2081. https://doi.org/10.1073/pnas.90.5.2078

Lovelace, J. W., Ethell, I. M., Binder, D. K., & Razak, K. A. (2018). Translation-relevant EEG phenotypes in a mouse model of Fragile X Syndrome. *Neurobiology of Disease*, *115*, 39–48.

Lovelace, J. W., Rais, M., Palacios, A. R., Shuai, X. S., Bishay, S., Popa, O., Pirbhoy, P. S., Binder, D. K., Nelson, D. L., Ethell, I. M., & Razak, K. A. (2020). Deletion of Fmr1 from Forebrain Excitatory Neurons Triggers Abnormal Cellular, EEG, and Behavioral Phenotypes in the Auditory Cortex of a Mouse Model of Fragile X Syndrome. *Cerebral Cortex*, *30*(3), 969–988. https://doi.org/10.1093/cercor/bhz141

Luo, Q., Holroyd, T., Jones, M., Hendler, T., & Blair, J. (2007). Neural dynamics for facial threat processing as revealed by gamma band synchronization using MEG. *Neuroimage*, *34*(2), 839–847.

Luo, Q., Mitchell, D., Cheng, X., Mondillo, K., McCaffrey, D., Holroyd, T., Carver, F., Coppola, R., & Blair, J. (2009). Visual awareness, emotion, and gamma band synchronization. *Cerebral Cortex*, *19*(8), 1896–1904. https://doi.org/10.1093/cercor/bhn216

Lussier, A. L., Romay-Tallón, R., Caruncho, H. J., & Kalynchuk, L. E. (2013). Altered GABAergic and glutamatergic activity within the rat hippocampus and amygdala in rats subjected to repeated corticosterone administration but not restraint stress. *Neuroscience*, *231*, 38–48. https://doi.org/10.1016/j.neuroscience.2012.11.037

Luxem, K., Mocellin, P., Fuhrmann, F., Kürsch, J., Remy, S., & Bauer, P. (2020). Identifying Behavioral Structure from Deep Variational Embeddings of Animal Motion. *BioRxiv*, 1–19.

Maccaferri, G., David, J., Roberts, B., Szucs, P., Cottingham, C. A., & Somogyi, P. (2000). Cell surface domain specific postsynaptic currents evoked by identified GABAergic neurones in rat hippocampus in vitro. *Journal of Physiology*, *524*(1), 91–116. https://doi.org/10.1111/j.1469-7793.2000.t01-3-00091.x

Maccaferri, G., & Lacaille, J. C. (2003). Interneuron Diversity series: Hippocampal interneuron classifications - Making things as simple as possible, not simpler. *Trends in Neurosciences*, *26*(10), 564–571. https://doi.org/10.1016/j.tins.2003.08.002

Maggio, N., & Segal, M. (2007a). Striking variations in corticosteroid modulation of long-term potentiation along the septotemporal axis of the hippocampus. *Journal of Neuroscience*, *27*(21), 5757–5765. https://doi.org/10.1523/JNEUROSCI.0155-07.2007

Maggio, N., & Segal, M. (2007b). Unique regulation of long term potentiation in the rat ventral hippocampus. *Hippocampus*, *17*(1), 10–25. https://doi.org/10.1002/hipo.20237

Maggio, N., & Segal, M. (2011). Persistent changes in ability to express long-term potentiation/depression in the rat hippocampus after juvenile/adult stress. *Biological Psychiatry*, *69*(8), 748–753. https://doi.org/10.1016/j.biopsych.2010.11.026

Maier, N., Morris, G., Johenning, F. W., & Schmitz, D. (2009). An approach for reliably investigating hippocampal sharpwave-ripples in vitro. *PLoS ONE*, *4*(9). https://doi.org/10.1371/journal.pone.0006925

Maier, N., Morris, G., Schuchmann, S., Korotkova, T., Ponomarenko, A., Böhm, C., Wozny, C., & Schmitz, D. (2012). Cannabinoids disrupt hippocampal sharp wave-ripples via inhibition of glutamate release. *Hippocampus*, *22*(6), 1350–1362. https://doi.org/10.1002/hipo.20971

Maier, N., Nimmrich, V., & Draguhn, A. (2003). Cellular and network mechanisms underlying spontaneous sharp wave-ripple complexes in mouse hippocampal slices. *The Journal of Physiology*, *550*(3), 873–887. https://doi.org/10.1113/jphysiol.2003.044602

Maier, N., Tejero-Cantero, Á., Dorrn, A. L., Winterer, J., Beed, P. S., Morris, G., Kempter, R., Poulet, J. F. A., Leibold, C., & Schmitz, D. (2011). Coherent Phasic Excitation during Hippocampal Ripples. *Neuron*, *72*(1), 137–152. https://doi.org/10.1016/j.neuron.2011.08.016

Maingret, N., Girardeau, G., Todorova, R., Goutierre, M., & Zugaro, M. B. (2016). Hippocampo-cortical coupling mediates memory consolidation during sleep. *Nature Neuroscience*, *19*(7), 959–964. https://doi.org/10.1038/nn.4304

Makkar, S. R., Zhang, S. Q., & Cranney, J. (2010). Behavioral and neural analysis of GABA in the acquisition, consolidation, reconsolidation, and extinction of fear memory. *Neuropsychopharmacology*, *35*(8), 1625–1652. https://doi.org/10.1038/npp.2010.53

Mamiya, N., Fukushima, H., Suzuki, A., Matsuyama, Z., Homma, S., Frankland, P. W., & Kida, S. (2009). Brain region-specific gene expression activation required for reconsolidation and extinction of contextual fear memory. *Journal of Neuroscience*, *29*(2), 402–413. https://doi.org/10.1523/JNEUROSCI.4639-08.2009

Manabe, H., Kusumoto-Yoshida, I., Ota, M., & Mori, K. (2011). Olfactory cortex generates synchronized top-down inputs to the olfactory bulb during slow-wave sleep. *Journal of Neuroscience*, *31*(22), 8123–8133. https://doi.org/10.1523/JNEUROSCI.6578-10.2011

Mann, E. O., & Mody, I. (2010). Control of hippocampal gamma oscillation frequency by tonic inhibition and excitation of interneurons. *Nature Neuroscience*, *13*(2), 205–212. https://doi.org/10.1038/nn.2464

Maren, S., & Fanselow, M. S. (1995). Synaptic plasticity in the basolateral amygdala induced by hippocampal formation stimulation in vivo. *Journal of Neuroscience*, *15*(11), 7548–7564. https://doi.org/10.1523/jneurosci.15-11-07548.1995

Marr, D. (1971). Simple memory: a theory of the archicortex. *Philosophical Transactions of the Royal Society B: Biological Sciences*, *262*, 23–81.

Martin, B. S., Corbin, J. G., & Huntsman, M. M. (2014). Deficient tonic GABAergic conductance and synaptic balance in the fragile X syndrome amygdala. *Journal of Neurophysiology*, *112*(4), 890–902. https://doi.org/10.1152/jn.00597.2013

Maruki, K., Izaki, Y., Nomura, M., & Yamauchi, T. (2001). Differences in paired-pulse facilitation and long-term potentiation between dorsal and ventral CA1 regions in anesthetized rats. *Hippocampus*, *11*(6), 655–661. https://doi.org/10.1002/hipo.1080

Matovic, S., Ichiyama, A., Igarashi, H., Salter, E. W., Sunstrum, J. K., Wang, X. F., Henry, M., Kuebler, E. S., Vernoux, N., Martinez-Trujillo, J., Tremblay, M. E., & Inoue, W. (2020). Neuronal hypertrophy dampens neuronal intrinsic excitability and stress responsiveness during chronic stress. *Journal of Physiology*, *598*(13), 2757–2773. https://doi.org/10.1113/JP279666

McEwen, B. S. (2004). Protection and damage from acute and chronic stress: Allostasis and allostatic overload and relevance to the pathophysiology of psychiatric disorders. *Annals of the New York Academy of Sciences*, *1032*, 1–7. https://doi.org/10.1196/annals.1314.001

Merino, J. J., Cordero, M. I., & Sandi, C. (2000). Regulation of hippocampal cell adhesion molecules NCAM and L1 by contextual fear conditioning is dependent upon time and stressor intensity. *European Journal of Neuroscience*, *12*(9), 3283–3290. https://doi.org/10.1046/j.1460-9568.2000.00191.x

Michalon, A., Sidorov, M., Ballard, T. M., Ozmen, L., Spooren, W., Wettstein, J. G., Jaeschke, G., Bear, M. F., & Lindemann, L. (2012). Chronic Pharmacological mGlu5 Inhibition Corrects Fragile X in Adult Mice. *Neuron*, *74*(1), 49–56. https://doi.org/10.1016/j.neuron.2012.03.009

Milad, M. R., & Quirk, G. J. (2002). Neuronsinmedialprefrontalcortexsignal memory for fear extinction. *Nature*, *420*(6911), 70–74. https://doi.org/10.1038/nature01144.1.

Milad, M. R., & Quirk, G. J. (2012). Fear extinction as a model for translational neuroscience: Ten years of progress. *Annual Review of Psychology*, *63*, 129–151. https://doi.org/10.1146/annurev.psych.121208.131631

Mizunuma, M., Norimoto, H., Tao, K., Egawa, T., Hanaoka, K., Sakaguchi, T., Hioki, H., Kaneko, T., Yamaguchi, S., Nagano, T., Matsuki, N., & Ikegaya, Y. (2014). Unbalanced excitability underlies offline reactivation of behaviorally activated neurons. *Nature Neuroscience*, *17*(4), 503–505. https://doi.org/10.1038/nn.3674

Möhler, H. (2012). The GABA system in anxiety and depression and its therapeutic potential. *Neuropharmacology*, *62*(1), 42–53. https://doi.org/10.1016/j.neuropharm.2011.08.040

Montgomery, S. M., & Buzsáki, G. (2007). Gamma oscillations dynamically couple hippocampal CA3 and CA1 regions during memory task performance. *Proceedings of the National Academy of Sciences of the United States of America*, *104*(36), 14495–14500. https://doi.org/10.1073/pnas.0701826104

Morgan, M. A., Romanski, L. M., & LeDoux, J. E. (1993). Extinction of emotional learning: Contribution of medial prefrontal cortex. *Neuroscience Letters*, *163*(1), 109–113. https://doi.org/10.1016/0304-3940(93)90241-C

Moser, M.-B., Moser, E. I., Forrest, E., Andersen, P., & Morris, R. G. M. (1995). *Spatial learning with a minislab in the dorsal hippocampus*. *92*(October), 9697–9701.

Müller, I., Çalışkan, G., & Stork, O. (2015). The GAD65 knock out mouse - A model for GABAergic processes in fear- and stress-induced psychopathology. *Genes, Brain and Behavior*, *14*(1), 37–45. https://doi.org/10.1111/gbb.12188

Myers, K. M., & Davis, M. (2007). Mechanisms of fear extinction. *Molecular Psychiatry*, *12*(2), 120–150. https://doi.org/10.1038/sj.mp.4001939

Nadel, L., & Moscovitch, M. (1997). Memory consolidation, retrograde amnesia and the hippocampal complex. *Current Opinion in Neurobiology*, *7*(2), 217–227. https://doi.org/10.1016/S0959-4388(97)80010-4

Nagode, D. A., Tang, A. H., Yang, K., & Alger, B. E. (2014). Optogenetic identification of an intrinsic cholinergically driven inhibitory oscillator sensitive to cannabinoids and opioids in hippocampal CA1. *Journal of Physiology*, *592*(1), 103–123. https://doi.org/10.1113/jphysiol.2013.257428

Nakashiba, T., Buhl, D. L., McHugh, T. J., & Tonegawa, S. (2009). Hippocampal CA3 Output Is Crucial for Ripple-Associated Reactivation and Consolidation of Memory. *Neuron*, *62*(6), 781–787. https://doi.org/10.1016/j.neuron.2009.05.013

Narikiyo, K., Manabe, H., & Mori, K. (2014). Sharp wave-associated synchronized inputs from the piriform cortex activate olfactory tubercle neurons during slow-wave sleep. *Journal of Neurophysiology*, *111*(1), 72–81. https://doi.org/10.1152/jn.00535.2013

Neves, G., Cooke, S. F., & Bliss, T. V. P. (2008). Synaptic plasticity, memory and the hippocampus: A neural network approach to causality. *Nature Reviews Neuroscience*, *9*(1), 65–75. https://doi.org/10.1038/nrn2303

Nguyen, R., Morrissey, M. D., Mahadevan, V., Cajanding, J. D., Woodin, M. A., Yeomans, J. S., Takehara-Nishiuchi, K., & Kim, J. C. (2014). Parvalbumin and GAD65 Interneuron Inhibition in the Ventral Hippocampus Induces Distinct Behavioral Deficits Relevant to Schizophrenia. *Journal of Neuroscience*, *34*(45), 14948–14960. https://doi.org/10.1523/JNEUROSCI.2204-14.2014

Nomura, T. (2021). Interneuron dysfunction and inhibitory deficits in autism and fragile X syndrome. *Cells*, *10*(10). https://doi.org/10.3390/cells10102610

Nuss, P. (2015). Anxiety disorders and GABA neurotransmission: A disturbance of modulation. *Neuropsychiatric Disease and Treatment*, *11*, 165–175. https://doi.org/10.2147/NDT.S58841

O'Keefe, J. (1976). Place units in the hippocampus of the freely moving rat. *Experimental Neurology*, *51*(1), 78–109. https://doi.org/10.1016/0014-4886(76)90055-8

O'Keefe, J., & Nadel, L. (1978). The Hippocampus as a Cognitive Map. *Oxford University Press*.

O'Neill, J., Pleydell-Bouverie, B., Dupret, D., & Csicsvari, J. (2010). Play it again: reactivation of waking experience and memory. *Trends in Neurosciences*, *33*(5), 220–229. https://doi.org/10.1016/j.tins.2010.01.006

O'Neill, J., Senior, T., & Csicsvari, J. (2006). Place-selective firing of CA1 pyramidal cells during sharp wave/ripple network patterns in exploratory behavior. *Neuron*, *49*(1), 143–155. https://doi.org/10.1016/j.neuron.2005.10.037

Oliva, A., Fernández-Ruiz, A., Buzsáki, G., & Berényi, A. (2016). Role of Hippocampal CA2 Region in Triggering Sharp-

Wave Ripples. *Neuron*, *91*(6), 1342–1355. https://doi.org/10.1016/j.neuron.2016.08.008

Olmos-Serrano, J. L., Paluszkiewicz, S. M., Martin, B. S., Kaufmann, W. E., Corbin, J. G., & Huntsman, M. M. (2010). Defective GABAergic neurotransmission and pharmacological rescue of neuronal hyperexcitability in the amygdala in a mouse model of fragile X syndrome. *Journal of Neuroscience*, *30*(29), 9929–9938. https://doi.org/10.1523/JNEUROSCI.1714-10.2010

Oren, I., & Paulsen, O. (2010). Currents in space: Understanding inhibitory field potentials. *Journal of Physiology*, *588*(12), 2015–2016. https://doi.org/10.1113/jphysiol.2010.192443

Padilla-Coreano, N., Bolkan, S. S., Pierce, G. M., Blackman, D. R., Hardin, W. D., Garcia-Garcia, A. L., Spellman, T. J., & Gordon, J. A. (2016). Direct Ventral Hippocampal-Prefrontal Input Is Required for Anxiety-Related Neural Activity and Behavior. *Neuron*, *89*(4), 857–866. https://doi.org/10.1016/j.neuron.2016.01.011

Pálhalmi, J., Paulsen, O., Freund, T. F., & Hájos, N. (2004). Distinct properties of carbachol- and DHPG-induced network oscillations in hippocampal slices. *Neuropharmacology*, *47*(3), 381–389. https://doi.org/10.1016/j.neuropharm.2004.04.010

Paluszkiewicz, S. M., Martin, B. S., & Huntsman, M. M. (2011). Fragile X syndrome: The GABAergic system and circuit dysfunction. *Developmental Neuroscience*, *33*(5), 349–364. https://doi.org/10.1159/000329420

Pangalos, M., Donoso, J. R., Winterer, J., Zivkovic, A. R., Kempter, R., Maier, N., & Schmitz, D. (2013). Recruitment of oriens-lacunosum-moleculare interneurons during hippocampal ripples. *Proceedings of the National Academy of Sciences of the United States of America*, *110*(11), 4398–4403. https://doi.org/10.1073/pnas.1215496110

Papatheodoropoulos, C. (2007). NMDA receptor-dependent high-frequency network oscillations (100-300 Hz) in rat hippocampal slices. *Neuroscience Letters*, *414*(3), 197–202. https://doi.org/10.1016/j.neulet.2006.10.036

Papatheodoropoulos, C., & Kostopoulos, G. (2000a). Decreased ability of rat temporal hippocampal CA1 region to produce long-term potentiation. *Neuroscience Letters*, *279*(3), 177–180. https://doi.org/10.1016/S0304-3940(99)01002-2

Papatheodoropoulos, C., & Kostopoulos, G. (2000b). Dorsal-ventral differentiation of short-term synaptic plasticity in rat CA1 hippocampal region. *Neuroscience Letters*, *286*(1), 57–60. https://doi.org/10.1016/S0304-3940(00)01084-3

Papatheodoropoulos, C., & Kostopoulos, G. (2002a). Spontaneous, low frequency (∼2-3 Hz) field activity generated in rat ventral hippocampal slices perfused with normal medium. *Brain Research Bulletin*, *57*(2), 187–193. https://doi.org/10.1016/S0361-9230(01)00738-9

Papatheodoropoulos, C., & Kostopoulos, G. (2002b). Spontaneous GABAA-dependent synchronous periodic activity in adult rat ventral hippocampal slices. *Neuroscience Letters*, *319*(1), 17–20. https://doi.org/10.1016/S0304-3940(01)02505-8

Pavlides, C., Ogawa, S., Kimura, A., & McEwen, B. S. (1996). Role of adrenal steroid mineralocorticoid and glucocorticoid receptors in long-term potentiation in the CA1 field of hippocampal slices. *Brain Research*, *738*(2), 229–235. https://doi.org/10.1016/S0006-8993(96)00776-7

Pavlides, C., Watanabe, Y., & McEwen, B. S. (1993). Effects of glucocorticoids on hippocampal long-term potentiation. *Hippocampus*, *3*(2), 183–192. https://doi.org/10.1002/hipo.450030210

Pavlov, I. P. (1927). Conditioned reflexes. *New York, NY:Dover*.

Peier, A. M., McIlwain, K. L., Kenneson, A., Warren, S. T., Paylor, R., & Nelson, D. L. (2000). (Over)correction of FMR1 deficiency with YAC transgenics: Behavioral and physical features. *Human Molecular Genetics*, *9*(8), 1145–1159. https://doi.org/10.1093/hmg/9.8.1145

Penttonen, M., & Buzsáki, G. (2003). Natural logarithmic relationship between brain oscillators. *Thalamus and Related Systems*, *2*(2), 145–152. https://doi.org/10.1016/S1472-9288(03)00007-4

Percelay, S., Billard, J. M., Freret, T., Andrieux, A., Boulouard, M., & Bouet, V. (2021). Functional dysregulations in ca1 hippocampal networks of a 3-hit mouse model of schizophrenia. *International Journal of Molecular Sciences*, *22*(5), 1–13. https://doi.org/10.3390/ijms22052644

Perumal, M. B., Latimer, B., Xu, L., Stratton, P., Nair, S., & Sah, P. (2021). Microcircuit mechanisms for the generation

of sharp-wave ripples in the basolateral amygdala: A role for chandelier interneurons. *Cell Reports*, *35*(6). https://doi.org/10.1016/j.celrep.2021.109106

Pfeiffer, B. E., & Foster, D. J. (2013). Hippocampal place-cell sequences depict future paths to remembered goals. *Nature*, *497*(7447), 74–79. https://doi.org/10.1038/nature12112

Phelps, E. A. (2004). Human emotion and memory: Interactions of the amygdala and hippocampal complex. *Current Opinion in Neurobiology*, *14*(2), 198–202. https://doi.org/10.1016/j.conb.2004.03.015

Phillips, R. G., & LeDoux, J. E. (1994). Lesions of the dorsal hippocampal formation interfere with background but not foreground contextual fear conditioning. *Learning Memory*, *1*(1), 34–44. https://doi.org/10.1101/lm.1.1.34

Pietersen, A. N. J., Ward, P. D., Hagger-Vaughan, N., Wiggins, J., Jefferys, J. G. R., & Vreugdenhil, M. (2014). Transition between fast and slow gamma modes in rat hippocampus area CA1 in vitro is modulated by slow CA3 gamma oscillations. *Journal of Physiology*, *592*(4), 605–620. https://doi.org/10.1113/jphysiol.2013.263889

Pinault, D., & Deschenes, M. (1992). Voltage-dependent 40-Hz oscillations in rat reticular thalamic neurons in vivo. *Neuroscience*, *51*(2), 245–258. https://doi.org/10.1016/0306-4522(92)90312-p

Pirbhoy, P. S., Rais, M., Lovelace, J. W., Woodard, W., Razak, K. A., Binder, D. K., & Ethell, I. M. (2020). Acute pharmacological inhibition of matrix metalloproteinase-9 activity during development restores perineuronal net formation and normalizes auditory processing in Fmr1 KO mice. *Journal of Neurochemistry*, *155*(5), 538–558. https://doi.org/10.1111/jnc.15037

Pitkänen, A., Pikkarainen, M., Nurminen, N., & Ylinen, A. (2000). Reciprocal connections between the amygdala and the hippocampal formation, perirhinal cortex, and postrhinal cortex in rat. A review. *Annals of the New York Academy of Sciences*, *911*, 369–391. https://doi.org/10.1111/j.1749-6632.2000.tb06738.x

Polepalli, J. S., Wu, H., Goswami, D., Halpern, C. H., Südhof, T. C., & Malenka, R. C. (2017). Modulation of excitation on parvalbumin interneurons by neuroligin-3 regulates the hippocampal network. *Nature Neuroscience*, *20*(2), 219–229. https://doi.org/10.1038/nn.4471

Ponomarenko, A. A., Korotkova, T. M., & Haas, H. L. (2003). High frequency (200 Hz) oscillations and firing patterns in the basolateral amygdala and dorsal endopiriform nucleus of the behaving rat. *Behavioural Brain Research*, *141*(2), 123–129. https://doi.org/10.1016/S0166-4328(02)00327-3

Ponomarenko, A. A., Li, J. S., Korotkova, T. M., Huston, J. P., & Haas, H. L. (2008). Frequency of network synchronization in the hippocampus marks learning. *European Journal of Neuroscience*, *27*(11), 3035–3042. https://doi.org/10.1111/j.1460-9568.2008.06232.x

Qi, J., Kim, M., Sanchez, R., Ziaee, S. M., Kohtz, J. D., & Koh, S. (2018). Enhanced susceptibility to stress and seizures in GAD65 deficient mice. *PLoS ONE*, *13*(1), 1–17. https://doi.org/10.1371/journal.pone.0191794

Qiu, S., Wu, Y., Lv, X., Li, X., Zhuo, M., & Koga, K. (2018). Reduced synaptic function of Kainate receptors in the insular cortex of Fmr1 Knock-out mice. *Molecular Brain*, *11*(1), 1–11. https://doi.org/10.1186/s13041-018-0396-1

Quirk, G. J., Garcia, R., & González-Lima, F. (2006). Prefrontal Mechanisms in Extinction of Conditioned Fear. *Biological Psychiatry*, *60*(4), 337–343. https://doi.org/10.1016/j.biopsych.2006.03.010

Quirk, G. J., Russo, G. K., Barron, J. L., & Lebron, K. (2000). The role of ventromedial prefrontal cortex in the recovery of extinguished fear. *Journal of Neuroscience*, *20*(16), 6225–6231. https://doi.org/10.1523/jneurosci.20-16-06225.2000

Radwan, B., Dvorak, D., & Fenton, A. A. (2016). Impaired cognitive discrimination and discoordination of coupled theta-gamma oscillations in Fmr1 knockout mice. *Neurobiology of Disease*, *88*, 125–138. https://doi.org/10.1016/j.nbd.2016.01.003

Ramirez-Villegas, J. F., Willeke, K. F., Logothetis, N. K., & Besserve, M. (2018). Dissecting the Synapse- and Frequency-Dependent Network Mechanisms of In Vivo Hippocampal Sharp Wave-Ripples. *Neuron*, *100*(5), 1224-1240.e13. https://doi.org/10.1016/j.neuron.2018.09.041

Raza, S. A., Albrecht, A., Çalışkan, G., Müller, B., Demiray, Y. E., Ludewig, S., Meis, S., Faber, N., Hartig, R., Schraven, B., Lessmann, V., Schwegler, H., & Stork, O. (2017). HIPP neurons in the dentate gyrus mediate the cholinergic modulation of background context memory salience. *Nature Communications*, *8*(1), 189.

https://doi.org/10.1038/s41467-017-00205-3

Rehberg, K., Kliche, S., Madencioglu, D. A., Thiere, M., Müller, B., Manuel Meineke, B., Freund, C., Budinger, E., & Stork, O. (2014). The serine/threonine kinase Ndr2 controls integrin trafficking and integrin-dependent neurite growth. *Journal of Neuroscience*, *34*(15), 5342–5354. https://doi.org/10.1523/JNEUROSCI.2728-13.2014

Richardson, D. J., Elhai, J. D., & Sarreen, J. (2011). Predictors of Treatment Response in Canadian Combat and Peacekeeping Veterans With Military-Related Posttraumatic Stress Disorder. *The Journal of Nervous and Mental Disease*, *199*(9). https://journals.lww.com/jonmd/Fulltext/2011/09000/Predictors_of_Treatment_Response_in_Canadian.5.aspx

Richardson, M. P., Strange, B. A., & Dolan, R. J. (2004). Encoding of emotional memories depends on amygdala and hippocampus and their interactions. *Nature Neuroscience*, *7*(3), 278–285. https://doi.org/10.1038/nn1190

Richter, J. D., Bassell, G. J., & Klann, E. (2015). Dysregulation and restoration of translational homeostasis in fragile X syndrome. *Nature Reviews Neuroscience*, *16*(10), 595–605. https://doi.org/10.1038/nrn4001

Rogers, J. L., Hunsaker, M. R., & Kesner, R. P. (2006). Effects of ventral and dorsal CA1 subregional lesions on trace fear conditioning. *Neurobiology of Learning and Memory*, *86*(1), 72–81. https://doi.org/10.1016/j.nlm.2006.01.002

Roth, F. C., & Draguhn, A. (2012). GABA metabolism and transport: Effects on synaptic efficacy. *Neural Plasticity*, *2012*. https://doi.org/10.1155/2012/805830

Rubinson, D. A., Dillon, C. P., Kwiatkowski, A. V., Sievers, C., Yang, L., Kopinja, J., Zhang, M., McManus, M. T., Gertler, F. B., Scott, M. L., & Van Parijs, L. (2003). A lentivirus-based system to functionally silence genes in primary mammalian cells, stem cells and transgenic mice by RNA interference. *Nature Genetics*, *33*(3), 401–406. https://doi.org/10.1038/ng1117

Sangha, S., Ilenseer, J., Sosulina, L., Lesting, J., & Pape, H. C. (2012). Differential regulation of glutamic acid decarboxylase gene expression after extinction of a recent memory vs. intermediate memory. *Learning and Memory*, *19*(5), 194–200. https://doi.org/10.1101/lm.025874.112

Sangha, S., Narayanan, R. T., Bergado-Acosta, J. R., Stork, O., Seidenbecher, T., & Pape, H. C. (2009). Deficiency of the 65 kDa isoform of glutamic acid decarboxylase impairs extinction of cued but not contextual fear memory. *Journal of Neuroscience*, *29*(50), 15713–15720. https://doi.org/10.1523/JNEUROSCI.2620-09.2009

Santos, A. R., Kanellopoulos, A. K., & Bagni, C. (2014). Learning and behavioral deficits associated with the absence of the fragile X mental retardation protein: What a fly and mouse model can teach us. *Learning and Memory*, *21*(10), 543–555. https://doi.org/10.1101/lm.035956.114

Schlingloff, D., Káli, S., Freund, T. F., Hájos, N., & Gulyás, A. I. (2014). Mechanisms of sharp wave initiation and ripple generation. *Journal of Neuroscience*, *34*(34), 11385–11398. https://doi.org/10.1523/JNEUROSCI.0867-14.2014

Schomburg, E. W., Anastassiou, C. A., Buzsáki, G., & Koch, C. (2012). The spiking component of oscillatory extracellular potentials in the rat hippocampus. *Journal of Neuroscience*, *32*(34), 11798–11811. https://doi.org/10.1523/JNEUROSCI.0656-12.2012

Schomburg, E. W., Fernández-Ruiz, A., Mizuseki, K., Berényi, A., Anastassiou, C. A., Koch, C., & Buzsáki, G. (2014). Theta Phase Segregation of Input-Specific Gamma Patterns in Entorhinal-Hippocampal Networks. *Neuron*, *84*(2), 470–485. https://doi.org/10.1016/j.neuron.2014.08.051

Scoville, W. B., & Milner, B. (1957). Loss of recent memory after bilateral hippocampal lesions. 1957. *Journal Neurol. Neurosurg. Psychiatry*, *20*(11). https://doi.org/10.1176/jnp.12.1.103-a

Scremin, O. U., Roch, M., Norman, K. M., Djazayeri, S., & Liu, Y. Y. (2015). Brain acetylcholine and choline concentrations and dynamics in a murine model of the Fragile X syndrome: Age, sex and region-specific changes. *Neuroscience*, *301*, 520–528. https://doi.org/10.1016/j.neuroscience.2015.06.036

Sederberg, P. B., Schulze-Bonhage, A., Madsen, J. R., Bromfield, E. B., Litt, B., Brandt, A., & Kahana, M. J. (2007). Gamma oscillations distinguish true from false memories: Research report. *Psychological Science*, *18*(11), 927–932. https://doi.org/10.1111/j.1467-9280.2007.02003.x

Sederberg, P. B., Schulze-Bonhage, A., Madsen, J. R., Bromfield, E. B., McCarthy, D. C., Brandt, A., Tully, M. S., & Kahana, M. J. (2007). Hippocampal and neocortical gamma oscillations predict memory formation in humans. *Cerebral Cortex*, *17*(5), 1190–1196. https://doi.org/10.1093/cercor/bhl030

Seidenbecher, T., Laxmi, T. R., Stork, O., & Pape, H. C. (2003). Amygdalar and Hippocampal Theta Rhythm Synchronization During Fear Memory Retrieval. *Science*, *301*(5634), 846–850. https://doi.org/10.1126/science.1085818

Seney, M. L., Chang, L. C., Oh, H., Wang, X., Tseng, G. C., Lewis, D. A., & Sibille, E. (2013). The role of genetic sex in affect regulation and expression of GABA-related genes across species. *Frontiers in Psychiatry*, *4*(SEP), 1–18. https://doi.org/10.3389/fpsyt.2013.00104

Senkowski, D., Kautz, J., Hauck, M., Zimmermann, R., & Engel, A. K. (2011). Emotional facial expressions modulate pain-induced beta and gamma oscillations in sensorimotor cortex. *Journal of Neuroscience*, *31*(41), 14542–14550. https://doi.org/10.1523/JNEUROSCI.6002-10.2011

Shin, L. M., Rauch, S. L., & Pitman, R. K. (2006). Amygdala, medial prefrontal cortex, and hippocampal function in PTSD. *Annals of the New York Academy of Sciences*, *1071*, 67–79. https://doi.org/10.1196/annals.1364.007

Shors, T. J., Seib, T. B., Levine, S., & Thompson, R. F. (1989). Inescapable versus escapable shock modulates long-term potentiation in the rat hippocampus. *Science*, *244*(4901), 224–226. https://doi.org/10.1126/science.2704997

Siegmund, A., & Wotjak, C. T. (2006). Toward an animal model of posttraumatic stress disorder. *Annals of the New York Academy of Sciences*, *1071*, 324–334. https://doi.org/10.1196/annals.1364.025

Singer, W. (1993). Synchronization of Cortical Activity and and Learning. *Brain*.

Soghomonian, J. J., & Martin, D. L. (1998). Two isoforms of glutamate decarboxylase: Why? *Trends in Pharmacological Sciences*, *19*(12), 500–505. https://doi.org/10.1016/S0165-6147(98)01270-X

Song, C., & Leonard, B. E. (2005). The olfactory bulbectomised rat as a model of depression. *Neuroscience and Biobehavioral Reviews*, *29*(4–5), 627–647. https://doi.org/10.1016/j.neubiorev.2005.03.010

Song, I., Savtchenko, L., & Semyanov, A. (2011). Tonic excitation or inhibition is set by GABAA conductance in hippocampal interneurons. *Nature Communications*, *2*(1), 310–376. https://doi.org/10.1038/ncomms1377

Squire, L. R., & Zola-Morgan, S. (1991). The Medial Temporal Lobe Memory System. *Science*, *253*.

Stark, E., Roux, L., Eichler, R., Senzai, Y., Royer, S., & Buzsáki, G. (2014). Pyramidal cell-interneuron interactions underlie hippocampal ripple oscillations. *Neuron*, *83*(2), 467–480. https://doi.org/10.1016/j.neuron.2014.06.023

Steullet, P., Cabungcal, J. H., Cuénod, M., & Do, K. Q. (2014). Fast oscillatory activity in the anterior cingulate cortex: Dopaminergic modulation and effect of perineuronal net loss. *Frontiers in Cellular Neuroscience*, *8*(AUG), 1–10. https://doi.org/10.3389/fncel.2014.00244

Stork, O., Ji, F. Y., Kaneko, K., Stork, S., Yoshinobu, Y., Moriya, T., Shibata, S., & Obata, K. (2000). Postnatal development of a GABA deficit and disturbance of neural functions in mice lacking GAD65. *Brain Research*, *865*(1), 45–58. https://doi.org/10.1016/S0006-8993(00)02206-X

Stork, O., Yamanaka, H., Stork, S., Kume, N., & Obata, K. (2003). Altered conditioned fear behavior in glutamate decarboxylase 65 null mutant mice. *Genes, Brain and Behavior*, *2*(2), 65–70. https://doi.org/10.1034/j.1601-183X.2003.00008.x

Strange, B. A., Witter, M. P., Lein, E. S., & Moser, E. I. (2014). Functional organization of the hippocampal longitudinal axis. *Nature Reviews Neuroscience*, *15*(10), 655–669. https://doi.org/10.1038/nrn3785

Stujenske, J. M., Likhtik, E., Topiwala, M. A., & Gordon, J. A. (2014). Fear and Safety Engage Competing Patterns of Theta-Gamma Coupling in the Basolateral Amygdala. *Neuron*, *83*(4), 919–933. https://doi.org/10.1016/j.neuron.2014.07.026

Suh, J., Foster, D. J., Davoudi, H., Wilson, M. A., & Tonegawa, S. (2013). Impaired Hippocampal Ripple-Associated Replay in a Mouse Model of Schizophrenia. *Neuron*, *80*(2), 484–493. https://doi.org/10.1016/j.neuron.2013.09.014

Sullivan, D., Csicsvari, J., Mizuseki, K., Montgomery, S. M., Diba, K., & Buzsáki, G. (2011). Relationships between

hippocampal sharp waves, ripples, and fast gamma oscillation: Influence of dentate and entorhinal cortical activity. *Journal of Neuroscience*, *31*(23), 8605–8616. https://doi.org/10.1523/JNEUROSCI.0294-11.2011

ter Wal, M., & Tiesinga, P. (2013). Hippocampal Oscillations, Mechanisms (PING, ING, Sparse). *Encyclopedia of Computational Neuroscience*.

Thiere, M., Kliche, S., Müiler, B., Teuber, J., Nold, I., & Stork, O. (2016). Integrin activation through the hematopoietic adapter molecule ADAP regulates dendritic development of hippocampal neurons. *Frontiers in Molecular Neuroscience*, *9*(SEP2016), 1–14. https://doi.org/10.3389/fnmol.2016.00091

Thomson, S. R., Seo, S. S., Barnes, S. A., Louros, S. R., Muscas, M., Dando, O., Kirby, C., Wyllie, D. J. A., Hardingham, G. E., Kind, P. C., & Osterweil, E. K. (2017). Cell-Type-Specific Translation Profiling Reveals a Novel Strategy for Treating Fragile X Syndrome. *Neuron*, *95*(3), 550-563.e5. https://doi.org/10.1016/j.neuron.2017.07.013

Tian, N., Petersen, C., Kash, S., Baekkeskov, S., Copenhagen, D., & Nicoll, R. (1999). *The role of the synthetic enzyme GAD65 in the control of neuronal ⇗ -aminobutyric acid release*.

Traub, R. D., Cunningham, M. O., Gloveli, T., LeBeau, F. E. N., Bibbig, A., Buhl, E. H., & Whittington, M. A. (2003). GABA-enhanced collective behavior in neuronal axons underlies persistent gamma-frequency oscillations. *Proceedings of the National Academy of Sciences of the United States of America*, *100*(19), 11047–11052. https://doi.org/10.1073/pnas.1934854100

Traub, R. D., Whittington, M. A., Buhl, E. H., Jefferys, J. G. R., & Faulkner, H. J. (1999). On the mechanism of the γ → β frequency shift in neuronal oscillations induced in rat hippocampal slices by tetanic stimulation. *Journal of Neuroscience*, *19*(3), 1088–1105. https://doi.org/10.1523/jneurosci.19-03-01088.1999

Traub, R. D., & Wong, R. K. (1982). Cellular Mechanism of Neuronal Synchronization in Epilepsy. *Science*, *216*(4547), 745–747. https://doi.org/10.1126/science.7079735

Tripathi, K., Demiray, Y. E., Kliche, S., Jing, L., Hazra, S., Hazra, J. D., Richter-Levin, G., & Stork, O. (2021). Reducing glutamic acid decarboxylase in the dorsal dentate gyrus attenuates juvenile stress induced emotional and cognitive deficits. *Neurobiology of Stress*, *15*(December 2020), 100350. https://doi.org/10.1016/j.ynstr.2021.100350

Tukker, J. J., Fuentealba, P., Hartwich, K., Somogyi, P., & Klausberger, T. (2007). Cell type-specific tuning of hippocampal interneuron firing during gamma oscillations in vivo. *Journal of Neuroscience*, *27*(31), 8184–8189. https://doi.org/10.1523/JNEUROSCI.1685-07.2007

Vaiva, G., Boss, V., Ducrocq, F., Fontaine, M., Devos, P., Brunet, A., Laffargue, P., Goudemand, M., & Thomas, P. (2006). Relationship between posttrauma GABA plasma levels and PTSD at 1-year follow-up. *American Journal of Psychiatry*, *163*(8), 1446–1448. https://doi.org/10.1176/ajp.2006.163.8.1446

Vaiva, G., Thomas, P., Ducrocq, F., Fontaine, M., Boss, V., Devos, P., Rascle, C., Cottencin, O., Brunet, A., Laffargue, P., & Goudemand, M. (2004). Low posttrauma GABA plasma levels as a predictive factor in the development of acute posttraumatic stress disorder. *Biological Psychiatry*, *55*(3), 250–254. https://doi.org/10.1016/j.biopsych.2003.08.009

Vandecasteele, M., Varga, V., Berényi, A., Papp, E., Barthó, P., Venance, L., Freund, T. F., & Buzsáki, G. (2014). Optogenetic activation of septal cholinergic neurons suppresses sharp wave ripples and enhances theta oscillations in the hippocampus. *Proceedings of the National Academy of Sciences of the United States of America*, *111*(37), 13535–13540. https://doi.org/10.1073/pnas.1411233111

Vanderwolf, C. H. (1969). Hippocampal Electrical Activity and Voluntary Movement in the Rat. *Electroencephalography and Clinical Neurophysiology*, *26*, 407–418.

Veeraragavan, S., Bui, N., Perkins, J. R., Yuva-Paylor, L. A., Carpenter, R. L., & Paylor, R. (2011). Modulation of behavioral phenotypes by a muscarinic M1 antagonist in a mouse model of fragile X syndrome. *Psychopharmacology*, *217*(1), 143–151. https://doi.org/10.1007/s00213-011-2276-6

Volk, L. J., Pfeiffer, B. E., Gibson, J. R., & Huber, K. M. (2007). Multiple Gq-coupled receptors converge on a common protein synthesis-dependent long-term depression that is affected in fragile X syndrome mental retardation. *Journal of Neuroscience*, *27*(43), 11624–11634. https://doi.org/10.1523/JNEUROSCI.2266-07.2007

Wang, Dayong, Noda, Y., Tsunekawa, H., Zhou, Y., Miyazaki, M., Senzaki, K., & Nabeshima, T. (2007). Behavioural and

neurochemical features of olfactory bulbectomized rats resembling depression with comorbid anxiety. *Behavioural Brain Research*, *178*(2), 262–273. https://doi.org/10.1016/j.bbr.2007.01.003

Wang, J., Ethridge, L. E., Mosconi, M. W., White, S. P., Binder, D. K., Pedapati, E. V., Erickson, C. A., Byerly, M. J., & Sweeney, J. A. (2017). A resting EEG study of neocortical hyperexcitability and altered functional connectivity in fragile X syndrome Refining translational treatment development in fragile X syndrome. *Journal of Neurodevelopmental Disorders*, *9*(1), 1–12. https://doi.org/10.1186/s11689-017-9191-z

Wang, Dong V., Yau, H. J., Broker, C. J., Tsou, J. H., Bonci, A., & Ikemoto, S. (2015). Mesopontine median raphe regulates hippocampal ripple oscillation and memory consolidation. *Nature Neuroscience*, *18*(5), 728–735. https://doi.org/10.1038/nn.3998

Wang, X.-J., & Buzsáki, G. (1996). Gamma oscillation by synaptic inhibition in a hippocampal interneuronal network model. *Journal of Neuroscience*, *16*(20), 6402–6413. https://doi.org/10.1523/jneurosci.16-20-06402.1996

Weeden, C. S. S., Roberts, J. M., Kamm, A. M., & Kesner, R. P. (2015). The role of the ventral dentate gyrus in anxiety-based behaviors. *Neurobiology of Learning and Memory*, *118*, 143–149. https://doi.org/10.1016/j.nlm.2014.12.002

Weiss, E. K., Krupka, N., Bähner, F., Both, M., & Draguhn, A. (2008). Fast effects of glucocorticoids on memory-related network oscillations in the mouse hippocampus. *Journal of Neuroendocrinology*, *20*(5), 549–557. https://doi.org/10.1111/j.1365-2826.2008.01699.x

Wen, T. H., Lovelace, J. W., Ethell, I. M., Binder, D. K., & Razak, K. A. (2019). Developmental Changes in EEG Phenotypes in a Mouse Model of Fragile X Syndrome. *Neuroscience*, *398*, 126–143. https://doi.org/10.1016/j.neuroscience.2018.11.047

Whittington, M. A., Cunningham, M. O., LeBeau, F. E. N., Racca, C., & Traub, R. D. (2011). Multiple origins of the cortical gamma rhythm. *Developmental Neurobiology*, *71*(1), 92–106. https://doi.org/10.1002/dneu.20814

Whittington, M. A., Traub, R. D., & Jefferys, J. G. R. (1995). Synchronized oscillations in interneuron networks glutamate receptor activation. *Nature*, *373*(February), 612–615.

Whittington, M. A., Traub, R. D., Kopell, N., Ermentrout, B., & Buhl, E. H. (2000). Inhibition-based rhythms: Experimental and mathematical observations on network dynamics. *International Journal of Psychophysiology*, *38*(3), 315–336. https://doi.org/10.1016/S0167-8760(00)00173-2

Wittner, L., Henze, D. A., Záborszky, L., & Buzsáki, G. (2007). Three-dimensional reconstruction of the axon arbor of a CA3 pyramidal cell recorded and filled in vivo. *Brain Structure and Function*, *212*(1), 75–83. https://doi.org/10.1007/s00429-007-0148-y

Wójtowicz, A. M., Van Boom, L. Den, Chakrabarty, A., Maggio, N., Haq, R. U., Behrens, C. J., & Heinemann, U. (2009). Monoamines block kainate- And carbachol-induced. γ-oscillations but augment stimulus-induced γ-oscillations in rat hippocampus in vitro. *Hippocampus*, *19*(3), 273–288. https://doi.org/10.1002/hipo.20508

Wong, H., Hooper, A. W. M., Niibori, Y., Lee, S. J., Hategan, L. A., Zhang, L., Karumuthil-Melethil, S., Till, S. M., Kind, P. C., Danos, O., Bruder, J. T., & Hampson, D. R. (2020). Sexually dimorphic patterns in electroencephalography power spectrum and autism-related behaviors in a rat model of fragile X syndrome. *Neurobiology of Disease*, *146*(August). https://doi.org/10.1016/j.nbd.2020.105118

Wu, C., Asl, M. N., Gillis, J., Skinner, F. K., & Zhang, L. (2005). An in vitro model of hippocampal sharp waves: Regional initiation and intracellular correlates. *Journal of Neurophysiology*, *94*(1), 741–753. https://doi.org/10.1152/jn.00086.2005

Wu, C., Shen, H., Luk, W. P., & Zhang, L. (2002). A fundamental oscillatory state of isolated rodent hippocampus. *Journal of Physiology*, *540*(2), 509–527. https://doi.org/10.1113/jphysiol.2001.013441

Xu, C., Krabbe, S., Gründemann, J., Botta, P., Fadok, J. P., Osakada, F., Saur, D., Grewe, B. F., Schnitzer, M. J., Callaway, E. M., & Lüthi, A. (2016). Distinct Hippocampal Pathways Mediate Dissociable Roles of Context in Memory Retrieval. *Cell*, *167*(4), 961-972.e16. https://doi.org/10.1016/j.cell.2016.09.051

Zelikowsky, M., Hersman, S., Chawla, M. K., Barnes, C. A., & Fanselow, M. S. (2014). Neuronal ensembles in amygdala, hippocampus, and prefrontal cortex track differential components of contextual fear. *Journal of Neuroscience*, *34*(25), 8462–8466. https://doi.org/10.1523/JNEUROSCI.3624-13.2014

Zeng, H., Chattarji, S., Barbarosie, M., Rondi-Reig, L., Philpot, B. D., Miyakawa, T., Bear, M. F., & Tonegawa, S. (2001). Forebrain-specific calcineurin knockout selectively impairs bidirectional synaptic plasticity and working/episodic-like memory. *Cell*, *107*(5), 617–629. https://doi.org/10.1016/S0092-8674(01)00585-2

Zhang, J., Hou, L., Klann, E., & Nelson, D. L. (2009). Altered hippocampal synaptic plasticity in the Fmr1 gene family knockout mouse models. *Journal of Neurophysiology*, *101*(5), 2572–2580. https://doi.org/10.1152/jn.90558.2008

Zhang, W. N., Bast, T., Xu, Y., & Feldon, J. (2014). Temporary inhibition of dorsal or ventral hippocampus by muscimol: Distinct effects on measures of innate anxiety on the elevated plus maze, but similar disruption of contextual fear conditioning. *Behavioural Brain Research*, *262*, 47–56. https://doi.org/10.1016/j.bbr.2013.10.044

Zucker, R. S., & Regehr, W. G. (2002). Short-term synaptic plasticity. *Annual Review of Physiology*, *64*, 355–405. https://doi.org/10.1146/annurev.physiol.64.092501.114547